

# Renormalization Group Flows of Hamiltonian QCD in Coulomb Gauge

DISSERTATION

der Mathematisch-Naturwissenschaftlichen Fakultät  
der Eberhard Karls Universität Tübingen  
zur Erlangung des Grades eines  
Doktors der Naturwissenschaften  
(Dr. rer. nat.)

vorgelegt von  
**MARKUS LEDER**  
aus Passau

Tübingen  
2011

Tag der mündlichen Qualifikation: 13.02.2012

Dekan:

Prof. Dr. Wolfgang Rosenstiel

1. Berichterstatter:

Prof. Dr. Hugo Reinhardt

2. Berichterstatter:

Prof. Dr. Dr. h.c. mult. Amand Fäßler

## Zusammenfassung

In der vorliegenden Dissertation wird die Yang-Mills-Theorie in Coulombbeichung in der Hamilton-Formulierung unter Anwendung der Funktionalen Renormierungsgruppenflüsse untersucht. Yang-Mills-Theorien bilden die Grundlage des Standardmodells der Elementarteilchenphysik. Der Fokus dieser Arbeit liegt insbesondere auf der Quantenchromodynamik, die die Starke Wechselwirkung beschreibt.

In Kap. 1 wird die Methode der Funktionalen Renormierungsgruppe eingeführt. Sie wird dabei zunächst in ihrer üblichen Formulierung innerhalb des Lagrange-Zugangs zur Quantenfeldtheorie präsentiert. Die Flussgleichung für den Propagator der skalaren Quantenfeldtheorie wird hergeleitet.

Kap. 2 enthält einen Überblick über die Yang-Mills-Theorie in Coulombbeichung in der Hamilton-Formulierung, als Gegensatz Lagrange-Formulierung.

In Kap. 3 wird die Funktionale Renormierungsgruppe auf den Hamilton-Zugang zur Yang-Mills-Theorie in Coulombbeichung übertragen. Mit diesem neuen Werkzeug werden die Flussgleichungen für den Gluon- und den Geistpropagator hergeleitet. Die Gleichungen werden numerisch unter Benutzung zweier verschiedener Näherungen gelöst und die Ergebnisse mit jenen aus dem Variationszugang verglichen.

Kap. 4 hat die Herleitung und Lösung einer Flussgleichung für das Farb-Coulomb-Potential zwischen zwei schweren Farbladungen zum Thema. Die entsprechende Dyson-Schwinger-Gleichung wird hergeleitet und die Bedingungen für die Existenz von Lösungen für diese Gleichung werden untersucht.

Die Einbeziehung dynamischer Quarks in diesen Formalismus wird in Kap. 5 behandelt. Der statische Quark-Propagator wird berechnet, um die Massenfunktion zu erhalten, die die dynamische Erzeugung der Konstituentenquarkmasse beschreibt. Der Einfluss des Gluonpropagators und der Quark-Vier-Punkt-Funktion auf die Massenfunktion werden untersucht.

Im letzten Kapitel werden eine kurze Zusammenfassung und ein Ausblick gegeben. Einige Definitionen und mehrere längere Rechnungen werden in den Anhängen dargestellt.



## Abstract

In this thesis, Yang-Mills theory in Coulomb gauge in its Hamiltonian formulation is investigated by applying the method of the Functional Renormalization Group. Yang-Mills theories form the basis of the Standard Model of elementary particle physics. The focus of this work is in particular on Quantum Chromodynamics, which describes the Strong Interaction.

In Chap. 1, the method of the Functional Renormalization Group is introduced. At first, it is presented in its usual formulation in Lagrangian Quantum Field Theory. The flow equation for the propagator of scalar quantum field theory is derived.

Chap. 2 contains an overview of Yang-Mills theory in Coulomb gauge in its Hamiltonian formulation as opposed to the Lagrangian approach.

In Chap. 3 the Functional Renormalization Group is transferred to the Hamiltonian setting of Yang-Mills theory in Coulomb gauge. With this new tool, the flow equations for the gluon and ghost propagators are derived. The equations are solved numerically using two different approximations. The results are compared to those obtained in the variational approach.

Chap. 4 deals with the derivation and solution of a flow equation for the colour Coulomb potential between two heavy colour charges. The corresponding Dyson-Schwinger equation is derived and the conditions for the existence of solutions are examined.

The inclusion of dynamic quarks into this formalism is the subject of Chap. 5. The static quark propagator is calculated in order to obtain the mass function, which shows the dynamic generation of the constituent quark mass. The influence of the gluon propagator and of the quark four-point function on the mass function are examined.

In the last chapter, a short summary and an outlook are given. Some definitions and several longer calculations are presented in the appendices.



## Acknowledgments

First of all, I would like to thank my supervisor Prof. Dr. Hugo Reinhardt for giving me the opportunity to work in his group. With his many good ideas and his continuous interest he contributed decisively to the advancement of this thesis. I also wish to thank him for giving me the opportunity to participate in the Confinement 8 in Mainz and in the ERG 2010 in Corfu.

I also would like to thank Prof. Dr. Jan M. Pawłowski for sharing with me his vast knowledge about the renormalization group in innumerable phone calls and emails as well as for taking the time for long discussions during his stays in Tübingen and my day trips to Heidelberg.

Special thanks go to Prof. Dr. Axel Weber, not only for teaching me many aspects of the renormalization group during his time in Tübingen but especially for giving me the opportunity to visit him two times at the Universidad Michoacana de San Nicolás de Hidalgo, Morelia. These two stays have not only advanced my scientific work substantially but I will also remember them for the Mexican hospitality extended to me there.

It is a pleasure to thank my office mate Dr. Davide R. Campagnari for numerous discussions about topics inside and outside physics, especially for his competent advice in graphic design and layout matters, as well as Markus Pak in the neighbouring office for always welcoming me warmly there to discuss all kinds of problems. I would also like to thank them for all the activities outside the Institute as well as for a critical reading of the manuscript.

I am thankful to PD Dr. Markus Quandt, Dr. Oliver Plohl and to Dr. Valery Lyubovitskij for collaborating with me on the administration of our workstation network and especially to Dr. Dominik Epple for sharing with me his broad knowledge about computers, Linux and networks.

At the beginning of my time at the Institute for Theoretical Physics, the help of Burghard Grüter and Dr. Wolfgang Schleifenbaum was invaluable to get started on the subject. Later on, the discussions with Dr. Peter Watson were especially helpful. I am grateful to all the members of the Institute for debating many physics and non-physics topics.

I have experienced both financial and educational support from the Internationales Graduiertenkolleg Basel-Graz-Tübingen and I very much appreciate the work of its Tübingen speakers Prof. Dr. Dr. h.c. mult. Amand Fäßler and Prof. Dr. Josef Jochum.

Es ist mir eine Freude, mich bei meinen Freunden und Kollegen Stephan Feuerer und Ralf Geretshauer zu bedanken für die viele gemeinsam verbrachte Zeit beim Mittagssandln und abends in Tübingen, für die Urlaube und Ausflüge sowie für die zahlreichen Gespräche über Themen jedweder Art.

Mein ganz besonderer Dank geht an Sandra Forster für ihr immer offenes Ohr und ihre unschätzbare, stetige Unterstützung.





# Contents

<b>1</b>	<b>The Functional Renormalization Group</b>	<b>13</b>
<b>2</b>	<b>Hamiltonian Yang-Mills Theory in Coulomb Gauge</b>	<b>21</b>
<b>3</b>	<b>The Gluon and Ghost Propagators</b>	<b>29</b>
3.1	FRG in Hamiltonian Yang-Mills Theory . . . . .	29
3.2	The Gluon and Ghost Propagator Flows . . . . .	33
3.3	Uniqueness of Infrared Scaling . . . . .	36
3.4	Truncation of the Propagator Flows . . . . .	37
3.5	Approximation without Tadpoles . . . . .	38
3.6	Optimization . . . . .	41
<b>4</b>	<b>The Colour Coulomb Potential</b>	<b>47</b>
4.1	Defining the Colour Coulomb Potential . . . . .	47
4.2	The Flow Equation for the Coulomb Form Factor . . . . .	50
4.3	An Alternative Derivation of the Coulomb Form Factor Flow . . . . .	52
4.4	The Dyson-Schwinger Equation for the Coulomb Form Factor . . . . .	57
4.5	Infrared Analysis . . . . .	58
4.5.1	Overall power laws . . . . .	58
4.5.2	The angular approximation . . . . .	59
4.5.3	Assessment of the angular approximation . . . . .	62
4.6	Numerical Solutions . . . . .	64
4.6.1	Iterative solution of the flow equation . . . . .	64
4.6.2	Solution of the DSE based on matrix inversion . . . . .	66
4.6.3	Iterative solution of the DSE with the angular approximation . . . . .	73
<b>5</b>	<b>The Quark Propagator</b>	<b>77</b>
5.1	Derivation of the Flow Equation for the Quark Propagator . . . . .	77
5.2	Inclusion of the Gluon Propagator Diagram . . . . .	84
5.2.1	Non-vanishing current quark mass . . . . .	84
5.2.2	Input from the variational approach in the chiral limit . . . . .	86
5.3	Inclusion of the Tadpole Diagram . . . . .	91
5.3.1	Derivation of the mass equation . . . . .	91
5.3.2	Results obtained in the framework of Adler and Davis . . . . .	93
5.4	Solving the Mass Equation . . . . .	96
5.4.1	A Hamiltonian ansatz for the four-quark function . . . . .	96
5.4.2	A perturbatively improved four-quark function . . . . .	99

---

<b>6</b>	<b>Summary and Outlook</b>	<b>107</b>
<b>A</b>	<b>Notations and Conventions</b>	<b>111</b>
<b>B</b>	<b>Derivation of the Propagator Flow</b>	<b>113</b>
B.1	Details of the Propagator Flow Derivation . . . . .	113
B.2	Ghost Number Conservation . . . . .	116
<b>C</b>	<b>Numerical Methods</b>	<b>119</b>
C.1	Chebyshev Representation . . . . .	119
C.2	Gauss-Legendre Integration . . . . .	120
C.3	Iterative Solution and Fine Tuning . . . . .	121
<b>D</b>	<b>Calculation of Two-Point Integrals</b>	<b>123</b>
<b>E</b>	<b>Calculations for the Quark Propagator Flow</b>	<b>127</b>
E.1	Calculation of the Two-Quark Kernels . . . . .	127
E.2	Perturbative Calculation of the Four-Quark Function . . . . .	128
E.3	Calculation of the Quark Tadpole Term . . . . .	132

# List of Figures

1.1	Typical regulator function . . . . .	16
1.2	Flow equation of the effective action . . . . .	18
1.3	Theory space . . . . .	19
1.4	Flow equation of the scalar propagator . . . . .	20
3.1	Flow equation of the gluon propagator . . . . .	34
3.2	Flow equation of the ghost propagator . . . . .	34
3.3	Truncated flow equation of the gluon propagator . . . . .	35
3.4	Truncated flow equation of the ghost propagator . . . . .	35
3.5	Gluon correlation function $\omega$ for different minimal cutoffs $k_{min}$ . . . . .	40
3.6	Ghost dressing function $d$ for different minimal cutoffs $k_{min}$ . . . . .	40
3.7	Flow of the ghost dressing function, $d_k(p)$ . . . . .	41
3.8	Comparison gluons, optimized and without tadpoles . . . . .	42
3.9	Comparison ghosts, optimized and without tadpoles . . . . .	42
3.10	Comparison optimized flow and variational approach . . . . .	43
3.11	Optimized flow equation of the gluon propagator . . . . .	44
3.12	Optimized flow equation of the ghost propagator . . . . .	44
3.13	Running coupling . . . . .	45
4.1	Error of the angular approximation . . . . .	64
4.2	Coulomb form factor $f$ for different minimal cutoffs $k_{min}$ . . . . .	65
4.3	Coulomb form factor $f$ for different $k_{min}$ with optimized input . . . . .	66
4.4	Coulomb form factor $f$ from the DSE . . . . .	68
4.5	Coulomb form factor $f$ from the DSE, half-logarithmic . . . . .	68
4.6	Coulomb form factor $f$ from the DSE with $d \equiv 1$ . . . . .	69
4.7	Gluon two-point function, critical and subcritical . . . . .	69
4.8	Ghost dressing function, critical and subcritical . . . . .	70
4.9	Coulomb form factor $f$ from the DSE with critical $d$ . . . . .	71
4.10	Coulomb form factor $f$ from the DSE with subcritical $d$ . . . . .	71
4.11	Coulomb form factor $f$ from the DSE for different scaling inputs . . . . .	72
4.12	Coulomb form factor $f$ from the DSE with angular approximation . . . . .	73
4.13	Comparison of $f$ from DSE with and without angular approximation . . . . .	74
5.1	Flow equation of the quark propagator . . . . .	80
5.2	Truncated flow equation of the quark propagator . . . . .	82
5.3	DSE of the quark propagator with a bare quark-gluon vertex . . . . .	84
5.4	Mass function from the DSE for different couplings . . . . .	85

5.5	Comparison mass function for gluon and photon propagator input . .	86
5.6	Two-quark kernel $\varphi$ from the variational approach . . . . .	88
5.7	Quark propagator dressings for $\varphi$ from the variational approach . . .	88
5.8	Approximated quark propagator flow with quark tadpole . . . . .	91
5.9	Mass function of Adler/Davis . . . . .	95
5.10	Mass function of Adler/Davis, half-logarithmic . . . . .	95
5.11	Mass function with Hamiltonian four-quark function, chiral . . . . .	97
5.12	Mass function with Hamiltonian four-quark function, chiral, half-log.	98
5.13	Mass function with Hamiltonian four-quark function, non-chiral . . .	98
5.14	Comparison mass functions . . . . .	99
5.15	Comparison mass functions, double-logarithmic . . . . .	100
5.16	Mass function with improved four-quark function, chiral . . . . .	103
5.17	Mass function with improved four-quark function, high IR regulator .	103
5.18	Mass function with improved four-quark function, low IR regulator .	104

# Chapter 1

## The Functional Renormalization Group

In this chapter, we introduce the technique of the Functional Renormalization Group (FRG) in the formulation by Wetterich [1] for a general quantum field theory, following mainly Ref. [2].

Quantum Field Theories (QFT) can be treated using different methods and approaches which all have their strengths and weaknesses. These different methods complement each other and therefore they should be and actually are applied simultaneously to the same theory in order to provide multiple checks on the results: for small couplings, perturbation theory has been successfully utilized like in low-energy quantum electrodynamics or in high-energy quantum chromodynamics (QCD). For large couplings, however, perturbation theory fails. In contrast, numerical methods like Monte Carlo simulations in the framework of lattice gauge theory [3] can be applied for arbitrary couplings and are therefore genuinely non-perturbative. But although the systematic and statistical errors of these methods are under control, the path from the basic definition of the theory to observable results is obscured due to its statistical nature, which may leave some dissatisfaction behind regarding a thorough understanding of the theory. Moreover, due to the finite size of the lattice, it becomes increasingly costly to push the simulations into the infrared, i.e., long-distance regime, which is the significant scale for confinement in QCD. For introductions to lattice gauge theory, see [4–6].

Another approach to solving quantum field theories non-perturbatively are functional methods. They consist in determining generating functionals for the expectation values of field operators, i.e., the correlation functions of the theory, which as a whole contain all the physical information about a particular QFT. Functional methods combine the advantage of perturbation theory, in allowing a largely analytical treatment, with the advantage of lattice simulations, in not being restricted to weak coupling, to the expense, however, that often approximations have to be made whose errors may be hard to estimate. Rather than calculating expectation values directly like in lattice simulations, where discretized path integrals are evaluated, in the functional approach equations are set up which relate different field operator expectation values to one another. The theory is then solved in terms of

these expectation values without the need to calculate a path integral directly. The infrared limit can be taken without the problems encountered in lattice simulations. Their downside lies in the fact that these equations couple the correlation functions of interest (which usually are of low order, the propagator to mention above all) to correlation functions of higher order which are usually unknown as well. Therefore, either terms of presumably minor influence on the quantities of interest have to be neglected, a process commonly known as truncation, or suitable ansatzes have to be made for them. One such functional method is the method of Dyson-Schwinger equations, sometimes also called the quantum equations of motion, see Refs. [7–9] and the reviews [10, 11] focussed on QCD.

In this thesis, however, we will employ another important functional method, the Functional Renormalization Group. The basic idea of the renormalization group is to take into account the influence of the different field modes on the correlation functions not all-at-once, like in the Dyson-Schwinger approach, but step-by-step, starting with the high-frequency modes, and thus the physics at small distance, going down to the low-frequency modes, describing long-distance physics. Although the process of renormalization had already been developed in quantum electrodynamics in order to deal with the occurring infinities of integrals, the first steps from this rather operational prescription backed by its success towards a more physical understanding were taken in statistical physics by Kadanoff [12] in form of the so-called block-spin transformations and were continued by Wilson and others [13–16] in order to describe critical phenomena, culminating in the award of the Nobel Prize in Physics to Kenneth Wilson in 1982.

This basic idea of the renormalization group has been shaped into different forms over the time, notably by Polchinski [17] who used it to prove the renormalizability of  $\phi^4$ -theory. In this work we will apply a formulation devised by Wetterich [1]. It is based on the notion of the effective action  $\Gamma_k$  which interpolates between the bare action  $S$  and the full quantum effective action  $\Gamma$  in a manner which will be detailed in this chapter. Although in the main part of this thesis we will apply the FRG to Yang-Mills theory in its Hamiltonian formulation, we will introduce it in the following within the framework in which it has commonly been used so far, i.e., the Lagrangian formulation of a general quantum field theory. For reviews and introductions, see Refs. [2, 18–25]. See also Ref. [26] for an early application to Yang-Mills theory and Ref. [27] for an application to quantum gravity.

The starting point for the derivation of the flow equation for the effective action is the generating functional of the Green functions,

$$Z[j] = \int \mathcal{D}\varphi \exp\{-S[\varphi] + j \cdot \varphi\}. \quad (1.1)$$

Here,  $\varphi$  and  $j$  denote collectively all fields involved and the corresponding sources. Furthermore, the scalar product  $j \cdot \varphi$  includes summation over all indices and integration over space-time. The theory is specified by the classical action  $S[\varphi]$  and the functional integral measure. In the FRG approach the generating functional is IR regularized by adding a regulator term  $\Delta S_k$  to the classical action  $S$ . It depends on

a cut-off momentum  $k$  and is chosen to be quadratic in the fields,

$$\Delta S_k[\varphi] := \frac{1}{2} \varphi \cdot R_k \cdot \varphi = \frac{1}{2} \int \frac{d^d p}{(2\pi)^d} \varphi(-p) R_k(p) \varphi(p). \quad (1.2)$$

Because of this form of the regulator term, the regulator function  $R_k(p)$  acts like an effective momentum dependent mass and is chosen to have the properties

$$\begin{aligned} \lim_{p \rightarrow 0} R_k(p) &> 0, \\ \lim_{k \rightarrow 0} R_k(p) &= 0, \\ \lim_{k \rightarrow \infty} R_k(p) &\rightarrow \infty. \end{aligned} \quad (1.3)$$

The first condition ensures that  $R_k(p)$  is indeed an infrared regulator and suppresses the propagation of the modes with momentum  $p \lesssim k$ . The second condition implies that the momentum modes with  $p \gtrsim k$  are unaffected by the regulator and that the full finite renormalized generating functional of the theory is recovered as the cut-off scale  $k$  is pushed to zero, because the only modification we have made of the theory is the term  $\Delta S_k[\varphi]$ . The third condition ensures that the initial condition at infinity for the cutoff-dependent effective action  $\Gamma_k$ , which we are going to define later in Eq. (1.10), coincides with the classical action  $S$ ,  $\lim_{k \rightarrow \infty} \Gamma_k = S$ , see the discussion below Eq. (1.11). A typical regulator function is sketched in Fig. 1.1.

In the FRG flow equation approach to Yang-Mills theory, we will start at a large cut-off scale  $k$ , where the theory is under control due to asymptotic freedom, and then let the cut-off  $k$  flow to the small momentum regime where the theory cannot be treated perturbatively anymore. The evolution of the Green's functions with the cut-off scale  $k$  is described by a flow equation which is obtained by taking the derivative of the regulated generating functional,

$$Z_k[j] = \int \mathcal{D}\varphi \exp\{-S[\varphi] - \Delta S_k[\varphi] + j \cdot \varphi\} =: e^{W_k[j]}, \quad (1.4)$$

w.r.t. the momentum scale  $k$ . The flow of  $Z_k$  is then derived as

$$\partial_t Z_k[j] = \left( -\frac{1}{2} \frac{\delta}{\delta j} \cdot \dot{R}_k \cdot \frac{\delta}{\delta j} \right) Z_k[j], \quad (1.5)$$

where the dot on  $R$  stands for the derivative w.r.t. the dimensionless variable  $t = \ln k/k_0$ . Here,  $k_0$  is an arbitrary reference scale. The functional derivative  $\delta/\delta j$  in momentum space is understood as

$$\frac{\delta}{\delta j}(p) := \frac{\delta}{\delta j(-p)}. \quad (1.6)$$

Expressing Eq. (1.5) in terms of the generating functional of the connected Green functions,  $W_k[j]$ , defined in Eq. (1.4), we get

$$\partial_t W_k[j] = -\frac{1}{2} \frac{\delta W_k}{\delta j} \cdot \dot{R}_k \cdot \frac{\delta W_k}{\delta j} - \frac{1}{2} \text{Tr} \dot{R}_k \frac{\delta^2 W_k}{\delta j \delta j}, \quad (1.7)$$

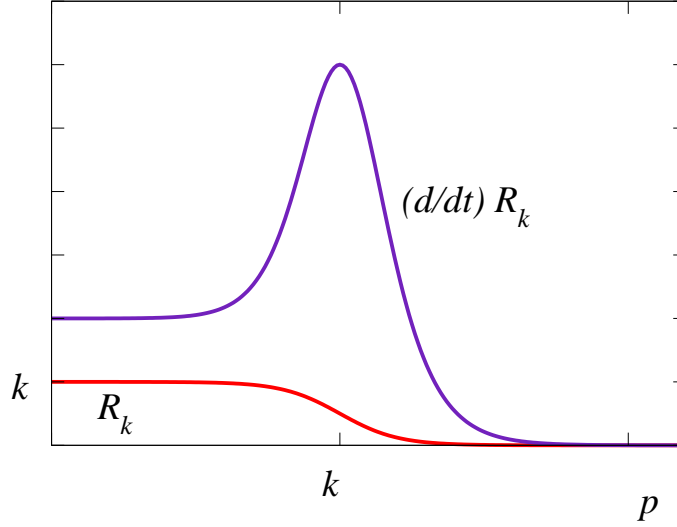


**Figure 1.1:** A typical regulator function  $R_k(p)$  and its scale derivative  $\partial_t R_k(p)$  are shown, where  $t := \ln k/k_0$  with an arbitrary reference scale  $k_0$ . It fulfils the properties of Eq. (1.3). Whereas for  $p \gtrsim k$  the regulator vanishes and the field modes therefore fully contribute to the generating functional, the modes with  $p \lesssim k$  are still suppressed by an effective mass term. The shape of the scale derivative  $\partial_t R_k(p)$ , which controls the loop integrals in the flow equations, see Eqs. (1.20), (1.27), and Figs. 1.2, 1.4, shows that only a narrow momentum shell around  $k \sim p$  contributes to the flow at  $k = p$ , in accordance with Wilson's picture of renormalization. (Picture taken from Ref. [2].)

where

$$\text{Tr } \dot{R}_k \frac{\delta^2 W_k}{\delta j \delta j} := \int \frac{d^d p}{(2\pi)^d} \dot{R}_k(p) \frac{\delta^2 W_k}{\delta j(-p) \delta j(p)}. \quad (1.8)$$

By taking derivatives of Eq. (1.7) w.r.t.  $j$  one obtains the flow equations for the connected Green's functions. By performing a Legendre transformation from the sources  $j$  to the classical field  $\phi$ , which defines the sources  $j_k[\phi]$  in terms of the classical field,

$$\phi = \left. \frac{\delta W_k[j]}{\delta j} \right|_{j=j_k[\phi]}, \quad (1.9)$$

we obtain the effective action

$$\Gamma_k[\phi] = (-W_k[j] + j \cdot \phi)_{j=j_k[\phi]} - \Delta S_k[\phi]. \quad (1.10)$$

This Legendre transformation is a slightly modified version of the usual one that defines the transition from the generating functional  $W$  of connected Green's functions to the generating functional  $\Gamma$  of proper Green's functions, which takes into account the regulator term quadratic in the fields. Eq. (1.10) also implies that

$$j_k[\phi] = \frac{\delta(\Gamma_k + \Delta S_k)}{\delta \phi}. \quad (1.11)$$



As the regulator vanishes for  $k \rightarrow 0$ , see Eq. (1.3), we retrieve the full quantum effective action,

$$\Gamma_{k \rightarrow 0}[\phi] = \Gamma[\phi]. \quad (1.12)$$

For the limit  $k \rightarrow \infty$  we consider the exponential of the definition of the effective action, Eq. (1.10),

$$\begin{aligned} e^{-\Gamma_k[\phi]} &= \int \mathcal{D}\varphi \exp \left\{ -S[\varphi] - \frac{1}{2}\varphi \cdot R_k \cdot \varphi + j_k[\phi] \cdot (\varphi - \phi) + \frac{1}{2}\phi \cdot R_k \cdot \phi \right\} \\ &= \int \mathcal{D}\varphi \exp \left\{ -S[\varphi] + \frac{\delta\Gamma_k[\phi]}{\delta\phi} \cdot (\varphi - \phi) - \frac{1}{2}(\varphi - \phi) \cdot R_k \cdot (\varphi - \phi) \right\} \end{aligned} \quad (1.13)$$

where we have used Eq. (1.11). As  $\lim_{k \rightarrow \infty} R_k(p) \rightarrow \infty$ , taking this limit, the last exponential is a representation of the delta functional (up to a factor):

$$\exp \left\{ -\frac{1}{2}(\varphi - \phi) \cdot R_k \cdot (\varphi - \phi) \right\} \xrightarrow{k \rightarrow \infty} \sim \delta[\varphi - \phi], \quad (1.14)$$

so that

$$e^{-\Gamma_k[\phi]} \sim \int \mathcal{D}\varphi \exp \left\{ -S[\varphi] + \frac{\delta\Gamma_k[\phi]}{\delta\phi} \cdot (\varphi - \phi) \right\} \delta[\varphi - \phi] = e^{-S[\phi]}. \quad (1.15)$$

Therefore,  $\Gamma_{k \rightarrow \infty}[\phi] \sim S[\phi] + \dots$ . More detailed considerations using the saddle point approximation, which becomes exact in the limit  $k \rightarrow \infty$ , show that indeed

$$\Gamma_{k \rightarrow \infty}[\phi] = S[\phi] \quad (1.16)$$

holds, up to a modification of the bare parameters contained in the action  $S$  of a renormalizable theory, see [28].

By taking the derivative of the effective action  $\Gamma_k$  w.r.t.  $t = \ln k/k_0$  and using its definition Eq. (1.10) together with Eq. (1.7), one arrives at

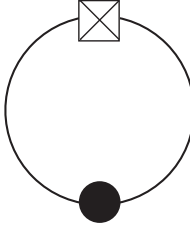
$$\partial_t \Gamma_k[\phi] = \frac{1}{2} \text{Tr} \dot{R}_k \frac{\delta^2 W_k}{\delta j \delta j}. \quad (1.17)$$

The second derivative of  $W_k$  w.r.t. the currents is the propagator (with non-vanishing sources). It is related to the inverse of the second derivative of the effective action,

$$\frac{\delta^2 W_k}{\delta j \delta j} = \left( \frac{\delta^2 \Gamma_k}{\delta \phi \delta \phi} + R_k \right)^{-1}. \quad (1.18)$$

Equation (1.18) follows from Eqs. (1.9) and (1.11) as well as

$$\frac{\delta}{\delta \phi} j = \left( \frac{\delta}{\delta j} \phi \right)^{-1} = \left( \frac{\delta^2 W_k}{\delta j \delta j} \right)^{-1}. \quad (1.19)$$

$$k\partial_k\Gamma_k[\phi] = \frac{1}{2} \text{Tr} \left[ \text{Regulator Insertion} \cdot \text{Propagator} \right]$$


**Figure 1.2:** The flow equation of the effective action, Eq. (1.20). The solid line with the filled black circle denotes the regularized scalar propagator at cut-off momentum  $k$  for non-vanishing field  $\phi$ , i.e.,  $\left(\Gamma_k^{(2)}[\phi] + R_k\right)^{-1}$ . The regulator insertion  $\dot{R}_k$  is represented by a square with a cross.

Inserting Eq. (1.18) into Eq. (1.17) we obtain Wetterich's flow equation for the effective action [1], which is the central equation of this approach and of the present work:

$$\dot{\Gamma}_k[\phi] = \frac{1}{2} \text{Tr} \dot{R}_k \left( \Gamma_k^{(2)}[\phi] + R_k \right)^{-1}, \quad (1.20)$$

where the dot denotes the derivative w.r.t.  $t$  and

$$\Gamma_{k,1\dots n}^{(n)}[\phi] := \frac{\delta^n \Gamma_k[\phi]}{\delta\phi_1 \dots \delta\phi_n} \quad (1.21)$$

are the one-particle irreducible  $n$ -point functions (proper vertices) at non-vanishing classical field  $\phi$ . We have also introduced a condensed notation where  $n$  stands for the space-time variable,  $\phi_n = \phi(x_n)$ . This equation is diagrammatically depicted in Fig. 1.2.

The structure of Eq. (1.20) is independent of the details of the underlying theory, i.e., of the explicit form of the action  $S[\phi]$ ; it is but a mere consequence of the form of the regulator term (1.2) being quadratic in the fields. Although we have started out with the generating functional  $Z[j]$  of Green's functions, which is defined by a functional integral, Eq. (1.20) and the equations we will derive from it involve no evaluation of a functional integral as they relate different expectation values to each other. The regulator function  $R_k(p)$  effects an infrared regularization, in form of the mass term in the propagator in Eq. (1.20) and in all the equations derived from it, as well as an ultraviolet regularization in form of the insertion  $\dot{R}_k(p)$  which cuts off the loop integral in the ultraviolet, see Fig. 1.1.

The flow equation (1.20) in general cannot be solved exactly. Therefore, we have to apply approximation methods which consist in systematically taking into account more and more operators in the effective action, e.g., in the gradient expansion, where the effective action is constructed from derivative operators of higher and higher order:

$$\Gamma_k[\phi] = \int d^d x \left[ V_k[\phi(x)] + \frac{1}{2} Z_k[\phi(x)] (\partial_\mu \phi(x))^2 + \mathcal{O}(\partial^4) \right] \quad (1.22)$$

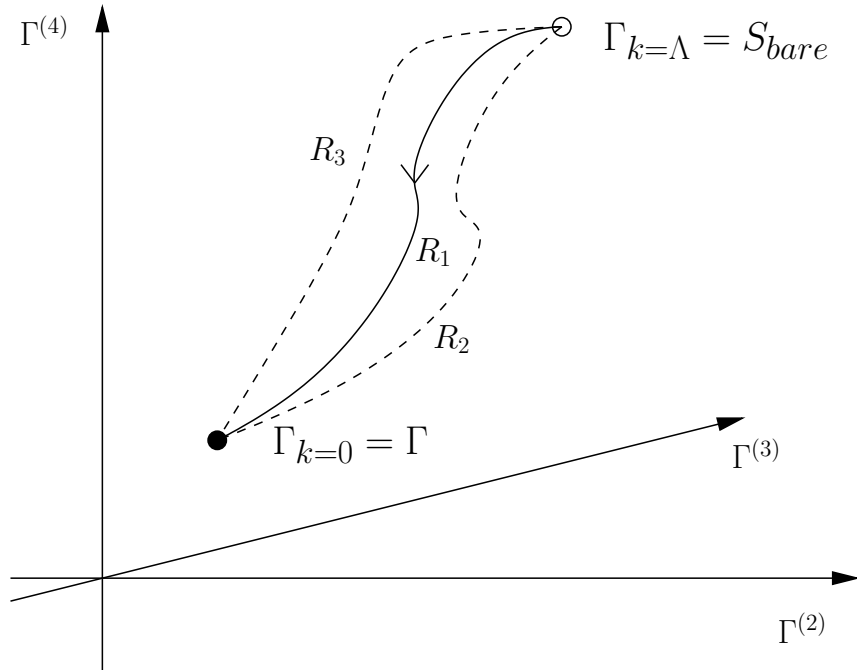


**Figure 1.3:** The space of all effective actions  $\Gamma[\phi]$  for a given field content is called theory space. The effective action  $\Gamma_k[\phi]$  describes a trajectory from the defining bare action  $\Gamma_{k=\Lambda} = S$  to the full quantum effective action  $\Gamma_{k=0} = \Gamma$ , determined by the flow equation (1.20). For the same bare action  $\Gamma_{k=\Lambda}$  the trajectories for different regulator functions  $R_k(p)$  always end in the same point. The depiction is highly simplified as theory space and even the correlation functions shown as axes are infinite dimensional.

In the present work, however, we apply the vertex expansion of the effective action,

$$\Gamma_k[\phi] = \sum_n \frac{1}{n!} \Gamma_{k,1\dots n}^{(n)} \cdot \phi_1 \cdots \phi_n \quad (1.23)$$

where the expansion coefficients are the proper vertices. (We denote  $\Gamma_{k,1\dots n}^{(n)} := \Gamma_{k,1\dots n}^{(n)}[\phi = 0]$ ). With this parameterization we can symbolically depict the flow of the effective action  $\Gamma_k[\phi]$  in theory space, which is the space of all effective actions for a given field content, here for the scalar field  $\phi$ , see Fig. 1.3. It is called theory space because each point in it is an effective action  $\Gamma[\phi]$  and therefore a whole quantum field theory, and consequently, the theory space is infinite dimensional. As axes we choose the vertex functions (which themselves are infinite dimensional). The flow starts at a high cut-off scale  $k = \Lambda$ , which should be chosen much larger than any other scale involved in the theory. There the bare action  $\Gamma_{k=\Lambda} = S$  defines the theory. The cut-off scale  $k$  is then lowered down to  $k = 0$ : as more and more lower frequency modes are taken into account, the effective action describes a path through theory space ending at the full quantum effective action  $\Gamma_{k=0} = \Gamma$  where all field modes now contribute. Depending on the exact shape of the regulator function  $R_k(p)$ , the exact paths may all be different but they always end at  $\Gamma$ , which is

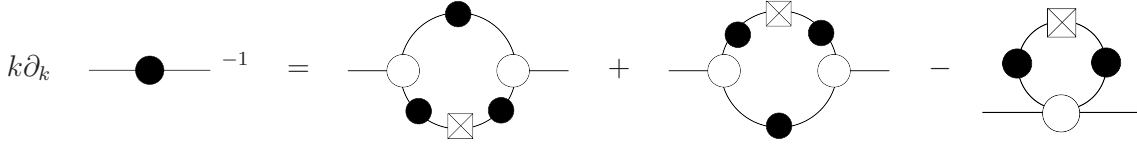


**Figure 1.4:** Flow equation (1.27) for the inverse propagator (two-point function)  $\Gamma_k^{(2)} = \langle \phi\phi \rangle^{-1}$ . Here and in all the following diagrammatic equations, lines with full circles represent  $(\Gamma_k^{(2)} + R_k)^{-1}$  on the r.h.s. of the equation, but only  $\Gamma_k^{(2)-1}$  on its l.h.s. Open circles represent full proper vertices  $\Gamma_k^{(n)}$ , while the square with a cross represents the regulator insertion  $\dot{R}_k$ .

guaranteed by the property  $R_{k=0}(p) = 0$  shared by all the regulator functions, see Eq. (1.3). Unfortunately, this need not be true any longer if truncations are applied.

By taking functional derivatives of the flow equation for the effective action (1.20) w.r.t. the fields one obtains the flow equations for the (inverse) propagators or vertices. From

$$\left(\Gamma_k^{(2)}[\phi] + R_k\right)^{-1} \left(\Gamma_k^{(2)}[\phi] + R_k\right) = \mathbf{1} \quad (1.24)$$

we obtain

$$\frac{\delta}{\delta\phi_i} \left(\Gamma_k^{(2)}[\phi] + R_k\right)^{-1} = - \left(\Gamma_k^{(2)}[\phi] + R_k\right)^{-1} \Gamma_{k,i}^{(3)}[\phi] \left(\Gamma_k^{(2)}[\phi] + R_k\right)^{-1}. \quad (1.25)$$

Taking one functional derivative of Eq. (1.20) w.r.t  $\phi_1$  we find (using the preceding equation)

$$\dot{\Gamma}_{k,1}^{(1)}[\phi] = -\frac{1}{2} \text{Tr} \dot{R}_k \left(\Gamma_k^{(2)}[\phi] + R_k\right)^{-1} \Gamma_{k,1}^{(3)}[\phi] \left(\Gamma_k^{(2)}[\phi] + R_k\right)^{-1} \quad (1.26)$$

and a second derivative w.r.t  $\phi_2$  as well as setting  $\phi = 0$  yields

$$\begin{aligned} \dot{\Gamma}_{k,12}^{(2)} = \frac{1}{2} \text{Tr} \dot{R}_k \left(\Gamma_k^{(2)} + R_k\right)^{-1} \left( -\Gamma_{k,12}^{(4)} + \left[ \Gamma_{k,1}^{(3)} \left(\Gamma_k^{(2)} + R_k\right)^{-1} \Gamma_{k,2}^{(3)} + (1 \leftrightarrow 2) \right] \right) \\ \left(\Gamma_k^{(2)} + R_k\right)^{-1}. \end{aligned} \quad (1.27)$$

We have suppressed here all internal indices, which are summed (integrated) over. Eq. (1.27) is diagrammatically illustrated in Fig. 1.4.

In this chapter we have presented the implementation of the FRG into the Lagrangian formulation of scalar QFT. In Chap. 3 we will implement it into the Hamiltonian formulation of Yang-Mills theory, which we will introduce in Chap. 2, and derive similar equations for the gluon and ghost propagators and also for the quark propagator in Chap. 5.

## Chapter 2

# Hamiltonian Yang-Mills Theory in Coulomb Gauge

In this chapter we introduce the Hamiltonian formulation of Yang-Mills theory in Coulomb gauge as opposed to the standard presentation of the theory in the Lagrangian formulation in Landau gauge. The Hamiltonian formulation provides the framework of the present work. In Chap. 3 we will incorporate the method of the Functional Renormalization Group, presented in Chap. 1, into this framework.

The Standard Model of Elementary Particle Physics describes the Electroweak Interaction and the Strong Interaction via a special kind of Quantum Field Theories, the non-Abelian gauge theories, also called Yang-Mills theories. In this work we focus on the Strong Interaction which is described by a Yang-Mills theory based on the non-Abelian Lie group  $SU(3)$ , called Quantum Chromodynamics (QCD). We will, however, mostly consider  $SU(N)$  gauge theories in general.

The term ‘gauge invariance’ was first used in 1919 by Weyl [29] for invariance under space-time dependent scale changes in order to unify gravity with electromagnetism, unsuccessfully though. Fock showed that scalar Quantum Electrodynamics (QED) can be based on what today is called the gauge principle [30], whose similarity to Weyl’s original scale change was pointed out by London [31]. Henceforth, the term ‘gauge invariance’ was used in the modern sense [32]. While it referred to Abelian  $U(1)$  symmetry then, the generalization to non-Abelian gauge groups was given by Yang and Mills in 1954 [33]. For detailed accounts of the history of Yang-Mills theory, see Refs. [34, 35], for introductory textbooks, see, e.g., [36–38].

The application of Yang-Mills theory to the Strong Interaction in form of QCD is rooted in the quark model proposed by Gell-Mann [39]. This rather schematic model of baryons and mesons is based on an internal quantum number called flavour, associated with the group  $SU(3)$ . In order to avoid problems with Fermi statistics, a further internal quantum number called colour was introduced that is also based on an  $SU(3)$ -symmetry. Gauging this colour symmetry then led to QCD [40]. Yang-Mills theories have been shown to exhibit asymptotic freedom [41, 42], which means that the force becomes arbitrarily small for short distances, and explained experimental results from deep inelastic scattering. Gross, Politzer, and Wilczek have been honoured with the Nobel Prize in Physics in 2004 for this insight. Con-

finement, however, could not yet be inferred from QCD. It means that asymptotic states must be colourless, which includes the fact that the quarks are ‘confined’ inside the hadrons and cannot be observed separately. An attempt at deducing this property from Yang-Mills theory is part of the present work, especially of Chap. 4.

In the following, we present the Hamiltonian approach to Yang-Mills theory in Coulomb gauge as set forth in [43]. Although we will not explicitly make use of the Hamiltonian operator and of canonical quantization in our approach, they provide the frame in which the present work is embedded.

Note that from here on until Eq. (2.22) excluded, we use the metric  $g_{\mu\nu} = \text{diag}(1, -1, -1, -1)$ . Greek indices refer to space-time, Latin indices to space only. Upper indices denote contravariant tensor components, lower indices covariant components. We will change this notation from Eq. (2.22) on.

The defining Lagrangian of Yang-Mills theory reads

$$\mathcal{L} = -\frac{1}{4}F_{\mu\nu}^a F_a^{\mu\nu} + \bar{\psi}(i\gamma^\mu D_\mu - m)\psi \quad (2.1)$$

where  $\psi$  is a collection of  $N$  Dirac fields,  $\psi = (\psi_1, \dots, \psi_N)$ , which transform in the fundamental representation of the gauge group and which we will refer to as matter or quark fields henceforth. In this work we will focus on the gauge group  $SU(N)$ . The gauge covariant derivative

$$D_\mu = \partial_\mu + igA_\mu^a T^a \quad (2.2)$$

affects the coupling of the quark sector to the gauge or gluon field  $A_\mu^a$ . The matrices  $T^a$  form the fundamental,  $N$ -dimensional, Hermitean representation of the gauge group  $SU(N)$ . The dynamics of the pure gauge field is governed by the first term in the Lagrangian where the field strength tensor is defined as

$$F_{\mu\nu}^a = \partial_\mu A_\nu^a - \partial_\nu A_\mu^a - gf^{abc}A_\mu^b A_\nu^c \quad (2.3)$$

where the  $f^{abc}$  are the structure constants of the gauge group defined via

$$[T^a, T^b] = if^{abc}T^c. \quad (2.4)$$

This Lagrangian is invariant under the local gauge transformations

$$\begin{aligned} \psi &\rightarrow \psi^U = U\psi \\ A_\mu &= A_\mu^a T^a \rightarrow A_\mu^U = UA_\mu U^\dagger - \frac{i}{g}U(\partial_\mu U^\dagger) \end{aligned} \quad (2.5)$$

with

$$U(x) = \exp(i\theta^a(x)T^a). \quad (2.6)$$

The transition to the Hamiltonian formulation is made by means of the usual Legendre transformation. To perform it, we need the momentum density of the fields:

$$\begin{aligned}
\Pi_A^{a,i}(x) &= \frac{\delta S}{\delta(\partial_0 A_i^a(x))} = -\frac{1}{2} \int d^4 y \frac{\delta}{\delta(\partial_0^x A_i^a(x))} F_{0j}^b(y) F^{b,0j}(y) \\
&= - \int d^4 y F^{b,0j}(y) \frac{\delta}{\delta(\partial_0^x A_i^a(x))} (\partial_0^y A_j^b(y) - \partial_j^y A_0^b(y) + \dots) \\
&= -F^{b,0j}(x) g_j^i = F^{a,i0}(x), \\
\Pi_\psi &= \frac{\delta S}{\delta(\partial_0 \psi)} = i\psi^\dagger.
\end{aligned} \tag{2.7}$$

Note that

$$\Pi_{A,0}^a = 0. \tag{2.8}$$

In analogy to electrodynamics, we can define a chromo-electric field  $E_i^a$  by

$$F_{i0}^a = \Pi_{A,i}^a = E_i^a. \tag{2.9}$$

The Hamiltonian is defined as the Legendre transform

$$H = \int d^3 x (\Pi_A^{a,i} \partial_0 A_i^a + \Pi_\psi \partial_0 \psi - \mathcal{L}). \tag{2.10}$$

From Eq. (2.3) we obtain the time derivative of the spatial gauge field components as

$$\partial_0 A_i^a = -\Pi_{A,i}^a + (\delta^{ab} \partial_i + g f^{abc} A_i^c) A_0^b = -\Pi_{A,i}^a + \hat{D}_i^{ab} A_0^b \tag{2.11}$$

where we have introduced the covariant derivative in the adjoint representation of the gauge group

$$\hat{D}_\mu^{ab} := \delta^{ab} \partial_\mu + g f^{abc} A_\mu^c. \tag{2.12}$$

The Hamiltonian becomes

$$\begin{aligned}
H &= \int d^3 x \left( -\Pi_A^{a,i} \Pi_{A,i}^a + \Pi_A^{a,i} \hat{D}_i^{ab} A_0^b + i\psi^\dagger \partial_0 \psi + \frac{1}{4} F_{ij}^a F_a^{ij} + \frac{1}{2} F_{0i}^a F_a^{0i} \right. \\
&\quad \left. - i\psi^\dagger \partial_0 \psi - i\bar{\psi} \gamma^i \partial_i \psi + g A_0^a \bar{\psi} \gamma^0 T^a \psi + g A_i^a \bar{\psi} \gamma^i T^a \psi + m \bar{\psi} \psi \right).
\end{aligned} \tag{2.13}$$

Motivated by electrodynamics, we can define a chromo-magnetic field  $B_i^a$  by

$$B_i^a = \frac{1}{2} \varepsilon_{imn} F_{mn}^a. \tag{2.14}$$

Furthermore, we perform an integration by parts in the  $\hat{D}$ -term, getting

$$\begin{aligned}
H &= \int d^3 x \left[ \frac{1}{2} (\Pi_{A,i}^{a2} + B_i^{a2}) + A_0^a \left( \hat{D}_i^{ab} \Pi_{A,i}^b + g \bar{\psi} T^a \gamma^0 \psi \right) \right. \\
&\quad \left. - i\psi^\dagger \alpha^i (\partial_i + ig A_i^a T^a) \psi + m \psi^\dagger \beta \psi \right].
\end{aligned} \tag{2.15}$$

The second of the two terms coupling to the time-component of the gauge field can be interpreted as the charge density of the matter field which we abbreviate as

$$\rho_m^a = \bar{\psi} T^a \gamma^0 \psi . \quad (2.16)$$

The Hamiltonian equation of motion for  $\Pi_0^a$ ,

$$\partial_0 \Pi_0^a = -\frac{\delta H}{\delta A_0^a} , \quad (2.17)$$

in view of Eq. (2.8) turns into

$$\hat{D}_i^{ab} \Pi_{A,i}^b + g \bar{\psi} T^a \gamma^0 \psi = 0 . \quad (2.18)$$

This equation is nothing but the non-Abelian analogue to the Gauss law in electrodynamics, as can be seen by choosing vanishing structure constants of the gauge group,  $f^{abc} = 0$ , which means returning to an Abelian gauge theory as electrodynamics is: the preceding equation indeed turns into

$$\partial_i E^{a,i} = g \rho_m^a . \quad (2.19)$$

The Hamiltonian equation of motion for  $A_0^a$  is

$$\partial_0 A_0^a = \frac{\delta H}{\delta \Pi_{A,0}^a} = 0 \quad (2.20)$$

so  $A_0^a$  is in fact no dynamic variable at all. The fact that its conjugate momentum  $\Pi_{A,0}^a$  vanishes, see Eq. (2.8), poses a problem for canonical quantization where the commutator of the field operator and its momentum operator,  $[A_0^a, \Pi_{A,0}^a]$ , cannot be zero everywhere. To avoid this problem, we can use the freedom to choose a gauge such that

$$A_0^a \equiv 0 \quad (2.21)$$

which is called temporal gauge or Weyl gauge.

Because no temporal vector components occur anymore, from now on we will exclusively use contravariant vector components which we denote with a subscript. Note that the partial derivative transforming covariantly  $\partial_i \equiv \partial/\partial x^i$  already involves the contravariant position vector.

In Weyl gauge the Hamiltonian simplifies to

$$H = \int d^3x \left[ \frac{1}{2} (\Pi_{A,i}^a)^2 + B_i^2 - i \psi^\dagger \alpha^i (\partial_i - ig A_i^a T^a) \psi + m \psi^\dagger \beta \psi \right] , \quad (2.22)$$

Now we can promote the fields and their conjugate momenta to operators which fulfil the canonical equal-time commutation relations (notice that we work in the Schrödinger picture),

$$\begin{aligned} [A_i^a(\mathbf{x}), \Pi_{A,j}^b(\mathbf{y})] &= i \delta^{ab} \delta_{ij} \delta^3(\mathbf{x} - \mathbf{y}) \\ [A_i^a(\mathbf{x}), A_j^b(\mathbf{y})] &= [\Pi_{A,i}^a(\mathbf{x}), \Pi_{A,j}^b(\mathbf{y})] = 0 , \end{aligned} \quad (2.23)$$



or anti-commutation relations in the case of the matter fields (note that the conjugate momentum is given by Eq. (2.7)),

$$\begin{aligned} \{\psi_\alpha^a(\mathbf{x}), \psi_\beta^{\dagger b}(\mathbf{y})\} &= \delta^{ab} \delta_{\alpha\beta} \delta^3(\mathbf{x} - \mathbf{y}) \\ \{\psi_\alpha^a(\mathbf{x}), \psi_\beta^b(\mathbf{y})\} &= \{\psi_\alpha^{\dagger a}(\mathbf{x}), \psi_\beta^{\dagger b}(\mathbf{y})\} = 0. \end{aligned} \quad (2.24)$$

After fixing the Weyl gauge, the Hamiltonian (2.22) still possesses an invariance under purely spatial gauge transformations  $U(\mathbf{x})$ . Fixing it poses no problem in the fermionic sector of the theory so we focus on the pure gauge part. In this work, we choose Coulomb gauge,

$$\partial_i A_i^a(\mathbf{x}) = 0, \quad (2.25)$$

and thereby resolve the quantum analogue to the classical Gauss law in Eq. (2.18) which is (without dynamical quark fields)

$$\hat{D}_i^{ab} \Pi_{A,i}^b |\phi\rangle = 0, \quad (2.26)$$

where  $|\phi\rangle$  is a state vector of the theory. It turns out that the Gauss operator  $\hat{D}_i^{ab} \Pi_{A,i}^b$  is just the generator of the operators  $\mathcal{U}$  which implement the spatial gauge transformations  $U(\mathbf{x})$  on the states  $|\phi\rangle$ . This means that the states fulfilling the Gauss law (2.26) are the gauge invariant ones. For further details regarding the Gauss law and the simultaneous choice of Weyl gauge and Coulomb gauge, which is possible only for one time slice but not for the whole space-time, see Ref. [44].

Fixing the Coulomb gauge implies that the transverse components  $A^\perp$  are the physical degrees of freedom. They are defined as

$$A_i^\perp(\mathbf{x}) := t_{ij}(\mathbf{x}) A_j(\mathbf{x}) \quad (2.27)$$

with the transverse projector

$$t_{ij}(\mathbf{x}) = \delta_{ij} - \frac{\partial_i \partial_j}{\partial^2}, \quad (2.28)$$

which reads in momentum space

$$A_i^\perp(\mathbf{p}) := t_{ij}(\mathbf{p}) A_j(\mathbf{p}), \quad t_{ij}(\mathbf{p}) = \delta_{ij} - \frac{p_i p_j}{\mathbf{p}^2}. \quad (2.29)$$

The field operator and its conjugate momentum have to fulfil the canonical commutation relations

$$[\hat{A}_i^{\perp a}(\mathbf{x}), \hat{\Pi}_{A,j}^{\perp b}(\mathbf{y})] = i \delta^{ab} t_{ij}(\mathbf{x}) \delta^3(\mathbf{x} - \mathbf{y}). \quad (2.30)$$

This can be achieved by choosing a representation where, in analogy to quantum mechanics, the field operator acts multiplicatively on the state in field representation, i.e., on the wave functional,

$$\langle A^\perp | \hat{A}_i^{\perp a}(\mathbf{x}) | \phi \rangle = A_i^{\perp a}(\mathbf{x}) \phi[A^\perp], \quad (2.31)$$

where

$$\langle A^\perp | \phi \rangle = \phi[A^\perp] \quad (2.32)$$

is the wave functional which describes the state the system is in and  $|A^\perp\rangle$  is an eigenstate of the field operator,

$$\hat{A}_i^{\perp a}(\mathbf{x})|A^\perp\rangle = A_i^{\perp a}(\mathbf{x})|A^\perp\rangle. \quad (2.33)$$

The momentum operator acts as a derivative on the wave functional

$$\langle A^\perp | \hat{\Pi}_{A,i}^{\perp a} | \phi \rangle = \frac{\delta}{i\delta A_i^{\perp a}(\mathbf{x})} \phi[A^\perp]. \quad (2.34)$$

Henceforth, we work with transverse fields and momenta exclusively and therefore drop the transversality sign as well as the hat denoting an operator. The pure gauge part of the Yang-Mills Hamiltonian in Weyl gauge (2.22) can be expressed using only transverse operators [45], turning into

$$H_g = \frac{1}{2} \int d^3x [J^{-1}\Pi_{A,i}^a(\mathbf{x})J\Pi_{A,i}^a(\mathbf{x}) + B_i^a(\mathbf{x})^2] + \frac{g^2}{2} \int d^3[xy] J^{-1}\rho^a(\mathbf{x})F^{ab}(\mathbf{x},\mathbf{y})J\rho^b(\mathbf{y}). \quad (2.35)$$

The Jacobian introduced by the transition to transverse fields,

$$J \equiv J[A] = \det(-\partial_i \hat{D}_i[A]) \quad (2.36)$$

is a functional determinant called the Faddeev-Popov determinant. The last term of the Hamiltonian is called the Coulomb term: it describes the interaction of the charge densities

$$\rho^a(\mathbf{x}) \equiv \rho[A, \Pi_A]^a(\mathbf{x}) = f^{abc} A_i^c(\mathbf{x}) \Pi_{A,i}^b(\mathbf{x}) + \rho_m^a(\mathbf{x}), \quad (2.37)$$

the first term of which describes the charge of the gauge field itself while the second term denotes the charge of the matter fields, which we have reintroduced here, through the Coulomb propagator

$$F^{ab}(\mathbf{x}, \mathbf{y}) \equiv F[A]^{ab}(\mathbf{x}, \mathbf{y}) = [(-\partial_i \hat{D}_i[A])^{-1}(-\partial^2)(-\partial_j \hat{D}_j[A])^{-1}]_{\mathbf{x},\mathbf{y}}^{ab}. \quad (2.38)$$

These terms can be made more transparent by reducing them to the familiar case of an Abelian theory like electrodynamics by setting  $f^{abc} = 0$ . The gauge covariant derivative then turns into the ordinary partial derivative,  $\hat{D}_{ED,i} = \partial_i$ , so the Faddeev-Popov determinant reduces to

$$J_{ED} = \det(-\partial^2), \quad (2.39)$$

and drops out of the Hamiltonian. The charge density reduces to the charge density of matter alone,

$$\rho_{ED}^a = \rho_m^a, \quad (2.40)$$

which shows that the electromagnetic field carries no charge itself, and the Coulomb propagator turns into

$$F_{ED}^{ab}(\mathbf{x}, \mathbf{y}) = [(-\partial^2)^{-1}(-\partial^2)(-\partial^2)^{-1}]_{\mathbf{x}, \mathbf{y}}^{ab} = [(-\partial^2)^{-1}]_{\mathbf{x}, \mathbf{y}}^{ab} = \frac{\delta^{ab}}{4\pi|\mathbf{x} - \mathbf{y}|}, \quad (2.41)$$

i.e., the ordinary Coulomb potential between two electric charges. In total, the Yang-Mills Hamiltonian transforms into the electrodynamics Hamiltonian,

$$H_{ED} = \frac{1}{2} \int d^3x [E_i^a(\mathbf{x}) + B_i^a(\mathbf{x})^2] + \frac{g^2}{2} \int d^3x [xy] \rho_m^a(\mathbf{x}) \frac{1}{4\pi|\mathbf{x} - \mathbf{y}|} \rho_m^a(\mathbf{y}). \quad (2.42)$$

Returning to Yang-Mills theory, the coordinate change to transverse gauge fields implies that its Jacobian is part of the measure of integration over these fields. Therefore, the matrix element of an operator  $\mathcal{O}[A, \Pi]$  between two states  $|\phi_1\rangle$  and  $|\phi_2\rangle$  in field space reads

$$\langle \phi_1 | \mathcal{O}[A, \Pi] | \phi_2 \rangle = \int \mathcal{D}A J[A] \phi_1^*[A] \mathcal{O}[A, \Pi] \phi_2[A]. \quad (2.43)$$

In the next chapter we will use this expression as the starting point to implement the functional renormalization group into the Hamiltonian approach to Yang-Mills theory in Coulomb gauge.

Most of the progress made so far in the formulation presented here has been achieved by applying the variational principle [43, 46–52], for a concise introduction see also Ref. [53]. There, the vacuum state  $|\phi\rangle$  of the theory, which is the eigenstate of the Yang-Mills Hamiltonian (without the charge density of matter) with the lowest energy,

$$H_g |\phi\rangle = E_{\min} |\phi\rangle, \quad (2.44)$$

is determined approximately by making a suitable ansatz for  $|\phi\rangle$  and minimizing its energy expectation value,

$$\frac{\langle \phi | H_g | \phi \rangle}{\langle \phi | \phi \rangle} \rightarrow \min. \quad (2.45)$$

With the vacuum wave functional so determined, the quantities of interest like the gluon propagator or the static quark potential can be calculated. As with other functional approaches, however, this method in general leads to a set of coupled integral equations which require further approximations. A specific advantage of the Hamiltonian formulation is its close connection to physics as demonstrated in the dual superconductor picture of the QCD vacuum, see, e.g., Ref. [54].

Another major approach to Yang-Mills theory is the application of the Dyson-Schwinger equations. Although the DSE approach has been used mainly in Landau gauge so far [10, 55–59], lately there have been many results obtained in Coulomb gauge, see, e.g., Refs. [60–62] or for some recent work also including quarks, see Refs. [63–66]. Its setting, however, is the Lagrangian formulation of the theory where the definition of a potential between colour charges is not as straightforward

as in the Hamiltonian approach, see Eq. (2.38) and Chap. 4. However, a connection can be established between the colour Coulomb potential and the  $\langle A_0 A_0 \rangle$  correlator [60].

Much progress in Coulomb gauge Yang-Mills theory has also been achieved in lattice gauge theory. Although it is an advantage of the lattice formulation that no gauge fixing is required and that, starting from the action, a direct access to observable quantities is provided, it can also be used to calculate gauge dependent quantities like correlation functions. Particularly, in Ref. [67] the simple form of the gluon propagator proposed by Gribov [68] has been confirmed. Moreover, a simple relation between the gluon propagators in Coulomb and Landau gauge has been shown [69]. Also the ghost and quark propagators are being incorporated [70]. For a short review of older results, see Ref. [71].

In this work now, the method of the Functional Renormalization Group is applied to Hamiltonian Yang-Mills theory in Coulomb gauge.

# Chapter 3

## The Gluon and Ghost Propagators

In this chapter, we will apply the method of renormalization group flows introduced in Chap. 1 to the Hamiltonian Yang-Mills theory in Coulomb gauge shown in Chap. 2. We will derive the flow equations for the static gluon and ghost propagators. A unique infrared scaling relation will be derived and the truncations necessary to make these two flow equations a closed system of equations will be discussed. This system of equations will be solved numerically using two different approximations. Both solutions will be shown to fulfill the so-called infrared scaling relation which relates the infrared behaviour of the gluon and the ghost propagator to each other.

Most of the content of this chapter is based on Ref. [72].

### 3.1 FRG in Hamiltonian Yang-Mills Theory

In Chap. 1, we have shown the derivation of the flow equation for the effective action in the Lagrangian formulation of QFT. In this section we derive the corresponding flow equation for Yang-Mills theory in Coulomb gauge in the Hamiltonian approach.

As in the Lagrangian approach, see Eq. (1.1), we start from the generating functional of the Green functions, which in this case are the static, equal-time Green functions. It can be obtained by using Eq. (2.43) to express the vacuum expectation value of several field operators  $A$  as

$$\begin{aligned}\langle\phi|A_1\cdots A_n|\phi\rangle &= \int \mathcal{D}A \det(-\partial_i\hat{D}_i)A_1\cdots A_n|\phi[A]|^2 \\ &= \frac{\delta^n}{\delta J_1\cdots\delta J_n} \int \mathcal{D}A \det(-\partial_i\hat{D}_i)|\phi[A]|^2 \exp(J\cdot A) \Big|_{J=0}\end{aligned}\quad (3.1)$$

with the abbreviation  $J\cdot A$  including the internal indices,

$$J\cdot A = \int \frac{d^3p}{(2\pi)^3} J_i^a(-\mathbf{p})A_i^a(\mathbf{p}). \quad (3.2)$$

The vacuum wave functional is denoted as  $\langle A|\phi\rangle = \phi[A]$ . Therefore, we recognize the expression

$$Z[J] = \int \mathcal{D}A \det(-\partial_i\hat{D}_i)|\phi[A]|^2 \exp(J\cdot A) \quad (3.3)$$

as the generating functional of Green functions. We represent the Faddeev-Popov functional determinant  $\det(-\partial_i \hat{D}_i)$  in the standard fashion as an integral over ghost fields  $c$  and  $\bar{c}$ ,

$$\det(-\partial_i \hat{D}_i) = \int \mathcal{D}[\bar{c}c] \exp \left( - \int d^3x \bar{c}^a(\mathbf{x}) (-\partial_i \hat{D}_i)^{ab} c^b(\mathbf{x}) \right). \quad (3.4)$$

Together with the absolute square of the vacuum wave functional, this permits the definition of an action  $S$  via

$$\exp(-S) := \exp \left( - \int d^3x \bar{c}^a(\mathbf{x}) (-\partial_i \hat{D}_i)^{ab} c^b(\mathbf{x}) \right) |\phi[A]|^2 \quad (3.5)$$

so that the generating functional becomes

$$Z[J, \sigma, \bar{\sigma}] = \int \mathcal{D}[A\bar{c}c] e^{-S+J \cdot A + \bar{\sigma} \cdot c + \bar{c} \cdot \sigma} \quad (3.6)$$

where the ghost sources  $\bar{\sigma}$  and  $\sigma$  have been introduced. This expression has precisely the standard form of the generating functional (1.1) in Lagrangian field theory, except that the functional integral extends over time-independent fields such that it generates static, equal-time correlation functions. Therefore, we can repeat, step by step, the derivation in Chap. 1 to obtain the corresponding FRG flow equation, which will have the same structure as Eq. (1.20). Introducing regulator terms for ghosts and gluons via  $\Delta S_k$ , see Eq. (1.2), the regulated generating functional (1.4) now reads

$$Z_k[J, \sigma, \bar{\sigma}] = \int \mathcal{D}[A\bar{c}c] e^{-S - \Delta S_k + J \cdot A + \bar{\sigma} \cdot c + \bar{c} \cdot \sigma}, \quad (3.7)$$

where the regulator term is chosen as

$$\Delta S_k[A, c, \bar{c}] = \frac{1}{2} A \cdot R_{A,k} \cdot A + \bar{c} \cdot R_{c,k} \cdot c. \quad (3.8)$$

Here we have again used the abbreviation for scalar products, e.g.,

$$A \cdot R_{A,k} \cdot A = \int \frac{d^3p}{(2\pi)^3} A_i^a(-\mathbf{p}) R_{A;k,ij}^{ab}(\mathbf{p}) A_j^b(\mathbf{p}). \quad (3.9)$$

Due to global colour symmetry and spatial rotational symmetry, the regulators take the form

$$\begin{aligned} R_{A;k,ij}^{ab}(\mathbf{p}) &= R_{A,k}(p) t_{ij}(\mathbf{p}) \delta^{ab}, \\ R_{c,k}^{ab}(\mathbf{p}) &= R_{c,k}(p) \delta^{ab}, \end{aligned} \quad (3.10)$$

with the notation  $p = |\mathbf{p}|$  that we will use from now on. Both regulators are chosen to depend on the same dimensionless shape function  $r_k(p)$ . Accounting for dimensions we set

$$\begin{aligned} R_{A,k}(p) &= 2p r_k(p), \\ R_{c,k}(p) &= g p^2 r_k(p) = g \bar{R}_{c,k}(p), \end{aligned} \quad (3.11)$$

see the remarks following Eq. (3.33) concerning the factor  $g$  included in the definition of  $R_{c,k}(p)$ .

From the regularized generating functional (3.7) and the regulator term (3.8) we first derive the flow equation for  $Z_k$ ,

$$\partial_t Z_k[J, \sigma, \bar{\sigma}] = \left( -\frac{1}{2} \frac{\delta}{\delta J} \cdot \dot{R}_{A,k} \cdot \frac{\delta}{\delta J} + \frac{\delta}{\delta \sigma} \cdot \dot{R}_{c,k} \cdot \frac{\delta}{\delta \bar{\sigma}} \right) Z_k[J, \sigma, \bar{\sigma}], \quad (3.12)$$

where the difference in signs of the gluon and ghost regulator term compared to Eq. (3.8) is due to the anticommutation property of the ghost fields and sources. The definition of the Schwinger functional  $W_k$  generating connected Green functions reads

$$W_k[J, \sigma, \bar{\sigma}] := \ln Z_k[J, \sigma, \bar{\sigma}], \quad (3.13)$$

and therefore its flow is expressed as

$$\begin{aligned} \partial_t W_k = & \left( -\frac{1}{2} \frac{\delta W_k}{\delta J} \cdot \dot{R}_{A,k} \cdot \frac{\delta W_k}{\delta J} - \frac{1}{2} \text{Tr} \dot{R}_{A,k} \frac{\delta^2 W_k}{\delta J \delta J} \right. \\ & \left. + \frac{\delta W_k}{\delta \sigma} \cdot \dot{R}_{c,k} \cdot \frac{\delta W_k}{\delta \bar{\sigma}} - \text{Tr} \dot{R}_{c,k} \frac{\delta^2 W_k}{\delta \bar{\sigma} \delta \sigma} \right). \end{aligned} \quad (3.14)$$

The effective action  $\Gamma_k$  is defined via a modified Legendre transformation,

$$\Gamma_k[A, \bar{c}, c] := -W_k[J_k, \sigma_k, \bar{\sigma}_k] + J_k \cdot A + \bar{\sigma}_k \cdot c + \bar{c} \cdot \sigma_k - \frac{1}{2} A \cdot R_{A,k} \cdot A - \bar{c} \cdot R_{c,k} \cdot c. \quad (3.15)$$

This modification of the Legendre transformation is chosen because it renders the flow equation for the effective action more elegant and it ensures that the effective action turns into the classical action for high cut-off momenta  $k$ , see the discussion starting at Eq. (1.13). However, it turns into the usual one upon taking  $k \rightarrow 0$ , because we will choose the regulator functions in compliance with Eq. (1.3),  $R_{A,k=0} = R_{c,k=0} = 0$ . In Eq. (3.15), the sources are functionals of the fields (that are not denoted), which are the expectation values of the corresponding field operators. The relations between sources and fields are given by

$$\begin{aligned} A_i^a(-\mathbf{p}) &= \frac{\delta W_k[J_k, \sigma_k, \bar{\sigma}_k]}{\delta J_i^a(\mathbf{p})}, \\ c^a(-\mathbf{p}) &= \frac{\delta W_k[J_k, \sigma_k, \bar{\sigma}_k]}{\delta \bar{\sigma}^a(\mathbf{p})}, \\ \bar{c}^a(-\mathbf{p}) &= -\frac{\delta W_k[J_k, \sigma_k, \bar{\sigma}_k]}{\delta \sigma^a(\mathbf{p})}, \end{aligned} \quad (3.16)$$

abbreviated as

$$A = \frac{\delta W_k}{\delta J}, \quad c = \frac{\delta W_k}{\delta \bar{\sigma}}, \quad \bar{c} = -\frac{\delta W_k}{\delta \sigma}. \quad (3.17)$$

With these definitions and with Eq. (3.14), the flow of the effective action is written as

$$\begin{aligned} \partial_t \Gamma_k &= -(\partial_t W_k)[J_k, \sigma_k, \bar{\sigma}_k] - \partial_t J_k \cdot \frac{\delta W_k}{\delta J} - \partial_t \sigma_k \cdot \frac{\delta W_k}{\delta \sigma} - \partial_t \bar{\sigma}_k \cdot \frac{\delta W_k}{\delta \bar{\sigma}} \\ &\quad + A \cdot \partial_t J_k + \partial_t \bar{\sigma}_k \cdot c - \partial_t \sigma_k \cdot \bar{c} - \frac{1}{2} A \cdot \dot{R}_{A,k} \cdot A - \bar{c} \cdot \dot{R}_{c,k} \cdot c \\ &= \left( \frac{1}{2} \text{Tr} \dot{R}_{A,k} \frac{\delta^2 W_k}{\delta J \delta J} + \text{Tr} \dot{R}_{c,k} \frac{\delta^2 W_k}{\delta \bar{\sigma} \delta \sigma} \right) \Big|_{J_k, \sigma_k, \bar{\sigma}_k} . \end{aligned} \quad (3.18)$$

In the present case, to keep the derivation of the propagator flows compact, it is convenient to switch to the superfield formalism<sup>1</sup>, i.e., we combine gluon and ghost fields into a superfield

$$\varphi = (A, c, \bar{c}), \quad \bar{\varphi} = (A, -\bar{c}, c). \quad (3.19)$$

Accordingly, we introduce the supersources

$$I = (J, \sigma, \bar{\sigma}), \quad \bar{I} = (J, -\bar{\sigma}, \sigma) \quad (3.20)$$

and supermatrices

$$\mathcal{R}_k = \text{diag}(R_{A,k}, R_{c,k}, R_{c,k}^T), \quad M = \text{diag}(\mathbf{1}, -\mathbf{1}, -\mathbf{1}), \quad (3.21)$$

where  $M$  enters the definition of the supertrace,

$$\text{STr}(\dots) := \text{Tr}(M \dots). \quad (3.22)$$

With this notation the effective action (3.15) is given by

$$\Gamma_k[\phi] = -W_k[I_k] + I_k \cdot \bar{\phi} - \frac{1}{2} \bar{\phi} \mathcal{R}_k M \phi, \quad (3.23)$$

where  $W_k[I_k]$  is defined by  $W_k := \ln Z_k$  and

$$\bar{\phi} = \frac{\delta W_k[I_k]}{\delta I_k} \quad (3.24)$$

is the classical superfield  $\phi = \langle \varphi \rangle$  with  $\phi = (A, c, \bar{c})$ , where we will use the same symbols for the components of  $\phi$  and  $\varphi$  as the latter will not turn up anymore in the following. The flow equation (3.18) of the effective action reads (cf. Eq. (1.17))

$$\partial_t \Gamma_k[\phi] = \frac{1}{2} \text{STr} \dot{\mathcal{R}}_k \frac{\delta^2 W_k}{\delta \bar{I} \delta I}. \quad (3.25)$$

---

<sup>1</sup>To maintain clarity of presentation, we have not started in the superfield formalism from the beginning. For a derivation that starts with the generating functional  $Z$  in the superfield formalism, see the discussion from Eq. (5.4) on, there with quark fields included.



With Eq. (3.24) we derive from (3.23) (cf. Eq. (1.18))

$$\frac{\delta^2 W_k}{\delta \bar{I} \delta I} = \left( \frac{\delta^2 \Gamma_k}{\delta \bar{\phi} \delta \phi} + \mathcal{R}_k \right)^{-1} \quad (3.26)$$

and obtain the flow equation (cf. Eq. (1.20))

$$\partial_t \Gamma_k = \frac{1}{2} \text{STr} \dot{\mathcal{R}}_k \left( \Gamma_k^{(2)} + \mathcal{R}_k \right)^{-1}, \quad (3.27)$$

where  $\Gamma_k^{(2)} := \delta^2 \Gamma_k / \delta \bar{\phi} \delta \phi$ . In components of the superfield, Eq. (3.27) reads

$$\partial_t \Gamma_k = \frac{1}{2} \text{Tr} \begin{pmatrix} \dot{R}_{A,k} & & & \\ & -\dot{R}_{c,k} & & \\ & & -\dot{R}_{c,k}^T & \\ & & & \end{pmatrix} \begin{pmatrix} \frac{\delta^2 \Gamma_k}{\delta A \delta A} + R_{A,k} & \frac{\delta^2 \Gamma_k}{\delta A \delta c} & \frac{\delta^2 \Gamma_k}{\delta A \delta \bar{c}} \\ -\frac{\delta^2 \Gamma_k}{\delta \bar{c} \delta A} & -\frac{\delta^2 \Gamma_k}{\delta \bar{c} \delta c} + R_{c,k} & -\frac{\delta^2 \Gamma_k}{\delta \bar{c} \delta \bar{c}} \\ \frac{\delta^2 \Gamma_k}{\delta c \delta A} & \frac{\delta^2 \Gamma_k}{\delta c \delta c} & \frac{\delta^2 \Gamma_k}{\delta c \delta \bar{c}} + R_{c,k}^T \end{pmatrix}^{-1} \quad (3.28)$$

From this equation we will derive the flow equations for the ghost and gluon propagators in Sec. 3.2 by taking functional derivatives w.r.t. the ghost and gluon fields.

In the present Hamiltonian formulation,  $\Gamma_k[\phi]$  – defined by Eqs. (3.5), (3.7), (3.8), (3.13), and (3.23) – is only determined by the vacuum wave functional  $\phi[A]$  and the Faddeev-Popov determinant. Importantly, the FRG approach does not require the knowledge of the full vacuum wave functional. It is sufficient to know the wave functional in the asymptotic region  $k \rightarrow \infty$ , where perturbation theory applies. The full quantum effective action  $\Gamma_{k \rightarrow 0}$  and therefore the full vacuum wave functional is then computed by solving the flow equation, making suitable ansatzes and truncations for  $\Gamma_k$  and its functional derivatives.

## 3.2 The Gluon and Ghost Propagator Flows

In this section we derive the flow equations for the gluon and the ghost propagator. The approximations made will be discussed in Sec. 3.4.

The propagator flows are obtained from the flow equation for the effective action (3.27) by differentiating twice w.r.t. the fields. These derivations are detailed in Appendix B.1, their outcome is represented diagrammatically in Figs. 3.1 and 3.2. All propagators and vertices, denoted by black and white circles, respectively, are fully dressed  $k$ -dependent correlation functions. It is interesting to compare this with the DSEs for the propagators where all diagrams contain one bare vertex.

For the approximations to be made, we rely on an expansion of the effective action in powers of the field,

$$\Gamma_k[\phi] = \sum_{N_A, N_c, N_{\bar{c}}} \frac{1}{N_A!} \frac{1}{N_c!} \frac{1}{N_{\bar{c}}!} \Gamma_{k, n_1 \dots n_N}^{(N)} \cdot \phi_{n_1} \cdots \phi_{n_N}, \quad (3.29)$$

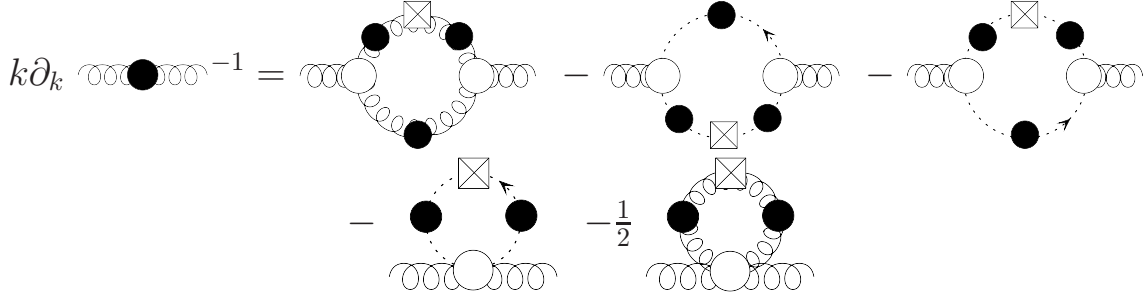


**Figure 3.1:** Flow equation of the gluon propagator, Eq. (B.8). Here and in the following, the spiral and dotted lines with the black circles denote the regularized gluon and ghost propagators at cutoff momentum  $k$ , respectively. White circles stand for proper vertices at cutoff  $k$ , a regulator insertion  $\hat{R}_k$  is represented by a square with a cross.

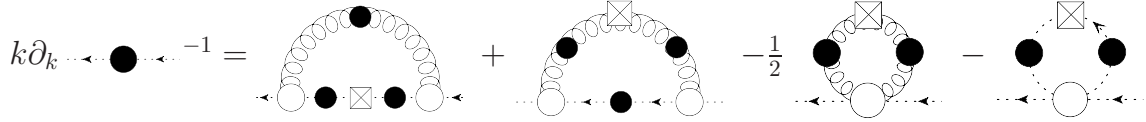


**Figure 3.2:** Flow equation of the ghost propagator, Eq. (B.7)

where the  $\phi_{n_i}$  stand for either the gluon fields ( $\phi = A$ ) or the ghost fields ( $\phi = c, \bar{c}$ ). In the following, we take into account the bare ghost-gluon vertex and the full momentum dependent propagators. All other vertices are set to zero. Therefore, in this minimal order of the approximation, the only non-vanishing  $n$ -point functions are the ghost and gluon (inverse) propagators and the ghost-gluon vertex. The flow equations truncated in this way are depicted in Figs. 3.3 and 3.4. In an improved approximation presented in Sec. 3.6 we will also take into account tadpole terms related to ghost and ghost-gluon vertices, which allows an error estimate for the approximation scheme set up here.

We parameterize the inverse gluon propagator as,

$$\frac{\delta^2 \Gamma_k}{\delta A_i^a(\mathbf{p}) \delta A_j^b(\mathbf{q})} = \delta^{ab} t_{ij}(\mathbf{p}) 2\omega_k(p) (2\pi)^3 \delta^3(\mathbf{p} + \mathbf{q}). \quad (3.30)$$

The diagonality in colour space is due to global colour symmetry. The transverse projector comes with the choice of Coulomb gauge where the gauge fields are transverse, see Eq. (2.29), and momentum conservation arises from spatial translational invariance of the theory. The only quantity left to be determined by the flow equation is  $\omega_k(p)$ , which depends only on the absolute value of the external momentum due to rotational invariance of the theory, and on the cutoff momentum  $k$ . The factor of 2 is mere convention. In the flow we need the gluon propagator  $G_{A,k} t_{ij} \delta^{ab}$  where

$$G_{A,k}(p) = \frac{1}{2\omega_k(p) + R_{A,k}(p)}. \quad (3.31)$$

$$k\partial_k \text{gluon propagator}^{-1} = - \text{diagram 1} - \text{diagram 2}$$

**Figure 3.3:** Truncated flow equation of the gluon propagator. Here and in the following, the bare vertices at  $k = \Lambda$  are symbolized by small dots.

$$k\partial_k \text{ghost propagator}^{-1} = \text{diagram 1} + \text{diagram 2}$$

**Figure 3.4:** Truncated flow equation of the ghost propagator.

The full gluon propagator at vanishing cut-off is given by  $G_A(p) = 1/2\omega(p)$ , with  $\omega(p) := \omega_0(p)$ .

The ghost two-point function can be expressed as

$$-\frac{\delta^2\Gamma_k}{\delta\bar{c}^a(\mathbf{p})\delta c^b(\mathbf{q})} = \delta^{ab}g\frac{p^2}{d_k(p)}(2\pi)^3\delta^3(\mathbf{p} + \mathbf{q}) , \quad (3.32)$$

where  $d_k(p)$  is the ghost form factor, which is the quantity to be calculated. The ghost propagator  $G_{c,k}\delta^{ab}$  comprises the scalar function

$$G_{c,k}(p) = \frac{1}{g}\bar{G}_{c,k}(p) \quad \text{with} \quad \bar{G}_{c,k}(p) = \frac{1}{p^2/d_k(p) + \bar{R}_{c,k}(p)} . \quad (3.33)$$

We have included an explicit constant factor of  $1/g$  in the definition of the ghost form factor in order to compare our results with the Dyson-Schwinger equations of the variational approach in Sec. 3.6. The full ghost propagator at vanishing cut-off is  $G_c(p) = d(p)/gp^2$ , where  $d(p) := d_0(p)$ .

The last quantity to be specified is the ghost-gluon vertex. We will argue in Sec. 3.4 that it is well approximated by its bare part,

$$\frac{\delta^3\Gamma_k}{\delta\bar{c}^a(\mathbf{p}_1)\delta c^b(\mathbf{p}_2)\delta A_i^c(\mathbf{p}_3)} = igf^{abc}p_{1,j}t_{ij}(\mathbf{p}_3)(2\pi)^3\delta^3(\mathbf{p}_1 + \mathbf{p}_2 + \mathbf{p}_3) , \quad (3.34)$$

where we have used the fact that the gauge field is transverse in Coulomb gauge.

These parameterizations are plugged into the propagator flow equations in Appendix B.1 with the result

$$\partial_t\omega_k(p) = -\frac{N_c}{2} \int \frac{d^3q}{(2\pi)^3} \left( \bar{G}_{c,k}\dot{\bar{R}}_{c,k}\bar{G}_{c,k} \right) (q) \bar{G}_{c,k}(|\mathbf{p} + \mathbf{q}|) q^2(1 - (\hat{\mathbf{p}} \cdot \hat{\mathbf{q}})^2) , \quad (3.35)$$

$$\begin{aligned}
\partial_t d_k^{-1}(p) = N_c \int \frac{d^3 q}{(2\pi)^3} & \left[ \left( G_{A,k} \dot{R}_{A,k} G_{A,k} \right) (q) \bar{G}_{c,k}(|\mathbf{p} + \mathbf{q}|) \right. \\
& \left. + \left( \bar{G}_{c,k} \dot{R}_{c,k} \bar{G}_{c,k} \right) (q) G_{A,k}(|\mathbf{p} + \mathbf{q}|) \frac{q^2}{(\mathbf{p} + \mathbf{q})^2} \right] (1 - (\hat{\mathbf{p}} \cdot \hat{\mathbf{q}})^2).
\end{aligned} \tag{3.36}$$

These equations are diagrammatically depicted in Figs. 3.3 and 3.4.

### 3.3 Uniqueness of Infrared Scaling

The Hamiltonian flow equation derived for Coulomb gauge Yang-Mills theory in Sec. 3.1 very much resembles the one in Landau gauge, but with one dimension less. It has already been speculated that there is a close connection between these two formulations, see Ref. [69]. Here we employ the similarities in order to derive unique scaling laws for the infrared behaviour of Coulomb gauge Yang-Mills theory.

It has been shown in Refs. [73, 74] that Landau gauge Yang-Mills theory admits a unique infrared scaling solution [75] in the sense that, if scaling is present, the scaling relations are unique. Moreover, this solution implies ghost dominance. Indeed, Landau gauge Yang-Mills theory also admits a solution without such a scaling behaviour, the decoupling solution, see Ref. [58] for further details. The scaling and decoupling solutions also exist for the DSE obtained in the Hamiltonian formulation of Yang-Mills theory in Coulomb gauge and are called critical and subcritical solutions there [51]. Furthermore, lattice calculations [69] show that it is actually the scaling or critical solution which is realized in Coulomb gauge. In the following, we will show that the scaling relation (3.42), which has already been found in Refs. [43, 49, 76], is unique.

The uniqueness proof in Ref. [73] is based on the comparison of the full hierarchies of DSE and FRG equations for the Green functions. This proof can be directly transferred to Coulomb gauge, the only missing piece is provided by the flow equation derived in Sec. 3.1. With the Hamiltonian Coulomb gauge DSEs and the FRGs we can derive the same set of constraint equations for the scaling coefficients as in Ref. [73]. We conclude that also Coulomb gauge Yang-Mills theory in its Hamiltonian formulation admits a unique scaling solution with the same scaling laws that are satisfied in Landau gauge in  $d = 3$ . The scaling relations relevant for the present work are that for the propagators,

$$\langle A(p)A(-p) \rangle \propto \frac{1}{p^{2(1+\kappa_A)}}, \quad \langle c(p)\bar{c}(-p) \rangle \propto \frac{1}{p^{2(1+\kappa_c)}}, \tag{3.37}$$

and for the ghost gluon vertex at the symmetric point,

$$\frac{\delta^3 \Gamma_k}{\delta \bar{c}^a \delta c^b \delta A_i^c} \propto p^{2\kappa_{\bar{c}cA}} \frac{\delta^3 S}{\delta \bar{c}^a \delta c^b \delta A_i^c}. \tag{3.38}$$

The scaling solution entails the non-renormalization of the ghost-gluon vertex,  $\kappa_{\bar{c}cA} =$

0, and a scaling relation for the scaling of the ghost and gluon propagator, summarized as

$$\kappa_{\bar{c}cA} = 0 \quad \text{and} \quad \kappa_A = -\frac{1}{2} - 2\kappa_c, \quad \text{with} \quad \kappa_A \leq -\frac{1}{4}. \quad (3.39)$$

Equation (3.39) implies

$$\kappa_c - \kappa_A \geq \frac{1}{8} > 0, \quad (3.40)$$

a relation which is called ghost-dominance, i.e., diagrams with ghost lines dominate in the infrared over diagrams with gluonic lines, see also [73]. The scaling coefficients  $\alpha, \beta$  used in Coulomb gauge are usually defined via

$$\langle A(p)A(-p) \rangle \propto p^\alpha, \quad \langle c(p)\bar{c}(-p) \rangle \propto \frac{1}{p^{2+\beta}}, \quad (3.41)$$

see Eq. (3.46). The coefficients  $\alpha$  and  $\beta$  relate to the  $\kappa$ 's via  $\alpha = -2 - 2\kappa_A$  and  $\beta = 2\kappa_c$ . Therefore, we find *unique* scaling laws in Coulomb gauge with the scaling relation

$$\alpha = 2\beta - 1. \quad (3.42)$$

Yet it must be noted that a numerical treatment is necessary after all because the uniqueness proof only shows that there is no scaling solution with a relation between the exponents other than  $\alpha = 2\beta - 1$ , it does, however, not yield the actual values of  $\alpha$  or  $\beta$ . These have to be calculated numerically, as will be done in Sections 3.5 and 3.6. It will be found there that the solutions indeed comply with the scaling relation (3.42).

### 3.4 Truncation of the Propagator Flows

To arrive at the flow equations of the gluon and the ghost propagator, Eqs. (3.35) and (3.36), we have approximated the full effective action with the bare ghost-gluon vertex and fully momentum dependent (inverse) propagators. As we are specifically interested in the infrared momentum regime where we assume scaling, and uniqueness of scaling as proven in Sec. 3.3 then implies ghost dominance, we have dropped the gluonic vertices and only kept the ghost vertices. The resulting flow equations for the gluon and ghost propagators are shown in Figs. 3.3 and 3.4.

We now discuss the meaning of and the justification for this truncation in detail. The generating functional (3.6) is a functional integral whose definition involves the full vacuum wave functional  $\phi[A]$ , see Eq. (3.5), which is, however, unknown. In Ref. [77] the vacuum functional has been determined explicitly to one-loop order through a perturbative solution of the Schrödinger equation for the Christ-Lee Hamiltonian of Eq. (2.35). As expected, it was found that gluonic terms give contributions to the static gluon propagator that are important to its ultraviolet behaviour, in particular its anomalous dimension. By neglecting the purely gluonic vertices in the truncation considered here, the ultraviolet behaviour of the two-point function

is not accurately reproduced, i.e., the power of the logarithmic correction in this kinematic regime is incorrect.

On the other hand, the three- and four-gluon couplings are not relevant to the infrared behaviour, which is our main concern here: it has been argued in Refs. [76, 78, 79] that in the infrared the static ghost propagator is strongly enhanced relative to its tree-level behaviour, while the gluon propagator is suppressed or even vanishing. This is precisely what happens for the unique scaling solution as discussed in Sec. 3.3: the infrared behaviour is dominated by the diagrams with the largest number of ghost propagators (ghost dominance). The approximation of keeping a bare or tree-level ghost-gluon vertex is based on the non-renormalization theorem for this vertex [80, 81], which can be carried over to the present situation. Indeed we have shown in Sec. 3.3 that it follows for the unique scaling solution. It has been confirmed on the non-perturbative level for the Landau gauge case in lattice [82, 83] and DSE [84] studies. As for the Coulomb gauge, a perturbative evaluation of the vertex (to one-loop level) at the symmetric point shows that the quantum corrections are finite and independent of the scale [77, 85].

In summary, we can drop the gluonic vertices without changing the infrared behaviour of the propagators. We emphasize that for large momenta this is evidently not true. Finally, we also drop the tadpole diagrams in the flow equations for the static propagators. We assume that their contribution is negligible in the infrared, at least for the qualitative behaviour of the two-point correlation functions. We will partially mend this neglect of the tadpole terms in Sec. 3.6 by an optimized flow.

### 3.5 Approximation without Tadpoles

In this section we solve the flow equations for the propagators within the minimal truncation introduced above: the only non-vanishing vertex function is the bare ghost-gluon vertex of Eq. (3.34). In particular, this eliminates the tadpole diagrams.

Equations (3.35) and (3.36) are two coupled differential equations for  $\omega_k$  and  $d_k$ , which can be solved numerically. Due to our definition (3.32) of the ghost form factor  $d_k(p)$ , the bare coupling constant  $g$  has formally disappeared from the propagator flow equations. To incorporate the appropriate initial conditions it is convenient to cast the differential flow equations into an integral form,

$$\omega_k(p) - \omega_\Lambda(p) = \int_\Lambda^k \frac{dk'}{k'} \int \frac{d^3\ell}{(2\pi)^3} I_{k'}^\omega[d_{k'}](\ell, \mathbf{p}), \quad (3.43)$$

$$d_k^{-1}(p) - d_\Lambda^{-1}(p) = \int_\Lambda^k \frac{dk'}{k'} \int \frac{d^3\ell}{(2\pi)^3} I_{k'}^d[\omega_{k'}, d_{k'}](\ell, \mathbf{p}). \quad (3.44)$$

$I^\omega$  and  $I^d$  stand for the integrands of the loop integrals on the r.h.s. of Eqs. (3.35) and (3.36).

The initial conditions  $d_\Lambda(p)$  and  $\omega_\Lambda(p)$  for the flow can be determined by perturbation theory [77, 85]. Contributions with higher powers of momenta than the ones

in lowest-order perturbation theory,  $d^{(0)}(p) = 1$  and  $\omega^{(0)}(p) = p$ , are suppressed by the corresponding powers of  $\Lambda$ . In the case of  $d_\Lambda(p)$ , this implies that for a large initial cut-off scale  $k = \Lambda$  we only have to fix the constant  $d_\Lambda(p) \equiv d_\Lambda$ .

For the gluon the introduction of the regulator term enforces a mass-like term, i.e., a  $p$ -independent contribution to  $\omega_k(p)$ . For large initial cut-off scales  $k = \Lambda$  the inverse gluon propagator has two relevant parameters, the mass-like parameter  $a$  and the coefficient of the classical term. The latter is set to one and we have the initial condition for the gluon correlator  $\omega_\Lambda(p) = p + a$ .

It is evident from the form of the flow equations (3.43) and (3.44) that the solution will not show infrared scaling unless the parameter  $d_\Lambda^{-1}(p) \equiv d_\Lambda^{-1}$  is fine-tuned, at least for  $\beta > 0$ . Such fine-tuning of relevant parameters is a well-known initial condition problem for RG flows. In Ref. [58] it has been shown that in Landau gauge there is a family of solutions of the flow equations where only one shows a scaling behaviour whereas the other solutions show a decoupling behaviour: a gluon with a massive propagator and a ghost which is at most logarithmically enhanced. Such a scenario also applies to Coulomb gauge.

In the present case we have numerically solved the fine-tuning condition for  $d_\Lambda$  with the constraint of infrared scaling for the ghost dressing function. The parameter  $a$  in the initial condition  $\omega_\Lambda(p)$  is fixed by demanding that  $\omega(p)$  reduce to the perturbative form  $\omega(p) \propto p$  for large momenta  $p$  close to but below  $\Lambda$ . The regulator used in the numerical solution is

$$r_k(p) = \exp\left(\frac{k^2}{p^2} - \frac{p^2}{k^2}\right). \quad (3.45)$$

Our numerical procedure is detailed in Appendix C. The results for the inverse gluon propagator  $\omega_k(p)$  and the ghost dressing function  $d_k(p)$  are shown in Figs. 3.5 and 3.6 for different values of the minimal cutoff  $k_{min}$  down to which the flow integration has been carried out. For better comparison, a physical scale has been introduced such that the extremum of the gluon propagator coincides with the one determined on the lattice in [67]. It is seen that the power law behaviour in both cases extends towards the IR as the cutoff  $k_{min}$  is lowered, although we have implemented a scaling behaviour (not the horizon condition  $d_0^{-1}(p=0) = 0$ ) only for the ghost dressing. We also display the full flow of the ghost dressing function,  $d_k(p)$ , in Fig. 3.7.

The IR power laws are extracted from the numerical solution shown in Figs. 3.5 and 3.6. The scaling coefficients  $\alpha$  and  $\beta$  defined in Eq. (3.41) as

$$\omega(p \rightarrow 0) \sim p^{-\alpha}, \quad d(p \rightarrow 0) \sim p^{-\beta}. \quad (3.46)$$

are determined as

$$\alpha = 0.28, \quad \beta = 0.64, \quad (3.47)$$

so  $\alpha$  and  $\beta$  satisfy the sum rule (3.42) already found analytically for the Coulomb gauge DSE in Refs. [43, 49]. Thus, we arrive at the nontrivial result that a scaling solution for the flow equations for both the gluon and the ghost propagator can be found. Note, however, that the scaling coefficients themselves obtained in the present truncation differ from the ones obtained in the DSE. In Figs. 3.8 and 3.9 the

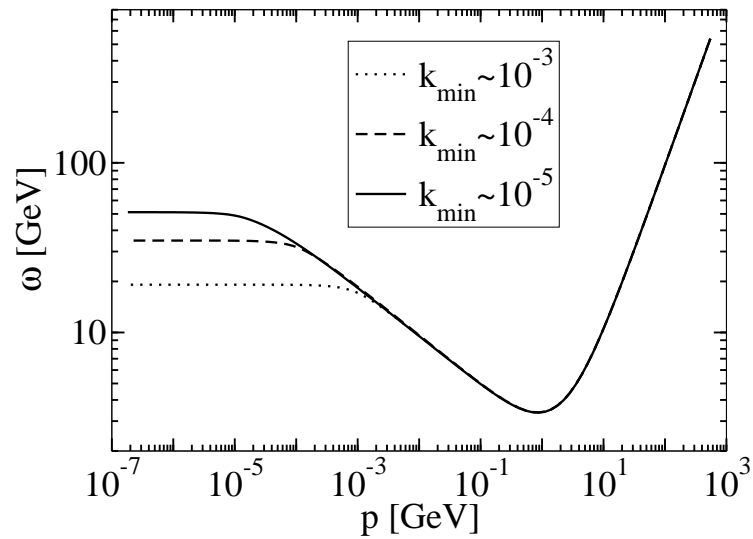


**Figure 3.5:** Gluon correlation function  $\omega$  for different minimal cutoffs  $k_{min}$ .

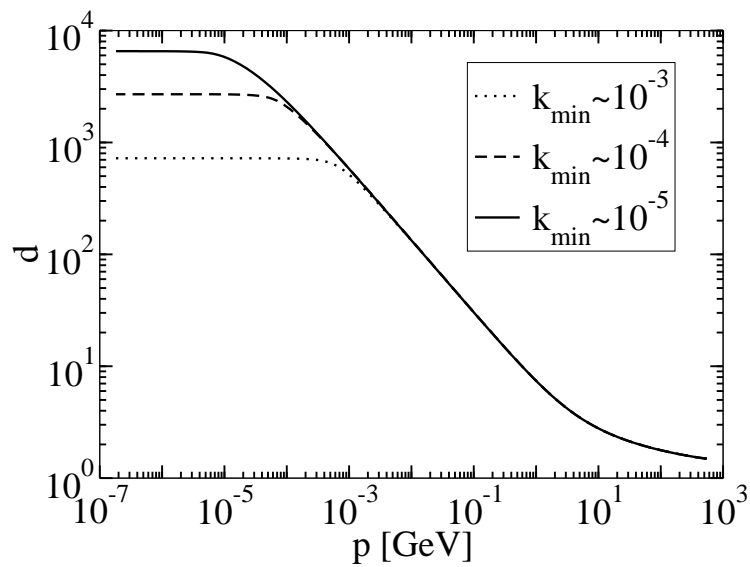


**Figure 3.6:** Ghost dressing function  $d$  for different minimal cutoffs  $k_{min}$ .



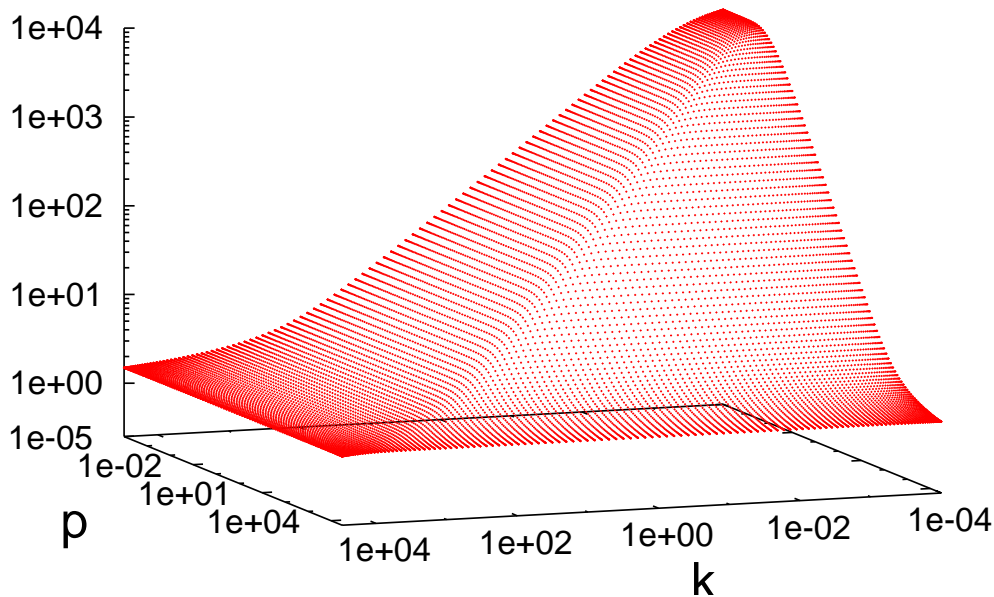


**Figure 3.7:** The flow of the full ghost form factor  $d_k(p)$  is shown. The gradual formation of the IR power law on lowering the cut-off scale  $k$  is explicitly seen.

solutions of the FRG flow equation for  $\omega(p)$  and  $d(p)$  are compared to the results which will be obtained from an optimized calculation in Sec. 3.6 which in turn are precisely the results found in [43] by the variational calculation, see Fig. 3.10. This variational calculation gave rise to the DSEs which will be found in Sec. 3.6 by an optimization of the truncated flow equations of Figs. 3.3 and 3.4.

While the curves in Figs. 3.8 and 3.9 match in the UV, the results of the FRG in the present minimal truncation are less infrared enhanced than the ones of the DSE. The scaling coefficients are actually expected to depend on the chosen regulator. It has already been proven in [86] for Landau gauge Yang-Mills theory that the scaling coefficients of FRG and DSE agree for optimized regulators if a bare ghost-gluon vertex is used, for details of the optimization theory for the FRG see, e.g., [22, 87].

## 3.6 Optimization

In this section we use optimization arguments in order to improve the present truncation. Similar arguments have already been used in Landau gauge for arriving at FRG results for the propagators that quantitatively agree with the lattice results [58]. Here we follow the arguments put forward in [86]. To that end we consider the following approximation: under the loop integrals we replace the propagators at the running momentum scale  $k$ ,  $\omega_k$  and  $d_k$ , by the propagators of the full theory, i.e.,

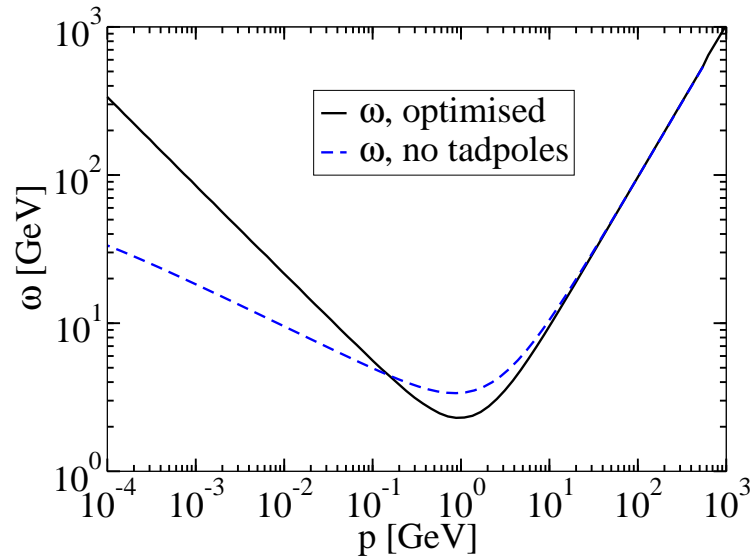


**Figure 3.8:** Comparison of the gluon two-point functions  $\omega$  calculated from the optimized flow and from the flow without tadpoles.

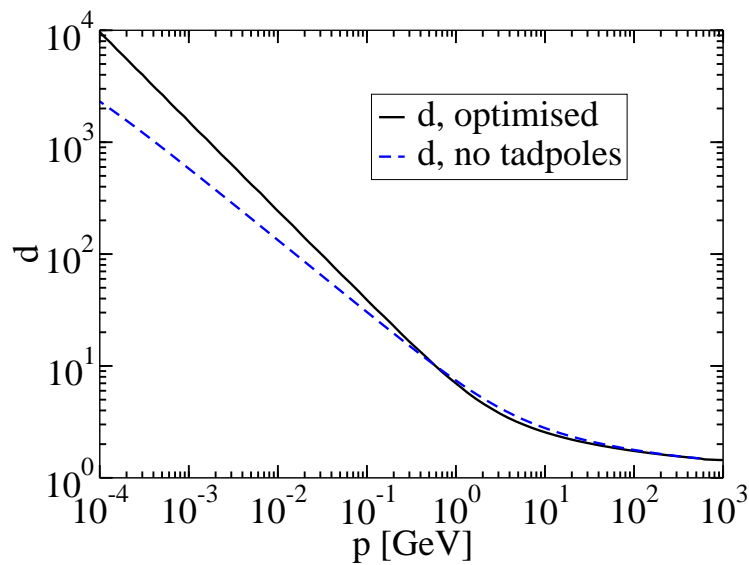


**Figure 3.9:** Comparison of the ghost dressings  $d$  calculated from the optimized flow and from the flow without tadpoles.

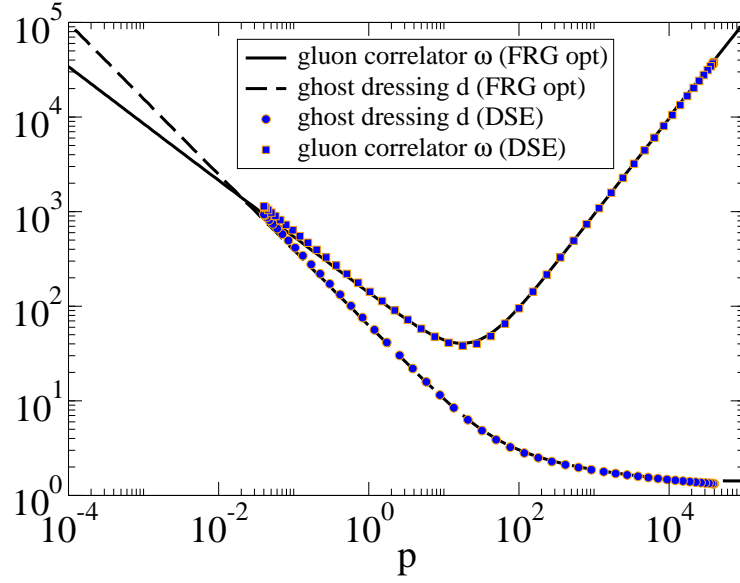


**Figure 3.10:** Gluon correlation function  $\omega$  and ghost dressing function  $d$  from the optimized flow equation in comparison with the results of the DSEs obtained from the variational ansatz in [43]. The results lie on top of each other as expected.

the ones at zero scale  $k = 0$ :

$$d_k(p) \rightarrow d_{k=0}(p) , \quad \omega_k(p) \rightarrow \omega_{k=0}(p) , \quad (3.48)$$

with the effect that the difference between the propagators at  $k = 0$  and the regularized ones at  $k$  drops out in the integrals. Indeed one can explicitly construct regulators for which this holds true in the asymptotic IR region, see [86]. Note that due to the strong infrared suppression introduced with the regulator choice (3.45) the approximation (3.48) is quantitatively reliable inside the loop integrals except for a small range of momenta  $p$  around the scale  $k$ . The approximation of Eq. (3.48) allows us to integrate the flow equations (3.35) and (3.36) over  $k$  analytically. The only  $k$ -dependence left is the explicit one on the regulator as the vertices are not  $k$ -dependent from the outset. Therefore, the flow can be rewritten as a total  $t$ -derivative of the loop integrals with full propagators. We arrive at

$$(\omega_0 - \omega_\Lambda)(p) = \frac{N_c}{4} \int \frac{d^3 q}{(2\pi)^3} \frac{q^2}{q^2 d_0^{-1}(q) + \bar{R}_{c,k}(q)} \frac{(1 - (\hat{\mathbf{p}} \cdot \hat{\mathbf{q}})^2)}{(\mathbf{p} + \mathbf{q})^2 d_0^{-1}(|\mathbf{p} + \mathbf{q}|) + \bar{R}_{c,k}(|\mathbf{p} + \mathbf{q}|)} \Big|_{k=\Lambda}^{k=0} , \quad (3.49)$$

$$(d_0^{-1} - d_\Lambda^{-1})(p) = -N_c \int \frac{d^3 q}{(2\pi)^3} \frac{1}{2\omega_0(q) + R_{A,k}(q)} \frac{(1 - (\hat{\mathbf{p}} \cdot \hat{\mathbf{q}})^2)}{(\mathbf{p} + \mathbf{q})^2 d_0^{-1}(|\mathbf{p} + \mathbf{q}|) + \bar{R}_{c,k}(|\mathbf{p} + \mathbf{q}|)} \Big|_{k=\Lambda}^{k=0} . \quad (3.50)$$

**Figure 3.11:** The integrated gluon flow equation of Eq. (3.49) is shown. It is equal to the gluon DSE where the purely gluonic terms are neglected and the ghost-gluon vertex is chosen bare.

**Figure 3.12:** The integrated ghost flow equation of Eq. (3.50). It is equal to the ghost DSE where the ghost-gluon vertex is chosen bare.

We notice that the flow equations (3.49) and (3.50) have acquired the form of truncated DSEs. They are shown diagrammatically in Figs. 3.11 and 3.12. Given the fact that  $R_{k=0} = 0$ , see Eq. (1.3), these equations coincide with the DSEs obtained in the variational approach of Ref. [43] (up to some additional contributions in the DSE for  $\omega(p)$  which are, however, subleading in the infrared), with a different UV-regularization realized here via the  $(k = \Lambda)$ -terms. Moreover, the optimization arguments in Refs. [22, 86] imply that the flows in the Eqs. (3.49) and (3.50) provide the best approximation to the full theory for the IR asymptotics.

That Eqs. (3.49) and (3.50) – shown in Figs. 3.11 and 3.12 – are a better approximation than Eqs. (3.35) and (3.36) – shown in Figs. 3.3 and 3.4 – can be seen also in the following way: without truncations, both the DSE and the flow equations are exact. Truncating the full ghost DSE by choosing the ghost-gluon vertex bare, we obtain Eq. (3.50), Fig. 3.12. Making the same approximation in the flow equation in Fig. 3.2 does not yield the truncated flow in Fig. 3.4 unless we additionally neglect the tadpole terms. Therefore, the truncated DSE in Fig. 3.12 is a better approximation than the truncated flow of Fig. 3.4. Truncating the full gluon DSE by also choosing the ghost-gluon vertex bare and by discarding the purely gluonic diagrams, we get Eq. (3.49), Fig. 3.11. Also here, the same approximation in the flow in Fig. 3.1 only yields the truncated flow in Fig. 3.3 if the additional approximation of neglecting the ghost tadpole is made. Therefore, the truncated DSE in Fig. 3.11 is a better approximation than the truncated flow in Fig. 3.3.

It remains to adjust the initial conditions. We could proceed in the same way as for the numerical solution in Sec. 3.5 to implement the condition of infrared scaling for the ghost dressing function. However, it is much simpler to use as an input the information from this numerical solution that  $\beta > 0$  and thus  $d_0^{-1}(p = 0) = 0$  (the horizon condition), so we can write

$$d_0^{-1}(p) = \int \frac{d^3q}{(2\pi)^3} [\text{int}(k, \mathbf{p}, \mathbf{q}) - \text{int}(k, \mathbf{p} = 0, \mathbf{q})] \Big|_{k=\Lambda}^{k=0}, \quad (3.51)$$

where  $\text{int}(k, \mathbf{p}, \mathbf{q})$  denotes the integrand in Eq. (3.50). The initial condition for the

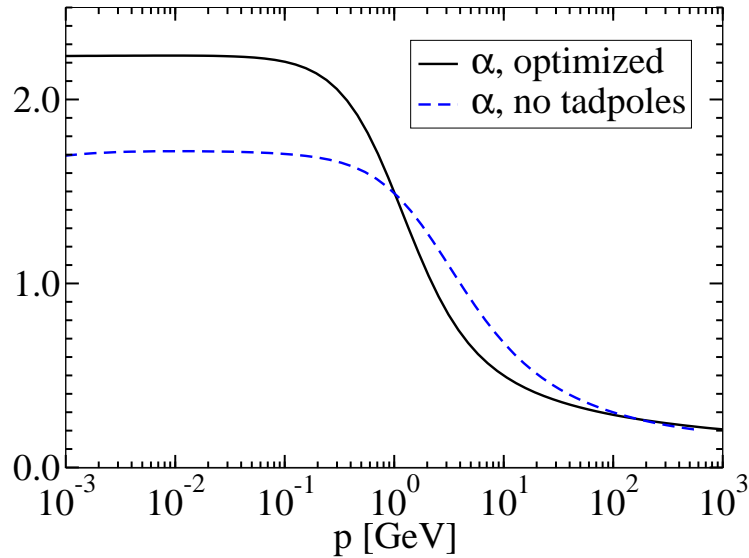


**Figure 3.13:** The running coupling  $\alpha$ , see Eq. (3.55), calculated from the optimized flow and from the flow without tadpoles.

gluon propagator is determined as before in Sec. 3.5. More details of the numerical procedure can be found in Appendix C.

The results of the iterative solution are shown in Fig. 3.10 in comparison to the results from the variational approach of Ref. [43], as well as in Figs. 3.8 and 3.9 in comparison with the non-optimized results of Sec. 3.5. A power law as parameterized in Eq. (3.46) emerges in the infrared region for both the gluon energy  $\omega(p)$  and the ghost dressing function  $d(p)$  with the IR exponents

$$\alpha = 0.60, \quad \beta = 0.80, \quad (3.52)$$

which is precisely one of the two possible IR solutions found analytically for the DSE in Ref. [49]. Furthermore, it corresponds to the solution found in the variational approach in Ref. [43] and it complies with the sum rule of Eq. (3.42) for the infrared exponents,

$$\alpha = 2\beta - 1. \quad (3.53)$$

The second possible solution in the analytical calculation of Ref. [49] with the infrared exponents

$$\alpha = 1, \quad \beta = 1 \quad (3.54)$$

has also been confirmed in a numerical calculation within the variational approach [50]. Although it might be present also in the optimized approximation, it has not been found numerically and it is not clear whether after the inclusion of the gluonic diagrams this solution would persist as an infrared stable one.

Finally, with the results for the propagator we can calculate the running coupling (recalling the definition in Eq. (3.32) including  $g$ ),

$$\alpha(p) = \frac{1}{4\pi} d^2(p) \frac{p}{\omega(p)}, \quad (3.55)$$

see Ref. [88]. The result is shown in Fig. 3.13, calculated using the propagators from the optimized flow equation as well as from the flow equation without the tadpoles. The plateau in the IR is due to the sum rule (3.42) which is fulfilled by the propagators resulting from both approximations of the flow equations.

In summary, we have shown that the method of Hamiltonian flows can be successfully applied to Yang-Mills theory in Coulomb gauge by calculating the gluon two-point function and the ghost form factor with it. The results have been obtained imposing the condition of infrared power law behaviour for the ghost form factor but without dictating the actual value of the exponent. Two different approximations have been used, where one of them can be argued to yield an optimized result. Both results fulfil a unique infrared scaling relation but with the optimized result possessing stronger infrared divergences than the non-optimized one. Moreover, the optimized result is in excellent quantitative agreement with the results obtained from the variational approach.

# Chapter 4

## The Colour Coulomb Potential

In this chapter we use the flow equation of the ghost form factor of Chap. 3 to derive a flow equation for the so-called Coulomb form factor. This quantity determines, together with the ghost propagator, the colour Coulomb potential which forms an upper bound for the static quark potential. We will find a linearly rising colour Coulomb potential from this equation. In contrast, the corresponding Dyson-Schwinger-like equation will be found to have no solution with the given gluon and ghost propagators. We will analyze this equation and the conditions for the existence of solutions in detail.

Part of the content of this chapter has already been presented in Ref. [89].

### 4.1 Defining the Colour Coulomb Potential

The Coulomb part of the Yang-Mills Hamiltonian in Coulomb gauge is, see Eq. (2.35),

$$H_{coul} = \frac{g^2}{2} \int d^3[xy] J^{-1}[A] \rho^a(\mathbf{x}) F[A]^{ab}(\mathbf{x}, \mathbf{y}) J[A] \rho^b(\mathbf{y}), \quad (4.1)$$

where the charge density  $\rho$  is composed of the charge of the gauge field itself and of the charge of the matter fields, see Eq. (2.37),

$$\rho^a(\mathbf{x}) \equiv \rho[A, \Pi_A]^a(\mathbf{x}) = \rho_{dyn}^a(\mathbf{x}) + \rho_m^a(\mathbf{x}), \quad (4.2)$$

where

$$\rho_{dyn}^a(\mathbf{x}) = f^{abc} A_i^c(\mathbf{x}) \Pi_{A,i}^b(\mathbf{x}). \quad (4.3)$$

It can be shown that mixing terms in the Hamiltonian, which are the terms with  $\rho_m F \rho_{dyn}$  and  $\rho_{dyn} F \rho_m$ , actually lower the potential between the matter fields [90]. Therefore, the term  $\rho_m F \rho_m$ , which is called the colour Coulomb potential, forms an upper bound to the full static quark potential, but it is much easier to obtain. We therefore restrict ourselves to the calculation of this quantity. As matter fields which we choose two point charges with opposite colour separated by the distance  $r = |\mathbf{r}|$ ,

$$\rho_m^a(\mathbf{x}) = \delta^{a0} \left[ \delta^3 \left( \mathbf{x} - \frac{\mathbf{r}}{2} \right) - \delta^3 \left( \mathbf{x} + \frac{\mathbf{r}}{2} \right) \right]. \quad (4.4)$$

The colour Coulomb potential for this charge distribution is

$$\begin{aligned}
V_C(r) &= \langle H_{\text{coul}} \rangle(r) = g^2 \langle F[A]^{00}(0, 0) - F[A]^{00}(0, \mathbf{r}) \rangle \\
&= g^2 \int \frac{d^3 p}{(2\pi)^3} F(p) (1 - e^{i\mathbf{p}\cdot\mathbf{r}}) \\
&= \frac{g^2}{2\pi^2} \frac{1}{r^3} \int_0^\infty dx F\left(\frac{x}{r}\right) x^2 \left(1 - \frac{\sin(x)}{x}\right),
\end{aligned} \tag{4.5}$$

where we denote as

$$\langle F[A]^{ab}(\mathbf{x}, \mathbf{y}) \rangle = \int \frac{d^3 p}{(2\pi)^3} \delta^{ab} F(p) e^{i\mathbf{p}\cdot(\mathbf{x}-\mathbf{y})} \tag{4.6}$$

the Fourier transform of the expectation value of the Coulomb kernel. The determination of  $F(p)$  is what we are aiming at in this chapter. We will find it to obey a (infrared) power law parameterized as

$$F(p \rightarrow 0) = \frac{a}{p^{\alpha_F}}. \tag{4.7}$$

Extending the IR behaviour of  $F$  to the whole momentum range, the potential becomes

$$V_C(r) = \frac{g^2 a}{2\pi^2} \frac{1}{r^{3-\alpha_F}} \int_0^\infty dx x^{1-\alpha_F} (x - \sin(x)), \tag{4.8}$$

which is convergent in the UV for  $\alpha_F > 3$  and convergent in the IR for  $\alpha_F < 5$ . Regularizing by a cut-off  $u$  in the UV as well as  $l$  in the IR and using integration by parts twice yields for the integral

$$\begin{aligned}
&\left[ \frac{1}{2-\alpha_F} x^{2-\alpha_F} (x - \sin(x)) - \frac{1}{(2-\alpha_F)(3-\alpha_F)} x^{3-\alpha_F} (1 - \cos(x)) \right] \Big|_l^u \\
&+ \int_l^u dx \frac{1}{(2-\alpha_F)(3-\alpha_F)} x^{3-\alpha_F} \sin(x).
\end{aligned} \tag{4.9}$$

Taking the limits  $u \rightarrow \infty$  and  $l \rightarrow 0$ , the boundary terms vanish and the integral becomes [91]

$$\int_0^\infty dx x^{1-\alpha_F} (x - \sin(x)) = \begin{cases} \frac{\Gamma(4-\alpha_F) \sin((4-\alpha_F)\frac{\pi}{2})}{(2-\alpha_F)(3-\alpha_F)} & \text{for } 3 < \alpha_F < 5; \alpha_F \neq 4 \\ \frac{\pi}{4} & \text{for } \alpha_F = 4. \end{cases} \tag{4.10}$$

The Coulomb potential itself finally reads

$$V_C(r) = \begin{cases} \frac{g^2 a}{2\pi^2} \frac{\Gamma(4-\alpha_F) \sin((4-\alpha_F)\frac{\pi}{2})}{(2-\alpha_F)(3-\alpha_F)} r^{\alpha_F-3} & \text{for } 3 < \alpha_F < 5; \alpha_F \neq 4 \\ \frac{g^2 a}{8\pi} r & \text{for } \alpha_F = 4 \end{cases} \tag{4.11}$$



In the case of a linearly rising potential, the slope is called the Coulomb string tension,

$$\sigma_C = \frac{g^2 a}{8\pi}, \quad (4.12)$$

and we get

$$g^2 F(p) = \frac{8\pi\sigma_C}{p^4}. \quad (4.13)$$

It has been shown in Ref. [90] that the Coulomb string tension  $\sigma_C$  forms an upper bound to the Wilson string tension  $\sigma$ ,

$$\sigma_C \geq \sigma, \quad (4.14)$$

which can be calculated from the Wilson loop and which describes the static quark potential, i.e., there is “no confinement without Coulomb confinement”.

We usually express the colour Coulomb potential with the Coulomb form factor  $f$  defined via

$$\begin{aligned} \langle F[A] \rangle &= \langle (-\partial\hat{D})^{-1}(-\partial^2)(-\partial\hat{D})^{-1} \rangle \\ &= \langle (-\partial\hat{D})^{-1} \rangle (-\partial^2) f (-\partial^2) \langle (-\partial\hat{D})^{-1} \rangle, \end{aligned} \quad (4.15)$$

or in momentum space

$$F(p) := \langle F[A] \rangle(p) = G_c(p) p^2 f(p) G_c(p). \quad (4.16)$$

In order to calculate the colour Coulomb potential, in Ref. [76] the Coulomb form factor was simply set equal to one, while in Refs. [43, 50] the DSE for this form factor was approximated by replacing in the loop integral the full ghost propagator  $\langle (-\partial\hat{D})^{-1} \rangle$  with the bare one, which results in an infrared finite Coulomb form factor. In this way, a strictly linear growth of the colour Coulomb potential with the distance between the colour sources (for sufficiently large distances) has been found in Ref. [50]. A natural improvement of this approximation would be the use of the full DSE for the Coulomb form factor. However, it turned out [51] that the full DSE for the Coulomb form factor cannot be consistently solved together with the DSEs for the static gluon and ghost propagators with an infrared-divergent ghost form factor, i.e., implementing the horizon condition. We will find that a solution for the Coulomb form factor equation with a ghost form factor complying with the horizon condition can be found only for a ghost form factor with an infrared divergence which is much milder than the ones found so far in various approaches.

In other words, a confining colour Coulomb potential cannot be obtained within the present approximation if the full DSE for the Coulomb form factor is used. In contrast, a consistent solution which exhibits scaling behaviour of the static propagators and of the colour Coulomb potential is found with the Hamiltonian flow equations without any additional approximation for the Coulomb form factor.

## 4.2 The Flow Equation for the Coulomb Form Factor

In the Hamiltonian approach to Yang-Mills theory in Coulomb gauge the potential between static colour sources is given by the vacuum expectation value of the Coulomb kernel

$$F[A]_{\mathbf{x},\mathbf{y}}^{ab} = \left[ (-\partial\hat{D})^{-1}(-\partial^2)(-\partial\hat{D})^{-1} \right]_{\mathbf{x},\mathbf{y}}^{ab}, \quad (4.17)$$

where  $-\partial\hat{D}$  is the Faddeev-Popov operator with

$$\hat{D}^{ab} = \delta^{ab}\partial + gf^{abc}A^c. \quad (4.18)$$

With these definitions the Coulomb kernel can be written as a derivative w.r.t. the coupling constant  $g$ ,

$$F[A] = \frac{\partial}{\partial g} [g(-\partial\hat{D})^{-1}], \quad (4.19)$$

because

$$\begin{aligned} \partial_g [g(-\partial\hat{D})^{-1}] &= (-\partial\hat{D})^{-1} - g(-\partial\hat{D})^{-1}[\partial_g(-\partial\hat{D})](-\partial\hat{D})^{-1} \\ &= (-\partial\hat{D})^{-1}[(-\partial\hat{D}) + gA\partial](-\partial\hat{D})^{-1} = (-\partial\hat{D})^{-1}(-\partial^2)(-\partial\hat{D})^{-1}. \end{aligned} \quad (4.20)$$

By taking the vacuum expectation value of Eq. (4.19) we get

$$\begin{aligned} F &= \langle F[A] \rangle = \int \mathcal{D}A \partial_g (g(-\partial\hat{D})^{-1}) e^{-S} \\ &= \partial_g \left( \int \mathcal{D}A g(-\partial\hat{D})^{-1} e^{-S} \right) + g \int \mathcal{D}A (\partial_g S) (-\partial\hat{D})^{-1} e^{-S} \\ &= \partial_g (gG_c) + g \left\langle (\partial_g S) (-\partial\hat{D})^{-1} \right\rangle, \end{aligned} \quad (4.21)$$

where

$$e^{-S} := |\psi(A)|^2 \det(-\partial\hat{D}). \quad (4.22)$$

Note that a possible normalization factor can be included in  $S$ . In the infrared, the first term of Eq. (4.21) reads (with the infrared parameterization  $d(p) = c(g)p^{-\beta(g)}$ )

$$\frac{\partial}{\partial g} (gG_c(p \rightarrow 0)) = [c'(g) - c(g)\beta'(g) \ln p] p^{-2-\beta(g)}. \quad (4.23)$$

Therefore,  $\partial_g(gG_c)$  has the same infrared behaviour as  $G_c$ , i.e.,  $p^{-2-\beta}$ , up to logarithms, so in principle it is crucial to keep the second term in Eq. (4.21) which might potentially be more divergent due to the insertion  $\partial_g S$ . Note that the desired  $1/p^4$  behaviour for  $F(p)$ , which yields a linearly rising potential, see Eq. (4.11), is achieved by the first term in Eq. (4.21) alone if  $\beta = 2$ . However, no solution nearly as divergent had been found in the explicit computations, the strongest divergence being  $\beta = 1$  [50].

As an alternative to keeping the term  $g\langle(\partial_g S)(-\partial\hat{D})^{-1}\rangle$  in Eq. (4.21), we can drop it and balance this neglect by taking into account only part of the first term in Eq. (4.21). This way of computation is chosen in the following, in order to make the computation of  $F$  by a flow equation feasible. We denote the  $g$ -dependence of  $S$ , which includes the vacuum wave functional as well as the Faddeev-Popov determinant, by a different variable  $g'$ :

$$\begin{aligned} F_k(g) &= \langle F[A](g) \rangle_k = \int \mathcal{D}A \partial_g(g(-\partial\hat{D})^{-1}(g))e^{-S_k(g')} \Big|_{g'=g} \\ &= \partial_g \left[ \int \mathcal{D}A g(-\partial\hat{D})^{-1}(g)e^{-S_k(g')} \right] \Big|_{g'=g} = \partial_g(gG_{c,k}(g, g')) \Big|_{g'=g} , \end{aligned} \quad (4.24)$$

where we have already included the cut-off dependence  $k$ . We denote the quantity occurring on the r.h.s. of Eq. (4.24) as

$$F_k(p; g, g') := \partial_g(gG_{c,k}(g, g')) , \quad (4.25)$$

so that

$$F_k(g) = F_k(p; g, g') \Big|_{g'=g} . \quad (4.26)$$

Motivated by Eq. (4.16), to which the following equation has to reduce at  $k = 0$ , we define the Coulomb form factor  $f_k$  as

$$F_k(p; g, g') =: G_{c,k}^2(p; g, g')p^2 f_k(p; g, g') = p^2 f_k(p; g, g') \frac{1}{g^2 \left( \frac{p^2}{d_k(p; g, g')} + \bar{R}_{c,k}(p) \right)^2} , \quad (4.27)$$

where Eq. (3.33) has been applied. (Note also that  $f_k(p; g, g') \Big|_{g'=g} = f_k(p; g)$ .) Given that

$$\partial_g(gG_{c,k}(p; g, g')) = \partial_g \frac{1}{\frac{p^2}{d_k(p; g, g')} + \bar{R}_{c,k}(p)} = \frac{-p^2}{\left( \frac{p^2}{d_k(p; g, g')} + \bar{R}_{c,k}(p) \right)^2} \partial_g d_k^{-1}(p; g, g') \quad (4.28)$$

we obtain

$$f_k(p; g, g') = -g^2 \partial_g d_k^{-1}(p; g, g') . \quad (4.29)$$

With this equation and recalling the definition in Eq. (3.33),

$$\bar{G}_{c,k}(p) = \frac{1}{p^2/d_k(p) + \bar{R}_{c,k}(p)} , \quad (4.30)$$

we can write

$$\partial_g \bar{G}_{c,k}(p; g, g') = -\bar{G}_{c,k}^2(p; g, g') \partial_g \bar{G}_{c,k}^{-1}(p; g, g') = \frac{1}{g^2} \bar{G}_{c,k}^2(p; g, g') p^2 f_k(p; g, g') . \quad (4.31)$$

Furthermore, because of

$$G_{A,k}(p; g, g') = \int \mathcal{D}A A(-\mathbf{p})A(\mathbf{p})e^{-S_k(g')} \quad (4.32)$$

we obtain

$$\partial_g G_{A,k}(p; g, g') = 0 . \quad (4.33)$$

Taking the  $g$ -derivative of Eq. (3.36), making use of Eqs. (4.29), (4.31), (4.33), and subsequently setting  $g = g'$  (which will not be denoted from now on) we get the flow equation for the Coulomb form factor:

$$\begin{aligned} \partial_t f_k(p) = -N_c \int \frac{d^3q}{(2\pi)^3} & \left[ \left( G_{A,k} \dot{R}_{A,k} G_{A,k} \right) (q) \bar{G}_{c,k}^2(\mathbf{p} + \mathbf{q})(\mathbf{p} + \mathbf{q})^2 f_k(\mathbf{p} + \mathbf{q}) \right. \\ & \left. + 2 \dot{R}_{c,k}(q) \bar{G}_{c,k}^3(q) q^2 f_k(q) G_{A,k}(\mathbf{p} + \mathbf{q}) \frac{q^2}{(\mathbf{p} + \mathbf{q})^2} \right] \\ & (1 - (\hat{\mathbf{p}} \cdot \hat{\mathbf{q}})^2) . \end{aligned} \quad (4.34)$$

As the Coulomb form factor  $f_k(p)$  does not enter the flow equations of ghost and gluon, we can use the flow of the gluon correlator  $\omega_k(p)$  and of the ghost form factor  $d_k(p)$  as input into Eq. (4.34) for  $f_k(p)$ . This is different in the variational approach [43], where the gap equation, following from minimizing the energy density with respect to the gluon energy, indeed contains the form factor  $f(p)$ .

### 4.3 An Alternative Derivation of the Coulomb Form Factor Flow

In this section, we will re-derive the flow equation for the Coulomb form factor  $f_k(p)$ , Eq. (4.34), in an alternative way.

We begin with the generating functional for static correlation functions of Yang-Mills theory in Coulomb gauge, where the Faddeev-Popov determinant has been expressed by a ghost-field integral, see Eqs. (3.6) and (3.5),

$$Z[J, \bar{\sigma}, \sigma] = \int \mathcal{D}A \int \mathcal{D}[\bar{c}c] \exp(-\bar{c}(-\partial\hat{D})c + \bar{\sigma} \cdot c + \bar{c} \cdot \sigma) \exp(-S[A] + J \cdot A) , \quad (4.35)$$

where for the moment we have included only the purely gluonic part into  $S$ . We evaluate the Gaussian ghost field integral by shifting the integration variable

$$c' = -c + (-\partial\hat{D})^{-1}\sigma , \quad \bar{c}' = -\bar{c} + \bar{\sigma}(-\partial\hat{D})^{-1} , \quad (4.36)$$

dropping the prime and using the path integral representation of the Faddeev-Popov determinant

$$\det(-\partial\hat{D}) = \int \mathcal{D}[\bar{c}c] \exp(-\bar{c}(-\partial\hat{D})c) \quad (4.37)$$

which leads to the second form of the generating functional

$$Z[J, \bar{\sigma}, \sigma] = \int \mathcal{D}A \det(-\partial\hat{D}) \exp(-S[A] + \bar{\sigma}(-\partial\hat{D})^{-1}\sigma + J \cdot A). \quad (4.38)$$

This is simply the generating functional where the introduction of the ghost fields has been reversed but the ghost sources kept.

Our aim is to relate the expectation value of two ghost operators  $(-\partial\hat{D})^{-1}$  to the expectation value of four ghost fields, which we will calculate using the flow equation of the ghost form factor. To this end we act with four derivatives w.r.t. the ghost sources on  $Z$  in both forms:

1st form, Eq. (4.35):

$$\frac{\delta^4}{\delta\bar{\sigma}_4\delta\sigma_3\delta\bar{\sigma}_2\delta\sigma_1} Z[J, \bar{\sigma}, \sigma] \Big|_0 = \langle c_4\bar{c}_3c_2\bar{c}_1 \rangle, \quad (4.39)$$

where the number subscripts stand for (adjoint) colour indices and spatial arguments condensed.

2nd form, Eq. (4.38): (showing only the ghost source exponential)

$$\begin{aligned} \frac{\delta}{\delta\sigma_1} e^{\bar{\sigma}(-\partial\hat{D})^{-1}\sigma} &= -\bar{\sigma}(-\partial\hat{D})_1^{-1} e^{\bar{\sigma}(-\partial\hat{D})^{-1}\sigma} \\ \frac{\delta}{\delta\bar{\sigma}_2} &\rightarrow [(-\partial\hat{D})_{21}^{-1} + (\bar{\sigma}(-\partial\hat{D})_1^{-1})((-\partial\hat{D})_2^{-1}\sigma)] e^{\bar{\sigma}(-\partial\hat{D})^{-1}\sigma} \\ \frac{\delta}{\delta\sigma_3} &\rightarrow [\bar{\sigma}(-\partial\hat{D})_3^{-1}(-\partial\hat{D})_{21}^{-1} - (-\partial\hat{D})_{23}^{-1}\bar{\sigma}(-\partial\hat{D})_1^{-1} \\ &\quad - (\bar{\sigma}(-\partial\hat{D})_3^{-1})(\bar{\sigma}(-\partial\hat{D})_1^{-1})((-\partial\hat{D})_2^{-1}\sigma)] e^{\bar{\sigma}(-\partial\hat{D})^{-1}\sigma} \\ \frac{\delta}{\delta\bar{\sigma}_4} &\xrightarrow{\sigma=\bar{\sigma}=0} (-\partial\hat{D})_{43}^{-1}(-\partial\hat{D})_{21}^{-1} - (-\partial\hat{D})_{23}^{-1}(-\partial\hat{D})_{41}^{-1}. \end{aligned} \quad (4.40)$$

This yields

$$\langle c_4\bar{c}_3c_2\bar{c}_1 \rangle = \langle (-\partial\hat{D})_{43}^{-1}(-\partial\hat{D})_{21}^{-1} \rangle - \langle (-\partial\hat{D})_{23}^{-1}(-\partial\hat{D})_{41}^{-1} \rangle. \quad (4.41)$$

Setting the sources to zero already after the second ghost source derivative, we additionally get the useful expression for the ghost propagator

$$\langle c_2\bar{c}_1 \rangle = \langle (-\partial\hat{D})_{21}^{-1} \rangle. \quad (4.42)$$

Now we insert the matrix elements of the negative Laplacian,  $(-\partial^2)_{32}$ , into Eq. (4.41), sum over 3 and 2 and write the condensed indices explicitly as  $4 \equiv (a, \mathbf{x})$ ,  $1 \equiv (b, \mathbf{y})$ , whereupon we can identify one of the terms as the Coulomb kernel  $F[A]$ :

$$\begin{aligned} \langle F[A]^{ab}(\mathbf{x}, \mathbf{y}) \rangle &= \langle F_{41}[A] \rangle = \langle (-\partial\hat{D})_{43}^{-1}(-\partial^2)_{32}(-\partial\hat{D})_{21}^{-1} \rangle \\ &= \langle c_4\bar{c}_3(-\partial^2)_{32}c_2\bar{c}_1 \rangle + \langle (-\partial\hat{D})_{41}^{-1}(-\partial^2)_{32}(-\partial\hat{D})_{23}^{-1} \rangle \\ &= \left\langle c^a(\mathbf{x}) \left( \int d^3x' \bar{c}^c(\mathbf{x}')(-\partial_{\mathbf{x}'}^2)c^c(\mathbf{x}') \right) \bar{c}^b(\mathbf{y}) \right\rangle \\ &\quad + \left\langle [(-\partial\hat{D})^{-1}]_{\mathbf{xy}}^{ab} \int d^3x' [(-\partial^2)(-\partial\hat{D})^{-1}]_{\mathbf{x}'\mathbf{x}'}^{cc} \right\rangle. \end{aligned} \quad (4.43)$$

This shows that there is no simple expression of the Coulomb propagator in terms of ghost field expectation values.

We are going to express the first term on the r.h.s. of Eq. (4.43) in terms of the generating functional of connected Green functions. For this purpose we define the scalar, Grassmann-even operator

$$K := \int d^3x' \bar{c}^c(\mathbf{x}') (-\partial_{\mathbf{x}'}^2) c^c(\mathbf{x}'), \quad (4.44)$$

which is a composite operator that we can add to the source terms of  $Z$  with a scalar source  $s$ ,

$$Z[J, \bar{\sigma}, \sigma, s] = \int \mathcal{D}A \int \mathcal{D}[\bar{c}c] \exp(-\bar{c}(-\partial\hat{D})c + \bar{\sigma} \cdot c + \bar{c} \cdot \sigma) \exp(-S[A] + J \cdot A + sK). \quad (4.45)$$

Taking the appropriate derivatives we obtain

$$\left. \frac{\delta^2}{\delta\bar{\sigma}\delta\sigma} \partial_s Z \right|_0 = -\langle cK\bar{c} \rangle, \quad (4.46)$$

and with  $W = \ln Z$  we get

$$\begin{aligned} \partial_s W &= Z^{-1} \partial_s Z \\ \frac{\delta}{\delta\sigma} \partial_s W &= -Z^{-2} \frac{\delta Z}{\delta\sigma} \partial_s Z + Z^{-1} \frac{\delta}{\delta\sigma} \partial_s Z \\ \left. \frac{\delta^2}{\delta\bar{\sigma}\delta\sigma} \partial_s W \right|_0 &= -Z^{-2} \left. \frac{\delta^2 Z}{\delta\bar{\sigma}\delta\sigma} \partial_s Z \right|_0 + Z^{-1} \left. \frac{\delta^2}{\delta\bar{\sigma}\delta\sigma} \partial_s Z \right|_0, \end{aligned} \quad (4.47)$$

which with Eq. (4.46) yields

$$\left. \frac{\delta^2}{\delta\bar{\sigma}\delta\sigma} \partial_s W \right|_0 = \langle c\bar{c} \rangle \langle K \rangle - \langle cK\bar{c} \rangle. \quad (4.48)$$

In the next step, we establish the relation to the corresponding 1PI-correlation function. The definition of the effective action with cut-off  $k$  in the superfield formalism reads (see Eq. (3.23) and the definitions there)

$$\Gamma_k[\phi, s] = -W_k[I_k[\phi, s], s] + I_k[\phi, s] \bar{\phi} - \frac{1}{2} \bar{\phi} \mathcal{R}_k M \phi, \quad \text{where} \quad \frac{\delta W_k[I_k[\phi, s], s]}{\delta I_k} = \bar{\phi}. \quad (4.49)$$

We take the derivative w.r.t.  $s$  on both sides,

$$\partial_s \Gamma_k[\phi, s] = -\partial_s I_k[\phi, s] \cdot \frac{\delta W_k}{\delta I_k} - \partial_s W_k + \partial_s I_k[\phi, s] \cdot \bar{\phi} = -\partial_s W_k[I_k[\phi, s], s], \quad (4.50)$$

and two ghost field derivatives to get

$$\frac{\delta}{\delta c} \partial_s \Gamma_k = - \left[ \frac{\delta}{\delta c} I_k \right] \frac{\delta \partial_s W_k}{\delta I_k} \quad (4.51)$$

$$\frac{\delta^2}{\delta\bar{c}\delta c} \partial_s \Gamma_k = - \left[ \frac{\delta^2}{\delta\bar{c}\delta c} I_k \right] \frac{\delta \partial_s W_k}{\delta I_k} - \left[ \frac{\delta}{\delta\bar{c}} \bar{I}_k \right] \frac{\delta^2 \partial_s W_k}{\delta \bar{I}_k \delta I_k} \left[ \frac{\delta I_k}{\delta c} \right]^T, \quad (4.52)$$

where derivatives w.r.t. the ghost fields  $\bar{c}$  and  $c$  are to be read as matrix rows and columns respectively. Going to the second line, we have used that in the terms of the scalar product  $\frac{\delta}{\delta c_i} I_k \cdot \frac{\delta \partial_s W_k}{\delta I_k}$  there is always one commuting factor, so we can commute  $\frac{\delta}{\delta c_i} I_k$  past  $\frac{\delta \partial_s W_k}{\delta I_k}$  without a sign. Setting  $s = 0$  and  $\phi = 0$  (which implies  $I_k = 0$ ), the term  $\frac{\delta \partial_s W_k}{\delta I_k}$  vanishes due to global colour symmetry.

What is left to be calculated are the field derivatives of the sources. From Eq. (4.49) we obtain

$$\frac{\delta}{\delta \bar{\phi}} I_k = \frac{\delta^2}{\delta \bar{\phi} \delta \phi} \Gamma_k B + B \mathcal{R}_k, \quad (4.53)$$

where

$$B := \begin{pmatrix} \mathbf{1} & 0 & 0 \\ 0 & 0 & -\mathbf{1} \\ 0 & \mathbf{1} & 0 \end{pmatrix}. \quad (4.54)$$

Using  $\bar{I}_k = B I_k$ , which implies (noting that we regard a single derivative operator as a left index)

$$\frac{\delta}{\delta \bar{\phi}} \bar{I}_k = \frac{\delta}{\delta \bar{\phi}} I_k B^T, \quad (4.55)$$

we are left with

$$\frac{\delta}{\delta \bar{\phi}} \bar{I}_k = \frac{\delta^2}{\delta \bar{\phi} \delta \phi} \Gamma_k + \mathcal{R}_k, \quad (4.56)$$

where  $\mathcal{R}_k^T = \mathcal{R}_k$  has been used. Taking into account that

$$-\frac{\delta}{\delta \bar{c}} \bar{I}_k = \frac{\delta}{\delta \bar{\phi}_2} \bar{I}_k \quad \text{and} \quad \frac{\delta}{\delta c} I_k = \frac{\delta}{\delta \bar{\phi}_3} I_k, \quad (4.57)$$

where the indices indicate the entries in the superfield of Eq. (3.19), Eq. (4.52) turns into

$$\begin{aligned} \frac{\delta^2}{\delta \bar{c} \delta c} \partial_s \Gamma_k \Big|_0 &= \left[ \frac{\delta \bar{I}_k}{\delta \bar{\phi}} \frac{\delta^2 \partial_s W_k}{\delta \bar{I}_k \delta I_k} \left( \frac{\delta I_k}{\delta \bar{\phi}} \right)^T \Big|_0 \right]_{23} \\ &= \left[ \left( \frac{\delta^2 \Gamma_k}{\delta \bar{\phi} \delta \phi} + \mathcal{R}_k \right) \frac{\delta^2 \partial_s W_k}{\delta \bar{I}_k \delta I_k} \left( B^T \frac{\delta^2 \Gamma_k}{\delta \bar{\phi} \delta \phi} + \mathcal{R}_k^T B^T \right) \Big|_0 \right]_{23} \\ &= - \left( -\frac{\delta^2 \Gamma_k}{\delta \bar{c} \delta c} + R_{c,k} \right) \frac{\delta^2 \partial_s W_k}{\delta \bar{\sigma}_k \delta \sigma_k} \left( -\frac{\delta^2 \Gamma_k}{\delta \bar{c} \delta c} + R_{c,k} \right) \Big|_0. \end{aligned} \quad (4.58)$$

Putting Eqs. (4.43), (4.48), and (4.58) together, we obtain

$$\begin{aligned} \langle F[A] \rangle &= \langle (-\partial \hat{D})^{-1} \rangle \frac{\delta^2 \partial_s \Gamma_0}{\delta \bar{c} \delta c} \Big|_0 \langle (-\partial \hat{D})^{-1} \rangle + \langle (-\partial \hat{D})^{-1} \rangle \langle \text{Tr} [(-\partial^2) (-\partial \hat{D})^{-1}] \rangle \\ &\quad + \langle (-\partial \hat{D})^{-1} \text{Tr} [(-\partial^2) (-\partial \hat{D})^{-1}] \rangle. \end{aligned} \quad (4.59)$$

In the last two terms on the r.h.s., the Laplacian is not connected to the external ghost propagators by ghost lines. However, judging from the perturbative expansion of  $\langle F \rangle$ , the opposite is expected. Therefore, there must also be such “ghost-disconnected” terms in the first term on the r.h.s. of Eq. (4.59) to balance the last two terms. We will neglect the last two terms and will account for this neglect later directly in the flow equation for  $\partial_s \delta_{\bar{c}} \delta_c \Gamma_k$  by inserting the  $K$ -operator only into the ghost lines connected with the external ghosts by ghost lines. This amounts to dropping the terms where the Laplacian is not connected to the external ghosts by ghost lines also in the first term on the r.h.s of Eq. (4.59). In the meantime, we denote this procedure by writing  $\partial'_s$  until we plug in the flow equation explicitly. After this treatment, the above equation becomes

$$\langle F \rangle = \langle (-\partial \hat{D})^{-1} \rangle \left. \frac{\delta^2 \partial'_s \Gamma_0}{\delta \bar{c} \delta c} \right|_0 \langle (-\partial \hat{D})^{-1} \rangle. \quad (4.60)$$

On the other hand, we define the Coulomb form factor  $f$  in momentum space as

$$\langle F \rangle(p) = \langle (-\partial \hat{D})^{-1} (-\partial^2) (-\partial \hat{D})^{-1} \rangle(p) =: \langle (-\partial \hat{D})^{-1} \rangle(p) p^2 f(p) \langle (-\partial \hat{D})^{-1} \rangle(p), \quad (4.61)$$

so we get

$$\left. \frac{\delta^2 \partial'_s \Gamma_0}{\delta \bar{c}^a(\mathbf{p}) \delta c^b(\mathbf{q})} \right|_0 = \delta^{ab} p^2 f(p) (2\pi)^3 \delta^3(\mathbf{p} + \mathbf{q}). \quad (4.62)$$

This equation motivates an obvious definition of the  $k$ -dependent Coulomb form factor  $f_k$  such that it becomes amenable to a flow equation treatment:

$$\left. \frac{\delta^2 \partial'_s \Gamma_k}{\delta \bar{c}^a(\mathbf{p}) \delta c^b(\mathbf{q})} \right|_0 =: \delta^{ab} p^2 f_k(p) (2\pi)^3 \delta^3(\mathbf{p} + \mathbf{q}). \quad (4.63)$$

With Eq. (3.32) we get

$$\left. \frac{\delta^2 \Gamma_k(s)}{\delta \bar{c}^a(\mathbf{p}) \delta c^b(\mathbf{q})} \right|_{c=\bar{c}=0} = -\delta^{ab} g \frac{p^2}{d_k(p, s)} (2\pi)^3 \delta^3(\mathbf{p} + \mathbf{q}), \quad (4.64)$$

where there is still the free argument  $s$ . We observe that the equations

$$\begin{aligned} \partial'_s d_k^{-1}(p, s)|_{s=0} &= -\frac{1}{g} f_k(p), \\ \partial'_s \bar{G}_k^{-1}(p, s)|_{s=0} &= -\frac{p^2}{g} f_k(p) \end{aligned} \quad (4.65)$$

hold. We are going to apply these relations to the flow equation of the ghost form factor  $d_k$ , Eq. (3.36), which is unchanged by the inclusion of the operator  $K$  except for an argument  $s$  in each vertex and propagator, which we do not denote,

$$\begin{aligned} \partial_t d_k^{-1}(p) &= N_c \int \frac{d^3 q}{(2\pi)^3} \left[ \left( G_{A,k} \dot{R}_{A,k} G_{A,k} \right) (q) \bar{G}_{c,k}(\mathbf{p} + \mathbf{q}) \right. \\ &\quad \left. + \left( \bar{G}_{c,k} \dot{R}_{c,k} \bar{G}_{c,k} \right) (q) G_{A,k}(\mathbf{p} + \mathbf{q}) \frac{q^2}{(\mathbf{p} + \mathbf{q})^2} \right] (1 - (\hat{\mathbf{p}} \cdot \hat{\mathbf{q}})^2). \end{aligned} \quad (4.66)$$



We act with  $\partial'_s$  on both sides of the equation and set  $s = 0$ . This procedure accounts for the neglect of the last two terms on the r.h.s. of Eq. (4.59), because it means that, taking the derivative  $\partial_s$  on the r.h.s., only the ghost propagators are hit. Thereby we avoid creating closed ghost loops without a ghost-line connection to the two external points, see the discussion below Eq. (4.59). This results in the same flow equation as in Eq. (4.34):

$$\begin{aligned} \partial_t f_k(p) = -N_c \int \frac{d^3q}{(2\pi)^3} & \left[ \left( G_{A,k} \dot{R}_{A,k} G_{A,k} \right) (q) \bar{G}_{c,k}^2(\mathbf{p} + \mathbf{q}) (\mathbf{p} + \mathbf{q})^2 f_k(\mathbf{p} + \mathbf{q}) \right. \\ & \left. + 2\dot{R}_{c,k}(q) \bar{G}_{c,k}^3(q) q^2 f_k(q) G_{A,k}(\mathbf{p} + \mathbf{q}) \frac{q^2}{(\mathbf{p} + \mathbf{q})^2} \right] \\ & (1 - (\hat{\mathbf{p}} \cdot \hat{\mathbf{q}})^2) . \end{aligned} \quad (4.67)$$

## 4.4 The Dyson-Schwinger Equation for the Coulomb Form Factor

As in the case of the flow equations for the gluon and the ghost propagator, see Sec. 3.6, we will at first resort to the replacement of  $f_k$ ,  $\omega_k$ , and  $d_k$  at the cut-off scale  $k$  by their values at zero cut-off  $k = 0$  in the loop integral of Eq. (4.34), i.e.,

$$f_k \rightarrow f_{k=0}, \quad \omega_k \rightarrow \omega_{k=0}, \quad d_k \rightarrow d_{k=0}. \quad (4.68)$$

Although we can apply the same optimization arguments as in the case of the gluon and the ghost propagator, the resulting equation has no solution for the previously found gluon and ghost propagator as input, as will be found. Said replacement allows us to integrate the flow equation analytically. Indeed,

$$\begin{aligned} & \partial_t \left[ N_c \int \frac{d^3q}{(2\pi)^3} \frac{1}{2\omega_0(q) + 2qr_k(q)} \frac{f_0(\mathbf{p} + \mathbf{q})}{(\mathbf{p} + \mathbf{q})^2} \frac{(1 - (\hat{\mathbf{p}} \cdot \hat{\mathbf{q}})^2)}{[d_0^{-1}(\mathbf{p} + \mathbf{q}) + r_k(\mathbf{p} + \mathbf{q})]^2} \right] \\ = - N_c \int \frac{d^3q}{(2\pi)^3} & \frac{2q\dot{r}_k(q)}{[2\omega_0(q) + 2qr_k(q)]^2} \frac{f_0(\mathbf{p} + \mathbf{q})}{(\mathbf{p} + \mathbf{q})^2} \frac{(1 - (\hat{\mathbf{p}} \cdot \hat{\mathbf{q}})^2)}{[d_0^{-1}(\mathbf{p} + \mathbf{q}) + r_k(\mathbf{p} + \mathbf{q})]^2} \\ & - 2N_c \int \frac{d^3q}{(2\pi)^3} \frac{1}{2\omega_0(q) + 2qr_k(q)} \frac{f_0(\mathbf{p} + \mathbf{q})}{(\mathbf{p} + \mathbf{q})^2} \frac{\dot{r}_k(\mathbf{p} + \mathbf{q}) (1 - (\hat{\mathbf{p}} \cdot \hat{\mathbf{q}})^2)}{[d_0^{-1}(\mathbf{p} + \mathbf{q}) + r_k(\mathbf{p} + \mathbf{q})]^3} \end{aligned} \quad (4.69)$$

which is just the r.h.s. of Eq. (4.34) with the approximation of Eq. (4.68) and Eqs. (3.11), (3.31), and (3.33) plugged in (which is explicitly seen after shifting  $\mathbf{q} \rightarrow -\mathbf{q} - \mathbf{p}$  in the 2nd term). Therefore, the integration of Eq. (4.34) over the cut-off momentum  $k$  yields

$$\begin{aligned} f_0(p) - f_\Lambda(p) = N_c \int \frac{d^3q}{(2\pi)^3} & \frac{1}{2\omega_0(q) + 2qr_k(q)} \frac{f_0(\mathbf{p} + \mathbf{q})}{(\mathbf{p} + \mathbf{q})^2} \\ & \frac{1}{[d_0^{-1}(\mathbf{p} + \mathbf{q}) + r_k(\mathbf{p} + \mathbf{q})]^2} (1 - (\hat{\mathbf{p}} \cdot \hat{\mathbf{q}})^2) \Big|_{k=\Lambda}^{k=0}. \end{aligned} \quad (4.70)$$

Separating the ultraviolet regularization, we obtain

$$f_0(p) = f_\Lambda(p) + \frac{N_c}{2} \int \frac{d^3q}{(2\pi)^3} \frac{1}{\omega_0(q)} \frac{f_0(\mathbf{p} + \mathbf{q})}{(\mathbf{p} + \mathbf{q})^2} d_0^2(\mathbf{p} + \mathbf{q}) (1 - (\hat{\mathbf{p}} \cdot \hat{\mathbf{q}})^2) - \left[ N_c \int \frac{d^3q}{(2\pi)^3} \frac{1}{2\omega_0(q) + 2qr_\Lambda(q)} \frac{f_0(\mathbf{p} + \mathbf{q})}{(\mathbf{p} + \mathbf{q})^2} \frac{(1 - (\hat{\mathbf{p}} \cdot \hat{\mathbf{q}})^2)}{[d_0^{-1}(\mathbf{p} + \mathbf{q}) + r_\Lambda(\mathbf{p} + \mathbf{q})]^2} \right]. \quad (4.71)$$

For  $f_\Lambda(p) \equiv 1$ , this is just the Dyson-Schwinger equation obtained in the variational approach [43] (up to the ultraviolet regularization terms in square brackets).

## 4.5 Infrared Analysis

In order to gain information about the infrared behaviour of the Coulomb form factor,  $f(p \rightarrow 0)$ , which is relevant for the long-distance behaviour of the Coulomb potential,  $V_C(r \rightarrow \infty)$ , aside from numerical calculations, which will be presented in Sec. 4.6, we perform infrared analyses on the Dyson-Schwinger equations obtained in Sec. 4.4: firstly, we will use the common method of extending the infrared power laws to the whole momentum range and subsequently scale the momenta. With this method we will find no information about the infrared behaviour of  $f$ ; secondly and more successfully, we will apply the angular approximation.

### 4.5.1 Overall power laws

First, one might proceed in a similar way as in Ref. [92]: making power law ansatzes for the functions occurring in the unregularized Eq. (4.71), taking the infrared exponents as exponents for the whole momentum range and using the bare form factor  $f_\Lambda \equiv 1$ . Then calculating the loop integral exactly, which becomes possible due to the simple power law form of the functions occurring, and making conclusions on the infrared exponents. Explicitly, with the ansatzes (dropping the indices ‘0’)

$$\omega(p) = Ap^{-\alpha}, \quad d(p) = Bp^{-\beta}, \quad f(p) = Cp^{-\gamma}, \quad (4.72)$$

where  $\omega$  and  $d$  obey the infrared power laws previously determined from the corresponding Dyson-Schwinger equations, we get

$$Cp^{-\gamma} = f_\Lambda + \int \frac{d^3q}{(2\pi)^3} \frac{C|\mathbf{p} + \mathbf{q}|^{-\gamma}}{Aq^{-\alpha}(\mathbf{p} + \mathbf{q})^2} B^2|\mathbf{p} + \mathbf{q}|^{-2\beta} (1 - (\hat{\mathbf{p}} \cdot \hat{\mathbf{q}})^2). \quad (4.73)$$

In the ultraviolet, the radial integral behaves like

$$\sim \int dq q^{2+\alpha-2\beta-2-\gamma} = \int dq q^{-\gamma-1}, \quad (4.74)$$

where the sum rule  $\alpha = 2\beta - 1$ , see Eq. (3.42), has been applied. This is convergent in the ultraviolet only on the condition that

$$\gamma > 0. \quad (4.75)$$

Under the assumption that the integral exists, which implies  $\gamma > 0$ , we can rescale the external momentum  $p \rightarrow \lambda p$  with a scale factor  $\lambda > 0$  and substitute the loop momentum  $q \rightarrow \lambda q$  :

$$\lambda^{-\gamma} C p^{-\gamma} = f_{\Lambda} + \lambda^{\alpha-2\beta+1-\gamma} \int \frac{d^3 q}{(2\pi)^3} \frac{C |\mathbf{p} + \mathbf{q}|^{-\gamma}}{A q^{-\alpha} (\mathbf{p} + \mathbf{q})^2} B^2 |\mathbf{p} + \mathbf{q}|^{-2\beta} (1 - (\hat{\mathbf{p}} \cdot \hat{\mathbf{q}})^2) \quad (4.76)$$

For the integral, we plug in Eq. (4.73),

$$\begin{aligned} \lambda^{-\gamma} C p^{-\gamma} &= f_{\Lambda} + \lambda^{-\gamma} (C p^{-\gamma} - f_{\Lambda}) \\ &= f_{\Lambda} (1 - \lambda^{-\gamma}) + \lambda^{-\gamma} C p^{-\gamma} , \end{aligned} \quad (4.77)$$

which leads to

$$\gamma = 0 , \quad (4.78)$$

contradictory to the assumption  $\gamma > 0$  which was necessary for the ultraviolet-convergence of the loop integral. This ansatz is therefore self-contradictory.

In summary, an infrared analysis by extension of the infrared power law behaviour to the whole momentum range fails because of the severe restriction forced on the exponents by the condition of ultraviolet convergence of the integral. One could relax this restriction by keeping (or introducing) the ultraviolet regularization or by using the true ultraviolet behaviour for the functions in the loop integral to make it converge. Then, however, the exact calculation of the integral, which the argument in Ref. [92] relied on, would be impossible. Therefore, another kind of infrared analysis is called for, which will be presented in the next subsection.

## 4.5.2 The angular approximation

An infrared analysis which can be performed also with an explicit ultraviolet regularization is carried out along the lines of Ref. [43]: for  $p \rightarrow 0$  and for a sharp cut-off function  $r_{\Lambda}(p)$  we can write Eq. (4.71) with a single ultraviolet integration cut-off  $\Lambda$ , turning it into (after substituting  $\mathbf{q} \rightarrow -\mathbf{q}$ )

$$f(p) = f_{\Lambda}(p) + I_f(p) \quad (4.79)$$

with

$$I_f(p) = \frac{N_c}{2} \int^{\Lambda} \frac{d^3 q}{(2\pi)^3} [1 - (\hat{\mathbf{p}} \cdot \hat{\mathbf{q}})^2] \frac{d^2(\mathbf{p} - \mathbf{q}) f(\mathbf{p} - \mathbf{q})}{(\mathbf{p} - \mathbf{q})^2 \omega(q)} \quad (4.80)$$

The so-called angular approximation is defined by approximating a function  $h(|\mathbf{p} - \mathbf{q}|)$  under a momentum integral by

$$h(|\mathbf{p} - \mathbf{q}|) = \theta(p - q) h(p) + \theta(q - p) h(q) . \quad (4.81)$$

This approximation has the benefit to render the angular integrals trivial. We can expect it to be a good approximation at least in the limits  $p/q \gg 1$  and  $p/q \ll 1$ .

We will use this approximation for the momentum differences  $\mathbf{p} - \mathbf{q}$  in the loop integral of Eq. (4.80), so we get

$$\begin{aligned} I_f(p) &= \frac{N_c}{8\pi^2} \underbrace{\int_0^\pi d\vartheta \sin^3 \vartheta}_{=4/3} \int_0^\Lambda dq q^2 \frac{1}{\omega(q)} \left[ \theta(p-q) \frac{d^2(p)f(p)}{p^2} + \theta(q-p) \frac{d^2(q)f(q)}{q^2} \right] \\ &= \frac{N_c}{6\pi^2} \left[ \frac{d^2(p)f(p)}{p^2} \int_0^p dq \frac{q^2}{\omega(q)} + \int_p^\Lambda dq \frac{d^2(q)f(q)}{\omega(q)} \right]. \end{aligned} \quad (4.82)$$

To avoid the necessity of evaluating the second integral, we take the  $p$ -derivative of this equation,

$$I'_f(p) = \frac{N_c}{6\pi^2} \frac{d}{dp} \left( \frac{d^2(p)f(p)}{p^2} \right) \int_0^p dq \frac{q^2}{\omega(q)}. \quad (4.83)$$

As we investigate the limit  $p \rightarrow 0$ , we use the infrared power law forms

$$\omega(p) = Ap^{-\alpha}, \quad d(p) = Bp^{-\beta}, \quad f(p) = Cp^{-\gamma} \quad (4.84)$$

and get

$$\begin{aligned} I'_f(p) &= \frac{N_c}{6\pi^2} B^2 C \frac{d}{dp} (p^{-2-2\beta-\gamma}) \frac{1}{A(3+\alpha)} [q^{3+\alpha}]_0^p \\ &= -\frac{N_c}{6\pi^2} \frac{B^2 C}{A} \frac{2+2\beta+\gamma}{2\beta+2} p^{-1-\gamma}, \end{aligned} \quad (4.85)$$

where the sum rule  $\alpha = 2\beta - 1$  of Eq. (3.42) for the infrared exponents of the gluon and ghost propagators has been plugged in. As  $f_\Lambda(p \rightarrow 0) \rightarrow \text{const.}$  for  $p \ll \Lambda$ , the  $p$ -derivative of Eq. (4.79) in the infrared regime is

$$f'(p \rightarrow 0) = I'_f(p \rightarrow 0) \quad (4.86)$$

and therefore

$$\gamma \left( \frac{N_c}{6\pi^2} \frac{B^2}{A} \frac{1}{2\beta+2} - 1 \right) = -\frac{N_c}{6\pi^2} \frac{B^2}{A}. \quad (4.87)$$

The same arguments can be applied to the ghost Dyson-Schwinger equation as has been done in Ref. [43]. This not only led to the sum rule (3.42), which has also been found in Sec. 3.3 using a different line of reasoning, but also to a relation between the prefactors of the infrared power laws and the infrared exponents,

$$\frac{N_c}{6\pi^2} \frac{B^2}{A} = \frac{2\beta(\beta+1)}{\beta+2}. \quad (4.88)$$

Therefore,  $\gamma$  only depends on the infrared exponent of the ghost form factor,

$$\gamma = \beta(\beta+1). \quad (4.89)$$

Under the assumption that this relation between the infrared exponents also holds in the case without the angular approximation, we will analyze for which values of  $\beta$  the original integral (4.80) exists at all. Because of the cut-off  $\Lambda$ , the convergence of the integral in the ultraviolet is guaranteed. Due to the power law ansatzes there might be a pole at  $\mathbf{q} = 0$ . However, this pole is integrable if  $3 + \alpha > 0$ , in view of Eq. (3.42) becoming  $\beta > -1$ , which is always true if the horizon condition  $\beta > 0$  is fulfilled. To examine the possible pole at  $\mathbf{q} = \mathbf{p}$ , we make the transformation  $\mathbf{q} \rightarrow \mathbf{q} - \mathbf{p}$  (note that the expression  $(1 - (\hat{\mathbf{p}} \cdot \hat{\mathbf{q}})^2)/(\mathbf{p} - \mathbf{q})^2$  is invariant under this momentum shift):

$$I_f(p) = \frac{N_c}{2} \int^{\Lambda} \frac{d^3q}{(2\pi)^3} \frac{d^2(q)}{\omega(\mathbf{p} - \mathbf{q})} f(q) \frac{1 - (\hat{\mathbf{p}} \cdot \hat{\mathbf{q}})^2}{(\mathbf{p} - \mathbf{q})^2}. \quad (4.90)$$

The pole, now at  $\mathbf{q} = 0$ , is integrable if  $3 - 2\beta - \gamma > 0$ , which means

$$\gamma < 3 - 2\beta. \quad (4.91)$$

If this is fulfilled, our line of reasoning leading to  $\gamma = \beta(\beta + 1)$  is valid, imposing the condition

$$\beta(\beta + 1) < 3 - 2\beta \quad (4.92)$$

on  $\beta$ , which becomes

$$\frac{1}{2}(-3 - \sqrt{21}) < \beta < \frac{1}{2}(-3 + \sqrt{21}) \quad (4.93)$$

or

$$-3.791 < \beta < 0.791, \quad (4.94)$$

i.e., for values of  $\beta$  outside this range the integral in the  $f$ -equation does not exist, for values inside it does exist and we have  $\gamma = \beta(\beta + 1)$ . In particular, the integral (4.80) in the  $f$ -equation does not exist for the values of  $\beta = 1$  and  $\beta = 0.796$  which have been found as two possible infrared exponents in an analytical infrared analysis of the Dyson-Schwinger equations in Ref. [49], and numerically in Refs. [43] and [50].

Note, however, that in a numerical treatment of Eq. (4.70) without the angular approximation, solutions will be found only for the stricter condition  $\beta \lesssim 0.5$ , see Fig. 4.11.

We may ask which value of  $\beta$ , in the present framework of the angular approximation, leads to a linearly rising Coulomb potential at large distances. To achieve this, the Fourier transform  $F(p)$  of the Coulomb potential must behave as

$$F(p \rightarrow 0) \sim p^{-4} \quad (4.95)$$

in the infrared. Recalling the definition (4.16) of the Coulomb form factor  $f$  via

$$F(p) = \frac{1}{g^2} \frac{1}{p^2} d^2(p) f(p), \quad (4.96)$$

we obtain an infrared behaviour of

$$F(p \rightarrow 0) \sim p^{-2-2\beta-\gamma} = p^{-2-3\beta-\beta^2} \stackrel{!}{=} p^{-4} \quad (4.97)$$

leading to

$$\beta_{1/2} = -\frac{1}{2} (3 \pm \sqrt{17}) \quad \text{or} \quad \beta_1 = -3.562, \beta_2 = 0.562. \quad (4.98)$$

Sticking to the horizon condition, we conclude that an infrared exponent of  $\beta \sim 0.56$  will produce a linearly rising confinement potential, a value considerably smaller than found so far in analytical and numerical studies, see again Refs. [43, 49, 50]. Note that for such a value of  $\beta$  the angular approximation will not be reliable anylonger, compare Fig. 4.11 to Fig. 4.12.

Without the angular approximation, in view of Fig. 4.11, no infrared strength greater than

$$F(p \rightarrow 0) \sim p^{-2-2\beta-\gamma} \sim p^{-3.75} \quad (4.99)$$

can build up. This holds true, however, only for the DSE for  $f$  but not for the flow equation.

### 4.5.3 Assessment of the angular approximation

In Subsec. 4.5.2 we have used the angular approximation to determine the infrared behaviour of the Coulomb form factor  $f$ . In this subsection we will assess the reliability of this approximation by applying it to a similar integral whose exact value is known. We will find a deviation of less than 5 percent in the parameter range this assessment can be carried out for.

We consider the integral in Eq. (4.80) with  $\Lambda \rightarrow \infty$  and the parameterizations of Eq. (4.72):

$$I_f(p) = \frac{N_c B^2 C}{2 A} \int \frac{d^3 q}{(2\pi)^3} \frac{1 - (\hat{\mathbf{p}} \cdot \hat{\mathbf{q}})^2}{|\mathbf{p} - \mathbf{q}|^{2\beta+\gamma+2} |\mathbf{q}|^{-\alpha}}. \quad (4.100)$$

Without the ultraviolet cut-off  $\Lambda$  we have to demand

$$\gamma > 0 \quad (4.101)$$

to ensure the ultraviolet convergence of the integral (the sum rule  $\alpha = 2\beta - 1$  is understood). For convergence at the two poles we demand

$$\alpha > -3, \text{ i.e., } \beta > -1 \quad \text{and} \quad 2\beta + \gamma < 3. \quad (4.102)$$

the last condition is seen by shifting  $\mathbf{q} \rightarrow \mathbf{q} + \mathbf{p}$  in the integral. This integral can be calculated by writing it as a sum of two integrals both evaluated in Appendix D

(along with the function  $K(\beta, \gamma)$ ),

$$\begin{aligned}
I_f(p) &= \frac{N_c B^2 C}{2 A} \left( \int \frac{d^3 q}{(2\pi)^3} (|\mathbf{q} - \mathbf{p}|^{-2\beta-\gamma-2} |\mathbf{q}|^\alpha) \right. \\
&\quad \left. - \frac{1}{\mathbf{p}^2} \int \frac{d^3 q}{(2\pi)^3} ((\mathbf{p} \cdot \mathbf{q})^2 |\mathbf{q} - \mathbf{p}|^{-2\beta-\gamma-2} |\mathbf{q}|^{\alpha-2}) \right) \\
&= \frac{N_c B^2 C}{2 A} \left[ \theta_0(-\alpha/2, \beta + \gamma/2 + 1) - \frac{1}{\mathbf{p}^2} \theta_2(-\alpha/2 + 1, \beta + \gamma/2 + 1) \right] \\
&= \frac{N_c B^2 C}{2 A} \frac{K(\beta, \gamma)}{(4\pi)^{3/2}} p^{-\gamma},
\end{aligned} \tag{4.103}$$

to the expense, however, that the parameter range has to be further restricted to

$$2\beta + \gamma < 1 \tag{4.104}$$

because both integrands are more divergent at  $\mathbf{q} = \mathbf{p}$  by a pole of the order 2 than is their difference.

On the other hand, the momentum derivative of the same integral has been calculated in Eq. (4.85) using the angular approximation (the ultraviolet cut-off  $\Lambda$  drops out by virtue of the derivative). Imposing the same UV asymptotics as for the exact integral,  $I_f(p \rightarrow \infty) = 0$ , this yields

$$I_f^{ang}(p) = \frac{N_c B^2 C}{6\pi^2 A} \frac{2 + 2\beta + \gamma}{(2\beta + 2)\gamma} p^{-\gamma}. \tag{4.105}$$

Therefore, the error made by using the angular approximation is

$$\frac{I_f^{ang}(p)}{I_f(p)} = \frac{4}{3\sqrt{\pi}} \frac{2 + 2\beta + \gamma}{K(\beta, \gamma)\gamma(\beta + 1)}. \tag{4.106}$$

This function is shown in Fig. 4.1, restricted to the parameter range of interest ( $\beta > 0$ , the horizon condition). The angular approximation turns out to be quite accurate, overestimating the exact value by less than 5 per cent throughout the parameter range. The numerical computations will indeed show that for  $\beta < 0.3$  the angular approximation yields good results, see Fig. 4.13. Note, however, that values of  $\beta > 0.3$  (with  $\gamma = \beta(\beta + 1)$ ) lie beyond the scope of the error estimate of this subsection. The numerical computations will show that the deviation from the value of  $\gamma$  computed using the angular approximation,  $\gamma = \beta(\beta + 1)$ , grows with  $\beta$  until at  $\beta \sim 0.5$  no power-law solution is possible any longer, see Fig. 4.11. Note also that it is not possible to use the exact value of the integral  $I_f(p)$  for an infrared analysis directly because the removal of the ultraviolet cut-off  $\Lambda$  enforces the condition  $\gamma > 0$  to ensure the ultraviolet convergence of the integral, which together with the ansatz of power laws on the whole momentum range leads to a contradiction in the equation for  $f$ , see Subsec. 4.5.1.

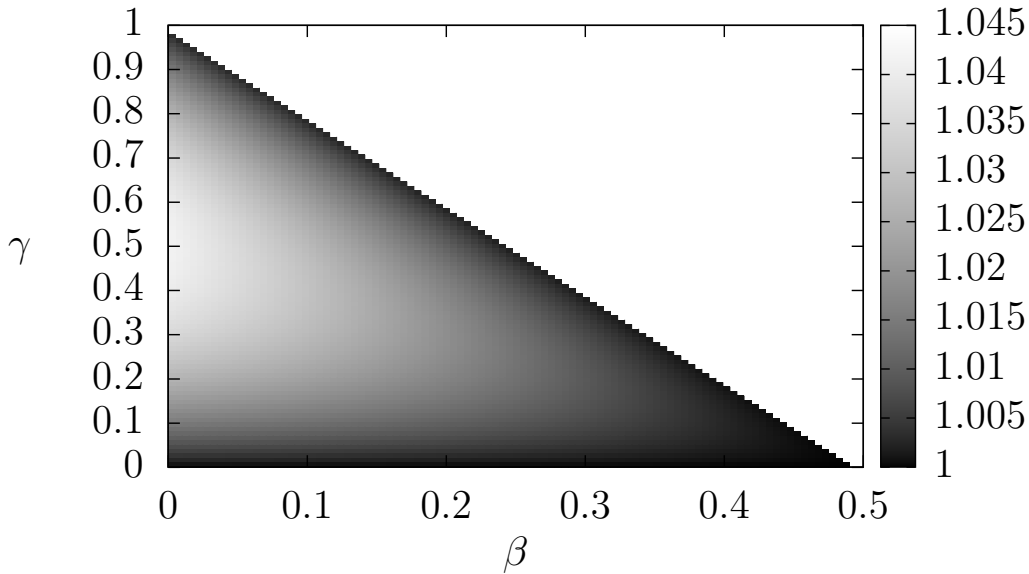


**Figure 4.1:** The error  $I_f^{ang}(p)/I_f(p)$  of the angular approximation with respect to its exact value, see Eq. (4.106), for those parameters  $\gamma$  and  $\beta$  where the exact value of the integral is known. The angular approximation turns out to be quite accurate, overestimating the exact value by less than 5 per cent throughout the parameter range.

## 4.6 Numerical Solutions

Both the full flow equation as well as the Dyson-Schwinger equation will be solved numerically using two different algorithms. First, the full flow equation will be solved iteratively after turning it into an integral equation in the same way as the flow equations for the gluon and ghost propagators, see Chap. 3. For the Dyson-Schwinger equation no solution could be found in this way because the iteration procedure does not converge unless the angular approximation is used; it has therefore been solved by turning it into a system of linear equations, which is possible because of the special structure of this equation.

### 4.6.1 Iterative solution of the flow equation

We will solve Eq. (4.34) numerically by integrating the flow and performing the iteration procedure as in Chap. 3. For this, we need the initial condition  $f_\Lambda$ . Because Eq. (4.34) is linear and homogeneous in  $f$ , it fixes  $f_k(p)$  only up to a multiplicative constant. This constant is chosen by considering the asymptotic value  $f_{k=0}(p \rightarrow \infty) = 1$ , which is known due to asymptotic freedom. In the numerical implementation we therefore set

$$f_{k_{min}}(p_{max} = \Lambda) \stackrel{!}{=} 1 \quad (4.107)$$

after each iteration step by adjusting  $f_\Lambda$ . The results are shown in Fig. 4.2. In the



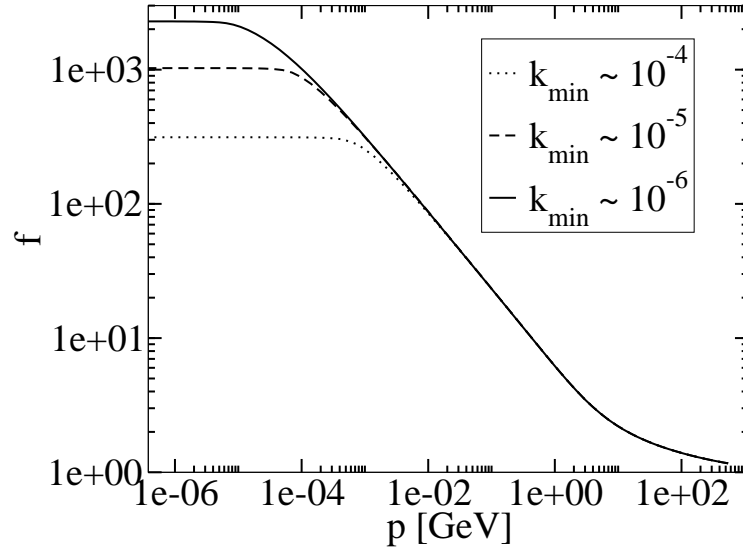


**Figure 4.2:** The Coulomb form factor  $f$  for three different values of  $k_{min}$  down to which the flow has been integrated. The input into the flow equation for  $f_k(p)$  are the flows of the gluon and ghost propagator,  $\omega_k(p)$  and  $d_k(p)$ , from the approximation without tadpoles in Sec. 3.5.

infrared,  $f(p)$  behaves as

$$f(p \rightarrow 0) \sim p^{-0.57}. \quad (4.108)$$

Together with the infrared behaviour  $d(p \rightarrow 0) \sim p^{-0.64}$ , this yields for the Coulomb potential, see Eq. (4.16),

$$F(p \rightarrow 0) \sim p^{-3.85}, \quad (4.109)$$

which results in an almost linearly rising Coulomb potential at large distances: a linear rise would be  $F(p) \sim p^{-4}$  in momentum space, see Eq. (4.11).

For Eq. (4.70), however, an iterative solution was not successful because no convergence could be achieved. Nevertheless, in order to use as input into the flow equation of the Coulomb form factor the ghost and the gluon propagators which have been calculated including tadpole terms, we set these propagators as infrared boundary conditions,  $\omega_{k_{min}}(p)$  and  $d_{k_{min}}^{-1}(p)$ , for the flow equations for  $\omega_k(p)$  and  $d_k(p)$ , and again solve these flow equations:

$$\omega_k(p) = \omega_{k_{min}}(p) + \int_{k_{min}}^k dk' I_\omega(k', p), \quad d_k^{-1}(p) = d_{k_{min}}^{-1}(p) + \int_{k_{min}}^k dk' I_d(k', p). \quad (4.110)$$

The so obtained  $\omega_k(p)$  and  $d_k(p)$  are plugged into Eq. (4.34), solving it iteratively as before. The result is shown in Fig. 4.3. We find an infrared behaviour of

$$f(p \rightarrow 0) \sim p^{-0.65}. \quad (4.111)$$

Together with the infrared behaviour of  $d(p \rightarrow 0) \sim p^{-0.80}$  for the ghost form factor from the optimized flow, see Eq. (3.52), this yields for the Coulomb potential, see

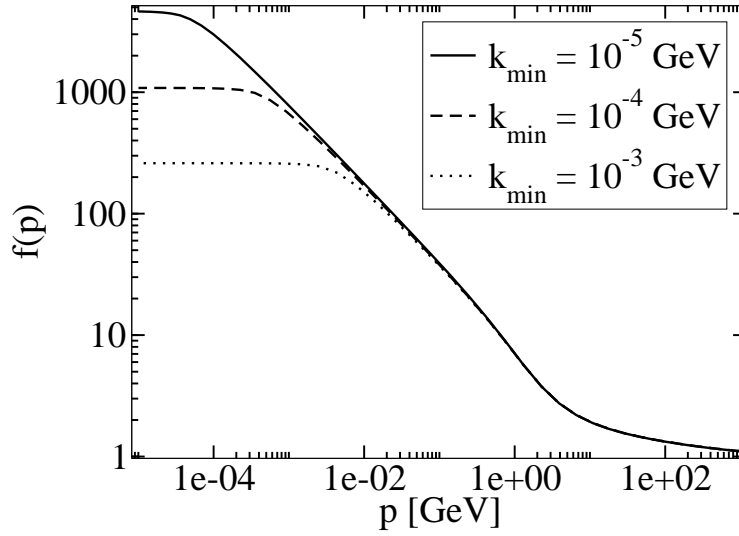


**Figure 4.3:** Like Fig. 4.2 but with gluon and ghost input from the approximation with inclusion of the tadpoles in Sec. 3.6.

Eq. (4.16),

$$F(p \rightarrow 0) \sim p^{-4.25}, \quad (4.112)$$

which rises slightly more than linearly at large distances.

### 4.6.2 Solution of the DSE based on matrix inversion

For the Dyson-Schwinger equation (4.70), a direct, i.e., non-iterative method of solving can be applied by turning it into a system of linear equations, which is possible because it is an inhomogeneous Fredholm integral equation: first, we perform the coordinate change  $\mathbf{q} \rightarrow \mathbf{q} - \mathbf{p}$  to get (dropping the indices ‘0’)

$$f(p) = f_\Lambda(p) + \int \frac{d^3q}{(2\pi)^3} \left[ \frac{N_c}{2} \frac{d^2(q)}{\omega(\mathbf{p} - \mathbf{q})} - N_c \frac{1}{[2\omega(\mathbf{p} - \mathbf{q}) + 2|\mathbf{p} - \mathbf{q}|r_\Lambda(\mathbf{p} - \mathbf{q})][d^{-1}(q) + r_\Lambda(q)]^2} \right] \frac{1 - (\hat{\mathbf{p}} \cdot \hat{\mathbf{q}})^2}{(\mathbf{p} - \mathbf{q})^2} f(q), \quad (4.113)$$

such that no extrapolation of  $f$  beyond its representation range is necessary. This can be rewritten as

$$f(p) = f_\Lambda(p) + \int_{q_{IR}}^{q_{UV}} dq \tilde{M}(p, q) f(q), \quad (4.114)$$

where

$$\tilde{M}(p, q) = \frac{N_c}{(2\pi)^2} \int_{-1}^1 dx \frac{q^2(1-x^2)}{q^2 + p^2 - 2pqx} \left[ \frac{d^2(q)}{2\omega(q^2 + p^2 - 2pqx)} - \frac{1}{[2\omega(q^2 + p^2 - 2pqx) + 2r_\Lambda(q^2 + p^2 - 2pqx)\sqrt{q^2 + p^2 - 2pqx}][d^{-1}(q) + r_\Lambda(q)]^2} \right], \quad (4.115)$$

with  $x := \hat{\mathbf{p}} \cdot \hat{\mathbf{q}}$ . As shown in Appendix C.2, we approximate the momentum integration by a sum over Gauss-Legendre nodes according to

$$\int_{x_1}^{x_2} f(x) dx \approx \sum_{i=1}^N w_i f(x_i). \quad (4.116)$$

We need to know  $f$  only on a Gauss-Legendre grid so we can drop the Chebyshev representation entirely. Eq. (4.114) then becomes

$$f(p_i) = f_\Lambda(p_i) + \sum_{j=1}^N w(q_j) \tilde{M}(p_i, q_j) f(q_j) =: f_\Lambda(p_i) + \sum_{j=1}^N M(p_i, q_j) f(q_j) \quad (4.117)$$

or

$$(\mathbb{1} - M)\mathbf{f} = \mathbf{f}_\Lambda \quad (4.118)$$

where

$$\mathbf{f} = (f(p_1), \dots, f(p_N)) \quad \text{and} \quad M_{ij} = M(p_i, p_j). \quad (4.119)$$

This system of linear equations is solved using Crout's algorithm with  $f_\Lambda(p_i) = 1$  and with gluon and ghost from the optimized flow as input, which have the infrared exponents of Eq. (3.52), i.e.,  $\omega(p \rightarrow 0) \sim p^{-0.6}$  and  $d(p \rightarrow 0) \sim p^{-0.8}$ . The results are shown in Figs. 4.4 and 4.5.

The Coulomb form factor  $f$  shows an oscillation around zero whose amplitude grows towards the infrared. This result has been used as the starting value of the iterative solving method. It is observed that the iteration diverges towards higher or lower function values depending on initial inaccuracies. This indicates that the above obtained solution is an unstable fixed point of the iterative solving procedure, thereby explaining its failure in the present case. Taking  $q_{IR} \rightarrow 0$ , the amplitude of the oscillation becomes larger and  $f$  changes not only in the infrared but over the whole momentum range. Therefore, there seems to be no finite solution to Eq. (4.113) in this limit.

In contrast, setting  $d(p) = 1$  in Eq. (4.113), we obtain an almost constant Coulomb form factor  $f$  as previously found in Ref. [43], see Fig. 4.6. A logarithmic ultraviolet behaviour is observed.

Using this solving method, the dependence of the Coulomb form factor  $f$  on the infrared behaviour of the gluon two-point function  $\omega$  and the ghost propagator dressing function  $d$  can be examined. The functions  $\omega$  and  $d$  are used as input into

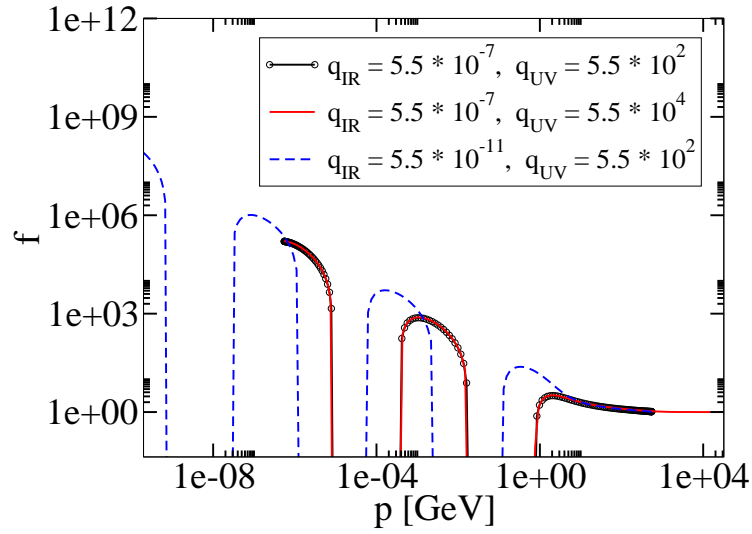


**Figure 4.4:** The Coulomb form factor  $f$  obtained from Eq. (4.113) for different boundaries  $q_{IR}$  and  $q_{UV}$  of the radial loop integral. The oscillation amplitude becomes larger as  $q_{IR}$  is lowered, and there are also modifications to  $f$  at momenta much higher than  $q_{IR}$ . This indicates that there is no finite solution to Eq. (4.113) for  $q_{IR} \rightarrow 0$ . In contrast, an increase of the upper boundary  $q_{UV}$  renders no modifications.

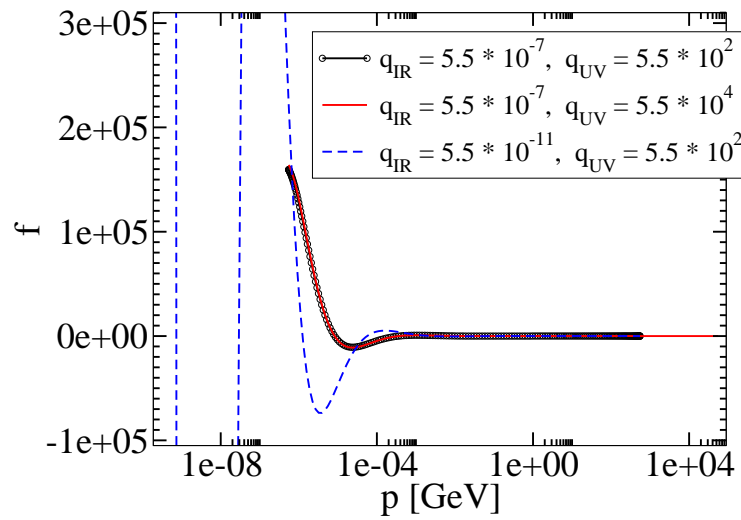


**Figure 4.5:** Like Fig. 4.4 but in a half-logarithmic plot.

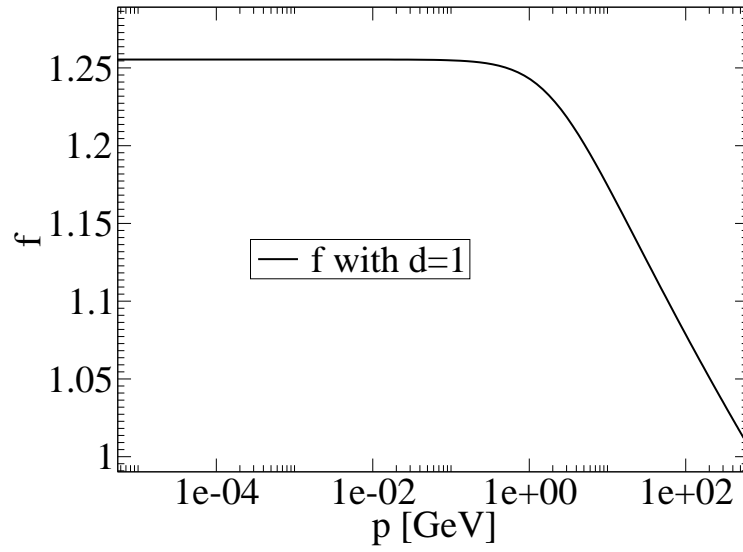


**Figure 4.6:** The Coulomb form factor  $f$  as a solution of Eq. (4.113) with  $d \equiv 1$  in a half-logarithmic plot. The logarithmic ultraviolet behaviour is explicitly seen as a linear descent in this plot.

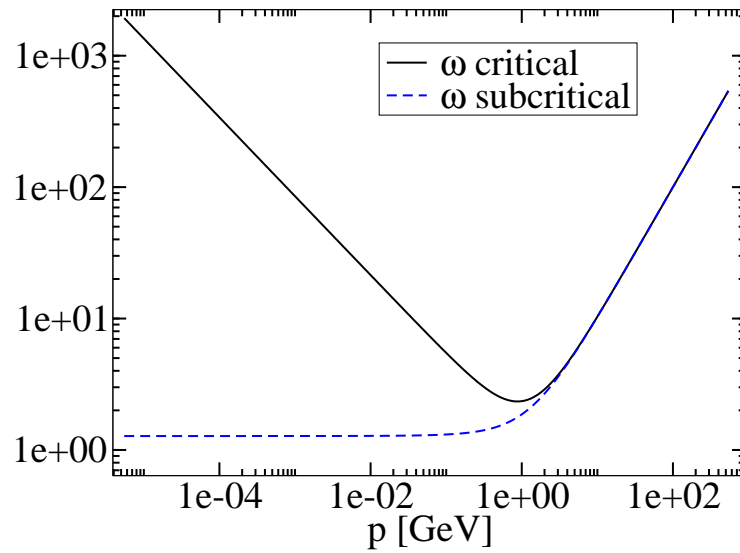


**Figure 4.7:** The gluon two-point function  $\omega$  as determined in Sec. 3.6 from an optimized flow equation, in its original critical form as well as in a modified subcritical form.

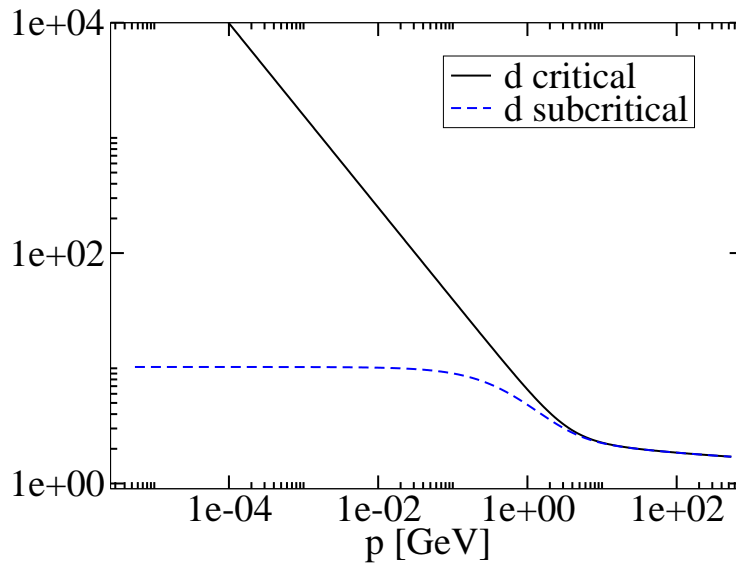


**Figure 4.8:** The ghost propagator dressing function  $d$  as determined in Sec. 3.6 from an optimized flow equation, in its original critical form as well as in a modified subcritical form.

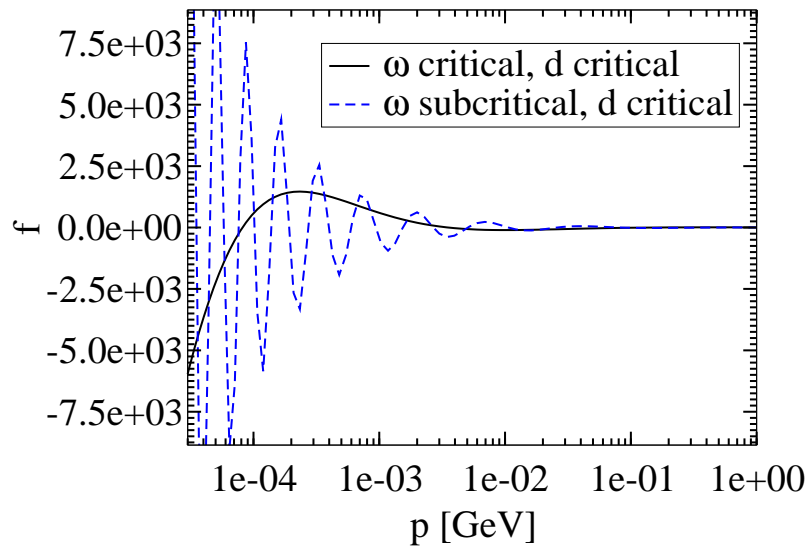
Eq. (4.113) in their original critical form as above, as well as in a modified form with a subcritical infrared behaviour. Both forms are shown in Figs. 4.7 and 4.8. Similar solutions have been found in Ref. [51].

Figure 4.9 shows that in the case where the critical, strongly divergent ghost form factor  $d$  is present, the oscillation of  $f$  cannot be mitigated or even avoided by a subcritical gluon two-point function  $\omega$ . On the contrary, a subcritical  $\omega$  further aggravates the oscillations concerning both their amplitude and their frequency, which points to the fact that (because it is  $\omega^{-1}$  that enters the equation) a larger integral kernel favours an oscillating behaviour of the solution  $f$ . In contrast, a subcritical ghost form factor  $d$  results in a non-oscillating and even infrared-constant Coulomb form factor  $f$  in both cases, see Fig. 4.10. Also in this case, different infrared behaviours of  $\omega$  only effect quantitative changes in the resulting  $f$ .

In the preceding analysis of Eq. (4.113) we have focussed on subcritical gluon and ghost propagators as input functions, namely those violating the scaling relation (3.42) between the infrared exponents. Now both the gluon as well as the ghost propagator are chosen critical: the infrared exponent  $\beta$  of the ghost form factor  $d$  is varied while  $\alpha$ , the infrared exponent of  $\omega$ , is adjusted according to

$$\alpha = 2\beta - 1. \quad (4.120)$$

Likewise, the infrared coefficient  $A$  of the gluon correlator  $\omega$  is chosen to fulfil Eq. (4.88) for given  $B$ . Equation (4.113) has been solved using the matrix inversion method as before and the infrared exponent  $\gamma$  of  $f$  has been determined wherever possible. The result is displayed in Fig. 4.11. Up to a value of  $\beta \sim 0.5$  there is no oscillation of  $f$  although for  $\beta = 0.475$  there is already a deviation (apart from



**Figure 4.9:** The Coulomb form factor  $f$  as solution of Eq. (4.113). For the critical and strongly infrared divergent ghost form factor  $d$ , see Fig. 4.8, an oscillating behaviour of  $f$  is obtained, regardless of the infrared behaviour of  $\omega$  as shown in Fig. 4.7.

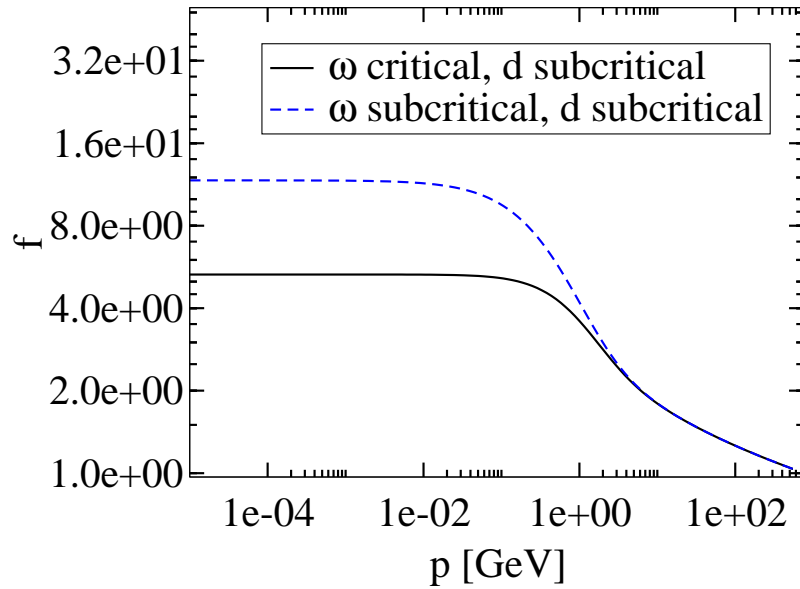


**Figure 4.10:** The Coulomb form factor  $f$  as solution of Eq. (4.113). For a subcritical ghost form factor  $d$ , see Fig. 4.8, a non-oscillating and even constant infrared-behaviour of  $f$  is obtained, regardless of the infrared behaviour of  $\omega$  as shown in Fig. 4.7.

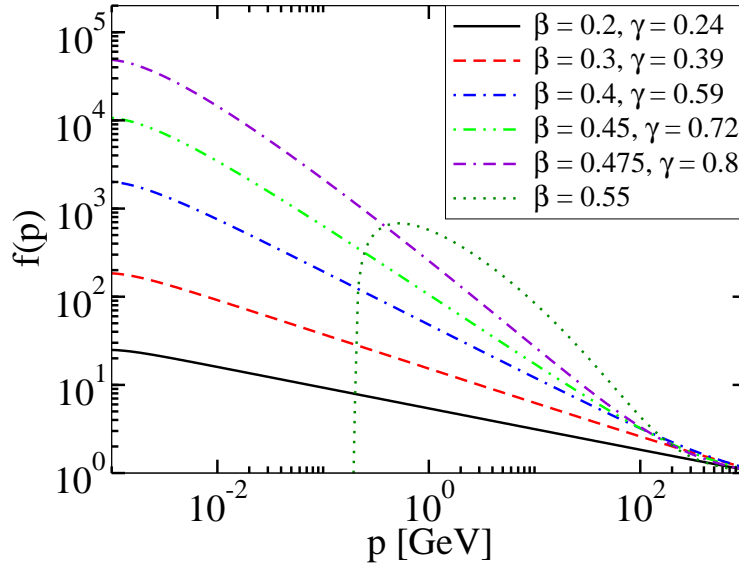


**Figure 4.11:** The Coulomb form factor  $f$  as solution of Eq. (4.113) for critical  $\omega$  and critical  $d$  whose infrared exponents  $\alpha$  and  $\beta$ , obey the sum rule  $\alpha = 2\beta - 1$  and whose infrared coefficients  $A$  and  $B$  fulfil Eq. (4.88). The transition to an oscillating behaviour of  $f$  takes place around the point where the Coulomb potential is about to become “overconfining”, i.e., where  $F(p)$  rises steeper than  $p^{-4}$  in the infrared. This happens roughly for  $\beta \sim 0.5$ .

fringe effects) of the infrared behaviour of  $f$  from a power law (therefore, the value of  $\gamma \sim 0.8$  is only an estimate.) The transition to an oscillating  $f$  for growing  $\beta$  is marked by a sign change of  $\det(\mathbb{1} - M)$ , which becomes negative for growing  $\beta$  at about  $\beta \sim 0.5$ .

Note that unlike in the case of Eq. (4.94), where the relations between the infrared exponents found from the angular approximation are used to determine the range of existence of the original integral without the angular approximation, here the reason that Eq. (4.113) ceases having a non-oscillating solution for growing  $\beta$  is not a possible infrared divergence of the loop integral. In the infrared, the radial part of the integral in Eq. (4.113) behaves as

$$\sim \int dq q^{2-2\beta-\gamma}, \quad (4.121)$$

which for the steepest non-oscillating solution  $\beta = 0.475$ ,  $\gamma \sim 0.8$  (see Fig. 4.11) becomes

$$\sim \int dq q^{0.25}, \quad (4.122)$$

so there is not even an infrared pole in the integrand, still less a divergence.

The Coulomb potential in the infrared behaves as

$$F(p) \sim \frac{d(p)^2 f(p)}{p^2} \underset{p \rightarrow 0}{\sim} p^{-2\beta-\gamma-2}. \quad (4.123)$$



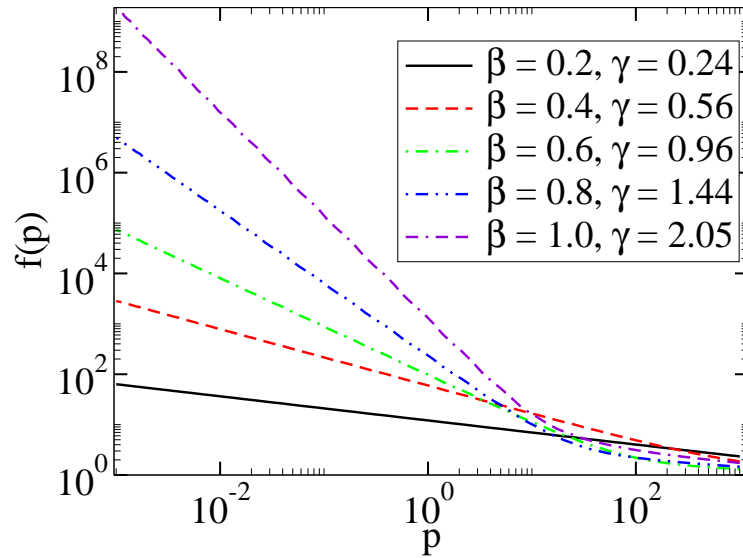


**Figure 4.12:** The Coulomb form factor  $f$  resulting from the iterative solution of Eq. (4.70) with angular approximation (4.81) is shown for different ghost and gluon propagators as input functions.  $\alpha$  has been determined according to the sum rule  $\alpha = 2\beta - 1$  for different values of  $\beta$ . The infrared coefficients  $A$  and  $B$  have been chosen to fulfil Eq. (4.88). It is seen that the result obeys an infrared power law over a wide range of different values of  $\beta$ . Moreover, the infrared exponent  $\gamma$  of the Coulomb form factor  $f$  with high accuracy fulfils the relation  $\gamma = \beta(\beta + 1)$  found in the infrared analysis, see Eq. (4.89).

see Eq. (4.16). If the Coulomb potential in position space is to rise linearly for large distances,  $V(r \rightarrow \infty) \sim r$ ,  $F(p)$  must behave like  $F(p \rightarrow 0) \sim p^{-4}$ , Eq. (4.11). For a value of  $\beta = 0.475$  we get  $-2\beta - \gamma - 2 = -3.75$ . Therefore, the transition of  $f$  to an oscillating behaviour occurs just before the point where the Coulomb potential is about to become “overconfining”, i.e., rising steeper than linearly at large distances.

This analysis shows that even if both  $\omega$  and  $d$  have critical infrared behaviour, with infrared exponents small enough a non-oscillating behaviour of  $f$  will result. Therefore, not criticality in itself, but a size of the infrared exponents too large prevents the  $f$ -equation from having a non-oscillating solution.

### 4.6.3 Iterative solution of the Dyson-Schwinger equation with the angular approximation

In contrast to the original Dyson-Schwinger equation for the Coulomb form factor  $f$ , Eq. (4.70), a solution can be found iteratively if the angular approximation (4.81) is used. Figure 4.12 shows the result for ghost and gluon propagators chosen again as explained at Eq. (4.120). It is seen that the result obeys an infrared power law over a wide range of different values of  $\beta$ . Moreover, the infrared exponent  $\gamma$  of the Coulomb form factor  $\beta$  fulfils Eq. (4.89),  $\gamma = \beta(\beta + 1)$ , found in the infrared

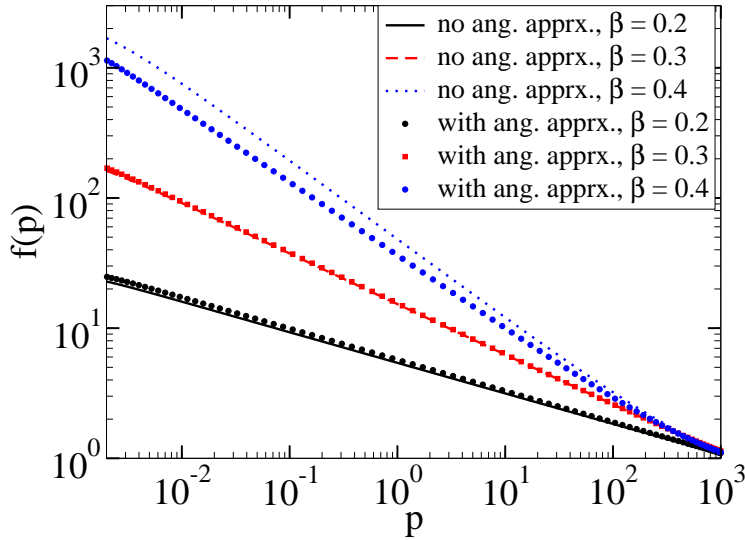


**Figure 4.13:** The Coulomb form factor  $f$  as solution of Eq. (4.70) with and without the angular approximation (4.81) is shown for small values of  $\beta$ . It is observed that for these small values of  $\beta$  the angular approximation indeed provides a good estimate, see also Fig. 4.1.

analysis, with great accuracy.

Compared to the original equation, the equation with the angular approximation is more benign because important contributions to the integral around  $\mathbf{q} = \mathbf{p}$  are neglected. This does not take much effect for small  $\beta$  as can be seen in a direct comparison of the solutions with and without the angular approximation in Fig. 4.13. For larger values of  $\beta$  these contributions become more and more important until for  $\beta \gtrsim 0.5$  the character of the solution changes to an oscillating behaviour.

In summary, we have derived a flow equation for the Coulomb form factor from the ghost form factor in two different ways with the same result. This flow equation has been solved with the flows of the ghost form factor and the gluon propagator as input. We have seen that the FRG is well suited to calculate the colour Coulomb potential: with the gluon and ghost propagators from the flow equations without tadpoles as input,  $\omega(p \rightarrow 0) \sim p^{-0.28}$  and  $d(p \rightarrow 0) \sim p^{-0.64}$ , we have obtained  $V_C(p \rightarrow 0) \sim p^{-3.85}$ . With the propagators from the optimized flow,  $\omega(p \rightarrow 0) \sim p^{-0.60}$  and  $d(p \rightarrow 0) \sim p^{-0.80}$ , we have even found  $V_C(p \rightarrow 0) \sim p^{-4.25}$ . This is an important result because a confining static quark potential implies a confining colour Coulomb potential [90], but an infrared exponent  $\alpha_F < 4$  of the colour Coulomb potential  $V_C(p \rightarrow 0) \sim p^{-\alpha_F}$  would lead to a  $V_C$  which rises weaker than linearly in position space, thereby excluding a linear static quark potential.

In contrast, the corresponding DSE for the Coulomb form factor has no non-oscillating solution for values of  $\beta \gtrsim 0.5$ , i.e., for all values found so far in various approaches, which has been shown using a solution method based on matrix inversion. Only for subcritical ghost form factor inputs or for critical inputs with a very

mild infrared divergence of the ghost form factor a solution is found. Such a weakly infrared divergent scaling solution for the propagators, however, has not been found. This method also shows that the angular approximation, although very accurate for values of  $\beta < 0.3$ , fails for higher values of  $\beta$ , which are those found so far. An analytical infrared analysis has been performed which has confirmed the numerical findings in its range of reliability.



# Chapter 5

## The Quark Propagator

Until now we have considered the pure gauge sector of Yang-Mills theory. Hadrons, however, which QCD is expected to describe, are also composed of quarks. Therefore, we will include quark fields into the present formalism in this chapter.

Besides confinement, the breaking of chiral symmetry is an outstanding feature of QCD: while the explicit chiral symmetry breaking by the current quark masses in the Lagrangian is very small, the dynamic chiral symmetry breaking by quantum corrections is the decisive mechanism which gives mass to the baryons. We use two quantities in order to show this generation of mass: a suitably defined mass function  $M(p)$  and the chiral condensate  $\langle\bar{\psi}\psi\rangle$ , which both can be calculated from the static quark propagator.

The two limits of the mass function in the UV and in the IR describe the current quark mass and the constituent quark mass, respectively:  $M(p \rightarrow \infty) = m$  and  $M(p \rightarrow 0) = M_{constit.} \sim 300$  MeV. The value of the chiral condensate can be inferred from the Gell-Mann-Oakes-Renner relation,  $(m_u + m_d)\langle\bar{\psi}\psi\rangle = -f_\pi^2 m_\pi^2$ , see Ref. [93] and the pedagogical introduction of Ref. [94]. Here,  $f_\pi \sim 92$  MeV is the pion decay constant,  $m_\pi \sim 135$  MeV is the pion mass, and  $m_u + m_d \sim 13$  MeV is the sum of the current masses of the up- and the down-quark. Moreover, we have set  $\langle\bar{\psi}\psi\rangle = \langle\bar{u}u\rangle \sim \langle\bar{d}d\rangle$ , which holds because of isospin symmetry. Accordingly, we expect a chiral condensate of about  $\langle\bar{\psi}\psi\rangle \sim -(230\text{MeV})^3$ .

A number of studies have been conducted so far in the field of chiral symmetry breaking with inclusion of a confining potential, see Refs. [95–102]. Also the functional renormalization group has been applied to study chiral symmetry breaking in QCD-like systems, see Refs. [103, 104]. In this work we use the FRG method to study chiral symmetry breaking in Hamiltonian QCD.

### 5.1 Derivation of the Flow Equation for the Quark Propagator

In order to derive the flow equation for the static quark propagator, we start with the generating functional of static Green functions that can be derived from a suitable

ansatz for the quark vacuum wave functional:

$$Z_k[J, \bar{\sigma}, \sigma, \Lambda^\dagger, \Lambda] = \int \mathcal{D}[A \bar{c} c \psi^\dagger \psi] \exp[-\psi^\dagger \Omega_{f,k} \psi - \psi^\dagger \Omega[A] \psi - S_k[A, \bar{c}, c] + JA + \bar{\sigma} c + \bar{c} \sigma + \Lambda^\dagger \psi + \psi^\dagger \Lambda] \quad (5.1)$$

where we define

$$\Lambda^\dagger \psi := \int \frac{d^3 p}{(2\pi)^3} (\Lambda_\alpha^m)^* (-\mathbf{p}) \psi_\alpha^m(\mathbf{p}). \quad (5.2)$$

The  $\Lambda$  are the quark sources,  $m$  are colour indices in the fundamental representation of the gauge group and  $\alpha$  are Dirac indices.  $S_k$  denotes the action of the gluon sector, that is to say, the vacuum wave functional, together with the regulator term, i.e.,  $S_k = S + \Delta S_k$  in the notation of Eq. (3.7). In the quark sector, we have the free part of the vacuum wave functional, i.e., the two-quark kernel  $\Omega_{f,k}$ , and the coupling of the quarks to the gluon field  $\Omega[A]$ . We choose the two-quark kernel as

$$\Omega_{f,k} := \Omega_f + R_{\psi,k}, \quad (5.3)$$

whereas  $\Omega[A]$  is  $k$ -independent because, due to the formalism of the FRG, the regulator term is added only to the two-point kernel  $\Omega_f$  in the action. For the following derivations it is convenient to switch to the superfield formalism which we have already used from Eq. (3.19) on. For this, we define

$$\begin{aligned} \phi &:= (A, c, \bar{c}, \psi, \psi^\dagger), & I &:= (J, \sigma, \bar{\sigma}, \Lambda, \Lambda^\dagger), \\ \bar{\phi} &:= (A, -\bar{c}, c, -\psi^\dagger, \psi), & \bar{I} &:= (J, -\bar{\sigma}, \sigma, -\Lambda^\dagger, \Lambda). \end{aligned} \quad (5.4)$$

In Eq. (5.1) we separate the regulator terms and introduce

$$\begin{aligned} M &:= \text{diag}(\mathbf{1}, -\mathbf{1}, -\mathbf{1}, -\mathbf{1}, -\mathbf{1}), \\ \mathcal{R}_k &:= \text{diag}(R_{A,k}, R_{c,k}, R_{c,k}^T, R_{\psi,k}, R_{\psi,k}^T) \end{aligned} \quad (5.5)$$

to get

$$Z_k[I] = \int \mathcal{D}\phi \exp \left[ -S[\phi] - \frac{1}{2} \bar{\phi} \mathcal{R}_k M \phi + I \bar{\phi} \right]. \quad (5.6)$$

Acting with the dimensionless flow derivative  $\partial_t := k \frac{\partial}{\partial k}$  on it we obtain

$$\begin{aligned} \partial_t Z_k[I] &= - \int \mathcal{D}\phi \frac{1}{2} \bar{\phi} \dot{\mathcal{R}}_k M \phi \exp \left[ -S[\phi] - \frac{1}{2} \bar{\phi} \mathcal{R}_k M \phi + I \bar{\phi} \right] \\ &= \left( -\frac{1}{2} \frac{\delta}{\delta I} \dot{\mathcal{R}}_k \frac{\delta}{\delta \bar{I}} \right) Z_k[I], \end{aligned} \quad (5.7)$$

where the dot denotes the  $t$ -derivative. The latter equality holds because of

$$\left( -\frac{1}{2} \frac{\delta}{\delta I} \dot{\mathcal{R}}_k \frac{\delta}{\delta \bar{I}} \right) e^{I \bar{\phi}} = \left( -\frac{1}{2} \frac{\delta}{\delta I} \dot{\mathcal{R}}_k \frac{\delta}{\delta \bar{I}} \right) e^{\bar{I} M \phi} = -\frac{1}{2} \frac{\delta}{\delta I} e^{I \bar{\phi}} \dot{\mathcal{R}}_k M \phi = -\frac{1}{2} \bar{\phi} \dot{\mathcal{R}}_k M \phi e^{I \bar{\phi}}. \quad (5.8)$$

We define the regularized generating functional for connected equal-time Green functions  $W_k$  as

$$W_k = \ln Z_k, \quad (5.9)$$

whose flow equation therefore is

$$\begin{aligned} \partial_t W_k &= Z_k^{-1} \partial_t Z_k = e^{-W_k} \left( -\frac{1}{2} \frac{\delta}{\delta I} \dot{\mathcal{R}}_k \frac{\delta}{\delta \bar{I}} \right) e^{W_k} = -e^{-W_k} \frac{1}{2} \frac{\delta}{\delta I} \dot{\mathcal{R}}_k \frac{\delta W_k}{\delta \bar{I}} e^{W_k} \\ &= -\frac{1}{2} \frac{\delta W_k}{\delta I} \dot{\mathcal{R}}_k \frac{\delta W_k}{\delta \bar{I}} - \frac{1}{2} \text{Tr} M \dot{\mathcal{R}}_k \frac{\delta^2 W_k}{\delta \bar{I} \delta I}. \end{aligned} \quad (5.10)$$

In accordance with Eqs. (5.6) and (5.9) the effective action is defined as

$$\Gamma_k[\phi] = -W_k[I_k[\phi]] + I_k[\phi] \bar{\phi} - \frac{1}{2} \bar{\phi} \mathcal{R}_k M \phi \quad \text{with} \quad \frac{\delta W_k[I_k[\phi]]}{\delta I} = \bar{\phi}. \quad (5.11)$$

Note that  $\phi$  denotes the field expectation value from here on. The flow of the effective action can be expressed as

$$\begin{aligned} \partial_t \Gamma_k &= -(\partial_t W_k)[I_k[\phi]] - \dot{I}_k[\phi] \frac{\delta W_k[I_k[\phi]]}{\delta I} + \dot{I}_k[\phi] \bar{\phi} - \frac{1}{2} \bar{\phi} \dot{\mathcal{R}}_k M \phi \\ &= \frac{1}{2} \frac{\delta W_k[I_k[\phi]]}{\delta I} \dot{\mathcal{R}}_k \frac{\delta W_k[I_k[\phi]]}{\delta \bar{I}} - \frac{1}{2} \bar{\phi} \dot{\mathcal{R}}_k M \phi + \frac{1}{2} \text{Tr} M \dot{\mathcal{R}}_k \frac{\delta^2 W_k[I_k[\phi]]}{\delta \bar{I} \delta I} \\ &= \frac{1}{2} \text{Tr} M \dot{\mathcal{R}}_k \frac{\delta^2 W_k[I_k[\phi]]}{\delta \bar{I} \delta I}, \end{aligned} \quad (5.12)$$

where

$$\frac{\delta W_k[I_k[\phi]]}{\delta I} = \bar{\phi} \quad \text{and} \quad \frac{\delta W_k[I_k[\phi]]}{\delta \bar{I}} = M \phi \quad (5.13)$$

have been used. With Eq. (3.26) this becomes (cf. Eq. (3.27))

$$\partial_t \Gamma_k[\phi] = \frac{1}{2} \text{Tr} M \dot{\mathcal{R}}_k \left( \frac{\delta^2 \Gamma_k}{\delta \bar{\phi} \delta \phi} + \mathcal{R}_k \right)^{-1}. \quad (5.14)$$

The derivation of the quark propagator flow is completely analogous to the derivation of the ghost propagator flow. Therefore, we can replace the ghost fields by quark fields in the ghost propagator flow equation which then becomes

$$\begin{aligned} \frac{\delta^2 \dot{\Gamma}_k}{\delta \psi_j^\dagger \delta \psi_i} &= \\ \text{Tr} \dot{R}_{A,k} \left( \frac{\delta^2 \Gamma_k}{\delta A \delta A} + R_{A,k} \right)^{-1} \frac{\delta^3 \Gamma_k}{\delta \psi_j^\dagger \delta A \delta \psi} \left( -\frac{\delta^2 \Gamma_k}{\delta \psi^\dagger \delta \psi} + R_{\psi,k} \right)^{-1} \frac{\delta^3 \Gamma_k}{\delta \psi_i \delta \psi^\dagger \delta A} \left( \frac{\delta^2 \Gamma_k}{\delta A \delta A} + R_{A,k} \right)^{-1} \\ &+ \text{Tr} \dot{R}_{\psi,k} \left( -\frac{\delta^2 \Gamma_k}{\delta \psi^\dagger \delta \psi} + R_{\psi,k} \right)^{-1} \frac{\delta^3 \Gamma_k}{\delta \psi_i \delta \psi^\dagger \delta A} \left( \frac{\delta^2 \Gamma_k}{\delta A \delta A} + R_{A,k} \right)^{-1} \frac{\delta^3 \Gamma_k}{\delta \psi_j^\dagger \delta A \delta \psi} \left( -\frac{\delta^2 \Gamma_k}{\delta \psi^\dagger \delta \psi} + R_{\psi,k} \right)^{-1} \\ &- \frac{1}{2} \text{Tr} \dot{R}_{A,k} \left( \frac{\delta^2 \Gamma_k}{\delta A \delta A} + R_{A,k} \right)^{-1} \frac{\delta^4 \Gamma_k}{\delta \psi_j^\dagger \delta \psi_i \delta A \delta A} \left( \frac{\delta^2 \Gamma_k}{\delta A \delta A} + R_{A,k} \right)^{-1} \\ &- \text{Tr} \dot{R}_{\psi,k} \left( -\frac{\delta^2 \Gamma_k}{\delta \psi^\dagger \delta \psi} + R_{\psi,k} \right)^{-1} \frac{\delta^4 \Gamma_k}{\delta \psi_j^\dagger \delta \psi_i \delta \psi^\dagger \delta \psi} \left( -\frac{\delta^2 \Gamma_k}{\delta \psi^\dagger \delta \psi} + R_{\psi,k} \right)^{-1}. \end{aligned} \quad (5.15)$$

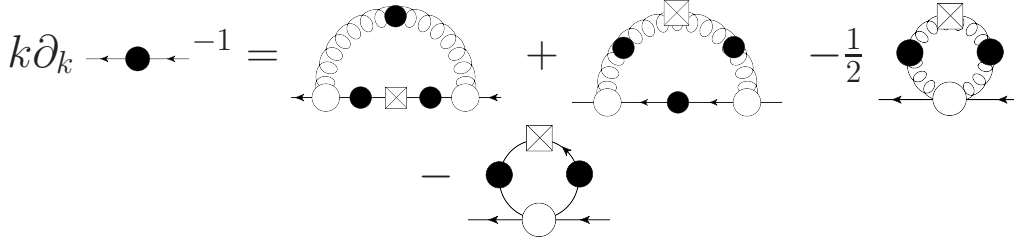


**Figure 5.1:** The flow equation of the quark propagator, Eq. (5.15). The spiral and solid lines with filled black circles denote the regularized gluon and quark propagators at cut-off momentum  $k$ , respectively. White circles stand for proper vertices at cut-off  $k$ , a regulator insertion  $\hat{R}_k$  is represented by a square with a cross.

This equation is diagrammatically illustrated in Fig. 5.1. The gluon propagator is specified as (see Eqs. (3.30) and (3.31))

$$\left[ \left( \frac{\delta^2 \Gamma_k}{\delta A \delta A} + R_A \right)^{-1} \right]_{ij}^{ab}(\mathbf{p}, \mathbf{q}) = \delta^{ab} t_{ij}(\mathbf{p}) (2\pi)^3 \delta^3(\mathbf{p} + \mathbf{q}) \frac{1}{2\omega_k(p) + 2p r_k(p)} \quad (5.16)$$

with

$$R_{A,ij}^{ab}(\mathbf{p}, \mathbf{q}) = \delta^{ab} t_{ij}(\mathbf{p}) (2\pi)^3 \delta^3(\mathbf{p} + \mathbf{q}) \cdot 2p r_k(p), \quad (5.17)$$

where  $\omega_k(p)$  as determined in Chap. 3 will be input into the equations. This is expected to be a good approximation as the effects of the quarks on the gluon sector are probably small as has been demonstrated in Landau gauge with DSEs [105] and on the lattice [106, 107].

The pure quark part of the Hamiltonian is (see Eq. (2.22))

$$\begin{aligned} H_{\psi^\dagger \psi} &= \int d^3x \psi^{m\dagger}(\mathbf{x}) [-i \boldsymbol{\alpha} \cdot \boldsymbol{\partial} + \beta m] \psi^m(\mathbf{x}) \\ &= \int \frac{d^3p}{(2\pi)^3} \psi^{m\dagger}(\mathbf{p}) [\boldsymbol{\alpha} \cdot \mathbf{p} + \beta m] \psi^m(\mathbf{p}). \end{aligned} \quad (5.18)$$

We use this structure also for the two-quark part of the effective action with two dressing functions  $A$  and  $B$ , so the two-point function in momentum space reads

$$\left( -\frac{\delta^2 \Gamma_k}{\delta \psi^\dagger \delta \psi} \right)^{mn}(\mathbf{p}, \mathbf{q}) = \delta^{mn} (2\pi)^3 \delta^3(\mathbf{p} + \mathbf{q}) [\boldsymbol{\alpha} \cdot \mathbf{p} A_k(p) + \beta B_k(p)], \quad (5.19)$$

where  $\psi^\dagger = \psi = 0$  is understood. The dimensions of the dressing functions, however, are  $[A] = -1$  and  $[B] = 0$  because the dimension of the effective action is one less than the dimension of the Hamiltonian.

To gain physical information from the quark two-point function, we rewrite it as

$$S^{-1}(\mathbf{p}) = \boldsymbol{\alpha} \cdot \mathbf{p} A_0(p) + \beta B_0(p) = A_0(p) [\boldsymbol{\alpha} \cdot \mathbf{p} + \beta M(p)], \quad (5.20)$$



where we have defined the mass function

$$M(p) := \frac{B_0(p)}{A_0(p)}. \quad (5.21)$$

In analogy to the free two-quark function

$$S_{free}^{-1}(\mathbf{p}) = \frac{2}{\sqrt{p^2 + m^2}}[\boldsymbol{\alpha} \cdot \mathbf{p} + \beta m], \quad (5.22)$$

where the coefficient in front of  $\beta$  is the mass of the free quark, we expect that the analogous term  $M(p)$  in the full two-quark function denotes the scale dependent mass where  $M(0)$  is the mass in the infrared, i.e., the constituent quark mass. Moreover, we define the quark regulator function as

$$R_{k,\psi}^{mn}(\mathbf{p}, \mathbf{q}) = \delta^{mn}(2\pi)^3 \delta^3(\mathbf{p} + \mathbf{q})[\boldsymbol{\alpha} \cdot \mathbf{p} R_{k,\alpha}(p) + \beta R_{k,\beta}(p)], \quad (5.23)$$

with

$$R_{k,\alpha}(p) = \frac{r_k(p)}{p}, \quad R_{k,\beta}(p) = r_k(p) \quad (5.24)$$

where  $r_k(q)$  is a dimensionless regulator shape function. Therefore, we get for the quark propagator

$$\begin{aligned} & \left( \left[ -\frac{\delta^2 \Gamma_k}{\delta \psi^\dagger \delta \psi} + R_{k,\psi} \right]^{-1} \right)^{mn}(\mathbf{p}, \mathbf{q}) \\ &= \delta^{mn}(2\pi)^3 \delta^3(\mathbf{p} + \mathbf{q}) \frac{\boldsymbol{\alpha} \cdot \mathbf{p}(A_k(p) + R_{k,\alpha}(p)) + \beta(B_k(p) + R_{k,\beta}(p))}{p^2(A_k(p) + R_{k,\alpha}(p))^2 + (B_k(p) + R_{k,\beta}(p))^2}, \end{aligned} \quad (5.25)$$

which becomes the full static quark propagator in the limit  $k \rightarrow 0$ .

For the quark-gluon vertex, which is not a priori known, we consider the structure of the quark-gluon coupling term in the Hamiltonian (see Eq. (2.22)),

$$H_{A\psi^\dagger\psi} = -g \int d^3x \psi^\dagger(\mathbf{x}) \alpha^i A_i^a(\mathbf{x}) T^a \psi(\mathbf{x}), \quad (5.26)$$

furnished with a dressing function  $h$  such that the vertex becomes

$$\left( \frac{\delta^3 \Gamma_k}{\delta A \delta \psi^\dagger \delta \psi} \right)_i^{a,mn}(\mathbf{p}_3, \mathbf{p}_2, \mathbf{p}_1) = g \alpha^j t_{ji}(\mathbf{p}_3) T^a h_k(\mathbf{p}_2, \mathbf{p}_1) (2\pi)^3 \delta^3(\mathbf{p}_1 + \mathbf{p}_2 + \mathbf{p}_3), \quad (5.27)$$

where the dressing function  $h$  has dimension  $[h] = -1$ .

Similarly, we consider the part of the Coulomb term of the Hamiltonian, where the colour density is generated by matter fields exclusively (see Eq. (2.35)),

$$H_C = \frac{g^2}{2} \int d^3[xy] \rho_m^a(\mathbf{x}) F^{ab}(\mathbf{x} - \mathbf{y}) \rho_m^b(\mathbf{y}), \quad (5.28)$$

**Figure 5.2:** Truncated flow equation of the quark propagator.

with the colour density (see Eq. (2.16)),

$$\rho_m^a(\mathbf{x}) = \psi^\dagger(\mathbf{x})T^a\psi(\mathbf{x}) . \quad (5.29)$$

As we neglect the reaction of the quarks on the gluon sector, we have plugged the Coulomb operator  $F = \langle F[A] \rangle$ , calculated in Chap. 4, into the Hamiltonian.

We take the four-quark part of the effective action to have the same structure as the corresponding part of the Hamiltonian,

$$\Gamma_{k,4\psi} = \frac{g^2}{2} \int d^3[xy] \psi^\dagger(\mathbf{x})T^a\psi(\mathbf{x})\delta^{ab}P_k(\mathbf{x}-\mathbf{y})\psi^\dagger(\mathbf{y})T^b\psi(\mathbf{y}) \quad (5.30)$$

which, after transformation into momentum space, leads to the quark four-point function

$$\begin{aligned} & \left( \frac{\delta^4 \Gamma_k}{\delta\psi^\dagger \delta\psi \delta\psi^\dagger \delta\psi} \right)_{\alpha_4 \alpha_3 \alpha_2 \alpha_1}^{m_4 m_3 m_2 m_1}(\mathbf{p}_4, \mathbf{p}_3, \mathbf{p}_2, \mathbf{p}_1) = \\ & (2\pi)^3 \delta^3(\mathbf{p}_4 + \mathbf{p}_3 + \mathbf{p}_2 + \mathbf{p}_1) g^2 [P_k(\mathbf{p}_1 + \mathbf{p}_2) \delta_{\alpha_2 \alpha_1} \delta_{\alpha_4 \alpha_3} (T^a)^{m_4 m_3} (T^a)^{m_2 m_1} \\ & - P_k(\mathbf{p}_2 + \mathbf{p}_3) \delta_{\alpha_3 \alpha_2} \delta_{\alpha_4 \alpha_1} (T^a)^{m_4 m_1} (T^a)^{m_2 m_3}] . \end{aligned} \quad (5.31)$$

The momentum-dependent function  $P_k(\mathbf{p})$  has the dimension  $[P] = -3$ .

We plug these parameterizations into Eq. (5.15) where, however, we omit the gluon tadpole term, which is unknown, see Fig. 5.2. For the flow of the dressing functions  $A$  and  $B$  we get (with  $C_2 = (N_c^2 - 1)/(2N_c)$ )

$$\begin{aligned} p\dot{A}_k(p) &= -g^2 C_2 \int \frac{d^3 q}{(2\pi)^3} h_k(-\mathbf{q}, \mathbf{p}) h_k(-\mathbf{p}, \mathbf{q}) \cdot 2q(\hat{\mathbf{p}} \cdot \widehat{\mathbf{p} - \mathbf{q}})(\hat{\mathbf{q}} \cdot \widehat{\mathbf{p} - \mathbf{q}}) \\ & \left[ \frac{2|\mathbf{p} - \mathbf{q}| \dot{r}_k(\mathbf{p} - \mathbf{q})}{[2\omega_k(\mathbf{p} - \mathbf{q}) + 2|\mathbf{p} - \mathbf{q}| r_k(\mathbf{p} - \mathbf{q})]^2} \frac{(A_k + R_{k,\alpha})(q)}{[q^2(A_k + R_{k,\alpha})^2 + (B_k + R_{k,\beta})^2](q)} \right. \\ & \left. + \frac{[2(A_k + R_{k,\alpha})(B_k + R_{k,\beta}) \dot{R}_{k,\beta} + q^2(A_k + R_{k,\alpha})^2 \dot{R}_{k,\alpha} - (B_k + R_{k,\beta})^2 \dot{R}_{k,\alpha}](q)}{[2\omega_k(\mathbf{p} - \mathbf{q}) + 2|\mathbf{p} - \mathbf{q}| r_k(\mathbf{p} - \mathbf{q})][q^2(A_k + R_{k,\alpha})^2 + (B_k + R_{k,\beta})^2](q)} \right] \\ & - g^2 C_2 \int \frac{d^3 q}{(2\pi)^3} \hat{\mathbf{p}} \cdot \hat{\mathbf{q}} q P_k(\mathbf{p} - \mathbf{q}) \\ & \frac{[2(A_k + R_{k,\alpha})(B_k + R_{k,\beta}) \dot{R}_{k,\beta} + q^2(A_k + R_{k,\alpha})^2 \dot{R}_{k,\alpha} - (B_k + R_{k,\beta})^2 \dot{R}_{k,\alpha}](q)}{[q^2(A_k + R_{k,\alpha})^2 + (B_k + R_{k,\beta})^2]^2(q)} \end{aligned} \quad (5.32)$$

and

$$\begin{aligned}
\dot{B}_k(p) = & -g^2 C_2 \int \frac{d^3 q}{(2\pi)^3} h_k(-\mathbf{q}, \mathbf{p}) h_k(-\mathbf{p}, \mathbf{q}) \\
& \left[ \frac{2|\mathbf{p} - \mathbf{q}| \dot{r}_k(\mathbf{p} - \mathbf{q})}{[2\omega_k(\mathbf{p} - \mathbf{q}) + 2|\mathbf{p} - \mathbf{q}| r_k(\mathbf{p} - \mathbf{q})]^2} \frac{2(B_k + R_{k,\beta})(q)}{[q^2(A_k + R_{k,\alpha})^2 + (B_k + R_{k,\beta})^2](q)} \right. \\
& \left. + \frac{2[2q^2(A_k + R_{k,\alpha})(B_k + R_{k,\beta}) \dot{R}_{k,\alpha} + (B_k + R_{k,\beta})^2 \dot{R}_{k,\beta} - q^2(A_k + R_{k,\alpha})^2 \dot{R}_{k,\beta}](q)}{[2\omega_k(\mathbf{p} - \mathbf{q}) + 2|\mathbf{p} - \mathbf{q}| r_k(\mathbf{p} - \mathbf{q})][q^2(A_k + R_{k,\alpha})^2 + (B_k + R_{k,\beta})^2](q)} \right] \\
& - g^2 C_2 \int \frac{d^3 q}{(2\pi)^3} P_k(\mathbf{p} - \mathbf{q}) \\
& \frac{[2q^2(A_k + R_{k,\alpha})(B_k + R_{k,\beta}) \dot{R}_{k,\alpha} + (B_k + R_{k,\beta})^2 \dot{R}_{k,\beta} - q^2(A_k + R_{k,\alpha})^2 \dot{R}_{k,\beta}](q)}{[q^2(A_k + R_{k,\alpha})^2 + (B_k + R_{k,\beta})^2](q)}.
\end{aligned} \tag{5.33}$$

As in the case of the gluon and ghost flow equations in Chap. 3 and of the Coulomb form factor flow equation in Chap. 4, we can transform the flow equations of the quark correlator form factors  $A$  and  $B$  into Dyson-Schwinger-like equations by making the replacements

$$A_k \rightarrow A_0, \quad B_k \rightarrow B_0, \quad \omega_k \rightarrow \omega_0, \quad h_k \rightarrow h_0, \quad P_k \rightarrow P_0 \tag{5.34}$$

in the loop integrals. This makes an analytic integration of the flow integral feasible because of

$$\begin{aligned}
& \partial_t \frac{A_0 + R_{k,\alpha}}{q^2(A_0 + R_{k,\alpha})^2 + (B_0 + R_{k,\beta})^2}(q) \\
& = \frac{-2(A_0 + R_{k,\alpha})(B_0 + R_{k,\beta}) \dot{R}_{k,\beta} - q^2(A_0 + R_{k,\alpha})^2 \dot{R}_{k,\alpha} + (B_0 + R_{k,\beta})^2 \dot{R}_{k,\alpha}}{[q^2(A_0 + R_{k,\alpha})^2 + (B_0 + R_{k,\beta})^2]^2}(q)
\end{aligned} \tag{5.35}$$

and

$$\begin{aligned}
& \partial_t \left[ \frac{1}{(2\omega_0 + 2|\mathbf{p} - \mathbf{q}| r_k)(\mathbf{p} - \mathbf{q})} \frac{A_0 + R_{k,\alpha}}{q^2(A_0 + R_{k,\alpha})^2 + (B_0 + R_{k,\beta})^2}(q) \right] \\
& = - \frac{2|\mathbf{p} - \mathbf{q}| \dot{r}_k(\mathbf{p} - \mathbf{q})}{(2\omega_0 + 2|\mathbf{p} - \mathbf{q}| r_k)^2(\mathbf{p} - \mathbf{q})} \frac{A_0 + R_{k,\alpha}}{q^2(A_0 + R_{k,\alpha})^2 + (B_0 + R_{k,\beta})^2}(q) \\
& \quad + \frac{[-2(A_0 + R_{k,\alpha})(B_0 + R_{k,\beta}) \dot{R}_{k,\beta} - q^2(A_0 + R_{k,\alpha})^2 \dot{R}_{k,\alpha} + (B_0 + R_{k,\beta})^2 \dot{R}_{k,\alpha}](q)}{[(2\omega_0 + 2|\mathbf{p} - \mathbf{q}| r_k)(\mathbf{p} - \mathbf{q})][q^2(A_0 + R_{k,\alpha})^2 + (B_0 + R_{k,\beta})^2](q)}
\end{aligned} \tag{5.36}$$

as well as the corresponding expressions for the dressing function  $B$ . Thus we arrive

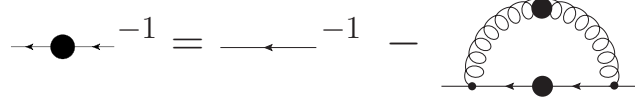


**Figure 5.3:** The approximated flow equation of the quark propagator, Eqs. (5.37) and (5.38), with the quark tadpole neglected and a bare quark-gluon vertex. The solid lines with filled black circles denote the quark propagators. The solid line without a circle is a bare quark propagator. Small dots represent a bare vertex.

at

$$A_0(p) = A_\Lambda(p) + g^2 C_2 \frac{1}{p} \int \frac{d^3 q}{(2\pi)^3} \left[ \frac{h_0(-\mathbf{q}, \mathbf{p}) h_0(-\mathbf{p}, \mathbf{q}) (\hat{\mathbf{p}} \cdot \widehat{\mathbf{p} - \mathbf{q}}) (\hat{\mathbf{q}} \cdot \widehat{\mathbf{p} - \mathbf{q}})}{2\omega_0(\mathbf{p} - \mathbf{q}) + 2|\mathbf{p} - \mathbf{q}| r_k(\mathbf{p} - \mathbf{q})} \right. \\ \left. \frac{2q(A_0 + R_{k,\alpha})(q)}{[q^2(A_0 + R_{k,\alpha})^2 + (B_0 + R_{k,\beta})^2](q)} + \frac{\hat{\mathbf{p}} \cdot \hat{\mathbf{q}} P_0(\mathbf{p} - \mathbf{q}) [q(A_0 + R_{k,\alpha})](q)}{[q^2(A_0 + R_{k,\alpha})^2 + (B_0 + R_{k,\beta})^2](q)} \right]_{k=\Lambda}^{k=0} \quad (5.37)$$

and

$$B_0(p) = B_\Lambda(p) + g^2 C_2 \int \frac{d^3 q}{(2\pi)^3} \left[ \frac{h_0(-\mathbf{q}, \mathbf{p}) h_0(-\mathbf{p}, \mathbf{q})}{2\omega_0(\mathbf{p} - \mathbf{q}) + 2|\mathbf{p} - \mathbf{q}| r_k(\mathbf{p} - \mathbf{q})} \right. \\ \left. \frac{2(B_0 + R_{k,\beta})(q)}{[q^2(A_0 + R_{k,\alpha})^2 + (B_0 + R_{k,\beta})^2](q)} + \frac{P_0(\mathbf{p} - \mathbf{q}) (B_0 + R_{k,\beta})(q)}{[q^2(A_0 + R_{k,\alpha})^2 + (B_0 + R_{k,\beta})^2](q)} \right]_{k=\Lambda}^{k=0}. \quad (5.38)$$

In the following sections we will make various approximations to these equations in order to calculate the dressing functions  $A$  and  $B$  as well as, ultimately, the mass function  $M$  and the chiral condensate  $\langle \bar{\psi} \psi \rangle$ .

## 5.2 Inclusion of the Gluon Propagator Diagram

In this section we study the approximated quark propagator flow equation of Sec. 5.1 without the quark tadpole in order to investigate the influence of the static gluon propagator on dynamic mass generation. The quark-gluon vertex is chosen bare. This results in an equation shown diagrammatically in Fig. 5.3.

### 5.2.1 Non-vanishing current quark mass

In this subsection we employ a bare quark propagator with non-vanishing current quark mass. The simplest choice for the bare quark dressing functions compatible with the dimensions  $[A] = -1$  and  $[B] = 0$  is

$$A_\Lambda(p) = \frac{1}{p} \quad \text{and} \quad B_\Lambda(p) = \frac{m}{p}, \quad (5.39)$$

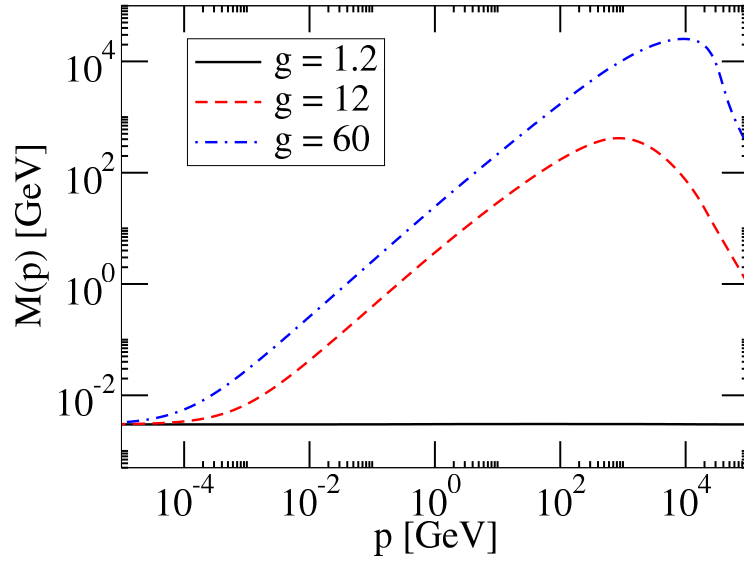


**Figure 5.4:** The mass function  $M(p)$  for different values of the coupling  $g$ , calculated with a bare quark-gluon vertex and the static gluon propagator as input.

where we choose the current quark mass  $m = 3 \text{ MeV}$ . For the transverse static gluon correlation function  $\omega$  we draw on the results obtained in Sec. 3.6 from the optimized flow equation. In accordance with perturbation theory [108], the bare static quark-gluon vertex dressing function  $h$  in Eq. (5.27) is

$$h(\mathbf{p}, \mathbf{q}) = \frac{1}{E_{\mathbf{p}}^{\psi} + E_{\mathbf{q}}^{\psi} + E_{\mathbf{p}+\mathbf{q}}^A} \quad (5.40)$$

with

$$E_{\mathbf{p}}^{\psi} = \sqrt{\mathbf{p}^2 + m^2} \quad \text{and} \quad E_{\mathbf{p}}^A = |\mathbf{p}|. \quad (5.41)$$

With these assumptions, Eqs. (5.37) and (5.38) without the tadpole are solved numerically. In Fig. 5.4 the result for the mass function  $M(p)$  is shown for different values of the coupling  $g$ . It is seen that for high couplings the mass function can reach high values for intermediate momenta but eventually drops to the current quark mass in the infrared. No dynamic generation of mass occurs. The same calculation has been performed with  $\omega(p) = p$  on the whole momentum range, which coincides with the photon two-point function in the infrared regime. It is seen in Fig. 5.5 that there is not only no qualitative difference between the two mass functions but that also the quantitative differences are negligibly small, if the coupling  $g$  is appropriately tuned, i.e., the effect of different infrared behaviours of the gauge field propagator can be balanced by adjusting one single number. Therefore, in the FRG approach there seems to be no effect on chiral symmetry breaking coming from the static gluon propagator alone. This is in accordance with the results from the variational approach in Ref. [109] where no chiral symmetry breaking occurs without the Coulomb term in the Hamiltonian.

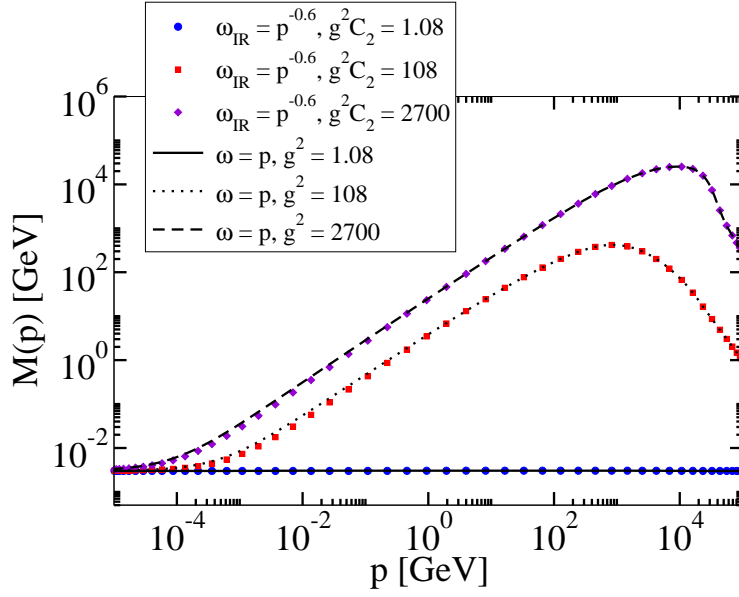


**Figure 5.5:** The mass function  $M(p)$  for different values of the coupling  $g$ , calculated for the Yang-Mills case with the static gluon propagator as input (symbols), as in Fig. 5.4, and for the case  $\omega(p) = p$  (lines). If the values for the coupling  $g$  are chosen appropriately, the curves coincide. Therefore, it is seen that the IR behaviour of the static, transverse gluon propagator has only negligible influence on the mass function.

### 5.2.2 Input from the variational approach in the chiral limit

In order to improve the input for the dressing functions  $A_\Lambda$  and  $B_\Lambda$ , we will use results from the variational approach. As these were obtained in the chiral limit, we now set  $m = 0$ .

In the Lagrangian formulation of QFT, the bare propagators and vertices occurring in the Dyson-Schwinger equations are the bare propagators and vertices in the classical action  $S$ . In the Hamiltonian formulation, however,  $S$  is actually defined via

$$\langle \phi | O[A, \psi^\dagger, \psi] | \phi \rangle = \int \mathcal{D}[A \psi^\dagger \psi] O[A, \psi^\dagger, \psi] e^{-S[A, \psi^\dagger, \psi]} \quad (5.42)$$

with

$$\exp(-S[A, \psi^\dagger, \psi]) := J[A] |\phi[A, \psi^\dagger, \psi]|^2. \quad (5.43)$$

Therefore,  $S$  is completely determined by the vacuum wave functional  $\phi$  and the gauge fixing procedure. Interpreting Eqs. (5.37) and (5.38) without the quark tadpole and with a bare quark-gluon vertex as Dyson-Schwinger equations, the propagator functions  $A_\Lambda$  and  $B_\Lambda$  at cutoff momentum  $\Lambda$  are the “bare” propagator functions in the exponent  $S$  of the vacuum wave functional. They can be determined by applying the variational principle,

$$\frac{\langle \phi | H | \phi \rangle}{\langle \phi | \phi \rangle} \rightarrow \min., \quad (5.44)$$

with a suitable ansatz for  $\phi$ , and used as input into the present equation. In Ref. [110] the action

$$S[\psi^\dagger, \psi] = \int \psi^\dagger \tilde{\Omega} \psi \quad \text{with} \quad \tilde{\Omega} = S^{(+)} + S^{(+)} K S^{(-)} + S^{(-)} \bar{K} S^{(+)} - S^{(-)}, \quad (5.45)$$

has been proposed where

$$S^{(\pm)}(\mathbf{p}) = \frac{1}{2} \left( \mathbb{1} \pm \frac{h(\mathbf{p})}{E_{\mathbf{p}}} \right) \quad \text{with} \quad h(\mathbf{p}) = \boldsymbol{\alpha} \cdot \mathbf{p} + \beta m \quad \text{and} \quad E_{\mathbf{p}} = \sqrt{\mathbf{p}^2 + m^2} \quad (5.46)$$

are the projectors on particle and antiparticle states, respectively. If we choose the quark kernel  $K$  as

$$K(\mathbf{p}) = \beta \varphi(p), \quad (5.47)$$

i.e., without coupling to the gluons, the above ansatz corresponds to the ground state used in Ref. [99]. We obtain

$$\tilde{\Omega}^{mn}(p) = \delta^{mn} [\boldsymbol{\alpha} \cdot \mathbf{p} A_\Lambda(p) + \beta B_\Lambda(p)] \quad (5.48)$$

with

$$A_\Lambda(p) = \frac{1}{E_{\mathbf{p}}} - \frac{m}{E_{\mathbf{p}}^2} \varphi(p) \quad \text{and} \quad B_\Lambda(p) = \frac{m}{E_{\mathbf{p}}} + \frac{\mathbf{p}^2}{E_{\mathbf{p}}^2} \varphi(p) \quad (5.49)$$

where the indices  $m$  and  $n$  are indices in the fundamental representation of the gauge group. This calculation is detailed in Appendix E.1. The determination of  $\varphi(p)$  by means of the variational principle has been performed in Ref. [99] (see also [109]) in the chiral limit  $m = 0$  where the kernels read

$$A_\Lambda(p) = \frac{1}{p} \quad \text{and} \quad B_\Lambda(p) = \varphi(p). \quad (5.50)$$

For the calculation and subsequent minimization of the energy expectation value, the Coulomb part  $H_C$  of the Hamiltonian containing the confinement potential has been fully included in addition to the kinetic part  $H_{\psi^\dagger \psi}$ . The kernels  $A_\Lambda$  and  $B_\Lambda$  are shown in Fig. 5.6 together with their asymptotic behaviour.

Using these  $A_\Lambda$  and  $B_\Lambda$  as input, the dressed propagator functions  $A_0(p)$  and  $B_0(p)$  (the indices ‘0’ will be dropped from now on) have been calculated in the chiral limit. The results are shown in Fig. 5.7 together with the mass function  $M(p) = B(p)/A(p)$ . It is seen that although mass builds up from the ultraviolet region towards the mid-momentum region, the mass function reaches a peak value of  $M = 270$  MeV at  $p = 580$  MeV and falls down towards the infrared region like  $M \sim p$ . Therefore, the gluon propagator term does not seem to be sufficient to maintain chiral symmetry breaking in the infrared.

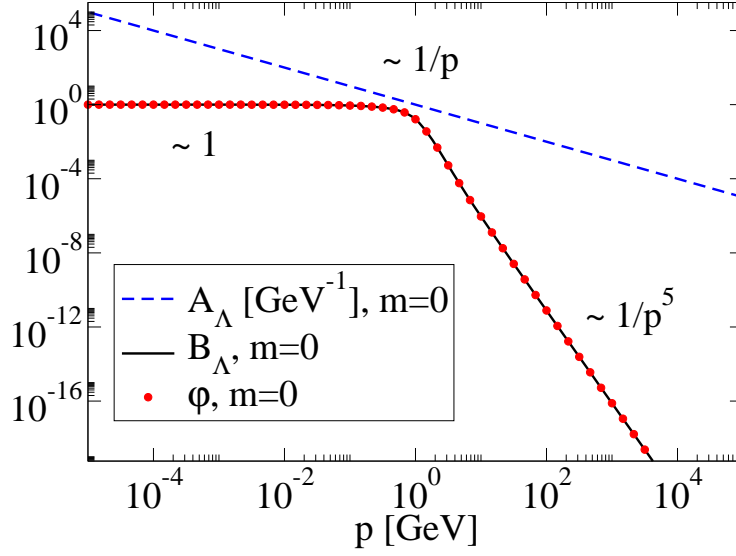


**Figure 5.6:** The variational parameter  $\varphi(p)$  of Eq. (5.45) as calculated in Ref. [99] (see also [109]) with  $m = 0$  is shown together with the two-quark kernels  $A_\Lambda$  and  $B_\Lambda$  shown of Eq. (5.50). The respective asymptotic behaviour is indicated.

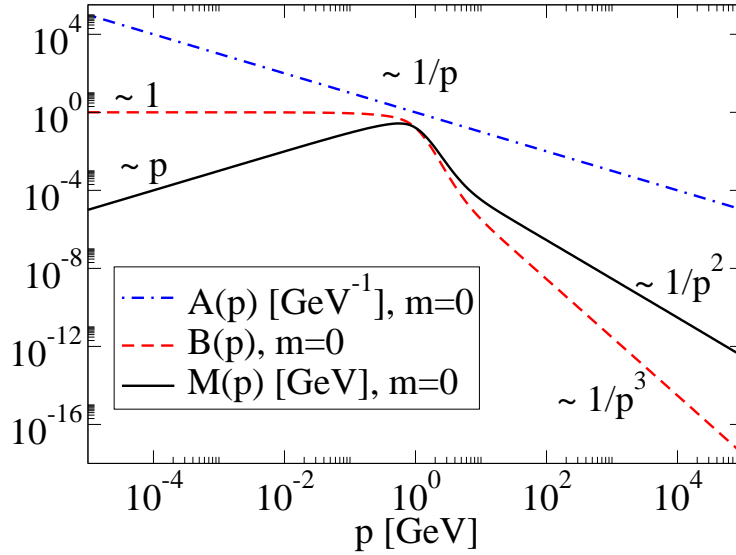


**Figure 5.7:** The dressing functions of the static quark propagator,  $A(p)$  and  $B(p)$ , as a solution of the equation in Fig. 5.3 in the chiral limit with input from the variational approach [99, 109] is shown. The mass function  $M(p)$  has a peak value of  $M = 270$  MeV at  $p = 580$  MeV. However, the mass function falls off towards the infrared region like  $M \sim p$ .



### Infrared analysis

Concerning the numerical solution of Eqs. (5.37) and (5.38), note that in the loop integrals the only momentum argument of the dressing functions  $A$  and  $B$  is the loop momentum  $q$ . In particular, no sums of the external momentum and the loop momentum like  $|\mathbf{p} - \mathbf{q}|$  or  $|\mathbf{p} + \mathbf{q}|$  occur. As a consequence, the range of the radial loop integration momentum  $q$  and the range of the Chebyshev representation momentum  $p$  can be chosen to coincide without the need to extrapolate  $A$  and  $B$  outside their representation range and, therefore, without the need to perform an analysis of their asymptotic behaviour as an input into the numerical computation. However, in order to check up on the numerical calculations, we will carry out such an analysis for the infrared region in the following.

As a reference, we first list the infrared behaviour of  $\omega(p)$  and  $\varphi(p)$  and, as a consequence, of  $A_\Lambda(p)$  and  $B_\Lambda(p)$  according to Eq. (5.50):

$$\omega(p \rightarrow 0) \sim p^{-\alpha}, \quad \varphi(p \rightarrow 0) \sim p^0, \quad A_\Lambda(p \rightarrow 0) \sim p^{-1}, \quad B_\Lambda(p \rightarrow 0) \sim p^0. \quad (5.51)$$

For the quark dressing functions we assume a power law behaviour in the infrared region and define the infrared exponents

$$A(p \rightarrow 0) \sim p^{-\eta} \quad \text{and} \quad B(p \rightarrow 0) \sim p^{-\tau}. \quad (5.52)$$

In the deep infrared region we can write the loop integrals in Eqs. (5.37) and (5.38) with the present approximations using a single ultraviolet cut-off:

$$A(p) = A_\Lambda(p) + g^2 C_2 \frac{1}{p} \int^\Lambda \frac{d^3 q}{(2\pi)^3} \frac{h(-\mathbf{q}, \mathbf{p}) h(-\mathbf{p}, \mathbf{q}) (\hat{\mathbf{p}} \cdot \widehat{\mathbf{p} - \mathbf{q}}) (\hat{\mathbf{q}} \cdot \widehat{\mathbf{p} - \mathbf{q}}) q \cdot 2A(q)}{2\omega(\mathbf{p} - \mathbf{q}) [q^2 A^2 + B^2](q)} \quad (5.53)$$

and

$$B(p) = B_\Lambda(p) + g^2 C_2 \int^\Lambda \frac{d^3 q}{(2\pi)^3} h(-\mathbf{q}, \mathbf{p}) h(-\mathbf{p}, \mathbf{q}) \frac{1}{2\omega(\mathbf{p} - \mathbf{q})} \frac{2B(q)}{[q^2 A^2 + B^2](q)}. \quad (5.54)$$

In the infrared analysis, we make the assumption that in the infrared region the infrared behaviour dominates the integral and therefore we replace the correlation functions under the integral with their infrared asymptotic behaviour given in Eqs. (5.51) and (5.52). We then scale the external momentum  $p$  as well as the loop momentum  $q$  by a positive factor of  $\lambda$ ,  $p \rightarrow \lambda p$ ,  $q \rightarrow \lambda q$ , where  $\lambda < 1$ . Two cases have to be distinguished:

$\tau < \eta - 1$  In this case the term  $q^2 A^2$  dominates over the term  $B^2$  in the denominator of the loop integrals in Eqs. (5.53) and (5.54), so we get for the  $B$ -equation (in view of Eq. (5.40) with  $m = 0$ )

$$\lambda^{-\tau} B(p) = \lambda^0 B_\Lambda(p) + \lambda^{2\eta - \tau + \alpha - 1} \text{Loop}(p). \quad (5.55)$$

Again, we have to distinguish two cases:

$2\eta - \tau + \alpha - 1 < 0$ : In this case the loop is dominant, so  $2\eta - \tau + \alpha - 1 = -\tau \rightarrow \eta = \frac{1-\alpha}{2}$ .

$2\eta - \tau + \alpha - 1 \geq 0$ : In this case  $B_\Lambda$  is dominant, so  $\tau = 0$ .

For the  $A$ -equation we get

$$\lambda^{-\eta}A(p) = \lambda^{-1}A_\Lambda(p) + \lambda^{\eta+\alpha-1}\text{Loop}(p) . \quad (5.56)$$

We have to distinguish

$\eta + \alpha < 0$ : Loop dominates,  $\eta + \alpha - 1 = -\eta \rightarrow \eta = \frac{1-\alpha}{2}$ .

$\eta + \alpha \geq 0$ :  $A_\Lambda$  dominates,  $\eta = 1$ .

$\tau \geq \eta - 1$  In this case the term  $B^2$  dominates over the term  $q^2A^2$  in the denominator of the loop integrals in Eqs. (5.53) and (5.54), so we get for the  $B$ -equation

$$\lambda^{-\tau}B(p) = \lambda^0B_\Lambda(p) + \lambda^{1+\alpha+\tau}\text{Loop}(p) . \quad (5.57)$$

$\alpha + \tau + 1 < 0$ : Loop dominates,  $1 + \alpha + \tau = -\tau \rightarrow \tau = -\frac{1+\alpha}{2}$ .

$\alpha + \tau + 1 \geq 0$ :  $B_\Lambda$  dominates,  $\tau = 0$ .

For the  $A$ -equation:

$$\lambda^{-\eta}A(p) = \lambda^{-1}A_\Lambda(p) + \lambda^{1+\alpha-\eta+2\tau}\text{Loop}(p) . \quad (5.58)$$

$\alpha - \eta + 2\tau + 2 < 0$ : Loop dominates,  $1 + \alpha + 2\tau - \eta = -\eta \rightarrow \tau = -\frac{1+\alpha}{2}$ .

$\alpha - \eta + 2\tau + 2 \geq 0$ :  $A_\Lambda$  dominates,  $\eta = 1$ .

In the following, we check the above case distinctions for consistency and we find that there is only one infrared behaviour of  $A$  and  $B$  which can be realized. We use the condition that  $\alpha > -1$ , which is easily fulfilled not only for the optimized result of Chap. 3 ( $\alpha = 0.60$ ) used in the numerical solution of Eqs. (5.37) and (5.38), but also for the result without inclusion of the tadpoles ( $\alpha = 0.28$ ) and for the result ( $\alpha = 1$ ) of the variational approach [50].

First, we consider the case of  $\tau < \eta - 1$ : for the  $A$ -equation, the result  $\eta = \frac{1-\alpha}{2}$  with the prerequisite  $\eta + \alpha < 0$  contradicts  $\alpha > -1$ . Therefore, we must have  $\eta = 1$  which, considering the  $B$ -equation and again the condition  $\alpha > -1$ , leads to the possibility  $\tau = 0$ . These results, however, conflict with the condition  $\tau < \eta - 1$ , which is therefore ruled out.

Next, we consider the case  $\tau \geq \eta - 1$ : for the  $B$ -equation, the result  $\tau = -\frac{1+\alpha}{2}$  with the prerequisite  $\alpha + \tau + 1 < 0$  contradicts  $\alpha > -1$ . Therefore, we must have  $\tau = 0$  which, considering the  $A$ -equation and again the condition  $\alpha > -1$ , leads to the possibility  $\eta = 1$ . Both values of  $\tau$  and  $\eta$  are now in accord with the condition  $\tau \geq \eta - 1$ , even with  $\tau = \eta - 1$ . Therefore, none of the terms  $q^2A^2$  and  $B^2$  in the denominator of the quark propagator actually dominates the infrared behaviour.

In summary, the only case where the result does not contradict any of the assumptions made for its derivation is  $\tau = 0$  and  $\eta = 1$  in the case of  $\tau \geq \eta - 1$  with

**Figure 5.8:** The approximated equation for the quark propagator, Eqs. (5.37) and (5.38), with inclusion of the quark tadpole only.

$\alpha + \tau \geq -1$  and  $\alpha - \eta + 2\tau + 2 \geq 0$ . This leads to the infrared behaviour

$$A(p \rightarrow 0) \sim \frac{1}{p} \quad \text{and} \quad B(p \rightarrow 0) \sim 1, \quad \text{and therefore} \quad M(p \rightarrow 0) \sim p, \quad (5.59)$$

which excellently confirms our numerical calculation, see Fig. 5.7.

## 5.3 Inclusion of the Tadpole Diagram

The foregoing considerations have shown that despite the improvement by using input from the variational approach, the mass function vanishes in the infrared. The static gluon propagator obviously has little influence on dynamic mass generation in the FRG approach. Therefore, we will neglect it in the following and consider only the quark tadpole in Eqs. (5.37) and (5.38). The resulting approximated flow equation is shown in Fig. 5.8.

### 5.3.1 Derivation of the mass equation

In order to write down an integral equation for the quantity of interest itself, the mass function, rather than for the dressing functions  $A$  and  $B$ , we make an ansatz for the proper self energy as in Ref. [99], such that the energy-dependent quark two-point function reads

$$S^{-1}(p^0, \mathbf{p}) = -i[\gamma^0 p^0 - \boldsymbol{\gamma} \cdot \mathbf{p} \tilde{A}(\mathbf{p}) - \mathbb{1} \tilde{B}(\mathbf{p})], \quad (5.60)$$

and therefore

$$S(p^0, \mathbf{p}) = i \frac{\gamma^0 p^0 - \boldsymbol{\gamma} \cdot \mathbf{p} \tilde{A}(\mathbf{p}) + \mathbb{1} \tilde{B}(\mathbf{p})}{(p^0)^2 - \mathbf{p}^2 \tilde{A}^2(\mathbf{p}) - \tilde{B}^2(\mathbf{p})}. \quad (5.61)$$

The static quark two-point function has been parameterized as

$$S^{-1}(\mathbf{p}) = \boldsymbol{\gamma} \cdot \mathbf{p} A(\mathbf{p}) + \mathbb{1} B(\mathbf{p}), \quad (5.62)$$

see Eq. (5.19), and therefore

$$S(\mathbf{p}) = \frac{-\boldsymbol{\gamma} \cdot \mathbf{p} A(\mathbf{p}) + \mathbb{1} B(\mathbf{p})}{p^2 A^2(\mathbf{p}) + B^2(\mathbf{p})}. \quad (5.63)$$

The static propagator is defined as the integral over the  $p^0$ -component of the time-dependent propagator:

$$\begin{aligned}
S(\mathbf{p}) &= \int \frac{dp^0}{2\pi} S(p^0, \mathbf{p}) = \frac{i}{2\pi} (-\boldsymbol{\gamma} \cdot \mathbf{p} \tilde{A} + \mathbb{1} \tilde{B}) \int dp^0 \frac{1}{(p^0)^2 - \mathbf{p}^2 \tilde{A}^2 - \tilde{B}^2 + i\epsilon} \\
&= \frac{i}{4\pi} \frac{(-\boldsymbol{\gamma} \cdot \mathbf{p} \tilde{A} + \mathbb{1} \tilde{B})}{\sqrt{\mathbf{p}^2 \tilde{A}^2 + \tilde{B}^2}} \int dp^0 \left[ \frac{1}{p^0 - \left( \sqrt{\mathbf{p}^2 \tilde{A}^2 + \tilde{B}^2} - i\epsilon \right)} \right. \\
&\quad \left. - \frac{1}{p^0 - \left( -\sqrt{\mathbf{p}^2 \tilde{A}^2 + \tilde{B}^2} + i\epsilon \right)} \right] \\
&= \frac{1}{2} \frac{(-\boldsymbol{\gamma} \cdot \mathbf{p} \tilde{A} + \mathbb{1} \tilde{B})}{\sqrt{\mathbf{p}^2 \tilde{A}^2 + \tilde{B}^2}},
\end{aligned} \tag{5.64}$$

where the residue theorem has been used. Comparison of Eqs. (5.63) and (5.64) yields the conditions

$$\frac{\tilde{A}}{2\sqrt{\mathbf{p}^2 \tilde{A}^2 + \tilde{B}^2}} = \frac{A}{p^2 A^2 + B^2} \quad \text{and} \quad \frac{\tilde{B}}{2\sqrt{\mathbf{p}^2 \tilde{A}^2 + \tilde{B}^2}} = \frac{B}{p^2 A^2 + B^2}, \tag{5.65}$$

which can be solved for  $A$  and  $B$  giving

$$A(\mathbf{p}) = \frac{2}{\sqrt{M(\mathbf{p})^2 + \mathbf{p}^2}} \quad \text{and} \quad B(\mathbf{p}) = \frac{2M(\mathbf{p})}{\sqrt{M(\mathbf{p})^2 + \mathbf{p}^2}} \tag{5.66}$$

with

$$M(\mathbf{p}) = \frac{\tilde{B}(\mathbf{p})}{\tilde{A}(\mathbf{p})} = \frac{B(\mathbf{p})}{A(\mathbf{p})}. \tag{5.67}$$

Therefore, using an energy independent ansatz for the quark self energy allows us to express the dressing functions  $A$  and  $B$  of the static quark two-point function in terms of the mass function  $M$ . In the ultraviolet, the dressing functions turn into the ones of the bare propagator (see Ref. [44]),

$$A(\mathbf{p} \rightarrow \infty) = \frac{2}{\sqrt{m^2 + \mathbf{p}^2}} \quad \text{and} \quad B(\mathbf{p} \rightarrow \infty) = \frac{2m}{\sqrt{m^2 + \mathbf{p}^2}}, \tag{5.68}$$

so the mass function approaches the current quark mass for high momenta,

$$M(\mathbf{p} \rightarrow \infty) = \frac{B(\mathbf{p} \rightarrow \infty)}{A(\mathbf{p} \rightarrow \infty)} = m. \tag{5.69}$$

On the other hand, Eq. (5.65) yields the constraint

$$\mathbf{p}^2 A^2(p) + B^2(p) = 4. \tag{5.70}$$

We choose the bare dressing functions  $A_\Lambda$  and  $B_\Lambda$  according to Eq. (5.68) as

$$A_\Lambda(p) = \frac{2}{\sqrt{m^2 + p^2}} \quad \text{and} \quad B_\Lambda(p) = \frac{2m}{\sqrt{m^2 + p^2}}. \quad (5.71)$$

This result is also obtained directly in the case  $g = 0$ , because then we have  $A = A_\Lambda$  and  $B = B_\Lambda$  and the bare time-dependent two-point function in Eq. (5.60) is parameterized with  $\tilde{A}(p) = 1$  and  $\tilde{B}(p) = m$ . Together with Eq. (5.65) this yields again the above equations.

We plug these bare propagators into Eqs. (5.37) and (5.38), without the gluon term, and those into the definition of the mass function, Eq. (5.67). As the regulator functions only occur with the argument  $q$ , we can replace the UV regulator terms with an integration cut-off  $\Lambda$  and get

$$M(p) = \left\{ \frac{2m}{\sqrt{m^2 + p^2}} + g^2 C_2 \int^\Lambda \frac{d^3 q}{(2\pi)^3} \frac{M(q) P(\mathbf{p} - \mathbf{q})}{2\sqrt{M^2(q) + q^2}} \right\} / \left\{ \frac{2}{\sqrt{m^2 + p^2}} + g^2 C_2 \int^\Lambda \frac{d^3 q}{(2\pi)^3} \frac{\hat{\mathbf{p}} \cdot \hat{\mathbf{q}} q P(\mathbf{p} - \mathbf{q})}{2p\sqrt{M^2(q) + q^2}} \right\}, \quad (5.72)$$

where the dressing functions  $A$  and  $B$  have been expressed in terms of the mass function, Eq. (5.66), and the constraint (5.70) has been taken into account. This is the equation we are going to solve in the following. It can also be written in an alternative form,

$$M(p) = m + g^2 C_2 \frac{\sqrt{m^2 + p^2}}{2} \int^\Lambda \frac{d^3 q}{(2\pi)^3} P(\mathbf{p} - \mathbf{q}) \frac{M(q) - \hat{\mathbf{p}} \cdot \hat{\mathbf{q}} \frac{q}{p} M(p)}{2\sqrt{M^2(q) + q^2}} \quad (5.73)$$

### 5.3.2 Results obtained in the framework of Adler and Davis

In Ref. [99] by Adler and Davis, chiral symmetry breaking in Coulomb gauge QCD has been studied. An equation for the mass function, however, has not been derived explicitly. We will use this framework to calculate the mass function and to compare it later on with our own results. There, the static quark propagator has been parameterized as

$$S(\mathbf{p}) = \frac{p\bar{A}(p)\beta + (1 + \bar{B}(p))\boldsymbol{\alpha} \cdot \mathbf{p}}{2p\sqrt{A(p)^2 + (1 + B(p))^2}}. \quad (5.74)$$

With this parameterization the mass function reads

$$M(p) = \frac{p\bar{A}}{1 + \bar{B}}(p), \quad (5.75)$$

see Eq. (5.67). The equation for the dressing functions in the approximation of a bare quark-gluon vertex, which has been applied there, yields

$$\begin{aligned} p\bar{A}(p) &= \frac{16\pi}{3} \int \frac{d^3q}{(2\pi)^3} F(\mathbf{p} - \mathbf{q}) \frac{\bar{A}}{2\sqrt{\bar{A}^2 + (1 + \bar{B})^2}}(q), \\ p\bar{B}(p) &= \frac{16\pi}{3} \int \frac{d^3q}{(2\pi)^3} F(\mathbf{p} - \mathbf{q}) \hat{\mathbf{p}} \cdot \hat{\mathbf{q}} \frac{1 + \bar{B}}{2\sqrt{\bar{A}^2 + (1 + \bar{B})^2}}(q). \end{aligned} \quad (5.76)$$

With these expressions we can formulate an equation for the mass function only:

$$\begin{aligned} M(p) &= \left\{ \frac{16\pi}{3} \int \frac{d^3q}{(2\pi)^3} F(\mathbf{p} - \mathbf{q}) \frac{\bar{A}}{2\sqrt{\bar{A}^2 + (1 + \bar{B})^2}}(q) \right\} \\ &\quad / \left\{ 1 + \frac{16\pi}{3} \frac{1}{p} \int \frac{d^3q}{(2\pi)^3} F(\mathbf{p} - \mathbf{q}) \hat{\mathbf{p}} \cdot \hat{\mathbf{q}} \frac{1 + \bar{B}}{2\sqrt{\bar{A}^2 + (1 + \bar{B})^2}}(q) \right\} \\ &= \left\{ \frac{16\pi}{3} \int \frac{d^3q}{(2\pi)^3} F(\mathbf{p} - \mathbf{q}) \frac{M}{2\sqrt{M^2 + q^2}}(q) \right\} \\ &\quad / \left\{ 1 + \frac{16\pi}{3} \int \frac{d^3q}{(2\pi)^3} F(\mathbf{p} - \mathbf{q}) \frac{\frac{q}{p} \hat{\mathbf{p}} \cdot \hat{\mathbf{q}}}{2\sqrt{M(q)^2 + q^2}} \right\}. \end{aligned} \quad (5.77)$$

This can be rewritten as

$$M(p) = \frac{16\pi}{3} \int \frac{d^3q}{(2\pi)^3} F(\mathbf{p} - \mathbf{q}) \frac{M(q) - \frac{q}{p} \hat{\mathbf{p}} \cdot \hat{\mathbf{q}} M(p)}{2\sqrt{M(q)^2 + q^2}}. \quad (5.78)$$

Note that this equation is very similar to ours in the chiral limit, Eq. (5.73). The structural differences are that our equation comprises the four-quark function  $P(p)$  instead of the colour Coulomb potential  $F(p)$  and that in our equation the integral is multiplied by the free quark energy  $E_{\mathbf{p}} = p$ .

To solve this equation numerically, we introduce an infrared regulator  $\varepsilon$  into the Coulomb potential,

$$F(p) \sim \frac{1}{p^4} \rightarrow \frac{1}{p^2(p^2 + \varepsilon^2)}. \quad (5.79)$$

It turns out that the equation in the form of (5.78) is less amenable to a numerical iterative treatment than in the form of (5.77). The results are shown in Figs. 5.9 and 5.10. The mass function decreases in the ultraviolet like  $M(p) \sim 1/p^4$  and it reaches a plateau value of  $M(0) = 0.19$  in the infrared. With a Coulomb string tension of about  $\sigma_C \sim 2\sigma$  [111–114] and the Wilson string tension  $\sigma = (440\text{MeV})^2$ , the constituent quark mass becomes  $M(0) = 120\text{MeV}$ , a value considerably smaller than the phenomenological  $300\text{MeV}$ .

Furthermore, we can calculate the chiral condensate, an order parameter of chiral

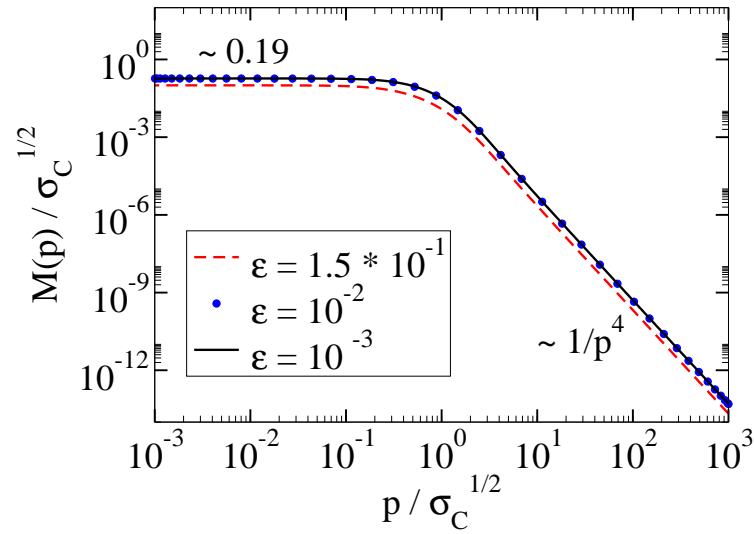


**Figure 5.9:** The mass function calculated within the framework of Adler and Davis [99] in a double-logarithmic plot. The infrared plateau value gives the constituent quark mass  $M(0) = 0.19\sqrt{\sigma_C}$ . With  $\sigma_C \sim 2\sigma = 2 \cdot (440\text{MeV})^2$ , the constituent quark mass is  $M(0) = 120\text{MeV}$ .

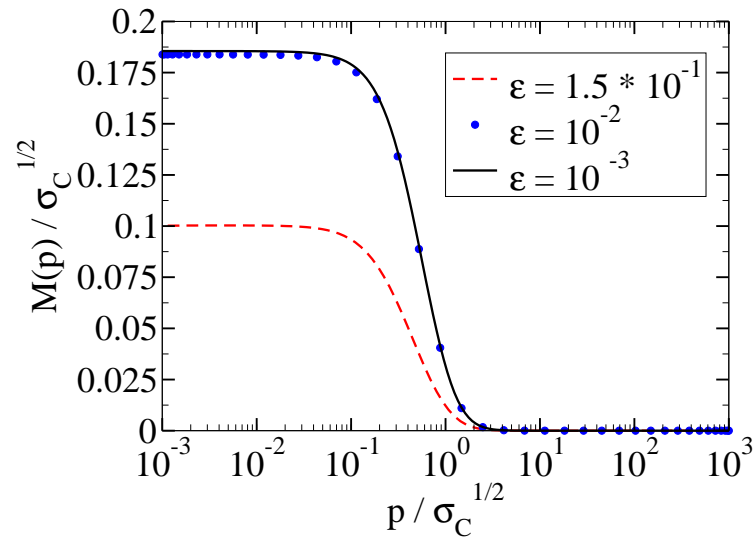


**Figure 5.10:** Like Fig. 5.9 in a half-logarithmic plot. The convergence of the procedure on lowering the infrared regulator  $\epsilon$  is explicitly seen.

symmetry breaking. It is defined as

$$\begin{aligned}
\langle \bar{\psi}(\mathbf{x})\psi(\mathbf{x}) \rangle &= \beta_{\beta\alpha} \langle \psi_{\beta}^{\dagger m}(\mathbf{x})\psi_{\alpha}^m(\mathbf{x}) \rangle = \beta_{\beta\alpha} \langle \delta^{mm} \delta_{\alpha\beta} \delta^3(\mathbf{0}) - \psi_{\alpha}^m(\mathbf{x})\psi_{\beta}^{\dagger m}(\mathbf{x}) \rangle \\
&= \delta^{mm} \text{Tr} \beta \delta^3(\mathbf{0}) - \beta_{\beta\alpha} \int \frac{d^3[pq]}{(2\pi)^6} \delta^{mm} S(\mathbf{p})_{\beta\alpha} (2\pi)^3 \delta^3(\mathbf{p} + \mathbf{q}) e^{i(\mathbf{p}+\mathbf{q})\cdot\mathbf{x}} \\
&= -N_c \int \frac{d^3p}{(2\pi)^3} \text{Tr} \frac{(1 + \bar{B})\boldsymbol{\gamma} \cdot \mathbf{p} + p\bar{A}\mathbf{1}}{2p\sqrt{A^2 + (1 + \bar{B})^2}}(p) = -N_c \int \frac{d^3p}{(2\pi)^3} \frac{2M(p)}{\sqrt{M(p)^2 + p^2}}
\end{aligned} \tag{5.80}$$

In the case at hand the chiral condensate is

$$\langle \bar{\psi}\psi \rangle = -1.84 \cdot 10^{-2} \sigma_C^{3/2} = -(164\text{MeV})^3, \tag{5.81}$$

which is substantially lower than the expected value of about  $\langle \bar{\psi}\psi \rangle \sim -(230\text{MeV})^3$ .

## 5.4 Solving the Mass Equation

In this section, we use two different ansatzes for the four-quark function, which enters the quark tadpole term, in order to calculate the mass function: an ansatz that is inspired by the form of the corresponding term in the Hamiltonian and a perturbatively improved ansatz.

### 5.4.1 A Hamiltonian ansatz for the four-quark function

In the derivation of the quark propagator flow equation in Sec. 5.1 we have already used the ansatz of Eq. (5.31) for the four-quark function,

$$\begin{aligned}
&\left( \frac{\delta^4 \Gamma_k}{\delta\psi^{\dagger} \delta\psi \delta\psi^{\dagger} \delta\psi} \right)_{\alpha_4 \alpha_3 \alpha_2 \alpha_1}^{m_4 m_3 m_2 m_1}(\mathbf{p}_4, \mathbf{p}_3, \mathbf{p}_2, \mathbf{p}_1) = \\
&(2\pi)^3 \delta^3(\mathbf{p}_4 + \mathbf{p}_3 + \mathbf{p}_2 + \mathbf{p}_1) g^2 [P_k(\mathbf{p}_1 + \mathbf{p}_2) \delta_{\alpha_2 \alpha_1} \delta_{\alpha_4 \alpha_3} (T^a)^{m_4 m_3} (T^a)^{m_2 m_1} \\
&\quad - P_k(\mathbf{p}_2 + \mathbf{p}_3) \delta_{\alpha_3 \alpha_2} \delta_{\alpha_4 \alpha_1} (T^a)^{m_4 m_1} (T^a)^{m_2 m_3}],
\end{aligned} \tag{5.82}$$

that has been modelled after the Coulomb term (5.28) in the Hamiltonian,

$$H_C = \frac{g^2}{2} \int d^3[xy] \psi^{\dagger}(\mathbf{x}) T^a \psi(\mathbf{x}) F^{ab}(\mathbf{x} - \mathbf{y}) \psi^{\dagger}(\mathbf{y}) T^b \psi(\mathbf{y}). \tag{5.83}$$

Making the appropriate approximations in the loop integral, we have arrived at Eq. (5.72) for the mass function. Approaching the chiral limit,  $m = 0$ , this equation becomes

$$\begin{aligned}
M(p) &= \left\{ C_2 \int^{\Lambda} \frac{d^3q}{(2\pi)^3} g^2 P(\mathbf{p} - \mathbf{q}) \frac{M(q)}{2\sqrt{M^2(q) + q^2}} \right\} \\
&\quad / \left\{ \frac{2}{p} + C_2 \int^{\Lambda} \frac{d^3q}{(2\pi)^3} g^2 P(\mathbf{p} - \mathbf{q}) \frac{\hat{\mathbf{p}} \cdot \hat{\mathbf{q}} \frac{q}{p}}{2\sqrt{M^2(q) + q^2}} \right\}.
\end{aligned} \tag{5.84}$$



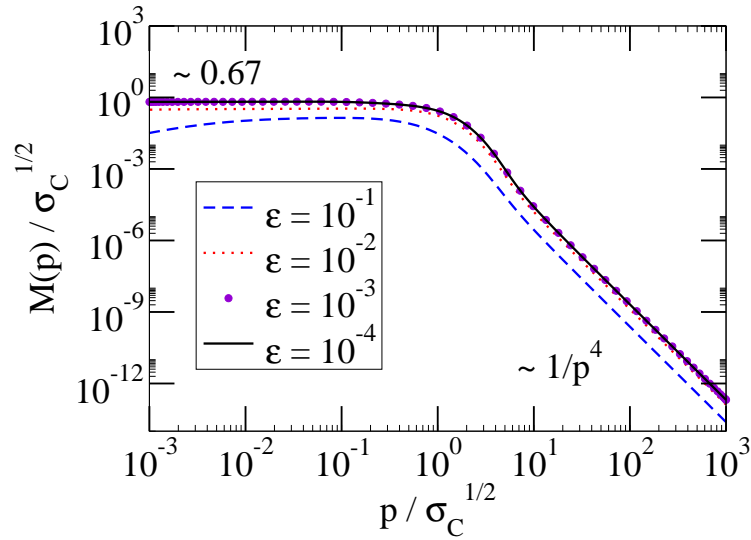


**Figure 5.11:** The mass function calculated with the ansatz of Eq. (5.82) for the four-quark function, in a double-logarithmic plot. The infrared plateau value gives the constituent quark mass  $M(0) = 0.67\sqrt{\sigma_C}$ . With  $\sigma_C \sim 2\sigma = 2 \cdot (440 \text{ MeV})^2$ , the constituent quark mass is  $M(0) \sim 420 \text{ MeV}$ .

It has assumed almost the same structure as the equation for the mass function in the framework of Adler and Davis, Eq. (5.77). There are two important differences: the term  $2/p$  in the sum in the denominator occurs instead of the term 1 in the sum in the denominator of Eq. (5.77), and the four-quark function  $P(\mathbf{p} - \mathbf{q})$  appears instead of the colour Coulomb potential  $F(\mathbf{p} - \mathbf{q})$ . As the four-quark function is not known, we go by the dimension  $[P] = -3$ , which is one less than the dimension of the colour Coulomb potential,  $[F] = -2$ , and in view of Eq. (4.13) we use the ansatz

$$g^2 P(\mathbf{p} - \mathbf{q}) = \frac{8\pi\sigma_C}{|\mathbf{p} - \mathbf{q}|^5}. \quad (5.85)$$

This ansatz can be justified a posteriori by the observation that the UV behaviour of the mass function  $M(p \rightarrow \infty) \sim 1/p^4$  will turn out to be same as in the case of Adler and Davis, see Fig. 5.9, and that the behaviour of  $P$  is the same in the UV as well as in the IR as it is the case for the colour Coulomb potential  $F$  used before in Eq. (5.77). We can therefore expect similar results as in the case of Subsec. 5.3.2, also in the IR. Obviously, this is indeed true qualitatively: the result of the numerical calculation for the chiral limit is shown in Figs. 5.11 and 5.12, the result for a current quark mass of  $m \sim 4 \text{ MeV}$  is given in Fig. 5.13, each with a decreasing infrared regulator  $\varepsilon$  as in Subsec. 5.3.2.

We observe that with this choice of the four-quark function the ultraviolet behaviour in the chiral limit is  $M(p \rightarrow \infty) \sim 1/p^4$  like in the framework of Adler and Davis, see Fig. 5.9. In the infrared a plateau develops at a value of  $M(0) = 0.67\sqrt{\sigma_C} \sim 420 \text{ MeV}$  in the chiral limit and of  $M(0) = 0.69\sqrt{\sigma_C} \sim 430 \text{ MeV}$  in the case of  $m \sim 4 \text{ MeV}$ . In contrast to Subsec. 5.3.2, both results lie higher than

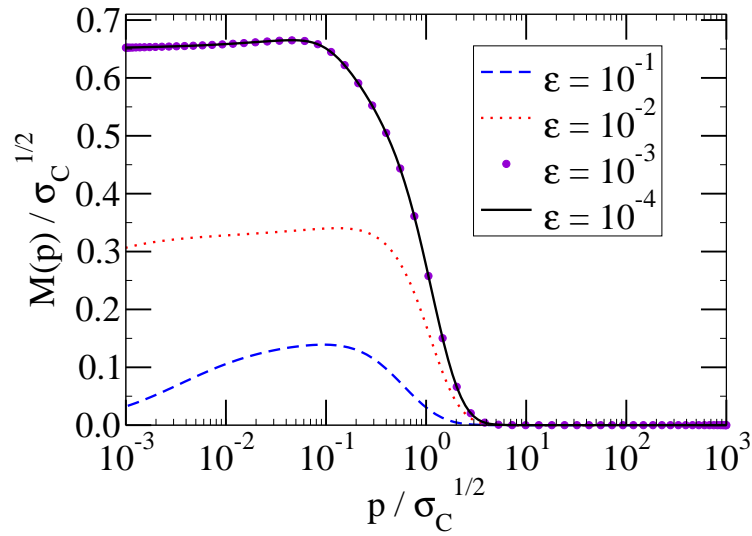


**Figure 5.12:** Like Fig. 5.11, in a half-logarithmic plot. The convergence on lowering the infrared regulator  $\varepsilon$  is explicitly seen.

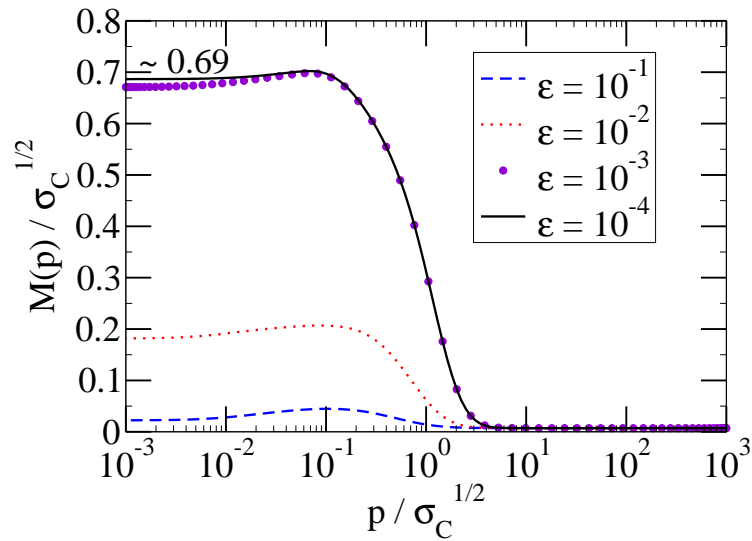


**Figure 5.13:** Like Fig. 5.11 but with a current quark mass  $m \sim 4$  MeV, giving  $M(0) \sim 430$  MeV.

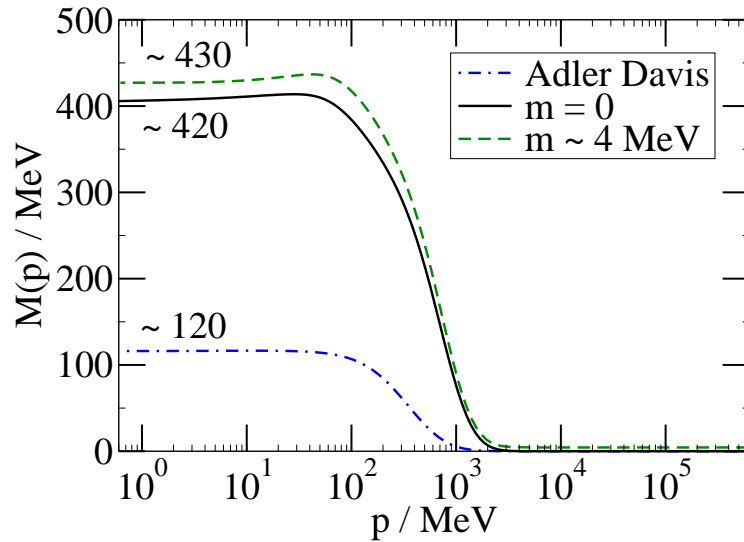


**Figure 5.14:** Comparison of the mass function obtained with the simple ansatz for the four-quark function in the chiral and massive case with the mass function obtained from the equation of Ref. [99].

the phenomenological 300 MeV, but still at a reasonably good value considering the model ansatz for the four-quark function. In Figs. 5.14 and 5.15 we compare our results obtained for the chiral case and for the massive case to the results from the equation in the framework of Adler and Davis. Our results are higher by a factor of about 3.5.

With the knowledge of the mass function we can again calculate the chiral condensate defined in Eq. (5.80) and get

$$\langle \bar{\psi}\psi \rangle = 1.48 \cdot 10^{-1} \sigma_C^{3/2} = -(329 \text{ MeV})^3, \quad (5.86)$$

which lies considerably higher than the experimental value of about  $\sim -(230 \text{ MeV})^3$ .

Note again that without the replacements of Eq. (5.34) a solution for the flow equations for  $A$  and  $B$  was not found.

### 5.4.2 A perturbatively improved four-quark function

In the previous section, we have used a sophisticated guess to determine the four-quark function as an input into the equation for the mass function, where the model was the Coulomb term of the Hamiltonian. In this section we use perturbation theory to improve the ansatz of Eq. (5.31) in order to get a hint at the form of the four-quark function. The perturbative calculation to the lowest order is shown in

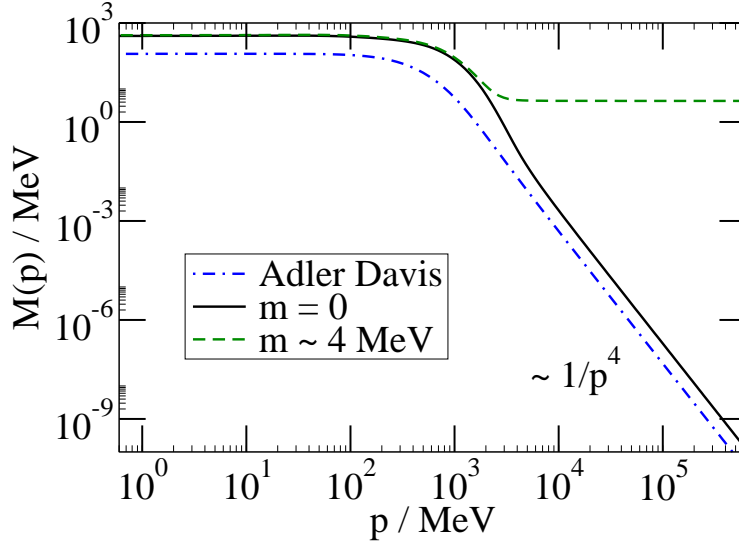


**Figure 5.15:** Like Fig. 5.14, in a double-logarithmic plot.

Appendix E.2, and the result is

$$\begin{aligned}
 & \left( \frac{\delta^4 \Gamma}{\delta \psi^\dagger \delta \psi \delta \psi^\dagger \delta \psi} \right)_{\alpha_4 \alpha_3 \alpha_2 \alpha_1}^{m_4 m_3 m_2 m_1}(\mathbf{p}_4, \mathbf{p}_3, \mathbf{p}_2, \mathbf{p}_1) = \frac{64g^2(2\pi)^3 \delta^3(\mathbf{p}_1 + \mathbf{p}_2 + \mathbf{p}_3 + \mathbf{p}_4)}{E_{\mathbf{p}_1} + \dots + E_{\mathbf{p}_4}} \\
 & \left\{ (T^a)^{m_4 m_3} (T^a)^{m_2 m_1} \left[ (S^{(+)}(\mathbf{p}_4) S^{(-)}(-\mathbf{p}_3))_{\alpha_4 \alpha_3} (S^{(+)}(\mathbf{p}_2) S^{(-)}(-\mathbf{p}_1))_{\alpha_2 \alpha_1} \right. \right. \\
 & \quad \left. \left. + (S^{(-)}(\mathbf{p}_4) S^{(+)}(-\mathbf{p}_3))_{\alpha_4 \alpha_3} (S^{(-)}(\mathbf{p}_2) S^{(+)}(-\mathbf{p}_1))_{\alpha_2 \alpha_1} \right] F(\mathbf{p}_1 + \mathbf{p}_2) \right. \\
 & \quad \left. - (T^a)^{m_4 m_1} (T^a)^{m_2 m_3} \left[ (S^{(+)}(\mathbf{p}_4) S^{(-)}(-\mathbf{p}_1))_{\alpha_4 \alpha_1} (S^{(+)}(\mathbf{p}_2) S^{(-)}(-\mathbf{p}_3))_{\alpha_2 \alpha_3} \right. \right. \\
 & \quad \left. \left. + (S^{(-)}(\mathbf{p}_4) S^{(+)}(-\mathbf{p}_1))_{\alpha_4 \alpha_1} (S^{(-)}(\mathbf{p}_2) S^{(+)}(-\mathbf{p}_3))_{\alpha_2 \alpha_3} \right] F(\mathbf{p}_2 + \mathbf{p}_3) \right\}. \tag{5.87}
 \end{aligned}$$

We plug the improved four-quark function of Eq. (5.87) into the flow equation of the two-quark function, see Eq. (5.15), retaining only the quark tadpole term. This calculation is detailed in Appendix E.3. For the flows of the dressing functions  $A$

and  $B$  we get

$$\begin{aligned} \mathbf{p}^2 \dot{A}_k(p) &= 16g^2 C_2 \int \frac{d^3 q}{(2\pi)^3} F_k(\mathbf{p} - \mathbf{q}) \frac{m\mathbf{p}^2(\mathbf{q}^2 - \mathbf{p} \cdot \mathbf{q}) + m\mathbf{p} \cdot \mathbf{q} E_{\mathbf{p}}(E_{\mathbf{p}} - E_{\mathbf{q}})}{(E_{\mathbf{p}} + E_{\mathbf{q}}) E_{\mathbf{p}}^2 E_{\mathbf{q}}^2} \\ &\frac{1}{[q^2(A_k + R_{\alpha,k})^2 + (B_k + R_{\beta,k})^2]^2(q)} \\ &\left[ m \left( \dot{R}_{\alpha,k}(B_k + R_{\beta,k})^2 - \dot{R}_{\alpha,k} q^2 (A_k + R_{\alpha,k})^2 - 2\dot{R}_{\beta,k}(A_k + R_{\alpha,k})(B_k + R_{\beta,k}) \right) (q) \right. \\ &\left. + \left( 2\dot{R}_{\alpha,k} q^2 (A_k + R_{\alpha,k})(B_k + R_{\beta,k}) + \dot{R}_{\beta,k}(B_k + R_{\beta,k})^2 - \dot{R}_{\beta,k} q^2 (A_k + R_{\alpha,k})^2 \right) (q) \right] \end{aligned} \quad (5.88)$$

and

$$\begin{aligned} \dot{B}_k(p) &= -16g^2 C_2 \int \frac{d^3 q}{(2\pi)^3} F_k(\mathbf{p} - \mathbf{q}) \frac{(m^2 - E_{\mathbf{p}} E_{\mathbf{q}}) \mathbf{p} \cdot \mathbf{q} + \mathbf{p}^2 \mathbf{q}^2}{(E_{\mathbf{p}} + E_{\mathbf{q}}) E_{\mathbf{p}}^2 E_{\mathbf{q}}^2} \\ &\frac{1}{[q^2(A_k + R_{\alpha,k})^2 + (B_k + R_{\beta,k})^2]^2(q)} \\ &\left[ m \left( \dot{R}_{\alpha,k}(B_k + R_{\beta,k})^2 - \dot{R}_{\alpha,k} q^2 (A_k + R_{\alpha,k})^2 - 2\dot{R}_{\beta,k}(A_k + R_{\alpha,k})(B_k + R_{\beta,k}) \right) (q) \right. \\ &\left. + \left( 2\dot{R}_{\alpha,k} q^2 (A_k + R_{\alpha,k})(B_k + R_{\beta,k}) + \dot{R}_{\beta,k}(B_k + R_{\beta,k})^2 - \dot{R}_{\beta,k} q^2 (A_k + R_{\alpha,k})^2 \right) (q) \right] \end{aligned} \quad (5.89)$$

As usual, in order to make the analytic integration of the flow possible, at first we replace  $\{A_k, B_k, F_k\} \rightarrow \{A_0, B_0, F_0\}$  in the loop integral. We can then again use the total derivatives of Eqs. (5.35) and (5.36) as well as the corresponding expressions for  $B$  to get

$$\begin{aligned} \mathbf{p}^2 A_0(p) &= \mathbf{p}^2 A_{\Lambda}(p) + 16g^2 C_2 \int^{\Lambda} \frac{d^3 q}{(2\pi)^3} F_0(\mathbf{p} - \mathbf{q}) \\ &\frac{m\mathbf{p}^2(\mathbf{q}^2 - \mathbf{p} \cdot \mathbf{q}) + m\mathbf{p} \cdot \mathbf{q} E_{\mathbf{p}}(E_{\mathbf{p}} - E_{\mathbf{q}})}{4(E_{\mathbf{p}} + E_{\mathbf{q}}) E_{\mathbf{p}}^2 E_{\mathbf{q}}^2} (mA_0(q) - B_0(q)) \end{aligned} \quad (5.90)$$

and

$$\begin{aligned} B_0(p) &= B_{\Lambda}(p) - 16g^2 C_2 \int^{\Lambda} \frac{d^3 q}{(2\pi)^3} F_0(\mathbf{p} - \mathbf{q}) \\ &\frac{(m^2 - E_{\mathbf{p}} E_{\mathbf{q}}) \mathbf{p} \cdot \mathbf{q} + \mathbf{p}^2 \mathbf{q}^2}{4(E_{\mathbf{p}} + E_{\mathbf{q}}) E_{\mathbf{p}}^2 E_{\mathbf{q}}^2} (mA_0(q) - B_0(q)). \end{aligned} \quad (5.91)$$

The effect of the perturbatively improved four-quark function, besides the emergence of several kinematic factors, is that, compared to Eqs. (5.37) and (5.38), the dressing function  $B$  is mixed into the equation for  $A$  and vice versa, apart from the term in the denominator which is a constant at  $k = 0$ , according to Eq. (5.70). With these

two dressing functions and using Eq. (5.68) for the bare dressing functions as well as Eqs. (5.66) and (5.70), we can write the mass function (5.67) as

$$M(p) = \left\{ \frac{2m}{E_{\mathbf{p}}} + 16g^2 C_2 \int^{\Lambda} \frac{d^3 q}{(2\pi)^3} F_0(\mathbf{p} - \mathbf{q}) \right. \\ \left. \frac{(m^2 - E_{\mathbf{p}} E_{\mathbf{q}}) \mathbf{p} \cdot \mathbf{q} + \mathbf{p}^2 \mathbf{q}^2}{2(E_{\mathbf{p}} + E_{\mathbf{q}}) E_{\mathbf{p}}^2 E_{\mathbf{q}}^2} \frac{M(q) - m}{\sqrt{M^2(q) + \mathbf{q}^2}} \right\} \\ \left/ \left\{ \frac{2}{E_{\mathbf{p}}} + 16g^2 C_2 \int^{\Lambda} \frac{d^3 q}{(2\pi)^3} F_0(\mathbf{p} - \mathbf{q}) \right. \right. \\ \left. \left. \frac{m \mathbf{p}^2 (\mathbf{q}^2 - \mathbf{p} \cdot \mathbf{q}) + m \mathbf{p} \cdot \mathbf{q} E_{\mathbf{p}} (E_{\mathbf{p}} - E_{\mathbf{q}})}{2(E_{\mathbf{p}} + E_{\mathbf{q}}) E_{\mathbf{p}}^2 E_{\mathbf{q}}^2 \mathbf{p}^2} \frac{m - M(q)}{\sqrt{M^2(q) + \mathbf{q}^2}} \right\} \right. . \quad (5.92)$$

This equation simplifies considerably in the chiral limit  $m = 0$  as the loop integral in the denominator vanishes and we obtain

$$M(p) = 4C_2 p \int^{\Lambda} \frac{d^3 q}{(2\pi)^3} g^2 F(\mathbf{p} - \mathbf{q}) \frac{M(q)(1 - \hat{\mathbf{p}} \cdot \hat{\mathbf{q}})}{(p + q) \sqrt{M^2(q) + q^2}} . \quad (5.93)$$

We can now use a pure confining potential,

$$g^2 F(p) = \frac{8\pi\sigma_c}{p^4} , \quad (5.94)$$

as input into the equation. The numerical results are shown in Fig. 5.16. We see the ultraviolet behaviour of  $M(p) = 1/p^4$  unchanged, but instead of a plateau in the infrared, a divergence of  $M(p) \sim 1/p$  emerges, leading to an infinite constituent quark mass, which is, of course, unphysical.

The inclusion of a current quark mass even aggravates the situation: due to the differences occurring Eq. (5.92), in the numerical solution the mass function  $M(p)$  at some iteration step turns negative for sufficiently high values of the current quark mass  $m$ , regardless of the value of the infrared regulator  $\varepsilon$ . Two exemplary cases are shown in Figs. 5.17 and 5.18.

So far we have taken the perturbative form (5.87) of the four-quark function with the non-perturbative infrared behaviour  $F(p \rightarrow 0) \sim 1/p^4$  of the colour Coulomb potential  $F$  plugged in. This may seem inappropriate as we are dealing with entirely non-perturbative correlation functions, so we now go one step further and replace the energy terms of the free quarks in Eq. (5.87),

$$E_{\mathbf{p}} = \sqrt{m^2 + \mathbf{p}^2} \quad \text{by} \quad \mathcal{E}_{\mathbf{p}} = \sqrt{M(\mathbf{p})^2 + \mathbf{p}^2} \quad (5.95)$$

as well as the projectors

$$S^{(\pm)}(\mathbf{p}) = \frac{1}{2} \pm \frac{\boldsymbol{\alpha} \cdot \mathbf{p} + \beta m}{2E_{\mathbf{p}}} \quad \text{by} \quad \mathcal{S}^{(\pm)}(\mathbf{p}) = \frac{1}{2} \pm \frac{\boldsymbol{\alpha} \cdot \mathbf{p} + \beta M(\mathbf{p})}{2\mathcal{E}_{\mathbf{p}}} . \quad (5.96)$$

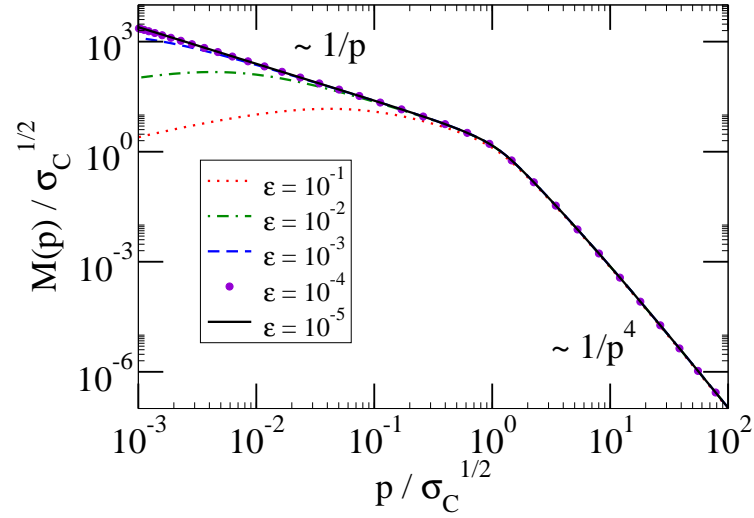


**Figure 5.16:** The mass function with the improved four-quark function of Eq. (5.87) as input is shown in the chiral limit  $m = 0$ . The regulator  $\varepsilon$  in  $F(\mathbf{p} - \mathbf{q}) = 1/[(\mathbf{p} - \mathbf{q})^2 + \varepsilon^2]$  is gradually lowered until convergence is reached. The ultraviolet behaviour of  $M(p) = 1/p^4$  is the same as in the cases before but in the infrared a divergence of  $M(p) \sim 1/p$  instead of a plateau emerges, leading to an infinite constituent quark mass, which is, of course, unphysical.

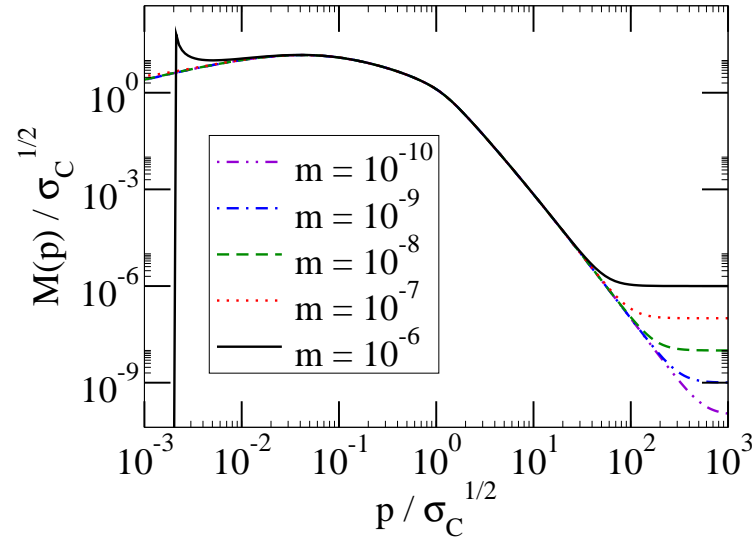


**Figure 5.17:** Like Fig. 5.16 but with non-vanishing current quark mass  $m$  and with the infrared regulator  $\varepsilon = 10^{-1}$ . As  $m$  is gradually increased, the mass function at some point becomes negative. This is caused by the differences occurring in Eq. (5.92).

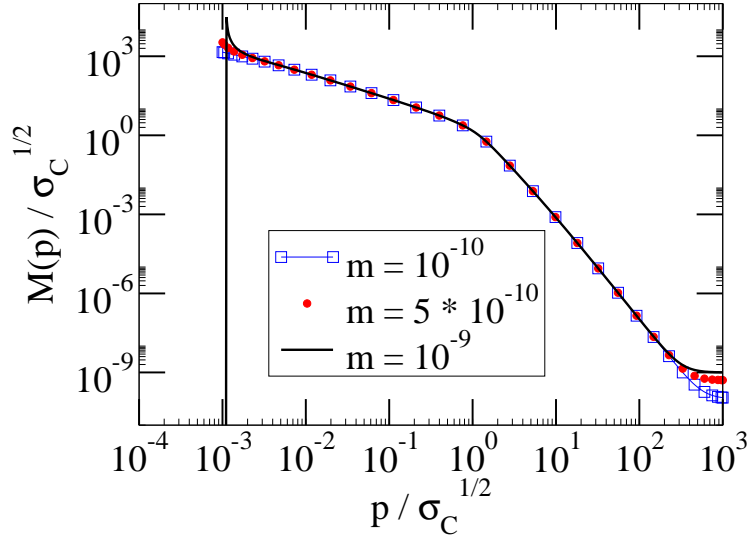


**Figure 5.18:** Like Fig. 5.17, but with the infrared regulator  $\varepsilon = 10^{-3}$ .

Plugging this four-quark function into Eq. (5.15) we can proceed as in Appendix E.3, but the Dirac structure of the equations now reads

$$\begin{aligned}
& \mathcal{S}^{(+)}(-\mathbf{p})\mathcal{S}^{(-)}(-\mathbf{q})\boldsymbol{\alpha}\cdot\mathbf{q}\mathcal{S}^{(+)}(-\mathbf{q})\mathcal{S}^{(-)}(-\mathbf{p}) \\
& + \mathcal{S}^{(-)}(-\mathbf{p})\mathcal{S}^{(+)}(-\mathbf{q})\boldsymbol{\alpha}\cdot\mathbf{q}\mathcal{S}^{(-)}(-\mathbf{q})\mathcal{S}^{(+)}(-\mathbf{p}) \\
& = \frac{M(q)}{2\mathcal{E}_p^2\mathcal{E}_q^2} [\boldsymbol{\alpha}\cdot\mathbf{p}(M(p)\mathbf{q}^2 - M(q)\mathbf{p}\cdot\mathbf{q}) \\
& \quad + \boldsymbol{\alpha}\cdot\mathbf{q}(M(q)\mathcal{E}_p^2 - M(p)\mathcal{E}_p\mathcal{E}_q) \\
& \quad + \beta(\mathbf{p}^2\mathbf{q}^2 + (M(p)M(q) - \mathcal{E}_p\mathcal{E}_q)\mathbf{p}\cdot\mathbf{q})]
\end{aligned} \tag{5.97}$$

and

$$\begin{aligned}
& \mathcal{S}^{(+)}(-\mathbf{p})\mathcal{S}^{(-)}(-\mathbf{q})\beta\mathcal{S}^{(+)}(-\mathbf{q})\mathcal{S}^{(-)}(-\mathbf{p}) \\
& + \mathcal{S}^{(-)}(-\mathbf{p})\mathcal{S}^{(+)}(-\mathbf{q})\beta\mathcal{S}^{(-)}(-\mathbf{q})\mathcal{S}^{(+)}(-\mathbf{p}) \\
& = \frac{1}{2\mathcal{E}_p^2\mathcal{E}_q^2} [\boldsymbol{\alpha}\cdot\mathbf{p}(M(p)\mathbf{q}^2 - M(q)\mathbf{p}\cdot\mathbf{q}) \\
& \quad + \boldsymbol{\alpha}\cdot\mathbf{q}(M(q)\mathcal{E}_p^2 - M(p)\mathcal{E}_p\mathcal{E}_q) \\
& \quad + \beta(\mathbf{p}^2\mathbf{q}^2 + (M(p)M(q) - \mathcal{E}_p\mathcal{E}_q)\mathbf{p}\cdot\mathbf{q})] .
\end{aligned} \tag{5.98}$$

Again the two terms are equal up to a mass factor, but the difference is that this time it is not the current quark mass  $m$  but the mass function  $M(q)$ . As we are dealing with a flow equation, the mass function is cut-off dependent as it is the quotient of the scalar and the vectorial part of the quark propagator in Eq. (5.25),

$$M_k(p) = \frac{B_k(p) + R_{\beta,k}(p)}{A_k(p) + R_{\alpha,k}(p)}, \tag{5.99}$$



so the flow equations become

$$\begin{aligned}
\mathbf{p}^2 \dot{A}_k(p) &= 16g^2 C_2 \int \frac{d^3 q}{(2\pi)^3} F_k(\mathbf{p} - \mathbf{q}) \\
\frac{M_k(p) q^2 p^2 - M_k(q) p^2 \mathbf{p} \cdot \mathbf{q} + M_k(q) \mathcal{E}_{k,\mathbf{p}}^2 \mathbf{p} \cdot \mathbf{q} - M_k(p) \mathcal{E}_{k,\mathbf{p}} \mathcal{E}_{k,\mathbf{q}} \mathbf{p} \cdot \mathbf{q}}{(\mathcal{E}_{k,\mathbf{p}} + \mathcal{E}_{k,\mathbf{q}}) \mathcal{E}_{k,\mathbf{p}}^2 \mathcal{E}_{k,\mathbf{q}}^2 [q^2 (A_k + R_{\alpha,k})^2 + (B_k + R_{\beta,k})^2]^2 (q)} \\
&\left[ M_k(q) \left( \dot{R}_{\alpha,k} (B_k + R_{\beta,k})^2 - \dot{R}_{\alpha,k} q^2 (A_k + R_{\alpha,k})^2 - 2\dot{R}_{\beta,k} (A_k + R_{\alpha,k}) (B_k + R_{\beta,k}) \right) (q) \right. \\
&\left. + \left( 2\dot{R}_{\alpha,k} q^2 (A_k + R_{\alpha,k}) (B_k + R_{\beta,k}) + \dot{R}_{\beta,k} (B_k + R_{\beta,k})^2 - \dot{R}_{\beta,k} q^2 (A_k + R_{\alpha,k})^2 \right) (q) \right]
\end{aligned} \tag{5.100}$$

and

$$\begin{aligned}
\dot{B}_k(p) &= -16g^2 C_2 \int \frac{d^3 q}{(2\pi)^3} F_k(\mathbf{p} - \mathbf{q}) \\
\frac{p^2 q^2 + \mathbf{p} \cdot \mathbf{q} (M_k(p) M_k(q) - \mathcal{E}_{k,\mathbf{p}} \mathcal{E}_{k,\mathbf{q}})}{(\mathcal{E}_{k,\mathbf{p}} + \mathcal{E}_{k,\mathbf{q}}) \mathcal{E}_{k,\mathbf{p}}^2 \mathcal{E}_{k,\mathbf{q}}^2} \frac{1}{[q^2 (A_k + R_{\alpha,k})^2 + (B_k + R_{\beta,k})^2]^2 (q)} \\
&\left[ M_k(q) \left( \dot{R}_{\alpha,k} (B_k + R_{\beta,k})^2 - \dot{R}_{\alpha,k} q^2 (A_k + R_{\alpha,k})^2 - 2\dot{R}_{\beta,k} (A_k + R_{\alpha,k}) (B_k + R_{\beta,k}) \right) (q) \right. \\
&\left. + \left( 2\dot{R}_{\alpha,k} q^2 (A_k + R_{\alpha,k}) (B_k + R_{\beta,k}) + \dot{R}_{\beta,k} (B_k + R_{\beta,k})^2 - \dot{R}_{\beta,k} q^2 (A_k + R_{\alpha,k})^2 \right) (q) \right]
\end{aligned} \tag{5.101}$$

However, again making the replacement  $\{A_k, B_k, F_k\} \rightarrow \{A_0, B_0, F_0\}$  in the loop integral, we cannot perform the flow integration analytically in this case. Moreover, also for the flow equations (5.100) and (5.101) without said replacement, no solution has been found. This is also true for Eqs. (5.32) and (5.33) as well as for Eqs. (5.88) and (5.89).

In summary, a flow equation for the static quark propagator has been derived. An approximation has been made which transforms the flow equation into an integral equation similar to a Dyson-Schwinger equation. With this equation, the effect of the gluon propagator and of the four-quark vertex on the dynamic generation of mass has been examined. It has been found that no dynamic generation of mass occurs if only the term involving the gluon propagator is taken into account. In contrast, with the quark tadpole term containing a simple ansatz for the four-quark vertex, a constituent quark mass emerges that even exceeds the phenomenological value of 300 MeV. For the quark propagator flow equation without the Dyson-Schwinger approximation, however, no solution has been found.



# Chapter 6

## Summary and Outlook

In this work a new approach to the non-perturbative calculation of the static correlation functions from the Hamiltonian formulation of Yang-Mills theory in Coulomb gauge has been presented. In the generating functional of the correlation functions at equal times, the absolute square of the vacuum wave functional plays the role of the exponential of the negative action in the usual Lagrangian approach. The functional renormalization group has been adapted to this Hamiltonian formulation.

Subsequently, the derivation of the flow equations for the gluon and ghost propagators has been presented. In order to arrive at a closed system of equations, the dressed ghost-gluon vertex has been replaced with the corresponding bare one, which is a good approximation according to perturbative arguments and lattice calculations, and all tadpole diagrams and vertices with three or more gluon lines have been discarded, which does not affect the infrared behaviour of the results. An approximation allowing for an analytical integration of the flow equations has been made that corresponds to an optimized choice of the regulator functions. The choice of the initial conditions has been discussed, which serve to implement the renormalization conditions corresponding to an infrared scaling solution for the propagators.

The result of the numerical solution of the flow equations has been compared to the solution of a system of Dyson-Schwinger equations derived from a variational principle for the vacuum wave functional. The solution of the optimized flow equations agrees with one of the two possible scaling solutions in the latter approach. In the approximation without tadpoles slightly different values for the infrared exponents have been obtained. The non-perturbative running coupling has been calculated, which forms a plateau in the infrared due to the scaling relation that both solutions fulfil.

Starting from the flow equation for the ghost propagator, a flow equation for the Coulomb form factor has been derived. Using the results for the flows of the gluon and ghost propagators as input, an infrared divergent Coulomb form factor has resulted without any further approximations. A confining colour Coulomb potential has been found, rising slightly more or less than linearly for large distances depending on the gluon and ghost propagator input.

In contrast, the Dyson-Schwinger-like integral equation for the Coulomb form factor found in the variational approach has no solution for the corresponding gluon and ghost propagators. Here, this equation has been re-derived from the flow equa-

tion and has been closely examined. It has been found that the equation indeed has a solution either for subcritical (or decoupling) input propagators or for critical (or scaling) propagators which are weakly infrared divergent (even more weakly than the one from the flow equation with the tadpoles neglected), which have, however, not been found in any approach.

Dynamic quarks have been included into the present formalism and a flow equation for the static quark propagator has been derived. An approximation has been made which turns the flow equation into a DSE-like equation with only the gluon propagator as input. With this approximation, only an infrared vanishing mass function has resulted. This confirms the result of the variational approach where no chiral symmetry breaking has been found by including transverse gluons without the Coulomb term of the Hamiltonian. In another approximation only the quark tadpole term has been considered. An ansatz for the four-quark function resembling the corresponding term in the Hamiltonian has been used. With this ansatz, an infrared constant mass function has been found, indicating a constituent quark mass slightly higher than expected. As there is no obvious direct connection to the colour Coulomb potential with this ansatz, the four-quark function has been calculated perturbatively to the lowest order, which contains the colour Coulomb potential. However, in this case no solution has been found with a finite current quark mass and in the chiral limit even an infrared divergent mass function emerged, which is, of course, unphysical. In any case, for the full flow equation, i.e., without the replacement leading to the DSE-like equation, no solution has been obtained.

The approach and results presented in this work motivate several additional investigations. In an analytical infrared analysis in Ref. [49] and also in a numerical calculation within the variational approach of Ref. [50], a second scaling solution with a stronger infrared divergence of the gluon correlator and the ghost form factor has been found. This solution has not been observed here as it poses an additional fine-tuning problem and is therefore difficult to obtain. The formalism put forward in the present work also allows to directly access the confining properties of the propagators. This can be done by using the Wilson loop potential evaluated along the lines of Ref. [115]. A first step in this direction is to implement the missing gluonic diagrams, which account for the correct ultraviolet behaviour, to allow a comparison with lattice data in the full momentum regime.

Concerning the quark sector, a better way to determine the quark four-point function should be found, as it is there where the information about the colour Coulomb potential enters. In the Lagrangian formulation, the potential can be identified with the time-time component of the gluon propagator. In the DSE for the quark propagator it couples to the quark via the quark-gluon vertex. One can speculate that a bare or some other kind of poor ansatz for this vertex fails to convey enough of the information about the potential from the gluon to the quark propagator, which might be the reason that in studies like in Ref. [99] only about a third of the expected constituent quark mass has been found. In our approach,

however, the gluon propagator has no time-time component and the information about the potential enters via the four-quark vertex. Therefore, a constituent quark mass has been obtained with the quark tadpole term alone. To corroborate these speculations, the ansatz for the quark tadpole should be improved and the equation be solved including both the quark-tadpole and the gluon propagator. In any case, the difficulties in finding a solution to the full quark propagator flow equation should be investigated more closely, especially the question whether it is a numerical issue or whether it hints to a deeper problem. Although the effect of dynamic quarks on the gluon sector is expected to be small, ultimately a solution of the full coupled system of the gluon and the quark sector should be undertaken.



# Appendix A

## Notations and Conventions

In this appendix we give some of the conventions used, mainly concerning the Fourier transformation.

We use the metric

$$g_{\mu\nu} = \text{diag}(1, -1, -1, -1) . \quad (\text{A.1})$$

Importantly, for the most part of this work we use contravariant tensor components which we denote with a subscript, except for the part of Chap. 2 from the beginning until and excluded Eq. (2.22). There we use upper indices to denote contravariant tensor components and lower indices to denote covariant components. Greek indices refer to space-time, Latin indices to space only.

We define the Fourier representation of a function in  $d$ -dimensional Euclidean position space as

$$f(\mathbf{x}) = \int \frac{d^d p}{(2\pi)^d} f(\mathbf{p}) e^{i\mathbf{p}\cdot\mathbf{x}} , \quad (\text{A.2})$$

where we do not use different symbols for the two functions but we distinguish them only by the names of their argument. The inverse transformation to momentum space then is

$$f(\mathbf{p}) = \int d^d x f(\mathbf{x}) e^{-i\mathbf{p}\cdot\mathbf{x}} . \quad (\text{A.3})$$

The functional derivatives transform as

$$\frac{\delta}{\delta f(\mathbf{x})} = \int \frac{d^d p}{(2\pi)^d} e^{-i\mathbf{p}\cdot\mathbf{x}} \frac{\delta}{\delta f(\mathbf{p})} \quad (\text{A.4})$$

and conversely

$$\frac{\delta}{\delta f(\mathbf{p})} = \int d^d x e^{i\mathbf{p}\cdot\mathbf{x}} \frac{\delta}{\delta f(\mathbf{x})} , \quad (\text{A.5})$$

where

$$\frac{\delta f(\mathbf{x})}{\delta f(\mathbf{y})} = \delta^d(\mathbf{x} - \mathbf{y}) \quad \text{and} \quad \frac{\delta f(\mathbf{p})}{\delta f(\mathbf{q})} = (2\pi)^d \delta^d(\mathbf{p} - \mathbf{q}) . \quad (\text{A.6})$$

In position space, the functional chain rule for functionals  $F, G$  and a function  $H$  is

$$\frac{\delta F[G[H]]}{\delta H(\mathbf{x})} = \int d^d y \frac{\delta F[G[H]]}{\delta G(\mathbf{y})} \frac{\delta G[H](\mathbf{y})}{\delta H(\mathbf{x})} , \quad (\text{A.7})$$

and in momentum space it is

$$\frac{\delta F[G[H]]}{\delta H(\mathbf{p})} = \int \frac{d^d q}{(2\pi)^d} \frac{\delta F[G[H]]}{\delta G(\mathbf{q})} \frac{\delta G[H](\mathbf{q})}{\delta H(\mathbf{p})}. \quad (\text{A.8})$$

Expressions like

$$D(\mathbf{x}, \mathbf{y}) = \int d^d z A(\mathbf{x}, \mathbf{z}) B(\mathbf{z}, \mathbf{y}) \quad (\text{A.9})$$

can be regarded as a continuous matrix multiplication that has the momentum representation

$$D(\mathbf{p}, \mathbf{q}) = \int \frac{d^d \ell}{(2\pi)^d} A(\mathbf{p}, \ell) B(-\ell, \mathbf{q}). \quad (\text{A.10})$$

Note the minus sign at one of the inner momentum arguments. Accordingly, the functional trace

$$\text{Tr} D = \int d^d x D(\mathbf{x}, \mathbf{x}) \quad (\text{A.11})$$

becomes

$$\text{Tr} D = \int \frac{d^d p}{(2\pi)^d} D(\mathbf{p}, -\mathbf{p}). \quad (\text{A.12})$$

An important special case of the matrix multiplication formula (A.9) is the inversion relation

$$\delta^d(\mathbf{x} - \mathbf{y}) = \int d^d z A(\mathbf{x}, \mathbf{z}) B(\mathbf{z}, \mathbf{y}) \quad (\text{A.13})$$

which has the Fourier representation

$$(2\pi)^d \delta^d(\mathbf{p} + \mathbf{q}) = \int \frac{d^d \ell}{(2\pi)^d} A(\mathbf{p}, \ell) B(-\ell, \mathbf{q}). \quad (\text{A.14})$$

Note that also here the difference in the argument of the delta function in position space turns into the sum of the external momenta in the Fourier representation of the delta function.



# Appendix B

## Derivation of the Propagator Flow

### B.1 Details of the Propagator Flow Derivation

In this appendix we derive the flow equations for the gluon and ghost propagators from the flow equation for the effective action, Eq. (3.28). A useful relation for the following concerns the commutation of fermionic derivatives past supermatrices. Consider a matrix with a block structure of commuting ( $c$ ) and anticommuting ( $a$ ) quantities and an anticommuting  $\eta$ :

$$\eta \begin{pmatrix} c & a & a \\ a & c & c \\ a & c & c \end{pmatrix} = \begin{pmatrix} c & -a & -a \\ -a & c & c \\ -a & c & c \end{pmatrix} \eta = M \begin{pmatrix} c & a & a \\ a & c & c \\ a & c & c \end{pmatrix} M \eta, \quad (\text{B.1})$$

with

$$M := \text{diag}(\mathbf{1}, -\mathbf{1}, -\mathbf{1}). \quad (\text{B.2})$$

This matrix structure is shared by  $\delta^2\Gamma_k/\delta\bar{\phi}\delta\phi$  as well as  $(\delta^2\Gamma_k/\delta\bar{\phi}\delta\phi + \mathcal{R}_k)^{-1}$ , the latter because of Eq. (3.26).

In the following,  $i$  and  $j$  are condensed external indices. They stand for colour indices, momenta and, in the case of gluon fields, also for contravariant Lorentz indices at the same time. They are, however, not part of the matrix notation. From the identity

$$\begin{aligned} 0 &= \frac{\delta}{\delta c_i} \left( \left( \frac{\delta^2\Gamma_k}{\delta\bar{\phi}\delta\phi} + \mathcal{R}_k \right) \left( \frac{\delta^2\Gamma_k}{\delta\bar{\phi}\delta\phi} + \mathcal{R}_k \right)^{-1} \right) \\ &= \frac{\delta^3\Gamma_k}{\delta c_i \delta\bar{\phi}\delta\phi} \left( \frac{\delta^2\Gamma_k}{\delta\bar{\phi}\delta\phi} + \mathcal{R}_k \right)^{-1} + M \left( \frac{\delta^2\Gamma_k}{\delta\bar{\phi}\delta\phi} + \mathcal{R}_k \right) M \frac{\delta}{\delta c_i} \left( \frac{\delta^2\Gamma_k}{\delta\bar{\phi}\delta\phi} + \mathcal{R}_k \right)^{-1} \end{aligned} \quad (\text{B.3})$$

it follows that

$$\frac{\delta}{\delta c_i} \left( \frac{\delta^2\Gamma_k}{\delta\bar{\phi}\delta\phi} + \mathcal{R}_k \right)^{-1} = -M \left( \frac{\delta^2\Gamma_k}{\delta\bar{\phi}\delta\phi} + \mathcal{R}_k \right)^{-1} M \frac{\delta^3\Gamma_k}{\delta c_i \delta\bar{\phi}\delta\phi} \left( \frac{\delta^2\Gamma_k}{\delta\bar{\phi}\delta\phi} + \mathcal{R}_k \right)^{-1}. \quad (\text{B.4})$$

For bosonic derivatives the same formula holds without the  $M$ 's. Using this, we can derive the ghost propagator flow equation from the flow of the effective action, Eq.

(3.28) by taking functional derivatives w.r.t. ghost fields:

$$\begin{aligned}
\frac{\delta^2 \dot{\Gamma}_k}{\delta \bar{c}_j \delta c_i} &= \frac{1}{2} \frac{\delta^2}{\delta \bar{c}_j \delta c_i} \text{STr} \left[ \dot{\mathcal{R}}_k \left( \frac{\delta^2 \Gamma_k}{\delta \phi \delta \phi} + \mathcal{R}_k \right)^{-1} \right] \\
&= \frac{1}{2} \frac{\delta}{\delta \bar{c}_j} \text{STr} \left[ -\dot{\mathcal{R}}_k M \left( \frac{\delta^2 \Gamma_k}{\delta \phi \delta \phi} + \mathcal{R}_k \right)^{-1} M \frac{\delta^3 \Gamma_k}{\delta c_i \delta \phi \delta \phi} \left( \frac{\delta^2 \Gamma_k}{\delta \phi \delta \phi} + \mathcal{R}_k \right)^{-1} \right] \\
&= \frac{1}{2} \text{STr} \left[ \dot{\mathcal{R}}_k \left( \frac{\delta^2 \Gamma_k}{\delta \phi \delta \phi} + \mathcal{R}_k \right)^{-1} M \frac{\delta^3 \Gamma_k}{\delta \bar{c}_j \delta \phi \delta \phi} \left( \frac{\delta^2 \Gamma_k}{\delta \phi \delta \phi} + \mathcal{R}_k \right)^{-1} M \frac{\delta^3 \Gamma_k}{\delta c_i \delta \phi \delta \phi} \left( \frac{\delta^2 \Gamma_k}{\delta \phi \delta \phi} + \mathcal{R}_k \right)^{-1} \right] \\
&\quad - \frac{1}{2} \text{STr} \left[ \dot{\mathcal{R}}_k \left( \frac{\delta^2 \Gamma_k}{\delta \phi \delta \phi} + \mathcal{R}_k \right)^{-1} M \frac{\delta^3 \Gamma_k}{\delta c_i \delta \phi \delta \phi} \left( \frac{\delta^2 \Gamma_k}{\delta \phi \delta \phi} + \mathcal{R}_k \right)^{-1} M \frac{\delta^3 \Gamma_k}{\delta \bar{c}_j \delta \phi \delta \phi} \left( \frac{\delta^2 \Gamma_k}{\delta \phi \delta \phi} + \mathcal{R}_k \right)^{-1} \right] \\
&\quad - \frac{1}{2} \text{STr} \left[ \dot{\mathcal{R}}_k \left( \frac{\delta^2 \Gamma_k}{\delta \phi \delta \phi} + \mathcal{R}_k \right)^{-1} \frac{\delta^4 \Gamma_k}{\delta \bar{c}_j \delta c_i \delta \phi \delta \phi} \left( \frac{\delta^2 \Gamma_k}{\delta \phi \delta \phi} + \mathcal{R}_k \right)^{-1} \right].
\end{aligned} \tag{B.5}$$

Setting the fields to zero,  $A = \bar{c} = c = 0$ , only the block matrices with the same number of ghosts and antighosts remain, see Appendix B.2. The first of the three terms in Eq. (B.5) becomes

$$\begin{aligned}
&\frac{1}{2} \text{Tr} \dot{R}_{A,k} \left( \frac{\delta^2 \Gamma_k}{\delta A \delta A} + R_{A,k} \right)^{-1} \frac{\delta^3 \Gamma_k}{\delta \bar{c}_j \delta A \delta c} \left( -\frac{\delta^2 \Gamma_k}{\delta \bar{c} \delta c} + R_{c,k} \right)^{-1} \\
&\quad \frac{\delta^3 \Gamma_k}{\delta c_i \delta \bar{c} \delta A} \left( \frac{\delta^2 \Gamma_k}{\delta A \delta A} + R_{A,k} \right)^{-1} \\
&+ \frac{1}{2} \text{Tr} \dot{R}_{c,k}^T \left( \frac{\delta^2 \Gamma_k}{\delta c \delta \bar{c}} + R_{c,k}^T \right)^{-1} \frac{\delta^3 \Gamma_k}{\delta \bar{c}_j \delta c \delta A} \left( \frac{\delta^2 \Gamma_k}{\delta A \delta A} + R_{A,k} \right)^{-1} \\
&\quad \frac{\delta^3 \Gamma_k}{\delta c_i \delta A \delta \bar{c}} \left( \frac{\delta^2 \Gamma_k}{\delta c \delta \bar{c}} + R_{c,k}^T \right)^{-1}.
\end{aligned} \tag{B.6}$$

The other two terms are treated alike. The ghost flow equation then reads (using  $R_{c,k}^T = R_{c,k}$ )

$$\begin{aligned}
\frac{\delta^2 \dot{\Gamma}_k}{\delta \bar{c}_j \delta c_i} &= \text{Tr} \dot{R}_{A,k} \left( \frac{\delta^2 \Gamma_k}{\delta A \delta A} + R_{A,k} \right)^{-1} \frac{\delta^3 \Gamma_k}{\delta \bar{c}_j \delta A \delta c} \left( -\frac{\delta^2 \Gamma_k}{\delta \bar{c} \delta c} + R_{c,k} \right)^{-1} \\
&\quad \frac{\delta^3 \Gamma_k}{\delta c_i \delta \bar{c} \delta A} \left( \frac{\delta^2 \Gamma_k}{\delta A \delta A} + R_{A,k} \right)^{-1} \\
&+ \text{Tr} \dot{R}_{c,k} \left( -\frac{\delta^2 \Gamma_k}{\delta \bar{c} \delta c} + R_{c,k} \right)^{-1} \frac{\delta^3 \Gamma_k}{\delta \bar{c}_j \delta \bar{c} \delta A} \left( \frac{\delta^2 \Gamma_k}{\delta A \delta A} + R_{A,k} \right)^{-1} \\
&\quad \frac{\delta^3 \Gamma_k}{\delta \bar{c}_j \delta A \delta c} \left( -\frac{\delta^2 \Gamma_k}{\delta \bar{c} \delta c} + R_{c,k} \right)^{-1} \\
&- \frac{1}{2} \text{Tr} \dot{R}_{A,k} \left( \frac{\delta^2 \Gamma_k}{\delta A \delta A} + R_{A,k} \right)^{-1} \frac{\delta^4 \Gamma_k}{\delta \bar{c}_j \delta c_i \delta A \delta A} \left( \frac{\delta^2 \Gamma_k}{\delta A \delta A} + R_{A,k} \right)^{-1} \\
&- \text{Tr} \dot{R}_{c,k} \left( -\frac{\delta^2 \Gamma_k}{\delta \bar{c} \delta c} + R_{c,k} \right)^{-1} \frac{\delta^4 \Gamma_k}{\delta \bar{c}_j \delta c_i \delta \bar{c} \delta c} \left( -\frac{\delta^2 \Gamma_k}{\delta \bar{c} \delta c} + R_{c,k} \right)^{-1}.
\end{aligned} \tag{B.7}$$

In much the same way, the gluon flow equation is derived from Eq. (3.28), and the result is

$$\begin{aligned}
 \frac{\delta^2 \dot{\Gamma}_k}{\delta A_j \delta A_i} = & \text{Tr } \dot{R}_{A,k} \left( \frac{\delta^2 \Gamma_k}{\delta A \delta A} + R_{A,k} \right)^{-1} \frac{\delta^3 \Gamma_k}{\delta A_j \delta A \delta A} \left( \frac{\delta^2 \Gamma_k}{\delta A \delta A} + R_{A,k} \right)^{-1} \\
 & \frac{\delta^3 \Gamma_k}{\delta A_i \delta A \delta A} \left( \frac{\delta^2 \Gamma_k}{\delta A \delta A} + R_{A,k} \right)^{-1} \\
 & - \text{Tr } \dot{R}_{c,k} \left( -\frac{\delta^2 \Gamma_k}{\delta \bar{c} \delta c} + R_{c,k} \right)^{-1} \frac{\delta^3 \Gamma_k}{\delta A_j \delta \bar{c} \delta c} \left( -\frac{\delta^2 \Gamma_k}{\delta \bar{c} \delta c} + R_{c,k} \right)^{-1} \\
 & \frac{\delta^3 \Gamma_k}{\delta A_i \delta \bar{c} \delta c} \left( -\frac{\delta^2 \Gamma_k}{\delta \bar{c} \delta c} + R_{c,k} \right)^{-1} \\
 & - \text{Tr } \dot{R}_{c,k} \left( -\frac{\delta^2 \Gamma_k}{\delta \bar{c} \delta c} + R_{c,k} \right)^{-1} \frac{\delta^3 \Gamma_k}{\delta A_i \delta \bar{c} \delta c} \left( -\frac{\delta^2 \Gamma_k}{\delta \bar{c} \delta c} + R_{c,k} \right)^{-1} \\
 & \frac{\delta^3 \Gamma_k}{\delta A_j \delta \bar{c} \delta c} \left( -\frac{\delta^2 \Gamma_k}{\delta \bar{c} \delta c} + R_{c,k} \right)^{-1} \\
 & - \frac{1}{2} \text{Tr } \dot{R}_{A,k} \left( \frac{\delta^2 \Gamma_k}{\delta A \delta A} + R_{A,k} \right)^{-1} \frac{\delta^4 \Gamma_k}{\delta A_j \delta A_i \delta A \delta A} \left( \frac{\delta^2 \Gamma_k}{\delta A \delta A} + R_{A,k} \right)^{-1} \\
 & - \text{Tr } \dot{R}_{c,k} \left( -\frac{\delta^2 \Gamma_k}{\delta \bar{c} \delta c} + R_{c,k} \right)^{-1} \frac{\delta^4 \Gamma_k}{\delta A_j \delta A_i \delta \bar{c} \delta c} \left( -\frac{\delta^2 \Gamma_k}{\delta \bar{c} \delta c} + R_{c,k} \right)^{-1} .
 \end{aligned} \tag{B.8}$$

These equations are represented diagrammatically in Figs. 3.1 and 3.2.

We now plug the parameterizations of the gluon and ghost propagators and the ghost-gluon vertex of Sect. 3.2 into these flow equations, dropping all the other vertices. As the ghost two-point function and the ghost regulator are both diagonal in colour space and momentum space, they can easily be inverted, yielding (see Eqs. (3.10), (3.32), and (3.33) )

$$\begin{aligned}
 \left[ \left( -\frac{\delta^2 \Gamma_k}{\delta \bar{c} \delta c} + R_{c,k} \right)^{-1} \right]_{\mathbf{p}\mathbf{q}}^{ab} &= \delta^{ab} [g p^2 / d_k(p) + R_{c,k}(p)]^{-1} (2\pi)^3 \delta^3(\mathbf{p} + \mathbf{q}) \\
 &= \delta^{ab} \frac{1}{g} \bar{G}_{c,k}(p) (2\pi)^3 \delta^3(\mathbf{p} + \mathbf{q}) .
 \end{aligned} \tag{B.9}$$

A similar formula holds for the gluon two-point function and the gluon regulator, which are invertible in the transverse subspace (see Eqs. (3.10), (3.30), and (3.31)):

$$\left[ \left( \frac{\delta^2 \Gamma_k}{\delta A \delta A} + R_{A,k} \right)^{-1} \right]_{ij, \mathbf{p}\mathbf{q}}^{ab} = \delta^{ab} t_{ij}(\mathbf{p}) G_{A,k}(p) (2\pi)^3 \delta^3(\mathbf{p} + \mathbf{q}) . \tag{B.10}$$

Therefore, the truncated gluon flow equation shown in Fig. 3.3 reduces to

$$\begin{aligned}
& 2\delta^{ab}t_{ij}(\mathbf{p})\dot{\omega}_k(p)(2\pi)^3\delta^3(\mathbf{p}+\mathbf{q}) = \\
& -\int\frac{d^3[p_{1\dots 6}]}{(2\pi)^{18}}\delta^{cd}g\dot{R}_{c,k}(p_1)(2\pi)^3\delta^3(\mathbf{p}_1-\mathbf{p}_2)\delta^{de}\frac{1}{g}\bar{G}_{c,k}(p_2)(2\pi)^3\delta^3(\mathbf{p}_2-\mathbf{p}_3) \\
& \quad gJ^{eaf}t_{im}(\mathbf{p})(ip_{4,m})(2\pi)^3\delta^3(\mathbf{p}+\mathbf{p}_3-\mathbf{p}_4)\delta^{fg}\frac{1}{g}\bar{G}_{c,k}(p_4)(2\pi)^3\delta^3(\mathbf{p}_4-\mathbf{p}_5) \quad (\text{B.11}) \\
& \quad gJ^{gbh}t_{jl}(\mathbf{q})(ip_{6,l})(2\pi)^3\delta^3(\mathbf{q}+\mathbf{p}_5-\mathbf{p}_6)\delta^{hc}\frac{1}{g}\bar{G}_{c,k}(p_6)(2\pi)^3\delta^3(\mathbf{p}_6-\mathbf{p}_1) \\
& + (i \leftrightarrow j).
\end{aligned}$$

Carrying out the index contractions and integrations we obtain the flow equation for  $\omega_k$ :

$$\partial_t\omega_k(p) = -\frac{N_c}{2}\int\frac{d^3q}{(2\pi)^3}\left(\bar{G}_{c,k}\dot{R}_{c,k}\bar{G}_{c,k}\right)(q)\bar{G}_{c,k}(|\mathbf{p}+\mathbf{q}|)q^2(1-(\hat{\mathbf{p}}\cdot\hat{\mathbf{q}})^2). \quad (\text{B.12})$$

In much the same way we treat the truncated ghost flow equation shown in Fig. 3.4 to get

$$\begin{aligned}
& -\delta^{ab}gp^2\partial_t d_k^{-1}(p)(2\pi)^3\delta^3(\mathbf{p}+\mathbf{q}) = \\
& \int\frac{d^3[p_{1\dots 6}]}{(2\pi)^{18}}\delta^{cd}t_{ij}(\mathbf{p}_1)\dot{R}_{A,k}(p_1)(2\pi)^3\delta^3(\mathbf{p}_1-\mathbf{p}_2)\delta^{de}t_{jh}(\mathbf{p}_2)G_{A,k}(p_2)(2\pi)^3\delta^3(\mathbf{p}_2-\mathbf{p}_3) \\
& \quad gJ^{fea}t_{lh}(\mathbf{p}_3)(-ip_{4,l})(2\pi)^3\delta^3(\mathbf{p}+\mathbf{p}_3-\mathbf{p}_4)\delta^{fg}\frac{1}{g}\bar{G}_{c,k}(p_4)(2\pi)^3\delta^3(\mathbf{p}_4-\mathbf{p}_5) \\
& \quad gJ^{bhg}t_{mn}(\mathbf{p}_6)(iq_m)(2\pi)^3\delta^3(\mathbf{q}+\mathbf{p}_5-\mathbf{p}_6)\delta^{hct}t_{ni}(\mathbf{p}_6)G_{A,k}(p_6)(2\pi)^3\delta^3(\mathbf{p}_6-\mathbf{p}_1) \\
& + \int\frac{d^3[p_{1\dots 6}]}{(2\pi)^{18}}\delta^{hc}g\dot{R}_{c,k}(p_1)(2\pi)^3\delta^3(\mathbf{p}_1-\mathbf{p}_2)\delta^{cd}\frac{1}{g}\bar{G}_{c,k}(p_2)(2\pi)^3\delta^3(\mathbf{p}_2-\mathbf{p}_3) \\
& \quad gJ^{bed}t_{mi}(\mathbf{p}_4)(iq_m)(2\pi)^3\delta^3(\mathbf{q}+\mathbf{p}_3-\mathbf{p}_4)\delta^{ef}t_{ij}(\mathbf{p}_4)G_{A,k}(p_4)(2\pi)^3\delta^3(\mathbf{p}_4-\mathbf{p}_5) \\
& \quad gJ^{gfa}t_{hj}(\mathbf{p}_5)(-ip_{6,h})(2\pi)^3\delta^3(\mathbf{p}+\mathbf{p}_5-\mathbf{p}_6)\delta^{gh}\frac{1}{g}\bar{G}_{c,k}(p_6)(2\pi)^3\delta^3(\mathbf{p}_6-\mathbf{p}_1). \quad (\text{B.13})
\end{aligned}$$

With the index contractions and integrations it turns into,

$$\begin{aligned}
\partial_t d_k^{-1}(p) = N_c \int \frac{d^3q}{(2\pi)^3} & \left[ \left( G_{A,k}\dot{R}_{A,k}G_{A,k} \right) (q)\bar{G}_{c,k}(|\mathbf{p}+\mathbf{q}|)(1-(\hat{\mathbf{p}}\cdot\hat{\mathbf{q}})^2) \right. \\
& \left. + \left( \bar{G}_{c,k}\dot{R}_{c,k}\bar{G}_{c,k} \right) (q)G_{A,k}(|\mathbf{p}+\mathbf{q}|)q^2\frac{1-(\hat{\mathbf{p}}\cdot\hat{\mathbf{q}})^2}{(\mathbf{p}+\mathbf{q})^2} \right]. \quad (\text{B.14})
\end{aligned}$$

## B.2 Ghost Number Conservation

In this appendix we show that correlation functions with a different number of ghosts and antighosts vanish.

Following Ref. [116], we consider a global phase transformation on the ghost fields and sources,

$$c \rightarrow c' = e^{i\lambda}c, \quad \bar{c} \rightarrow \bar{c}' = e^{-i\lambda}\bar{c}, \quad \sigma \rightarrow \sigma' = e^{i\lambda}\sigma, \quad \bar{\sigma} \rightarrow \bar{\sigma}' = e^{-i\lambda}\bar{\sigma} . \quad (\text{B.15})$$

The generating functional is invariant under this transformation,

$$\begin{aligned} Z_k[J, \sigma', \bar{\sigma}'] &= \int \mathcal{D}[A\bar{c}c] \exp \{ -S[A, c, \bar{c}] - \Delta S_k[A, c, \bar{c}] + J \cdot A + \bar{\sigma}' \cdot c + \bar{c} \cdot \sigma' \} \\ &= \int \mathcal{D}[A\bar{c}'c'] \exp \{ -S[A, c', \bar{c}'] - \Delta S_k[A, c', \bar{c}'] + J \cdot A + \bar{\sigma}' \cdot c' + \bar{c}' \cdot \sigma' \} \\ &= Z_k[J, \sigma, \bar{\sigma}] , \end{aligned} \quad (\text{B.16})$$

because of

$$\mathcal{D}\bar{c}'\mathcal{D}c' = \mathcal{D}\bar{c}\mathcal{D}c \quad \text{and} \quad (S + \Delta S_k)[A, c', \bar{c}'] = (S + \Delta S_k)[A, c, \bar{c}] . \quad (\text{B.17})$$

This holds because we only consider actions and regulators with terms containing the same number of ghosts and antighosts. We then get (suppressing the notation of the bosonic fields and sources)

$$W_k[\sigma', \bar{\sigma}'] = W_k[\sigma, \bar{\sigma}] . \quad (\text{B.18})$$

Taking the derivative of this equation w.r.t  $\bar{\sigma}$  gives

$$\frac{\delta}{\delta \bar{\sigma}} W_k[\sigma, \bar{\sigma}] = \frac{\delta \bar{\sigma}'}{\delta \bar{\sigma}} \frac{\delta}{\delta \bar{\sigma}'} W_k[\sigma', \bar{\sigma}'] = e^{-i\lambda} \frac{\delta}{\delta \bar{\sigma}'} W_k[\sigma', \bar{\sigma}'] . \quad (\text{B.19})$$

Plugging in

$$\sigma = \sigma_k[c, \bar{c}] \quad \text{and} \quad \bar{\sigma} = \bar{\sigma}_k[c, \bar{c}] \quad (\text{B.20})$$

we obtain

$$\begin{aligned} \frac{\delta}{\delta \bar{\sigma}'_k} W_k[\sigma'_k[c, \bar{c}], \bar{\sigma}'_k[c, \bar{c}]] &= e^{i\lambda} \frac{\delta}{\delta \bar{\sigma}_k} W_k[\sigma_k[c, \bar{c}], \bar{\sigma}_k[c, \bar{c}]] = e^{i\lambda} c = c' \\ &= \frac{\delta}{\delta \bar{\sigma}'_k} W_k[\sigma_k[c', \bar{c}'], \bar{\sigma}_k[c', \bar{c}']] . \end{aligned} \quad (\text{B.21})$$

Together with the analogous equation obtained by taking the derivative of Eq. (B.18) w.r.t  $\sigma$  we get

$$\sigma'_k[c, \bar{c}] = \sigma_k[c', \bar{c}'], \quad \bar{\sigma}'_k[c, \bar{c}] = \bar{\sigma}_k[c', \bar{c}'] . \quad (\text{B.22})$$

The effective average action now turns out to be invariant under this phase transformation:

$$\begin{aligned} \Gamma_k[\bar{c}', c'] &= -W_k[\sigma_k[\bar{c}', c'], \bar{\sigma}_k[\bar{c}', c']] + \bar{\sigma}_k[\bar{c}', c'] \cdot c' + \bar{c}' \cdot \sigma_k[\bar{c}', c'] - \bar{c}' \cdot R_{c,k} \cdot c' \\ &= -W_k[\sigma'_k[\bar{c}, c], \bar{\sigma}'_k[\bar{c}, c]] + \bar{\sigma}'_k[\bar{c}, c] \cdot c' + \bar{c}' \cdot \sigma'_k[\bar{c}, c] - \bar{c} \cdot R_{c,k} \cdot c \\ &= -W_k[\sigma_k[\bar{c}, c], \bar{\sigma}_k[\bar{c}, c]] + \bar{\sigma}_k[\bar{c}, c] \cdot c + \bar{c} \cdot \sigma_k[\bar{c}, c] - \bar{c} \cdot R_{c,k} \cdot c \\ &= \Gamma_k[\bar{c}, c] . \end{aligned} \quad (\text{B.23})$$

We conclude that derivatives w.r.t different numbers of ghosts and antighosts vanish at  $\bar{c} = c = 0$ :

$$\frac{\delta\Gamma_k[\bar{c}, c]}{\delta\bar{c}} = \frac{\delta\Gamma_k[\bar{c}', c']}{\delta\bar{c}} = \frac{\delta\bar{c}'}{\delta\bar{c}} \frac{\delta\Gamma_k[\bar{c}', c']}{\delta\bar{c}'} = e^{-i\lambda} \frac{\delta\Gamma_k[\bar{c}', c']}{\delta\bar{c}'} \xrightarrow{\bar{c}=c=0} \frac{\delta\Gamma_k[\bar{c}, c]}{\delta\bar{c}} \Big|_0 = 0 . \quad (\text{B.24})$$

The same holds for the derivative w.r.t  $c$ .

In contrast, if we take an equal number of ghost and anti-ghost derivatives, we get

$$\frac{\delta^2\Gamma_k[\bar{c}, c]}{\delta\bar{c}\delta c} = \frac{\delta}{\delta\bar{c}} \left( \frac{\delta c'}{\delta c} \frac{\delta\Gamma_k[\bar{c}', c']}{\delta c'} \right) = e^{i\lambda} \frac{\delta\bar{c}'}{\delta\bar{c}} \frac{\delta\Gamma_k[\bar{c}', c']}{\delta\bar{c}'\delta c'} = \frac{\delta^2\Gamma_k[\bar{c}', c']}{\delta\bar{c}'\delta c'} . \quad (\text{B.25})$$

The phase factors have cancelled and nothing can be inferred. Taking more derivatives, it can be shown in general that correlation functions with different numbers of ghosts and antighosts vanish.

# Appendix C

## Numerical Methods

In this appendix, the details of the numerical method used for solving the flow equations are presented. To be specific, the method is exemplified for the case of the gluon and ghost propagator equations.

### C.1 Chebyshev Representation

The functions  $\omega(p)$  and  $d(p)$  of Sec. 3.6 as well as  $\omega_k(p)$  and  $d_k(p)$  of Sec. 3.5 can be calculated numerically only for a finite number of sites  $(p_i)$  and  $(k_j, p_i)$ , respectively. The evaluation of these functions, however, cannot be restricted to these sites because the structure of the loop integrals enforces evaluations like  $\omega(\mathbf{p} + \mathbf{q})$ , where  $\mathbf{q}$  is the loop integration momentum, which will assume discrete values on a Gauss-Legendre grid. Therefore, these momentum arguments of the functions will in general not match the sites  $(p_i)$ . For this reason an approximation method has to be applied to approximate the function values between the momentum sites  $(p_i)$  they have originally been calculated for. Although not involved in loop integrals, this approximation method is necessary also for the cut-off momenta  $(k_j)$ , because the flow integrals with varying limits as in Eqs. (3.43) and (3.44) enforce an evaluation also between the grid sites  $(k_j)$ .

The function interpolation is accomplished by Chebyshev approximation using the implementation of Ref. [117]. In this method, the function is approximated by a sum of the Chebyshev polynomials of degree 0 to  $N - 1$ , weighted by coefficients that are calculated from the function to be approximated. It has the property that it is an exact representation of the function at the  $N$  zeros of the  $N$ -th Chebyshev polynomial. Moreover, the maximum error is getting smaller with increasing polynomial order, thereby avoiding Runge's phenomenon which is the observation that the error increases with the polynomial order due to strong oscillations if equidistant nodes are used. Indeed, the Chebyshev approximation polynomial comes close to the minimax polynomial which (out of all polynomials with the same degree) minimizes the maximum difference to the function to be approximated.

Therefore, the momentum sites  $(p_i)$  and  $(k_j, p_i)$  are chosen to be the Chebyshev nodes on suitably sized momentum ranges, spanning up to nine orders of magnitude. A logarithmic momentum scale is used in order to sample the behaviour of the functions equally well on all orders of magnitude. The function values are also taken

logarithmic because otherwise the power laws, that frequently occur as behaviour of the functions in the IR and in the UV, would turn into exponentials on the logarithmic momentum scale, which can, however, not be fitted well with polynomials. In a double logarithmic representation, power laws turn into straight lines, which can of course easily be fitted with polynomials. Altogether, a representation of the function  $y = \ln f(e^x)$  with  $x = \ln(p)$  on the range  $[\ln(p_{min}), \ln(p_{max})]$  is obtained rather than of  $f(p)$  on  $[p_{min}, p_{max}]$ , likewise for the cut-off momentum argument  $k$  if present. In the case of the flow functions  $\omega_k(p)$  and  $d_k(p)$ , which have the cut-off momentum as an additional argument, the coefficients along the  $p$ -direction for each value of ( $k_j$ ) are calculated; this results in functions of  $k$  for each of the  $p$ -coefficients. These functions are known just at the Chebyshev nodes ( $k_j$ ) and therefore their Chebyshev coefficients can be determined. To evaluate the functions this procedure is processed backwards. About 130 Chebyshev nodes in each direction have been used.

In the loop integrals of Sec. 3.5, the flow functions  $\omega_k(p)$  and  $d_k(p)$  need to be evaluated also outside the Chebyshev representation range of the external momentum  $p$ . Yet the IR extrapolation of the flow functions requires no extra assumptions about their IR behaviour: as long as  $k_{min}$  never reaches the lower boundary of the  $p$ -range, the functions can simply be chosen to be constant beyond this boundary, as clearly seen in Fig. 3.7. For their continuation in the UV, a power law has been fitted to their behaviour in the UV region of the  $p$ -range, which is  $\omega_k(p) \sim p$  and  $d_k(p) \sim const.$  As for the  $k$ -range, the functions are never evaluated outside the Chebyshev range anyway, so no extrapolation is necessary.

In contrast, the correlation functions  $\omega(p)$  and  $d(p)$  of Sec. 3.6 require also an IR-extrapolation because the cut-off momentum is set to  $k = 0$  there. As both  $\omega$  and  $d$  develop a power law in the IR, the form

$$f(p) = ap^b \tag{C.1}$$

is assumed for  $p < p_{min}$  and the values for  $a$  and  $b$  are determined within the range  $[p_{min}, 10p_{min}]$ . Similarly, the functions  $\omega(p) = ap$  and  $d(p) = const.$  are taken as fitting functions for the UV in the range  $[0.1p_{max}, p_{max}]$ .

## C.2 Gauss-Legendre Integration

The momentum integrals, for the loop as well as for the flow (in Sec. 3.5), have been calculated using the Gauss-Legendre quadrature as implemented in Ref. [117]. This method spreads  $N$  nodes ( $x_i$ ) over an integration range  $[a, b]$  together with weight factors ( $w_i$ ) such that

$$\int_a^b f(x)dx \approx \sum_{i=1}^N w_i f(x_i) . \tag{C.2}$$

This equation holds exactly if  $f$  is a polynomial of a degree not greater than  $2N - 1$  and approximately otherwise. The three-dimensional loop integrals have been



calculated as nested one-dimensional integrals according to Fubini's theorem,

$$\int d^3q f(\mathbf{p}, \mathbf{q}) = \int_{q_{min}}^{q_{max}} dq q^2 \int_{-1}^1 dx \int_0^{2\pi} d\varphi f(\mathbf{p}, \mathbf{q}) \quad \text{where} \quad x = \hat{\mathbf{q}} \cdot \hat{\mathbf{p}}. \quad (\text{C.3})$$

Whilst the integral over the azimuth angle  $\varphi$  of the  $\mathbf{p}$ -axis can be carried out trivially because the functions  $f$  occurring in this work are independent of it, the other two integrals are calculated numerically using the Gauss-Legendre approximation. As for the integral over  $x$ , it can be applied to the integral as it stands whereas for the radial integral the Gauss-Legendre nodes have to be calculated on a logarithmic momentum scale in order to appropriately sample the IR behaviour. To achieve this, the substitution

$$x := \ln q \quad (\text{C.4})$$

is performed such that a radial integral of a function  $g$  becomes

$$\int_{q_{min}}^{q_{max}} dq g(q) = \int_{\ln q_{min}}^{\ln q_{max}} dx e^x g(e^x). \quad (\text{C.5})$$

Just as for the Chebyshev nodes, the Gauss-Legendre nodes are now spread over the range  $[\ln q_{min}, \ln q_{max}]$  instead of  $[q_{min}, q_{max}]$ , so there are more nodes lying in the low momentum region where important contributions to the integrals evaluated in this work are coming from. These considerations can be verified and the programme be tested by calculating integrals that are similar in structure to the actual integrals but can be evaluated analytically and by subsequent comparison of the numerical result to the real value of the integral.

Moreover, the radial loop integrals in the case of the fully  $k$ -dependent flow equations of Sec. 3.5 have been confined to a range of one order of magnitude around the cutoff momentum  $k$ ,  $q_{min} \leq k \leq q_{max}$ , outside of which there is virtually no contribution to the integral owing to the regulator functions employed, see Eq. (3.45). The validity of this restriction can be checked by using a wider integration range which shows to have no effect on the result. Also for the optimized equations of Sec. 3.6 the integration range has to be broadened and the number of Gauss-Legendre nodes to be increased along with it until the results do not change anymore upon further extension, so effects coming from the choice of a momentum integration range too narrow can be excluded. For the flow integral in  $k$  as well as for the loop integral, about 70 nodes have been used.

### C.3 Iterative Solution and Fine Tuning

The sets of equations (3.43) and (3.44) as well as (3.50) and (3.49) have been solved iteratively. Starting from constant functions  $\omega$  and  $d$ , the r.h.s. of the equations are calculated. From the result, the initial values of the flow,  $d_\Lambda$  and  $\omega_\Lambda$ , are determined following the procedures described in the next paragraph, giving

temporary results  $\omega^{tmp}$  and  $d^{tmp}$ . To improve the convergence behaviour, a relaxation method is applied to determine the final result of the  $n$ -th iteration as  $\omega_{k_j}^{(n)}(p_i) = r\omega_{k_j}^{tmp}(p_i) + (1-r)\omega_{k_j}^{(n-1)}(p_i)$  for each Chebyshev node  $(k_j, p_i)$ , likewise for  $d_k(p)$ . Values of  $r \in [0.1, 0.5]$  have been used, depending on how much the functions change from one iteration to the next. This yields the new functions  $\omega^{(n)}$  and  $d^{(n)}$  which are then fed back into the r.h.s. of the equations as input to the  $(n+1)$ -th step of the iteration. This iteration is repeated until the functions do not change anymore from one step to the next, so convergence is reached. These functions are the solutions to the integral equations.

The initial conditions  $d_\Lambda$  and  $\omega_\Lambda$  are determined in the following way: the constant  $d_\Lambda(p) \equiv d_\Lambda$  in Eq. (3.44) is chosen such that  $d_{k_{min}}(p)$  fulfil a power law for  $p$  in the IR,  $d_{k_{min}}^{-1}(p \rightarrow 0) \sim p^\beta$ . First, we observe that for a power law  $f(p) = p^\beta$  the expression

$$p \frac{d}{dp} \ln f(p) = \beta \quad (\text{C.6})$$

yields a constant value, i.e., the exponent. Let  $g(p)$  be the r.h.s. of Eq. (3.44) (with  $k = k_{min}$ ). Demanding that

$$\frac{d}{dp} \left( p \frac{d}{dp} \ln (g(p) + d_\Lambda^{-1}) \right) \stackrel{!}{=} 0 \quad (\text{C.7})$$

is equivalent to demanding that  $g(p)$  fulfil a power law. Solving for  $d_\Lambda^{-1}$  and performing a least squares fit of a constant function to the infrared region of the expression obtained for  $d_\Lambda^{-1}$  (which will in general not yet be a constant) gives the optimal value for  $d_\Lambda^{-1}$  in order to achieve a power law behaviour for  $d_{k_{min}}^{-1}(p)$  in the IR region. This is done during each iteration step as described in the previous paragraph. In this way, a power law behaviour can be imposed on the ghost form factor without dictating its exponent. Concerning the Eqs. (3.43) (with  $k = k_{min}$ ) and (3.49), the expression  $-a + bp$  is fitted to the r.h.s. in the UV and  $\omega_\Lambda(p) = a + p$  is used to achieve  $\omega_{k=k_{min}}(p)|_{p \rightarrow \Lambda} \sim p$  for Eq. (3.43) and  $\omega_0(p)|_{p \rightarrow \Lambda} \sim p$  for Eq. (3.49), which is an expression of asymptotic freedom. For Eq. (3.50) the determination of the initial conditions is not a numerical issue anyway, see Eq. (3.51).

This method allows for a systematic, simultaneous determination of the solution together with originally unknown initial conditions to accomplish that the solution at  $k = k_{min}$  fulfil certain properties. Solving the differential equations in their original, i.e., differential form would require a trial-and-error search for the initial conditions to find a solution with the specified characteristics.

# Appendix D

## Calculation of Two-Point Integrals

Here we calculate the two-point integrals necessary for the assessment of the angular approximation in Subsec. 4.5.3. We define

$$\theta_m(a, b) := \int \frac{d^d q}{(2\pi)^d} \frac{(\mathbf{q} \cdot \mathbf{p})^m}{(\mathbf{q}^2)^a ((\mathbf{q} - \mathbf{p})^2)^b}. \quad (\text{D.1})$$

For the cases of our interest,  $m = 0$  and  $m = 2$ , the integral is convergent in the ultraviolet, at the pole  $\mathbf{q} = 0$ , and at the pole  $\mathbf{q} = \mathbf{p}$ , respectively, if

$$a + b > \frac{d}{2} + \frac{m}{2}, \quad a < \frac{d}{2} + \frac{m}{2}, \quad b < \frac{d}{2}. \quad (\text{D.2})$$

Using the Feynman parameterization [36] for the integrand,

$$\frac{1}{(\mathbf{q}^2)^a ((\mathbf{q} - \mathbf{p})^2)^b} = \int_0^1 dx \int_0^1 dy \delta(x + y - 1) \frac{x^{a-1} y^{b-1}}{(x\mathbf{q}^2 + y(\mathbf{q} - \mathbf{p})^2)^{a+b}} \frac{\Gamma(a+b)}{\Gamma(a)\Gamma(b)}, \quad (\text{D.3})$$

we get

$$\theta_m(a, b) = \int \frac{d^d q}{(2\pi)^d} \int_0^1 dx \int_0^1 dy \delta(x + y - 1) \frac{x^{a-1} y^{b-1} (\mathbf{q} \cdot \mathbf{p})^m}{(x\mathbf{q}^2 + y(\mathbf{q} - \mathbf{p})^2)^{a+b}} \frac{\Gamma(a+b)}{\Gamma(a)\Gamma(b)}. \quad (\text{D.4})$$

Shifting  $\mathbf{q} \rightarrow \mathbf{q} + y\mathbf{p}$  yields

$$\theta_m(a, b) = \frac{\Gamma(a+b)}{\Gamma(a)\Gamma(b)} \int_0^1 dx \int_0^1 dy \delta(x + y - 1) x^{a-1} y^{b-1} \int \frac{d^d q}{(2\pi)^d} \frac{(\mathbf{q} \cdot \mathbf{p} + y\mathbf{p}^2)^m}{(\mathbf{q}^2 + \mathbf{p}^2 xy)^{a+b}}. \quad (\text{D.5})$$

In the case of  $m = 0$  we obtain the integral [36]

$$\int \frac{d^d q}{(2\pi)^d} \frac{1}{(\mathbf{q}^2 + \mathbf{p}^2 xy)^{a+b}} = \frac{1}{(4\pi)^{d/2}} \frac{\Gamma(a+b-d/2)}{\Gamma(a+b)} (\mathbf{p}^2 xy)^{-a-b+d/2} \quad (\text{D.6})$$

and therefore

$$\theta_0(a, b) = \frac{1}{(4\pi)^{d/2}} \frac{\Gamma(a+b-d/2)}{\Gamma(a)\Gamma(b)} (\mathbf{p}^2)^{d/2-a-b} \int_0^1 d[xy] \delta(x + y - 1) x^{d/2-b-1} y^{d/2-a-1} \quad (\text{D.7})$$

Using the Feynman parameterization (D.3) in reverse we obtain

$$\theta_0(a, b) = \frac{1}{(4\pi)^{d/2}} \frac{\Gamma(a+b-d/2)\Gamma(d/2-b)\Gamma(d/2-a)}{\Gamma(a)\Gamma(b)\Gamma(d-a-b)} (\mathbf{p}^2)^{d/2-a-b}. \quad (\text{D.8})$$

In the case of  $m = 2$  we get with Feynman parameterization

$$\theta_2(a, b) = \frac{\Gamma(a+b)}{\Gamma(a)\Gamma(b)} \int_0^1 dx \int_0^1 dy \delta(x+y-1) x^{a-1} y^{b-1} [I_A + I_B] \quad (\text{D.9})$$

where

$$I_A := \int \frac{d^d q}{(2\pi)^d} \frac{(\mathbf{q} \cdot \mathbf{p})^2}{(\mathbf{q}^2 + \mathbf{p}^2 xy)^{a+b}} \quad \text{and} \quad I_B := \int \frac{d^d q}{(2\pi)^d} \frac{(y\mathbf{p}^2)^2}{(\mathbf{q}^2 + \mathbf{p}^2 xy)^{a+b}} \quad (\text{D.10})$$

because the integrand with the term  $2y\mathbf{p}^2 \mathbf{p} \cdot \mathbf{q}$  in the numerator is proportional to  $q$  and therefore this integral vanishes by symmetry. As in the case of  $m = 0$  we obtain

$$I_B = \frac{1}{(4\pi)^{d/2}} \frac{\Gamma(a+b-d/2)}{\Gamma(a+b)} x^{d/2-a-b} y^{d/2-a-b+2} (\mathbf{p}^2)^{2+d/2-a-b}. \quad (\text{D.11})$$

The integral  $I_A$  can be rewritten and solved [36], giving

$$I_A = p_i p_j \int \frac{d^d q}{(2\pi)^d} \frac{q_i q_j}{(\mathbf{q}^2 + \mathbf{p}^2 xy)^{a+b}} = \frac{p_i p_j \delta_{ij}}{2(4\pi)^{d/2}} \frac{\Gamma(a+b-d/2-1)}{\Gamma(a+b)} (\mathbf{p}^2 xy)^{1+d/2-a-b}. \quad (\text{D.12})$$

Altogether, we get

$$\begin{aligned} \theta_2(a, b) = & \frac{\Gamma(a+b-d/2-1)}{2(4\pi)^{d/2}\Gamma(a)\Gamma(b)} (\mathbf{p}^2)^{2+d/2-a-b} \int_0^1 d[xy] \delta(x+y-1) x^{1+d/2-b-1} y^{1+d/2-a-1} \\ & + \frac{1}{(4\pi)^{d/2}} \frac{\Gamma(a+b-d/2)}{\Gamma(a)\Gamma(b)} (\mathbf{p}^2)^{2+d/2-a-b} \int_0^1 d[xy] \delta(x+y-1) x^{d/2-b-1} y^{d/2-a+2-1}, \end{aligned} \quad (\text{D.13})$$

and removing the Feynman parameters with Eq. (D.3) finally yields

$$\begin{aligned} \theta_2(a, b) = \frac{1}{(4\pi)^{d/2}} & \left[ \frac{1}{2} \frac{\Gamma(a+b-d/2-1)\Gamma(1+d/2-b)\Gamma(1+d/2-a)}{\Gamma(a)\Gamma(b)\Gamma(2+d-a-b)} \right. \\ & \left. + \frac{\Gamma(a+b-d/2)\Gamma(d/2-b)\Gamma(d/2+2-a)}{\Gamma(a)\Gamma(b)\Gamma(d+2-a-b)} \right] (\mathbf{p}^2)^{2+d/2-a-b}. \end{aligned} \quad (\text{D.14})$$

The term in square brackets in Eq. (4.103) can now be written as

$$\theta_0(-\alpha/2, \beta + \gamma/2 + 1) - \frac{1}{\mathbf{p}^2} \theta_2(-\alpha/2 + 1, \beta + \gamma/2 + 1) = \frac{K(\beta, \gamma)}{(4\pi)^{3/2}} p^{-\gamma} \quad (\text{D.15})$$

with

$$\begin{aligned}
 K(\beta, \gamma) = & \frac{\Gamma(\beta + 1)\Gamma(1/2 - \beta - \gamma/2)\Gamma(\gamma/2)}{\Gamma(1/2 - \beta)\Gamma(\beta + \gamma/2 + 1)\Gamma(3/2 - \gamma/2)} \\
 & - \frac{\Gamma(\beta + 2)\Gamma(1/2 - \beta - \gamma/2)\Gamma(1 + \gamma/2)}{\Gamma(3/2 - \beta)\Gamma(\beta + \gamma/2 + 1)\Gamma(5/2 - \gamma/2)} \\
 & - \frac{1}{2} \frac{\Gamma(\beta + 1)\Gamma(3/2 - \beta - \gamma/2)\Gamma(\gamma/2)}{\Gamma(3/2 - \beta)\Gamma(\beta + \gamma/2 + 1)\Gamma(5/2 - \gamma/2)}.
 \end{aligned} \tag{D.16}$$



# Appendix E

## Calculations for the Quark Propagator Flow

### E.1 Calculation of the Two-Quark Kernels

Here we calculate the two-quark kernel  $\tilde{\Omega}$  of the wave functional in Eq. (5.45), as suggested in [110],

$$\tilde{\Omega} = S^{(+)} + S^{(+)}KS^{(-)} + S^{(-)}\bar{K}S^{(+)} - S^{(-)}. \quad (\text{E.1})$$

The part without  $\varphi$  is

$$S^{(+)} - S^{(-)} = \frac{\boldsymbol{\alpha} \cdot \mathbf{p} + \beta m}{E_{\mathbf{p}}}. \quad (\text{E.2})$$

The parts containing  $\varphi$  are

$$\begin{aligned} S^{(+)}KS^{(-)} &= \frac{1}{4}\varphi(p) \left( \mathbb{1} + \frac{\boldsymbol{\alpha} \cdot \mathbf{p} + \beta m}{E_{\mathbf{p}}} \right) \beta \left( \mathbb{1} - \frac{\boldsymbol{\alpha} \cdot \mathbf{p} + \beta m}{E_{\mathbf{p}}} \right) \\ S^{(-)}\bar{K}S^{(+)} &= \frac{1}{4}\varphi^*(p) \left( \mathbb{1} - \frac{\boldsymbol{\alpha} \cdot \mathbf{p} + \beta m}{E_{\mathbf{p}}} \right) \beta \left( \mathbb{1} + \frac{\boldsymbol{\alpha} \cdot \mathbf{p} + \beta m}{E_{\mathbf{p}}} \right) \end{aligned} \quad (\text{E.3})$$

With

$$\begin{aligned} &\left( \mathbb{1} \pm \frac{\boldsymbol{\alpha} \cdot \mathbf{p} + \beta m}{E_{\mathbf{p}}} \right) \beta \left( \mathbb{1} \mp \frac{\boldsymbol{\alpha} \cdot \mathbf{p} + \beta m}{E_{\mathbf{p}}} \right) \\ &= \beta \mp \frac{1}{E_{\mathbf{p}}}(\beta \boldsymbol{\alpha} \cdot \mathbf{p} + m) \pm \frac{1}{E_{\mathbf{p}}}(\boldsymbol{\alpha} \cdot \mathbf{p} \beta + m) - \frac{1}{E_{\mathbf{p}}^2}(\boldsymbol{\alpha} \cdot \mathbf{p} \beta \boldsymbol{\alpha} \cdot \mathbf{p} + 2\boldsymbol{\alpha} \cdot \mathbf{p} m + \beta m^2) \\ &= \beta \mp \frac{1}{E_{\mathbf{p}}}(2\beta \boldsymbol{\alpha} \cdot \mathbf{p}) - \frac{1}{E_{\mathbf{p}}^2}(-\beta \mathbf{p}^2 + 2m \boldsymbol{\alpha} \cdot \mathbf{p} + \beta m^2) \\ &= \beta \frac{2\mathbf{p}^2}{E_{\mathbf{p}}^2} + \boldsymbol{\alpha} \cdot \mathbf{p} \frac{-2m}{E_{\mathbf{p}}^2} \mp \beta \boldsymbol{\alpha} \cdot \mathbf{p} \frac{2}{E_{\mathbf{p}}} \end{aligned} \quad (\text{E.4})$$

we obtain

$$\begin{aligned} \tilde{\Omega} &= \beta \left[ \frac{m}{E_{\mathbf{p}}} + \frac{\mathbf{p}^2}{2E_{\mathbf{p}}^2}(\varphi(p) + \varphi^*(p)) \right] + \boldsymbol{\alpha} \cdot \mathbf{p} \left[ \frac{1}{E_{\mathbf{p}}} - \frac{m}{2E_{\mathbf{p}}^2}(\varphi(p) + \varphi^*(p)) \right] \\ &\quad + \beta \boldsymbol{\alpha} \cdot \mathbf{p} \left[ \frac{1}{2E_{\mathbf{p}}}(\varphi^*(p) - \varphi(p)) \right]. \end{aligned} \quad (\text{E.5})$$

For real  $\varphi$  this becomes

$$\tilde{\Omega} = \beta \left[ \frac{m}{E_{\mathbf{p}}} + \frac{\mathbf{p}^2}{E_{\mathbf{p}}^2} \varphi(p) \right] + \boldsymbol{\alpha} \cdot \mathbf{p} \left[ \frac{1}{E_{\mathbf{p}}} - \frac{m}{E_{\mathbf{p}}^2} \varphi(p) \right]. \quad (\text{E.6})$$

In the chiral limit,  $m = 0$ , the kernel further simplifies to

$$\tilde{\Omega} = \beta \varphi(p) + \boldsymbol{\alpha} \cdot \mathbf{p} \frac{1}{p}. \quad (\text{E.7})$$

## E.2 Perturbative Calculation of the Four-Quark Function

In this appendix we will apply perturbation theory to the lowest order to improve the ansatz for the four-quark function of Eq. (5.31). We use the notations and conventions of Ref. [44] where perturbation theory has been applied to the static quark propagator. Here we restrict ourselves to the purely fermionic part of the theory with the colour Coulomb potential  $F$ . The Hamiltonian then reads

$$\begin{aligned} H = H_{\psi^\dagger\psi} + g^2 H_F &= \int \frac{d^3p}{(2\pi)^3} \psi^\dagger(\mathbf{p}) (\boldsymbol{\alpha} \cdot \mathbf{p} + \beta m) \psi(\mathbf{p}) \\ &+ \frac{g^2}{2} \int \frac{d^3[p_1 p_2 p_3 p_4]}{(2\pi)^{12}} \psi^\dagger(\mathbf{p}_1) T^a \psi(\mathbf{p}_2) \\ &F(\mathbf{p}_1 - \mathbf{p}_2) \psi^\dagger(\mathbf{p}_3) T^a \psi(\mathbf{p}_4) (2\pi)^3 \delta^3(\mathbf{p}_1 - \mathbf{p}_2 + \mathbf{p}_3 - \mathbf{p}_4) \end{aligned} \quad (\text{E.8})$$

The quark field operator in momentum representation can be decomposed into its particle and anti-particle part as

$$\psi^m(\mathbf{p}) = \frac{1}{\sqrt{2E_{\mathbf{p}}}} \sum_s [b^m(\mathbf{p}, s) u(\mathbf{p}, s) + d^{m\dagger}(-\mathbf{p}, s) v(-\mathbf{p}, s)] \quad (\text{E.9})$$

where  $u$  and  $v$  are the solutions of the free Dirac equation,  $E_{\mathbf{p}} = \sqrt{m^2 + \mathbf{p}^2}$  is the free fermion energy and the particle and anti-particle creators and annihilators fulfil the anticommutation relations

$$\{b^m(\mathbf{p}, s), b^{n\dagger}(\mathbf{q}, t)\} = \{d^m(\mathbf{p}, s), d^{n\dagger}(\mathbf{q}, t)\} = \delta^{mn} \delta_{st} (2\pi)^3 \delta^3(\mathbf{p} - \mathbf{q}). \quad (\text{E.10})$$

All the other anti-commutators vanish. For the solutions of the free Dirac equation we obtain the relations

$$\sum_s \frac{u_\alpha(\mathbf{p}, s) u_\beta^\dagger(\mathbf{p}, s)}{2E_{\mathbf{p}}} = S_{\alpha\beta}^{(+)}(\mathbf{p}), \quad \sum_s \frac{v_\alpha(-\mathbf{p}, s) v_\beta^\dagger(-\mathbf{p}, s)}{2E_{\mathbf{p}}} = S_{\alpha\beta}^{(-)}(\mathbf{p}) \quad (\text{E.11})$$

where

$$S^{(\pm)}(\mathbf{p}) = \frac{1}{2} \pm \frac{h(\mathbf{p})}{2E_{\mathbf{p}}}, \quad h(\mathbf{p}) = \boldsymbol{\alpha} \cdot \mathbf{p} + \beta m. \quad (\text{E.12})$$



The  $S^{(\pm)}(\mathbf{p})$  are projectors on particle and anti-particle states, i.e.,

$$\begin{aligned} S^{(+)}(\mathbf{p})u(\mathbf{p}, s) &= u(\mathbf{p}, s), & S^{(+)}(\mathbf{p})v(-\mathbf{p}, s) &= 0, \\ S^{(-)}(\mathbf{p})v(-\mathbf{p}, s) &= v(-\mathbf{p}, s), & S^{(-)}(\mathbf{p})u(\mathbf{p}, s) &= 0, \end{aligned} \quad (\text{E.13})$$

$$S^{(+)}(\mathbf{p}) + S^{(-)}(\mathbf{p}) = \mathbf{1}, \quad S^{(+)}(\mathbf{p})S^{(-)}(\mathbf{p}) = 0, \quad S^{(\pm)^2}(\mathbf{p}) = S^{(\pm)}(\mathbf{p}). \quad (\text{E.14})$$

In the following we use abbreviations like

$$b_n := b^{m_n \dagger}(\mathbf{p}_n, s_n) \quad \text{and} \quad \psi_{-n} := \psi_{\alpha_n}^{m_n}(-\mathbf{p}_n) \quad (\text{E.15})$$

as well as obvious extensions thereof to other quantities. Our intent is to calculate the quark four-point function to first order in  $g^2$ ,

$$\begin{aligned} \langle \psi_1^\dagger \psi_2 \psi_3^\dagger \psi_4 \rangle &= ({}^1\langle 0 | g^2 + \langle 0 | \psi_1^\dagger \psi_2 \psi_3^\dagger \psi_4 (|0\rangle + g^2 |0\rangle^1) \\ &= g^2 \langle 0 | \psi_1^\dagger \psi_2 \psi_3^\dagger \psi_4 | 0 \rangle^1 + g^2 {}^1\langle 0 | \psi_1^\dagger \psi_2 \psi_3^\dagger \psi_4 | 0 \rangle, \end{aligned} \quad (\text{E.16})$$

where disconnected and higher order terms have been dropped. The first order correction in  $g^2$  to the non-interacting vacuum state is

$$|0\rangle^1 = - \sum_{n \neq 0} \frac{\langle n | H_F | 0 \rangle}{E_n} |n\rangle \quad (\text{E.17})$$

where the  $|n\rangle$  are the eigenstates of the free Dirac Hamiltonian  $H_{\psi^\dagger \psi}$ . The simplest non-trivial result is obtained using a two-quark-two-antiquark basis,

$$|0\rangle^1 \sim b_5^\dagger b_6^\dagger d_7^\dagger d_8^\dagger |0\rangle, \quad (\text{E.18})$$

as terms with a lower number of creation operators either vanish in Eq. (E.16) or give disconnected terms. For the evaluation of Eqs. (E.16) and (E.17) we need the expectation values

$$\begin{aligned} \langle 0 | \psi_1^\dagger \psi_2 \psi_3^\dagger \psi_4 b_5^\dagger b_6^\dagger d_7^\dagger d_8^\dagger | 0 \rangle &= \frac{1}{\prod_{i=1}^4 \sqrt{2E_{\mathbf{p}_i}}} \sum_{s_1 \dots s_4} v_{-1}^\dagger u_2 v_{-3}^\dagger u_4 \langle 0 | d_{-1} b_2 d_{-3} b_4 b_5^\dagger b_6^\dagger d_7^\dagger d_8^\dagger | 0 \rangle \\ &= \frac{1}{\prod_{i=1}^4 \sqrt{2E_{\mathbf{p}_i}}} \sum_{s_1 \dots s_4} v_{-1}^\dagger u_2 v_{-3}^\dagger u_4 (\delta_{-17} \delta_{26} \delta_{-38} \delta_{45} - \delta_{-18} \delta_{26} \delta_{-37} \delta_{45} \\ &\quad + \delta_{-18} \delta_{25} \delta_{-37} \delta_{46} - \delta_{-17} \delta_{25} \delta_{-38} \delta_{46}) \end{aligned} \quad (\text{E.19})$$

and

$$\begin{aligned} \langle 0 | d_8 d_7 b_6 b_5 \psi_1^\dagger \psi_2 \psi_3^\dagger \psi_4 | 0 \rangle &= \frac{1}{\prod_{i=1}^4 \sqrt{2E_{\mathbf{p}_i}}} \sum_{s_1 \dots s_4} v_{-4} u_3^\dagger v_{-2} u_1^\dagger (\delta_{-47} \delta_{36} \delta_{-28} \delta_{15} - \delta_{-48} \delta_{36} \delta_{-27} \delta_{15} \\ &\quad + \delta_{-48} \delta_{35} \delta_{-27} \delta_{16} - \delta_{-47} \delta_{35} \delta_{-28} \delta_{16}). \end{aligned} \quad (\text{E.20})$$

With these expressions, the first order correction to the ground state, Eq. (E.17), becomes

$$\begin{aligned}
|0\rangle^1 &= - (T^a)^{m_5 m_8} (T^a)^{m_6 m_7} \frac{1}{2} \int \frac{d^3[p_5 \cdots p_8]}{(2\pi)^{12}} (2\pi)^3 \delta^3(\mathbf{p}_5 + \cdots + \mathbf{p}_8) F(\mathbf{p}_5, -\mathbf{p}_8) \\
&\quad \frac{1}{\sqrt{E_{\mathbf{p}_5} \cdots E_{\mathbf{p}_8}} (E_{\mathbf{p}_5} + \cdots + E_{\mathbf{p}_8})} u_5^\dagger v_8 u_6^\dagger v_7 b_5^\dagger b_6^\dagger d_7^\dagger d_8^\dagger |0\rangle \\
&= : \int \frac{d^3[p_5 \cdots p_8]}{(2\pi)^{12}} K_{5867} b_5^\dagger b_6^\dagger d_7^\dagger d_8^\dagger |0\rangle
\end{aligned} \tag{E.21}$$

The first expectation value in Eq. (E.16) therefore becomes

$$\begin{aligned}
&\langle 0 | \psi_1^\dagger \psi_2 \psi_3^\dagger \psi_4 | 0 \rangle^1 \\
&= \frac{1}{4 \sqrt{E_{\mathbf{p}_1} \cdots E_{\mathbf{p}_4}}} \sum_{s_1 \dots s_4} v_{-1}^\dagger u_2 v_{-3}^\dagger u_4 (K_{4-32-1} - K_{4-12-3} + K_{2-14-3} - K_{2-34-1}) \\
&= \frac{4(2\pi)^3 \delta^3(\mathbf{p}_4 + \mathbf{p}_2 - \mathbf{p}_3 - \mathbf{p}_1)}{E_{\mathbf{p}_1} + \cdots + E_{\mathbf{p}_4}} \\
&\quad \left( (T^a)^{m_4 m_1} (T^a)^{m_2 m_3} (S^{(+)}(\mathbf{p}_4) S^{(-)}(\mathbf{p}_1))_{\alpha_4 \alpha_1} (S^{(+)}(\mathbf{p}_2) S^{(-)}(\mathbf{p}_3))_{\alpha_2 \alpha_3} F(\mathbf{p}_2 - \mathbf{p}_3) \right. \\
&\quad \left. - (T^a)^{m_4 m_3} (T^a)^{m_2 m_1} (S^{(+)}(\mathbf{p}_4) S^{(-)}(\mathbf{p}_3))_{\alpha_4 \alpha_3} (S^{(+)}(\mathbf{p}_2) S^{(-)}(\mathbf{p}_1))_{\alpha_2 \alpha_1} F(\mathbf{p}_1 - \mathbf{p}_2) \right).
\end{aligned} \tag{E.22}$$

Taking into account

$$(S^{(+)}(\mathbf{p}_4) S^{(-)}(\mathbf{p}_1))_{\alpha_4 \alpha_1}^* = (S^{(-)}(\mathbf{p}_1) S^{(+)}(\mathbf{p}_4))_{\alpha_1 \alpha_4}, \tag{E.23}$$

we obtain for the four-point function

$$\begin{aligned}
\langle \psi_{\alpha_4}^{m_4 \dagger}(\mathbf{p}_4) \psi_{\alpha_3}^{m_3}(\mathbf{p}_3) \psi_{\alpha_2}^{m_2 \dagger}(\mathbf{p}_2) \psi_{\alpha_1}^{m_1}(\mathbf{p}_1) \rangle &= \frac{4g^2 (2\pi)^3 \delta^3(\mathbf{p}_4 + \mathbf{p}_2 - \mathbf{p}_3 - \mathbf{p}_1)}{E_{\mathbf{p}_1} + \cdots + E_{\mathbf{p}_4}} \\
&\left\{ (T^a)^{m_4 m_1} (T^a)^{m_2 m_3} \left[ (S^{(+)}(\mathbf{p}_4) S^{(-)}(\mathbf{p}_1))_{\alpha_4 \alpha_1} (S^{(+)}(\mathbf{p}_2) S^{(-)}(\mathbf{p}_3))_{\alpha_2 \alpha_3} \right. \right. \\
&\quad \left. \left. + (S^{(-)}(\mathbf{p}_4) S^{(+)}(\mathbf{p}_1))_{\alpha_4 \alpha_1} (S^{(-)}(\mathbf{p}_2) S^{(+)}(\mathbf{p}_3))_{\alpha_2 \alpha_3} \right] F(\mathbf{p}_2 - \mathbf{p}_3) \right. \\
&\quad \left. - (T^a)^{m_4 m_3} (T^a)^{m_2 m_1} \left[ (S^{(+)}(\mathbf{p}_4) S^{(-)}(\mathbf{p}_3))_{\alpha_4 \alpha_3} (S^{(+)}(\mathbf{p}_2) S^{(-)}(\mathbf{p}_1))_{\alpha_2 \alpha_1} \right. \right. \\
&\quad \left. \left. + (S^{(-)}(\mathbf{p}_4) S^{(+)}(\mathbf{p}_3))_{\alpha_4 \alpha_3} (S^{(-)}(\mathbf{p}_2) S^{(+)}(\mathbf{p}_1))_{\alpha_2 \alpha_1} \right] F(\mathbf{p}_1 - \mathbf{p}_2) \right\}
\end{aligned} \tag{E.24}$$

Because of

$$\langle \psi_{\alpha_4}^{m_4 \dagger}(\mathbf{p}_4) \psi_{\alpha_3}^{m_3}(\mathbf{p}_3) \psi_{\alpha_2}^{m_2 \dagger}(\mathbf{p}_2) \psi_{\alpha_1}^{m_1}(\mathbf{p}_1) \rangle = W_{\alpha_4 \alpha_3 \alpha_2 \alpha_1}^{(4), m_4 m_3 m_2 m_1}(\mathbf{p}_4, -\mathbf{p}_3, \mathbf{p}_2, -\mathbf{p}_1) \tag{E.25}$$

and

$$\Gamma^{(4)} = -W_{\text{amp.}}^{(4)} , \quad (\text{E.26})$$

we still have to amputate the external propagators to get the one-particle irreducible four-quark vertex. In Ref. [44] the bare static quark propagator has been calculated as

$$S_{\alpha\beta}^{mn}(\mathbf{p}, \mathbf{q}) = \delta^{mn} \frac{h(\mathbf{p})_{\alpha\beta}}{2E_{\mathbf{p}}} (2\pi)^3 \delta^3(\mathbf{p} + \mathbf{q}) \quad (\text{E.27})$$

whose inverse is

$$\begin{aligned} (S^{-1})_{\alpha\beta}^{mn}(\mathbf{p}, \mathbf{q}) &= \delta^{mn} \frac{2h(\mathbf{p})_{\alpha\beta}}{E_{\mathbf{p}}} (2\pi)^3 \delta^3(\mathbf{p} + \mathbf{q}) \\ &= 2\delta^{mn} [S^{(+)}(\mathbf{p}) - S^{(-)}(\mathbf{p})]_{\alpha\beta} (2\pi)^3 \delta^3(\mathbf{p} + \mathbf{q}) . \end{aligned} \quad (\text{E.28})$$

Cutting off the external quark propagators, Eq. (E.24) involves terms like

$$\begin{aligned} &\int \frac{d^3 p'_4}{(2\pi)^3} (S^{-1})_{\alpha_4 \alpha'_4}(\mathbf{p}_4, -\mathbf{p}'_4) S_{\alpha'_4 \alpha_i}^{(\pm)}(\mathbf{p}'_4) (2\pi)^3 \delta^3(\mathbf{p}'_4 + \dots) \\ &= \int \frac{d^3 p'_4}{(2\pi)^3} 2 [S^{(+)}(\mathbf{p}_4) - S^{(-)}(\mathbf{p}_4)]_{\alpha_4 \alpha'_4} (2\pi)^3 \delta^3(\mathbf{p}_4 - \mathbf{p}'_4) S_{\alpha'_4 \alpha_i}^{(\pm)}(\mathbf{p}'_4) (2\pi)^3 \delta^3(\mathbf{p}'_4 + \dots) \\ &= \pm 2S_{\alpha_4 \alpha_i}^{(\pm)}(\mathbf{p}_4) \delta^3(\mathbf{p}_4 + \dots) \end{aligned} \quad (\text{E.29})$$

and

$$\begin{aligned} &\int \frac{d^3 p'_1}{(2\pi)^3} S_{\alpha_i \alpha'_1}^{(\pm)}(-\mathbf{p}'_1) (2\pi)^3 \delta^3(\mathbf{p}'_1 + \dots) (S^{-1})_{\alpha'_1 \alpha_1}(-\mathbf{p}'_1, \mathbf{p}_1) \\ &= \int \frac{d^3 p'_1}{(2\pi)^3} (2\pi)^3 \delta^3(\mathbf{p}'_1 + \dots) S_{\alpha_i \alpha'_1}^{(\pm)}(-\mathbf{p}'_1) \\ &\quad 2 [S^{(+)}(-\mathbf{p}'_1) - S^{(-)}(-\mathbf{p}'_1)]_{\alpha_1 \alpha'_1} (2\pi)^3 \delta^3(\mathbf{p}'_1 - \mathbf{p}_1) \\ &= \pm 2S_{\alpha_i \alpha_1}^{(\pm)}(-\mathbf{p}_1) \delta^3(\mathbf{p}_1 + \dots) , \end{aligned} \quad (\text{E.30})$$

where use has been made of Eq. (E.14). Therefore, cutting off a propagator at  $S^{(\pm)}$  yields a factor of  $\pm 2$ , so we get

$$\Gamma^{(4)} = -W_{\text{amp.}}^{(4)} = -16 W^{(4)} . \quad (\text{E.31})$$

The four-quark function finally becomes

$$\begin{aligned}
& \left( \frac{\delta^4 \Gamma}{\delta \psi^\dagger \delta \psi \delta \psi^\dagger \delta \psi} \right)_{\alpha_4 \alpha_3 \alpha_2 \alpha_1}^{m_4 m_3 m_2 m_1}(\mathbf{p}_4, \mathbf{p}_3, \mathbf{p}_2, \mathbf{p}_1) = \frac{64g^2(2\pi)^3 \delta^3(\mathbf{p}_1 + \mathbf{p}_2 + \mathbf{p}_3 + \mathbf{p}_4)}{E_{\mathbf{p}_1} + \dots + E_{\mathbf{p}_4}} \\
& \left\{ (T^a)^{m_4 m_3} (T^a)^{m_2 m_1} \left[ (S^{(+)}(\mathbf{p}_4) S^{(-)}(-\mathbf{p}_3))_{\alpha_4 \alpha_3} (S^{(+)}(\mathbf{p}_2) S^{(-)}(-\mathbf{p}_1))_{\alpha_2 \alpha_1} \right. \right. \\
& \quad \left. \left. + (S^{(-)}(\mathbf{p}_4) S^{(+)}(-\mathbf{p}_3))_{\alpha_4 \alpha_3} (S^{(-)}(\mathbf{p}_2) S^{(+)}(-\mathbf{p}_1))_{\alpha_2 \alpha_1} \right] F(\mathbf{p}_1 + \mathbf{p}_2) \right. \\
& \quad \left. - (T^a)^{m_4 m_1} (T^a)^{m_2 m_3} \left[ (S^{(+)}(\mathbf{p}_4) S^{(-)}(-\mathbf{p}_1))_{\alpha_4 \alpha_1} (S^{(+)}(\mathbf{p}_2) S^{(-)}(-\mathbf{p}_3))_{\alpha_2 \alpha_3} \right. \right. \\
& \quad \left. \left. + (S^{(-)}(\mathbf{p}_4) S^{(+)}(-\mathbf{p}_1))_{\alpha_4 \alpha_1} (S^{(-)}(\mathbf{p}_2) S^{(+)}(-\mathbf{p}_3))_{\alpha_2 \alpha_3} \right] F(\mathbf{p}_2 + \mathbf{p}_3) \right\}. \tag{E.32}
\end{aligned}$$

### E.3 Calculation of the Quark Tadpole Term

In the following, we calculate the flow equation for the quark two-point function retaining only the quark tadpole term. In condensed notation this equation reads, see Eq. (5.15),

$$\frac{\delta^2 \dot{\Gamma}_k}{\delta \psi_j^\dagger \delta \psi_i} = -\text{Tr} \dot{R}_{\psi, k} \left( -\frac{\delta^2 \Gamma_k}{\delta \psi^\dagger \delta \psi} + R_{\psi, k} \right)^{-1} \frac{\delta^4 \Gamma_k}{\delta \psi_j^\dagger \delta \psi_i \delta \psi^\dagger \delta \psi} \left( -\frac{\delta^2 \Gamma_k}{\delta \psi^\dagger \delta \psi} + R_{\psi, k} \right)^{-1}. \tag{E.33}$$

With Eq. (5.19) the l.h.s. becomes

$$\left( \frac{\delta^2 \dot{\Gamma}_k}{\delta \psi_j^\dagger \delta \psi_i} \right)_{\alpha_j \alpha_i}^{m_j m_i}(\mathbf{p}_j, \mathbf{p}_i) = -\delta^{m_j m_i} [(\boldsymbol{\alpha} \cdot \mathbf{p}_j) \dot{A}_k(\mathbf{p}_j) + \beta \dot{B}_k(\mathbf{p}_j)]_{\alpha_j \alpha_i} (2\pi)^3 \delta^3(\mathbf{p}_j + \mathbf{p}_i). \tag{E.34}$$

With Eqs. (5.23) and (5.25) the loop of the tadpole turns into

$$\begin{aligned}
& \left[ \left( -\frac{\delta^2 \Gamma_k}{\delta \psi^\dagger \delta \psi} + R_{\psi, k} \right)^{-1} \dot{R}_{\psi, k} \left( -\frac{\delta^2 \Gamma_k}{\delta \psi^\dagger \delta \psi} + R_{\psi, k} \right)^{-1} \right]_{\alpha_2 \alpha_1}^{m_2 m_1}(\mathbf{p}_2, \mathbf{p}_1) = \\
& \left[ (\boldsymbol{\alpha} \cdot \mathbf{p}_1)_{\alpha_2 \alpha_1} \left( \dot{R}_{\alpha, k} (B_k + R_{\beta, k})^2 - \dot{R}_{\alpha, k} p_1^2 (A_k + R_{\alpha, k})^2 \right. \right. \\
& \quad \left. \left. - 2\dot{R}_{\beta, k} (A_k + R_{\alpha, k})(B_k + R_{\beta, k}) \right) (p_1) \right. \\
& \quad \left. + \beta_{\alpha_2 \alpha_1} \left( 2\dot{R}_{\alpha, k} p_1^2 (A_k + R_{\alpha, k})(B_k + R_{\beta, k}) + \dot{R}_{\beta, k} (B_k + R_{\beta, k})^2 \right. \right. \\
& \quad \left. \left. - \dot{R}_{\beta, k} p_1^2 (A_k + R_{\alpha, k})^2 \right) (p_1) \right] \\
& \frac{\delta^{m_2 m_1} (2\pi)^3 \delta^3(\mathbf{p}_2 + \mathbf{p}_1)}{[p_1^2 (A_k + R_{\alpha, k})^2 + (B_k + R_{\beta, k})^2]^2 (p_1)}. \tag{E.35}
\end{aligned}$$

Using the four-quark function in Eq. (5.87) with a cut-off dependent Coulomb potential  $F_k(\mathbf{p})$ , the quark tadpole term in Eq. (E.33) is

$$\begin{aligned}
& - \int \frac{d^3[p_1 p_2]}{(2\pi)^6} \left[ \left( -\frac{\delta^2 \Gamma_k}{\delta \psi^\dagger \delta \psi} + R_{\psi,k} \right)^{-1} \dot{R}_{\psi,k} \left( -\frac{\delta^2 \Gamma_k}{\delta \psi^\dagger \delta \psi} + R_{\psi,k} \right)^{-1} \right]_{\alpha_2 \alpha_1}^{m_2 m_1} (\mathbf{p}_2, \mathbf{p}_1) \\
& \quad \left[ \frac{\delta^4 \Gamma_k}{\delta \psi^\dagger \delta \psi \delta \psi^\dagger \delta \psi} \right]_{\alpha_j \alpha_i \alpha_1 \alpha_2}^{m_j m_i m_1 m_2} (\mathbf{p}_j, \mathbf{p}_i, -\mathbf{p}_1, -\mathbf{p}_2) \\
& = - \int \frac{d^3 q}{(2\pi)^3} \frac{1}{[q^2(A_k + R_{\alpha,k})^2 + (B_k + R_{\beta,k})^2]^2(q)} \\
& \quad \left\{ (\boldsymbol{\alpha} \cdot \mathbf{q})_{\alpha_2 \alpha_1} \left( \dot{R}_{\alpha,k} (B_k + R_{\beta,k})^2 - \dot{R}_{\alpha,k} q^2 (A_k + R_{\alpha,k})^2 \right. \right. \\
& \quad \left. \left. - 2\dot{R}_{\beta,k} (A_k + R_{\alpha,k})(B_k + R_{\beta,k}) \right) (q) \right. \\
& \quad \left. + \beta_{\alpha_2 \alpha_1} \left( 2\dot{R}_{\alpha,k} q^2 (A_k + R_{\alpha,k})(B_k + R_{\beta,k}) + \dot{R}_{\beta,k} (B_k + R_{\beta,k})^2 \right. \right. \\
& \quad \left. \left. - \dot{R}_{\beta,k} q^2 (A_k + R_{\alpha,k})^2 \right) (q) \right\} \\
& \quad \left\{ - \underbrace{(T^a)^{m_j m_2} (T^a)^{m_2 m_i}}_{=C_2 \delta^{m_j m_i}} \left[ (S^{(+)}(-\mathbf{p}) S^{(-)}(-\mathbf{q}))_{\alpha_j \alpha_2} (S^{(+)}(-\mathbf{q}) S^{(-)}(-\mathbf{p}))_{\alpha_1 \alpha_i} \right. \right. \\
& \quad \left. \left. + (S^{(-)}(-\mathbf{p}) S^{(+)}(-\mathbf{q}))_{\alpha_j \alpha_2} (S^{(-)}(-\mathbf{q}) S^{(+)}(-\mathbf{p}))_{\alpha_1 \alpha_i} \right] \right. \\
& \quad \left. F(\mathbf{p} - \mathbf{q}) \right. \\
& \quad \left. + \underbrace{(T^a)^{m_2 m_2}}_{=0} \dots \right\} \frac{32g^2}{E_{\mathbf{p}} + E_{\mathbf{q}}} (2\pi)^3 \delta^3(\mathbf{0}) \\
& = \delta^{m_j m_i} [(\boldsymbol{\alpha} \cdot \mathbf{p})_{\alpha_j \alpha_i} \dot{A}_k(\mathbf{p}) - \beta_{\alpha_j \alpha_i} \dot{B}_k(\mathbf{p})] (2\pi)^3 \delta^3(\mathbf{0}), \tag{E.36}
\end{aligned}$$

where we have used the fact that the generators of the gauge group  $T^a$  are traceless and renamed  $\mathbf{p}_i \rightarrow \mathbf{p}$  and  $\mathbf{p}_1 \rightarrow \mathbf{q}$ . The lengthy products of Dirac matrices can be simplified to

$$\begin{aligned}
& S^{(+)}(-\mathbf{p}) S^{(-)}(-\mathbf{q}) \boldsymbol{\alpha} \cdot \mathbf{q} S^{(+)}(-\mathbf{q}) S^{(-)}(-\mathbf{p}) \\
& + S^{(-)}(-\mathbf{p}) S^{(+)}(-\mathbf{q}) \boldsymbol{\alpha} \cdot \mathbf{q} S^{(-)}(-\mathbf{q}) S^{(+)}(-\mathbf{p}) \\
& = \frac{m}{2E_{\mathbf{p}}^2 E_{\mathbf{q}}^2} (\boldsymbol{\alpha} \cdot \mathbf{p} m(\mathbf{q}^2 - \mathbf{p} \cdot \mathbf{q}) + \boldsymbol{\alpha} \cdot \mathbf{q} m E_{\mathbf{p}} (E_{\mathbf{p}} - E_{\mathbf{q}}) \\
& \quad + \beta((m^2 - E_{\mathbf{p}} E_{\mathbf{q}}) \mathbf{p} \cdot \mathbf{q} + \mathbf{p}^2 \mathbf{q}^2)) \tag{E.37}
\end{aligned}$$

and

$$\begin{aligned}
& S^{(+)}(-\mathbf{p})S^{(-)}(-\mathbf{q})\beta S^{(+)}(-\mathbf{q})S^{(-)}(-\mathbf{p}) + S^{(-)}(-\mathbf{p})S^{(+)}(-\mathbf{q})\beta S^{(-)}(-\mathbf{q})S^{(+)}(-\mathbf{p}) \\
&= \frac{1}{2E_{\mathbf{p}}^2E_{\mathbf{q}}^2}(\boldsymbol{\alpha} \cdot \mathbf{p} m(\mathbf{q}^2 - \mathbf{p} \cdot \mathbf{q}) + \boldsymbol{\alpha} \cdot \mathbf{q} mE_{\mathbf{p}}(E_{\mathbf{p}} - E_{\mathbf{q}}) \\
&\quad + \beta((m^2 - E_{\mathbf{p}}E_{\mathbf{q}})\mathbf{p} \cdot \mathbf{q} + \mathbf{p}^2\mathbf{q}^2)).
\end{aligned} \tag{E.38}$$

Note that these two expressions differ only by a factor of the current quark mass  $m$  which accounts for different dimensions. For the flows of the dressing functions  $A$  and  $B$  we finally obtain

$$\begin{aligned}
\mathbf{p}^2 \dot{A}_k(p) &= 16g^2 C_2 \int \frac{d^3q}{(2\pi)^3} F_k(\mathbf{p} - \mathbf{q}) \frac{m\mathbf{p}^2(\mathbf{q}^2 - \mathbf{p} \cdot \mathbf{q}) + m\mathbf{p} \cdot \mathbf{q}E_{\mathbf{p}}(E_{\mathbf{p}} - E_{\mathbf{q}})}{(E_{\mathbf{p}} + E_{\mathbf{q}})E_{\mathbf{p}}^2E_{\mathbf{q}}^2} \\
&\quad \frac{1}{[q^2(A_k + R_{\alpha,k})^2 + (B_k + R_{\beta,k})^2]^2(q)} \\
&\quad \left[ m \left( \dot{R}_{\alpha,k}(B_k + R_{\beta,k})^2 - \dot{R}_{\alpha,k}q^2(A_k + R_{\alpha,k})^2 - 2\dot{R}_{\beta,k}(A_k + R_{\alpha,k})(B_k + R_{\beta,k}) \right) (q) \right. \\
&\quad \left. + \left( 2\dot{R}_{\alpha,k}q^2(A_k + R_{\alpha,k})(B_k + R_{\beta,k}) + \dot{R}_{\beta,k}(B_k + R_{\beta,k})^2 - \dot{R}_{\beta,k}q^2(A_k + R_{\alpha,k})^2 \right) (q) \right]
\end{aligned} \tag{E.39}$$

and

$$\begin{aligned}
\dot{B}_k(p) &= -16g^2 C_2 \int \frac{d^3q}{(2\pi)^3} F_k(\mathbf{p} - \mathbf{q}) \frac{(m^2 - E_{\mathbf{p}}E_{\mathbf{q}})\mathbf{p} \cdot \mathbf{q} + \mathbf{p}^2\mathbf{q}^2}{(E_{\mathbf{p}} + E_{\mathbf{q}})E_{\mathbf{p}}^2E_{\mathbf{q}}^2} \\
&\quad \frac{1}{[q^2(A_k + R_{\alpha,k})^2 + (B_k + R_{\beta,k})^2]^2(q)} \\
&\quad \left[ m \left( \dot{R}_{\alpha,k}(B_k + R_{\beta,k})^2 - \dot{R}_{\alpha,k}q^2(A_k + R_{\alpha,k})^2 - 2\dot{R}_{\beta,k}(A_k + R_{\alpha,k})(B_k + R_{\beta,k}) \right) (q) \right. \\
&\quad \left. + \left( 2\dot{R}_{\alpha,k}q^2(A_k + R_{\alpha,k})(B_k + R_{\beta,k}) + \dot{R}_{\beta,k}(B_k + R_{\beta,k})^2 - \dot{R}_{\beta,k}q^2(A_k + R_{\alpha,k})^2 \right) (q) \right].
\end{aligned} \tag{E.40}$$

# Bibliography

- [1] C. Wetterich, “Exact evolution equation for the effective potential,” *Phys. Lett.* **B301** (1993) 90–94.
- [2] H. Gies, “Introduction to the functional RG and applications to gauge theories,” [arXiv:hep-ph/0611146](https://arxiv.org/abs/hep-ph/0611146).
- [3] K. G. Wilson, “Confinement of Quarks,” *Phys.Rev.* **D10** (1974) 2445–2459.
- [4] M. Creutz, *Quarks, Gluons and Lattices*. Cambridge University Press, 1985.
- [5] H. Rothe, “Lattice gauge theories: An Introduction,” *World Sci.Lect.Notes Phys.* **74** (2005) 1–605.
- [6] C. Gattringer and C. B. Lang, “Quantum chromodynamics on the lattice,” *Lect.Notes Phys.* **788** (2010) 1–211.
- [7] F. Dyson, “The S matrix in quantum electrodynamics,” *Phys.Rev.* **75** (1949) 1736–1755.
- [8] J. S. Schwinger, “On the Green’s functions of quantized fields. 1.,” *Proc.Nat.Acad.Sci.* **37** (1951) 452–455.
- [9] J. S. Schwinger, “On the Green’s functions of quantized fields. 2.,” *Proc.Nat.Acad.Sci.* **37** (1951) 455–459.
- [10] R. Alkofer and L. von Smekal, “The Infrared behavior of QCD Green’s functions: Confinement dynamical symmetry breaking, and hadrons as relativistic bound states,” *Phys.Rept.* **353** (2001) 281, [arXiv:hep-ph/0007355](https://arxiv.org/abs/hep-ph/0007355) [hep-ph].
- [11] C. D. Roberts and A. G. Williams, “Dyson-Schwinger equations and their application to hadronic physics,” *Prog.Part.Nucl.Phys.* **33** (1994) 477–575, [arXiv:hep-ph/9403224](https://arxiv.org/abs/hep-ph/9403224) [hep-ph].
- [12] L. Kadanoff, “Scaling laws for Ising models near T(c),” *Physics* **2** (1966) 263–272.
- [13] K. G. Wilson, “Renormalization group and critical phenomena. 1. Renormalization group and the Kadanoff scaling picture,” *Phys.Rev.* **B4** (1971) 3174–3183.

- 
- [14] K. G. Wilson, “Renormalization group and critical phenomena. 2. Phase space cell analysis of critical behavior,” *Phys.Rev.* **B4** (1971) 3184–3205.
- [15] K. Wilson and J. B. Kogut, “The Renormalization group and the epsilon expansion,” *Phys.Rept.* **12** (1974) 75–200.
- [16] F. J. Wegner and A. Houghton, “Renormalization group equation for critical phenomena,” *Phys.Rev.* **A8** (1973) 401–412.
- [17] J. Polchinski, “Renormalization and Effective Lagrangians,” *Nucl.Phys.* **B231** (1984) 269–295.
- [18] D. F. Litim and J. M. Pawłowski, “On gauge invariant Wilsonian flows,” [arXiv:hep-th/9901063](https://arxiv.org/abs/hep-th/9901063).
- [19] K. Aoki, “Introduction to the nonperturbative renormalization group and its recent applications,” *Int.J.Mod.Phys.* **B14** (2000) 1249–1326.
- [20] J. Berges, N. Tetradis, and C. Wetterich, “Nonperturbative renormalization flow in quantum field theory and statistical physics,” *Phys.Rept.* **363** (2002) 223–386, [arXiv:hep-ph/0005122](https://arxiv.org/abs/hep-ph/0005122) [hep-ph].
- [21] J. Polonyi, “Lectures on the functional renormalization group method,” *Central Eur.J.Phys.* **1** (2003) 1–71, [arXiv:hep-th/0110026](https://arxiv.org/abs/hep-th/0110026) [hep-th].
- [22] J. M. Pawłowski, “Aspects of the functional renormalisation group,” *Annals Phys.* **322** (2007) 2831–2915, [arXiv:hep-th/0512261](https://arxiv.org/abs/hep-th/0512261).
- [23] B. Delamotte, “An Introduction to the nonperturbative renormalization group,” [arXiv:cond-mat/0702365](https://arxiv.org/abs/cond-mat/0702365) [COND-MAT].
- [24] M. Reuter and F. Saueressig, “Functional Renormalization Group Equations, Asymptotic Safety, and Quantum Einstein Gravity,” [arXiv:0708.1317](https://arxiv.org/abs/0708.1317) [hep-th].
- [25] P. Kopietz, L. Bartosch, and F. Schutz, “Introduction to the functional renormalization group,” *Lect.Notes Phys.* **798** (2010) 1–380.
- [26] U. Ellwanger, M. Hirsch, and A. Weber, “Flow equations for the relevant part of the pure Yang- Mills action,” *Z. Phys.* **C69** (1996) 687–698, [arXiv:hep-th/9506019](https://arxiv.org/abs/hep-th/9506019).
- [27] M. Reuter, “Nonperturbative evolution equation for quantum gravity,” *Phys.Rev.* **D57** (1998) 971–985, [arXiv:hep-th/9605030](https://arxiv.org/abs/hep-th/9605030) [hep-th].
- [28] M. Reuter and C. Wetterich, “Quantum Liouville field theory as solution of a flow equation,” *Nucl.Phys.* **B506** (1997) 483–520, [arXiv:hep-th/9605039](https://arxiv.org/abs/hep-th/9605039) [hep-th].



- 
- [29] H. Weyl, “A new extension of relativity theory. (in German),” *Annalen Phys.* **59** (1919) 101–133.
- [30] V. Fock, “On the invariant form of the wave equation and the equations of motion for a charged point mass. (In German and English),” *Z.Phys.* **39** (1926) 226–232.
- [31] F. London, “Quantum mechanical interpretation of the Weyl theory. (In German and English),” *Z.Phys.* **42** (1927) 375–389.
- [32] H. Weyl, “Electron and Gravitation. 1. (In German),” *Z.Phys.* **56** (1929) 330–352.
- [33] C.-N. Yang and R. L. Mills, “Conservation of Isotopic Spin and Isotopic Gauge Invariance,” *Phys.Rev.* **96** (1954) 191–195.
- [34] L. O’Raifeartaigh and N. Straumann, “Gauge theory: Historical origins and some modern developments,” *Rev.Mod.Phys.* **72** (2000) 1–23.
- [35] J. D. Jackson and L. Okun, “Historical roots of gauge invariance,” *Rev.Mod.Phys.* **73** (2001) 663–680, arXiv:hep-ph/0012061 [hep-ph].
- [36] M. Peskin and E. Schroeder, *An Introduction to Quantum Field Theory*. Perseus Books, 1995.
- [37] S. Pokorski, *Gauge Field Theories*. Cambridge University Press, 2000.
- [38] S. Weinberg, *The Quantum Theory of Fields: Volume 2, Modern Applications*. Cambridge University Press, 2005.
- [39] M. Gell-Mann, “A Schematic Model of Baryons and Mesons,” *Phys.Lett.* **8** (1964) 214–215.
- [40] H. Fritzsch, M. Gell-Mann, and H. Leutwyler, “Advantages of the Color Octet Gluon Picture,” *Phys.Lett.* **B47** (1973) 365–368.
- [41] D. Gross and F. Wilczek, “Ultraviolet Behavior of Nonabelian Gauge Theories,” *Phys.Rev.Lett.* **30** (1973) 1343–1346.
- [42] H. Politzer, “Reliable Perturbative Results for Strong Interactions?,” *Phys.Rev.Lett.* **30** (1973) 1346–1349.
- [43] C. Feuchter and H. Reinhardt, “Variational solution of the Yang-Mills Schroedinger equation in Coulomb gauge,” *Phys. Rev.* **D70** (2004) 105021, arXiv:hep-th/0408236.
- [44] D. R. Campagnari, *The Yang-Mills Vacuum Wave Functional in Coulomb Gauge*. PhD thesis, University of Tübingen, 2010.

- 
- [45] N. Christ and T. Lee, “Operator Ordering and Feynman Rules in Gauge Theories,” *Phys.Rev.* **D22** (1980) 939.
- [46] D. Schutte, “Nonperturbative many body techniques applied to a Yang-Mills field theory,” *Phys.Rev.* **D31** (1985) 810–821.
- [47] A. P. Szczepaniak and E. S. Swanson, “Coulomb gauge QCD, confinement, and the constituent representation,” *Phys. Rev.* **D65** (2002) 025012, [arXiv:hep-ph/0107078](#).
- [48] H. Reinhardt and C. Feuchter, “On the Yang-Mills wave functional in Coulomb gauge,” *Phys. Rev.* **D71** (2005) 105002, [arXiv:hep-th/0408237](#).
- [49] W. Schleifenbaum, M. Leder, and H. Reinhardt, “Infrared analysis of propagators and vertices of Yang-Mills theory in Landau and Coulomb gauge,” *Phys. Rev.* **D73** (2006) 125019, [arXiv:hep-th/0605115](#).
- [50] D. Epple, H. Reinhardt, and W. Schleifenbaum, “Confining Solution of the Dyson-Schwinger Equations in Coulomb Gauge,” *Phys. Rev.* **D75** (2007) 045011, [arXiv:hep-th/0612241](#).
- [51] D. Epple, H. Reinhardt, W. Schleifenbaum, and A. P. Szczepaniak, “Subcritical solution of the Yang-Mills Schroedinger equation in the Coulomb gauge,” *Phys. Rev.* **D77** (2008) 085007, [arXiv:0712.3694 \[hep-th\]](#).
- [52] D. R. Campagnari and H. Reinhardt, “Non-Gaussian wave functionals in Coulomb gauge Yang-Mills theory,” *Phys.Rev.* **D82** (2010) 105021, [arXiv:1009.4599 \[hep-th\]](#).
- [53] H. Reinhardt *et al.*, “Coulomb gauge Yang-Mills theory in the Hamiltonian approach,” [arXiv:0807.4635 \[hep-th\]](#).
- [54] H. Reinhardt, “The dielectric function of the QCD vacuum,” *Phys. Rev. Lett.* **101** (2008) 061602, [arXiv:0803.0504 \[hep-th\]](#).
- [55] C. S. Fischer, “Infrared properties of QCD from Dyson-Schwinger equations,” *J.Phys.G* **G32** (2006) R253–R291, [arXiv:hep-ph/0605173 \[hep-ph\]](#).
- [56] L. von Smekal, “Landau Gauge QCD: Functional Methods versus Lattice Simulations,” [arXiv:0812.0654 \[hep-th\]](#).
- [57] D. Binosi and J. Papavassiliou, “Pinch Technique: Theory and Applications,” *Phys. Rept.* **479** (2009) 1–152, [arXiv:0909.2536 \[hep-ph\]](#).
- [58] C. S. Fischer, A. Maas, and J. M. Pawłowski, “On the infrared behavior of Landau gauge Yang-Mills theory,” *Annals Phys.* **324** (2009) 2408–2437, [arXiv:0810.1987 \[hep-ph\]](#).

- 
- [59] P. Boucaud *et al.*, “On the IR behaviour of the Landau-gauge ghost propagator,” *JHEP* **06** (2008) 099, arXiv:0803.2161 [hep-ph].
- [60] D. Zwanziger, “Renormalization in the Coulomb gauge and order parameter for confinement in QCD,” *Nucl. Phys.* **B518** (1998) 237–272.
- [61] P. Watson and H. Reinhardt, “Propagator Dyson-Schwinger equations of Coulomb gauge Yang-Mills theory within the first order formalism,” *Phys. Rev.* **D75** (2007) 045021, arXiv:hep-th/0612114.
- [62] R. Alkofer, A. Maas, and D. Zwanziger, “Truncating first-order Dyson-Schwinger equations in Coulomb-Gauge Yang-Mills theory,” *Few Body Syst.* **47** (2010) 73–90, arXiv:0905.4594 [hep-ph].
- [63] P. Watson and H. Reinhardt, “Two-Point Functions of Coulomb Gauge Yang-Mills Theory,” *Phys. Rev.* **D77** (2008) 025030, arXiv:0709.3963 [hep-th].
- [64] P. Watson and H. Reinhardt, “The Coulomb gauge ghost Dyson-Schwinger equation,” *Phys.Rev.* **D82** (2010) 125010, arXiv:1007.2583 [hep-th].
- [65] C. Popovici, P. Watson, and H. Reinhardt, “Quarks in Coulomb gauge perturbation theory,” *Phys.Rev.* **D79** (2009) 045006, arXiv:0810.4887 [hep-th].
- [66] C. Popovici, P. Watson, and H. Reinhardt, “Coulomb gauge confinement in the heavy quark limit,” *Phys.Rev.* **D81** (2010) 105011, arXiv:1003.3863 [hep-th].
- [67] G. Burgio, M. Quandt, and H. Reinhardt, “Coulomb gauge gluon propagator and the Gribov formula,” *Phys.Rev.Lett.* **102** (2009) 032002, arXiv:0807.3291 [hep-lat].
- [68] V. Gribov, “Quantization of Nonabelian Gauge Theories,” *Nucl.Phys.* **B139** (1978) 1.
- [69] G. Burgio, M. Quandt, and H. Reinhardt, “BRST symmetry vs. Horizon condition in Yang-Mills theories,” *Phys. Rev.* **D81** (2010) 074502, arXiv:0911.5101 [hep-lat].
- [70] G. Burgio, M. Quandt, M. Schrock, and H. Reinhardt, “Propagators in lattice Coulomb gauge and confinement mechanisms,” *PoS LATTICE2010* (2010) 272, arXiv:1011.0560 [hep-lat].
- [71] A. Cucchieri, “Lattice Results in Coulomb Gauge,” *AIP Conf.Proc.* **892** (2007) 22–28, arXiv:hep-lat/0612004 [hep-lat].

- [72] M. Leder, J. M. Pawłowski, H. Reinhardt, and A. Weber, “Hamiltonian Flow in Coulomb Gauge Yang-Mills Theory,” *Phys.Rev.* **D83** (2011) 025010, [arXiv:1006.5710 \[hep-th\]](#).
- [73] C. S. Fischer and J. M. Pawłowski, “Uniqueness of infrared asymptotics in Landau gauge Yang- Mills theory II,” *Phys. Rev.* **D80** (2009) 025023, [arXiv:0903.2193 \[hep-th\]](#).
- [74] R. Alkofer, M. Q. Huber, and K. Schwenzer, “Infrared singularities in Landau gauge Yang-Mills theory,” *Phys. Rev.* **D81** (2010) 105010, [arXiv:0801.2762 \[hep-th\]](#).
- [75] C. Lerche and L. von Smekal, “On the infrared exponent for gluon and ghost propagation in Landau gauge QCD,” *Phys. Rev.* **D65** (2002) 125006, [arXiv:hep-ph/0202194](#).
- [76] D. Zwanziger, “Analytic calculation of color-Coulomb potential and color confinement,” *Phys. Rev.* **D70** (2004) 094034, [arXiv:hep-ph/0312254](#).
- [77] D. Campagnari, A. Weber, H. Reinhardt, F. Astorga, and W. Schleifenbaum, “Equal-time two-point correlation functions in Coulomb gauge Yang-Mills theory,” *Nucl. Phys.* **B842** (2011) 501–528, [arXiv:0910.4548 \[hep-th\]](#).
- [78] D. Zwanziger, “Vanishing of zero momentum lattice gluon propagator and color confinement,” *Nucl. Phys.* **B364** (1991) 127–161.
- [79] D. Zwanziger, “Lattice Coulomb Hamiltonian and static color-Coulomb field,” *Nucl. Phys.* **B485** (1997) 185–240, [arXiv:hep-th/9603203](#).
- [80] J. C. Taylor, “Ward Identities and Charge Renormalization of the Yang-Mills Field,” *Nucl. Phys.* **B33** (1971) 436–444.
- [81] W. J. Marciano and H. Pagels, “Quantum Chromodynamics: A Review,” *Phys. Rept.* **36** (1978) 137.
- [82] A. Cucchieri, T. Mendes, and A. Mihara, “Numerical study of the ghost-gluon vertex in Landau gauge,” *JHEP* **12** (2004) 012, [arXiv:hep-lat/0408034](#).
- [83] A. Sternbeck, E. M. Ilgenfritz, M. Müller-Preussker, and A. Schiller, “Landau gauge ghost and gluon propagators and the Faddeev-Popov operator spectrum,” *Nucl. Phys. Proc. Suppl.* **153** (2006) 185–190, [arXiv:hep-lat/0511053](#).
- [84] W. Schleifenbaum, A. Maas, J. Wambach, and R. Alkofer, “Infrared behaviour of the ghost-gluon vertex in Landau gauge Yang-Mills theory,” *Phys.Rev.* **D72** (2005) 014017, [arXiv:hep-ph/0411052 \[hep-ph\]](#).

- 
- [85] D. R. Campagnari, H. Reinhardt, and A. Weber, “Perturbation theory in the Hamiltonian approach to Yang-Mills theory in Coulomb gauge,” *Phys. Rev.* **D80** (2009) 025005, arXiv:0904.3490 [hep-th].
- [86] J. M. Pawłowski, D. F. Litim, S. Nedelko, and L. von Smekal, “Infrared behaviour and fixed points in Landau gauge QCD,” *Phys. Rev. Lett.* **93** (2004) 152002, arXiv:hep-th/0312324.
- [87] D. F. Litim, “Optimisation of the exact renormalisation group,” *Phys. Lett.* **B486** (2000) 92–99, arXiv:hep-th/0005245.
- [88] C. S. Fischer and D. Zwanziger, “Infrared behaviour and running couplings in interpolating gauges in QCD,” *Phys. Rev.* **D72** (2005) 054005, arXiv:hep-ph/0504244.
- [89] M. Leder, H. Reinhardt, A. Weber, and J. M. Pawłowski, “Color Coulomb Potential in Yang-Mills Theory from Hamiltonian Flows,” arXiv:1105.0800 [hep-th].
- [90] D. Zwanziger, “No confinement without Coulomb confinement,” *Phys.Rev.Lett.* **90** (2003) 102001, arXiv:hep-lat/0209105 [hep-lat].
- [91] I. Gradshteyn and I. Ryzhik, *Table of Integrals, Series, and Products*. Academic Press, New York, 1980.
- [92] W. Schleifenbaum, *Nonperturbative aspects of Yang-Mills theory*. PhD thesis, University of Tübingen, 2008.
- [93] M. Gell-Mann, R. Oakes, and B. Renner, “Behavior of current divergences under  $SU(3) \times SU(3)$ ,” *Phys.Rev.* **175** (1968) 2195–2199.
- [94] W. Weise, “The QCD vacuum and its hadronic excitations,” arXiv:nucl-th/0504087 [nucl-th].
- [95] A. Amer, A. Le Yaouanc, L. Oliver, O. Pene, and J. Raynal, “Instability of the chiral invariant vacuum for a confining potential,” *Phys.Rev.Lett.* **50** (1983) 87–90.
- [96] J. R. Finger and J. E. Mandula, “Quark Pair Condensation and Chiral Symmetry Breaking in QCD,” *Nucl.Phys.* **B199** (1982) 168.
- [97] A. Le Yaouanc, L. Oliver, O. Pene, and J. Raynal, “Chiral noninvariant solutions of the gap equation for a confining potential,” *Phys.Lett.* **B134** (1984) 249.
- [98] A. Le Yaouanc, L. Oliver, S. Ono, O. Pene, and J. Raynal, “A Quark Model of Light Mesons with Dynamically Broken Chiral Symmetry,” *Phys.Rev.* **D31** (1985) 137.

- 
- [99] S. L. Adler and A. Davis, “Chiral Symmetry Breaking in Coulomb Gauge QCD,” *Nucl.Phys.* **B244** (1984) 469.
- [100] A. Le Yaouanc, L. Oliver, O. Pene, and J. Raynal, “Spontaneous Breaking of Chiral Symmetry for Confining Potentials,” *Phys.Rev.* **D29** (1984) 1233.
- [101] R. Alkofer and P. Amundsen, “Chiral symmetry breaking in an instantaneous approximation to Coulomb gauge QCD,” *Nucl.Phys.* **B306** (1988) 305–342.
- [102] A. P. Szczepaniak and P. Krupinski, “Spontaneous chiral symmetry breaking in the linked cluster expansion,” *Phys.Rev.* **D66** (2002) 096006, [arXiv:hep-ph/0204249](#) [hep-ph].
- [103] H. Gies and C. Wetterich, “Renormalization flow of bound states,” *Phys.Rev.* **D65** (2002) 065001, [arXiv:hep-th/0107221](#) [hep-th].
- [104] H. Gies and C. Wetterich, “Universality of spontaneous chiral symmetry breaking in gauge theories,” *Phys.Rev.* **D69** (2004) 025001, [arXiv:hep-th/0209183](#) [hep-th].
- [105] C. Fischer, P. Watson, and W. Cassing, “Probing unquenching effects in the gluon polarisation in light mesons,” *Phys.Rev.* **D72** (2005) 094025, [arXiv:hep-ph/0509213](#) [hep-ph].
- [106] P. O. Bowman, U. M. Heller, D. B. Leinweber, M. B. Parappilly, and A. G. Williams, “Unquenched gluon propagator in Landau gauge,” *Phys.Rev.* **D70** (2004) 034509, [arXiv:hep-lat/0402032](#) [hep-lat].
- [107] P. O. Bowman, U. M. Heller, D. B. Leinweber, M. B. Parappilly, A. G. Williams, *et al.*, “Unquenched quark propagator in Landau gauge,” *Phys.Rev.* **D71** (2005) 054507, [arXiv:hep-lat/0501019](#) [hep-lat].
- [108] D. Campagnari, “private communication.” 2011.
- [109] M. Pak and H. Reinhardt, “Chiral symmetry breaking in Hamiltonian QCD in Coulomb gauge,” [arXiv:1107.5263](#) [hep-ph].
- [110] H. Reinhardt, “private communication.” 2011.
- [111] J. Greensite, S. Olejnik, and D. Zwanziger, “Coulomb energy, remnant symmetry, and the phases of nonAbelian gauge theories,” *Phys.Rev.* **D69** (2004) 074506, [arXiv:hep-lat/0401003](#) [hep-lat].
- [112] K. Langfeld and L. Moyaerts, “Propagators in Coulomb gauge from SU(2) lattice gauge theory,” *Phys.Rev.* **D70** (2004) 074507, [arXiv:hep-lat/0406024](#) [hep-lat].

- 
- [113] A. Voigt, E.-M. Ilgenfritz, M. Muller-Preussker, and A. Sternbeck, “The Effective Coulomb potential in SU(3) lattice Yang-Mills theory,” *Phys.Rev.* **D78** (2008) 014501, [arXiv:0803.2307](#) [hep-lat].
- [114] Y. Nakagawa, A. Nakamura, T. Saito, and H. Toki, “Scaling study of the gluon propagator in Coulomb gauge QCD on isotropic and anisotropic lattices,” *Phys.Rev.* **D83** (2011) 114503, [arXiv:1105.6185](#) [hep-lat].
- [115] J. Braun, H. Gies, and J. M. Pawłowski, “Quark Confinement from Color Confinement,” *Phys. Lett.* **B684** (2010) 262–267, [arXiv:0708.2413](#) [hep-th].
- [116] A. Weber, *Exakte Renormierungsgruppengleichungen in der Quantenfeldtheorie*. PhD thesis, University of Heidelberg, 1995.
- [117] W. H. Press, B. P. Flannery, S. A. Teukolsky, and W. T. Vetterling, *Numerical Recipes in C: The Art of Scientific Computing*. Cambridge University Press, 1992.





